Cable-Driven Parallel Robots with Large Translation and Orientation Workspaces

Saman Lessanibahri

Thèse de doctorat de

L'ÉCOLE CENTRALE DE NANTES
COMUE UNIVERSITE BRETAGNE LOIRE

ECOLE DOCTORALE N° 602
Sciences pour l'Ingénieur
Spécialité : *Robotique - Mécanique*

Par

Saman LESSANIBAHRI

Cable-Driven Parallel Robots with Large Translation and Orientation Workspaces

Thèse présentée et soutenue à Nantes, le 12 mai 2020
Unité de recherche : Laboratoire des Sciences du Numérique de Nantes (LS2N)

Rapporteurs :

Marc GOUTTEFARDE   Directeur de recherche, Université de Montpellier
Med Amine LARIBI   Maître de conférences HDR, Université de Poitiers

Composition du Jury :

Président :   Marc GOUTTEFARDE   Directeur de recherche, Université de Montpellier

Examinateurs : Coralie GERMAIN   Enseignante Chercheuse, Agrocampus-Ouest, Rennes
          Darwin LAU   Professeur assistant, Université Chinoise de Hong Kong, Chine

Dir. de thèse :   Stéphane CARO   Directeur de recherche, École Centrale de Nantes
Co-dir. de thèse : Philippe CARDOU   Professeur, Université de Laval, Canada

Résumé

Les Robots Parallèles à Câbles (RPC) sont considérés comme des manipulateurs parallèles avec des câbles flexibles au lieu de liens rigides. Un RPC se compose d'un bâti, d'une plate-forme mobile et de câbles les reliant l'un à l'autre. Les RPC sont réputés pour leurs performances avantageuses par rapport aux robots parallèles classiques en termes d'espace de travail en translation, de reconfigurabilité, de capacité de charge utile importante et de performances dynamiques élevées. Cependant, l'amplitude de rotation de la plateforme mobile des RPC est généralement limitée en raison des collisions de types câble/câble et câble/plateforme mobile.

De nouveaux concepts sur le potentiel des RPC avec un espace de travail en orientation très large ont été introduits dans la littérature. L'un de ces concepts suggère l'utilisation d'un circuit de câble bi-actionné pour l'actionnement à distance d'un mécanisme parallèle intégré dans la plateforme mobile des RPC, formant des manipulateurs hybrides. Ces manipulateurs sont hybrides parce qu'ils combinent les avantages d'un grand espace de travail en translation des RPC et de grandes amplitudes de rotation des poignets actifs. Même s'il s'agit d'un concept prometteur pour l'augmentation de l'espace de travail en orientation des RPC, au meilleur de la connaissance de l'auteur, il n'a pas été réalisé. Les circuits de câble bi-actionnés, à savoir les boucles de câbles, sont l'essence même des RPC hybrides munis d'une plateforme articulée et actionnée au moyen de moteurs fixés au sol. Par conséquent, les plateformes mobiles n'ont pas besoin d'actionneurs embarqués, ce qui réduit l'inertie des parties mobiles des manipulateurs. Ainsi, l'objectif principal de cette thèse de doctorat est ainsi de concevoir, d'analyser et de prototyper des RPC hybrides ayant à la fois un grand espace de travail en translation et un grand espace de travail en orientation en utilisant des boucles de câbles.

Ce manuscrit est composé de cinq chapitres. Le premier chapitre présente des robots parallèles à câbles existants, l'état de l'art des manipulateurs hybrides, les concepts fondamentaux ainsi que les contributions de ce manuscrit.

Le deuxième chapitre traite de l'étude, de l'analyse et de la conception d'un manipulateur parallèle à câbles planaire composé d'une paire de câbles et dédié à des opérations de manutention dans de grands espaces. L'objectif principal est l'étude d'une approche innovante pour la construction de RPC hybrides par le biais de boucles de câbles. La modélisation, l'analyse et la conception optimale du RPC hybride proposé sont présentées dans le chapitre.

Un RPC muni d'un poignet à deux degrés de liberté est étudié dans le troisième chapitre. Le manipulateur combine les avantages des RPC, c'est-à-dire un grand espace de travail en translation, avec ceux des poignets, à savoir des amplitudes de rotation importantes autour de deux axes. L'effecteur comprend également huit degrés de liberté (ddl) contrôlables.

Le quatrième chapitre présente les travaux de recherche sur un RPC ayant un

poignet sphérique d'architecure parallèle à trois degrés de liberté intégré et un espace de travail en orientation considérablement augmenté. La plate-forme mobile sous-actionnée possède neuf degrés de liberté.

Finalement les conclusions et les perspectives pour les travaux futurs sont présentées dans le cinquième chapitre. Les recherches menées dans le cadre de cette thèse proposent des solutions inédites pour les RPC à grands espaces de travail en translation et d'orientation.

Mots clés: robot parallèle à câbles, robots hybrides, espace de travail, boucles de câbles, conception, poignet à deux degrés de liberté, poignet sphérique

Abstract

Cable-Driven Parallel Robots (CDPRs) also noted as wire-driven robots are parallel manipulators with flexible cables instead of rigid links. A CDPR consists of a base frame, a moving-platform and a set of cables connecting in parallel the moving-platform to the base frame. CDPRs are well-known for their advantageous performance over classical parallel robots in terms of large translational workspace, reconfigurability, large payload capacity and high dynamic performance. They have drawn interests towards industry thanks to their fundamental advantages and capabilities. However, most of the CDPRs provide only limited amplitudes of rotation of the moving-platform due to collisions between the cables and the moving parts.

Novel concepts towards the potential of CDPRs with drastically large orientation workspace have been introduced in literature. One of those concepts suggests using a bi-actuated cable circuit for remote actuation of a parallel mechanism embedded in the moving-platform of CDPRs, forming hybrid manipulators. Those manipulators are hybrid because they combine advantages of large translational workspace of CDPRs and large rotational amplitudes of active wrists. Even though it is a promising concept for augmentation of orientation workspace of CDPRs, to the best of author's knowledge, it has not been realized. Bi-actuated cable circuits, namely, cable-loops are the essence of the hybrid CDPRs with augmented orientation workspace, since they transmit power directly from motors fixed on the ground to the moving-platform. Consequently, the actuators do not have to be mounted on the moving-platform, which leads to lower inertia of the moving parts of the manipulators. The main objective of this doctoral thesis is to design, analyze and prototype hybrid CDPRs to enlarge the orientation workspace in addition to their large translational workspace by exploiting cable-loops.

This manuscript is composed of five chapters. The first chapter introduces CDPRs, the state of the art related to hybrid manipulators, the fundamental concepts and contribution of the manuscript.

The second chapter deals with the study, analysis and design of a planar cable-driven parallel crane as the fundamental step for construction of hybrid CDPRs with large translation and orientation workspaces. The primary objective is the investigation of an innovative approach for construction of hybrid CDPRs through cable-loops. Modeling, analysis and optimum design of the proposed hybrid CDPR are presented in this chapter.

A CDPR with an embedded tilt-roll wrist is studied in the third chapter. The manipulator combines the advantages of CDPRs, i.e., a large translational workspace, with those of tilt-roll wrists, namely, drastically large amplitudes of rotations about two axes. It also has eight controllable Degree of Freedom (DoF).

The fourth chapter introduces the research work on a CDPR with an embedded parallel spherical wrist with a substantially augmented orientation workspace,

i.e., more than fifty turns of rotation about three axes. The under-actuated moving-platform possesses nine-DoF.

Finally, the conclusions and perspectives are presented in the fifth chapter. The research that had been conducted in the context of this thesis proposes novel solutions for CDPRs with large translational and orientation workspaces.

Keywords: Cable-Driven Parallel Robots, Hybrid Robots, Workspace, Cable loops, Design, Tilt-roll wrist, Parallel spherical wrist

Acknowledgements

I would like to thank my thesis director, Stéphane Caro for offering me the opportunity of this doctorate position and moreover for his guidance during my PhD journey despite his busy schedule. I am greatly thankful to my supervisor, Philippe Cardou for his wonderful insight and clever propositions whenever I needed him. Moreover, I thank Philippe for his continuous encouragement and patience throughout this journey. Stéphane Jolivet, the mechanic of the laboratory helped me with prototyping and manufacturing of my thesis. I am really grateful for his substantial help and being always nice and amusing despite of my design mistakes. I have had the honor to work on my experimentations with Philippe Lemoine whom I admire for his engineering knowledge and personality. I am deeply thankful to talented and friendly master students, Marceau Métillon and Gaspard Bourgeois who enormously helped me out with my PhD thesis. Furthermore, I would like to extend my appreciation to my colleagues and staff of LS2n, namely, Sana Baklouti, Sébastien Rouquet, Rafael Balderas Philippe Perlot, Arnaud Hamon for their technical support and help.

My parents have always encouraged me for pursuing my goals and despite all the difficulties they have never stopped supporting me. I am eternally grateful to them, my two sisters Sarahs and my brother Sina for their endless love and support.

I am glad that I have befriended so many nice persons who made this journey easier for me by sharing so many happy moments with me. I am so grateful to my friends Abhilash, Caroline, Arushi, Rafael, Khaoula, David, Abdulah, Victor, Emmanuel, Antoine, Marlène, Beatriz, Stephanie, Elaheh, Mehrazin, Armel, Tahir, Swaminath, Ghita, Konstantin, Ginevra, Aleksandrea, Alessandra, Franco, Hajar, Kenza, Borzoo, Susana, Misbah, Simone, Avgi, Frank, Gabriel, Vignesh, Julia, Manon, Sébastien and Maxim.

Contents

List of Figures

List of Tables

Acronyms and Abbreviations

CDPR	**C**able-**D**riven **P**arallel **R**obot
WFW	**W**rench-**F**easible **W**orkspace
TFW	**T**wist-**F**easible **W**orkspace
SW	**S**tatic **W**orkspace
DoF	**D**egree-**o**f-**F**reedom
CoM	**C**enter of **M**ass
RCVS	**R**equired **C**able **V**elocity **S**et
ACVS	**A**vailable **C**able **V**elocity **S**et
RTS	**R**equired **T**wist **S**et
ATS	**A**vailable **T**wist **S**et
PSW	**P**arallel **S**pherical **W**rist
TRW	**T**ilt-**R**oll **W**rist
CDPC	**C**able-**D**riven **P**arallel **C**rane
CDPR\TRW	**C**able-**D**riven **P**arallel **R**obot with an **E**mbedded **T**ilt-**R**oll **W**rist
CDPR\PSW	**C**able-**D**riven **P**arallel **R**obot with an **E**mbedded **P**arallel **S**pherical **W**rist
CREATOR	robot parallèle à **C**âbles ayant un g**R**and **E**space de tr**A**vail en **T**ranslation et en **OR**ientation)
HSM	**H**yperplane **S**hifting **M**ethod
CMI	**C**apacity **M**argin **I**ndex

Chapter 1

Introduction

Contents

Parallel robots are closed-loop mechanisms with high performance in terms of accuracy, rigidity and payload capabilities. They have been used in a large variety of applications, like, astronomy and flight simulators. They have drawn many interests towards the machine-tool industry [Mer06]. Parallel architectures were originally proposed in the context of tire-testing machines and flight simulators [Gou57], [Ste65]. Since then, they have been used in other applications requiring manipulation of heavy loads with high accelerations such as vehicle driving simulators or a riding simulator developed for the french national riding School [KD04].

Parallel manipulators share the payload on theirs limbs leading to a high payload capacity. Moreover, due to the traction-compression in the joints of parallel robots, a better positioning precision is obtained by parallel manipulator compared to serial manipulators. Parallel manipulators have attracted the attention of the researchers and manufacturers due to their outperforming characteristics in terms of stiffness, precision, dynamic performance, compared to serial robots. Parallel robots include variety of industrial applications, such as flight simulation, machining and medical robotics.
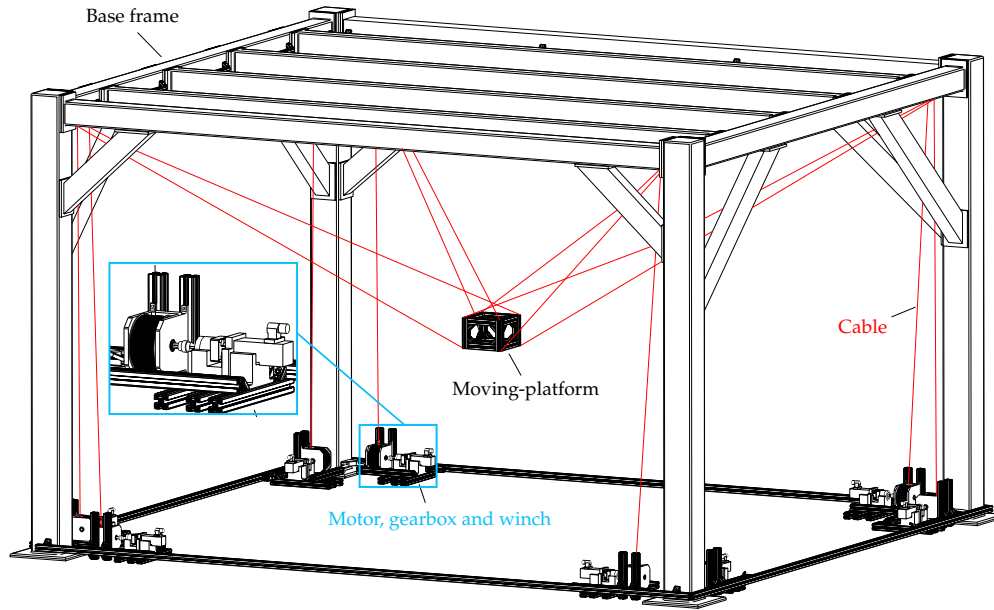
Figure 1.1: Architecture of the cable-driven parallel robot, developed in the framework of the CREATOR project, LS2N, Nantes, France

1.1   Cable-Driven Parallel Robots (CDPRs)

Cable-Driven Parallel Robots (CDPRs) also noted as wire-driven robots are parallel manipulators with flexible cables instead of rigid links. A CDPR consists in a base frame, a moving-Platform and a set of cables connecting in parallel the moving-platform to the base frame. The pose of the moving-platform is determined based on the geometry of the exit-points as well as the anchor-points. The former is the connection between a cable and a point on the fixed frame and the latter is the connection point between a cable and the moving-platform. Active cable lengths, i.e., the distance between exit and anchor points are adjusted by coiling the cables on motorized winches. A schematic of the architecture of CDPRs is presented in Fig. 1.1. CDPRs are well-known for their advantages over the classical parallel robots in terms of large workspace, reconfigurability, large payload capacity and high dynamic performance. Nevertheless, one of the main shortcomings of the CDPRs is their limited orientation workspace. The latter drawback is mainly due to cable interferences and collisions between cables and their surrounding environment.

The interest of researchers has been drawn toward CDPRs because of their novelty and open issues originated from the nature of cables. Despite of classical parallel robots, CDPRs consist in uni-directional force transmission limbs.

In spite of all the mentioned advantages of CDPRs, we can note the common drawbacks and challenges that should be dealt with. One of the main drawbacks of the CDPRs arises from the actuation of cables. Cables can only pull but not to push, as a result, the control of the robot is more complicated than the conventional parallel robots. Another challenge can be considered as lower stiffness due to nature of cables resulting to the instability and vibration of the moving-platform. The main characteristics of CDPRs are pointed in Table 1.1.

Table 1.1: Merits and demerits of Cable-Driven Parallel Robots (CDPRs)

Merits	Demerits
• Large translational Workspace	• Limited orientation workspace
• Inexpensive	• Repercussions due to cable ruptures
• Low inertia of the moving platform	• Cable interferences
• Reconfigurability and transportability	• Cable elongation and deformation
• Remote actuation of the moving-platform	• Poor accuracy
• Energy efficiency	
• High payload-to-weight ratio	

1.2 Applications

Due to the distinct merits of the CDPRs, they are used in variety of tasks from industrial to entertainment applications. NIST RoboCrane is one of the earliest CDPRs designed based on the idea of the Stewart platform. NIST RoboCrane is a suspended crane by six cables capable of performing tasks within its large workspace with six (Degree of Freedom) DoFs. Its example applications are mentioned as flexible-structure mobility, heavy structure and equipment handling [Bos+94; BJB99].

One distinct characteristic of CDPRs was demonstrated by FAST (Five-Hundred Meter Aperture Spherical Radio Telescope) where its moving-platform contains the receiver cabin of a large reflector dish as shown in Fig. 1.2. FAST is a large-scale CDPR with a suspended moving-platform while encountering two main challenges in terms of inverse kinematics and the stiffness due to sag in the cables [Dua99; KZW06; Dua+09; WR15].

Skycam is one of the most popular CDPRs used in sport broadcasting. Skycam was patented in 2005 as a three dimensional moving camera assembly with an informational cover housing. This CDPR consists of a cable driven trolley and a camera platform similar to Stewart platform and suspended by four cables. One instance of the application of skycam is presented in Fig. 1.3.

CDPRs have also engaged in entertainment and art. Thrill ride CDPR, i.e, an amusement park ride with cable-suspended vehicle is a patented concept shown in Fig. 1.4 by Disney [Pot18; CN12]. Two CDPRs each suspended by eight cables were simultaneously flying over head of visitors for entertainment and artistic purposes at EXPO 2015 in Milan as shown in Fig. 1.5. The safety, robustness and technical feasibility of the robots were demonstrated by showing its performance in front of audience for about 40 times a day within few months, [Tem+15].

Figure 1.2: FAST spherical radio telescope [Dua99; KZW06; Dua+09; WR15]

Figure 1.3: Skycam camera system at NRG Stadium in Texas [Skya; Skyb]
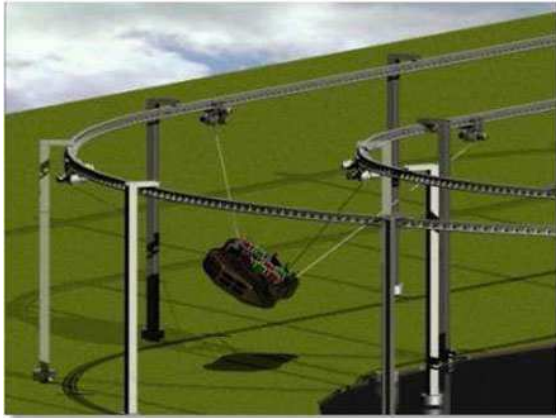
Figure 1.4: Amusement park ride with cable-suspended vehicle, [Pot18; CN12]

Figure 1.5: CDPRs flying over the heads of the visitors at the EXPO 2015, [Tem+15]

Several interesting CDPR prototypes and demonstrations employed in the medical and rehabilitation field. A Light-weight exoskeleton, namely, CAREX was proposed by Ying Mao et al. as shown in Fig. 1.6. This prototype is a rehabilitation and human movement training CDPR designed for upper arm movement training [Mao+14]. String-Man prototype is presented in [SB04]. The prototype is an advanced gait rehabilitation robot aiming at weight bearing, balancing and posture control in 6-DoFs as shown in Fig. 1.7. Another application of CDPRs in the field of medical science and specialized in surgical robotics is demonstrated in Fig. 1.8. The Raven-II system with a grasper which has 4 DoF (wrist roll, wrist yaw, and finger pitch times two fingers) actuated by cables.

Intralogistics, handling and sorting of goods at industrial level, are suitable application for CDPRs due to their advantages in terms of high payload capacity, large workspace and high dynamic performance. The prototype of FALCON-7 is the earliest CDPR with high-speed pick-and-place ability illustrated in Fig. 1.9. The moving-platform of FALCON-7 (FAst Load Conveyance robot with 7 wires) obtains ultra-high speed and more than 40 times of the gravitational acceleration with commercial actuators [Li94; KKW00b; KK15]. A lightweight and fast CDPR, namely, CABLAR prototype shown in Fig. 1.10, was developed for storage retrieval and
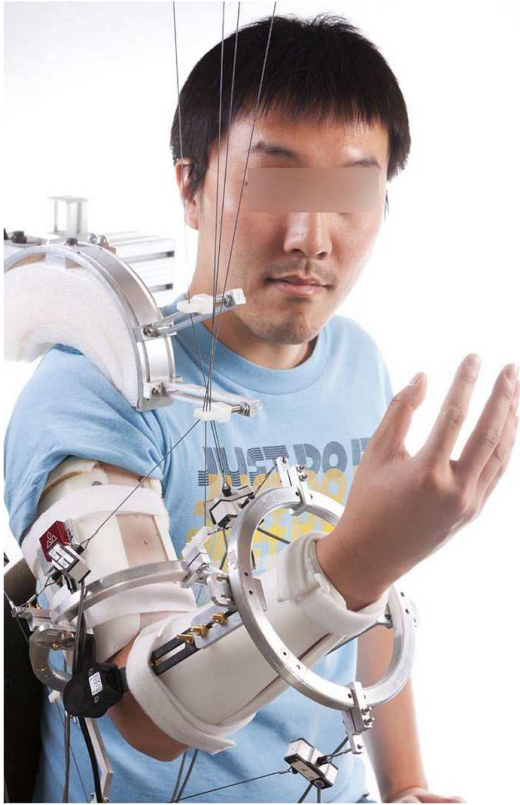
Figure 1.6: Cables routed through the cuffs and controlled in tension in CAR-TEX CDPR for arm training and rehabilitation purposes [Mao+14]
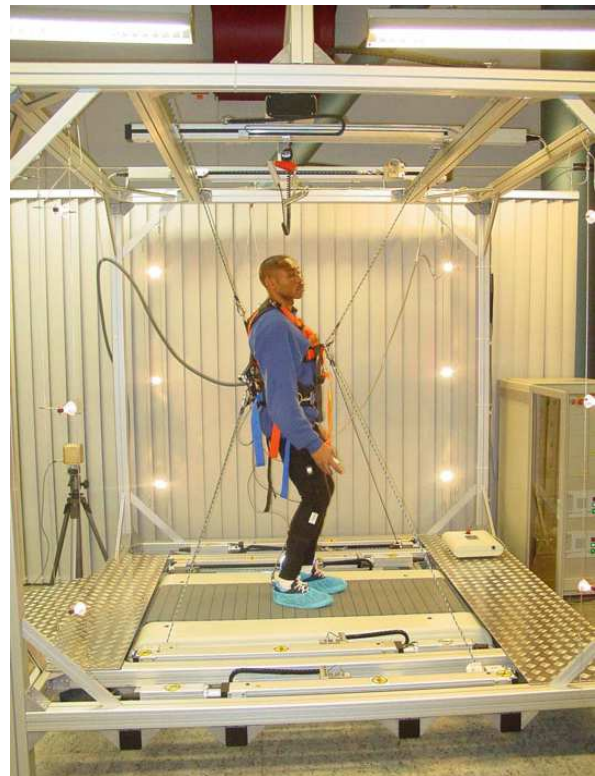
Figure 1.7: String-Man CDPR for gait rehabilitation and posture control [SB04; Pot18]

logistic by Bruckmann et al. in [Bru+13b; Bru+13a; LBS13]. Moreover, a mobile CDPR, named FASTKIT, with multiple mobile bases for logistics was introduced in [Ras+18; Ped+19] as shown in Fig. 1.11. The prototype was developed to be a faster and more versatile alternative solution for industrial logistics.

CDPRs have also been employed as measurements and calibration systems. In [Jeo+98; JKK99] a CDPR was introduced for measuring the pose of a robot end-effector. The position and orientation of the robot are computed through solving forward kinematic equations for the cable lengths of the CDPR. Similarly, IPAnema 2 (shown in Fig.1.12) estimates the pose of the end-effector of an industrial robot based on the measured cable lengths through optical absolute encoders [Pot+13]. Furthermore, Pott in [Pot10] developed an algorithm for real-time forward kinematics of CDPRs, which was employed for IPAnema 2.

A modular hybrid CDPR consists of standalone modules, an end-effector and a rover with a robotic manipulator. This architecture enables the manipulator for performing inspection and space exploration on celestial bodies as studied in [SGW16]. One application of the proposed manipulator is illustrated in Fig. 1.13. Moreover, comprehensive introduction to the history and development of CDPRs and their latest applications are presented in the literature, e.g., [Qia+18; Pot18].
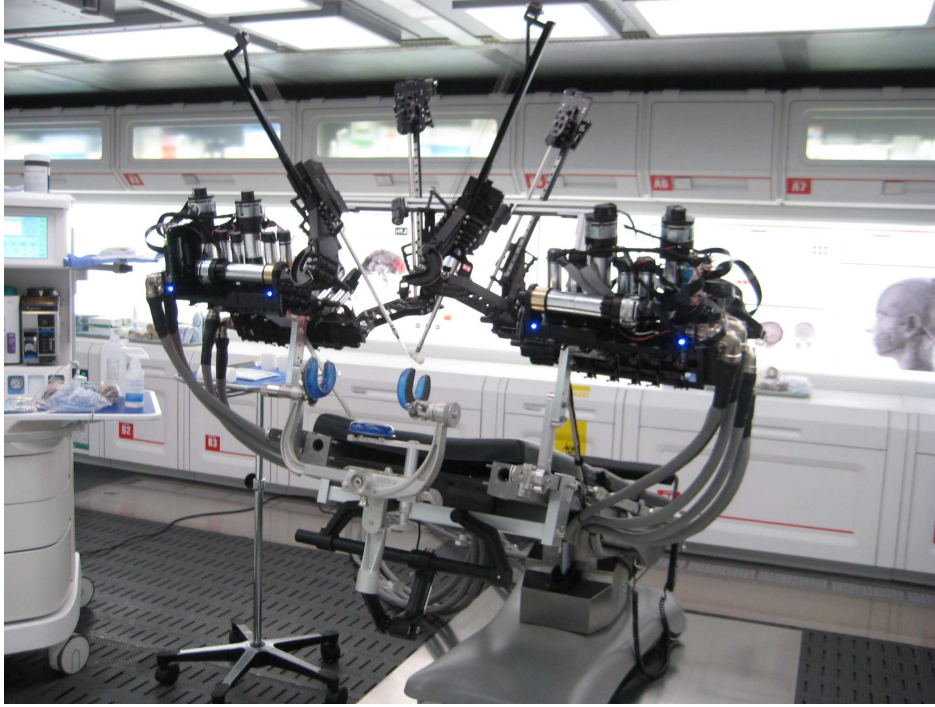
Figure 1.8: The Raven II robot of UW EE's BioRobotics is an open-source platform for surgical robotics research [Han+12; Lab]
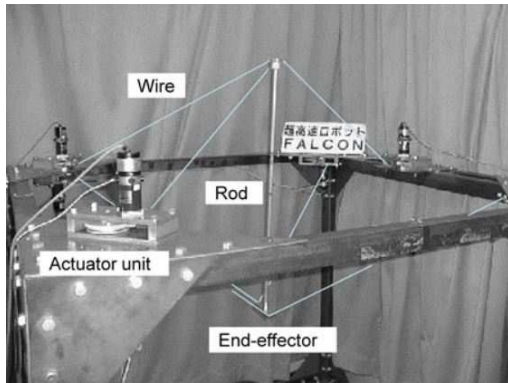
Figure 1.9: High-speed pick-and-place FALCON prototype [Li94; KKW00b; KK15]

Figure 1.10: CABLAR CDPR as a large-scale storage retrieval machine [Bru+13b; Bru+13a; LBS13]

1.3 Classification

CDPRs can be categorized into different groups based on their geometry, DoF, function, actuation, motion pattern and etc. In the following some CDPRs are classified based on their geometry.

A CDPR is kinematically categorized into under-constrained, fully-constrained and over-constrained in [Pot18; Min94]. By assuming number of cables denoted by m and the number of the DoF of the moving-platform as n, we proceed to distinguish CDPRs as follow:

In *Under-constrained* CDPRs, the number of cables is less than DoF of the moving-platform $m < n$ for instance, SpiderBot [CSS11], CaTraSys II [TOC06]. Therefore
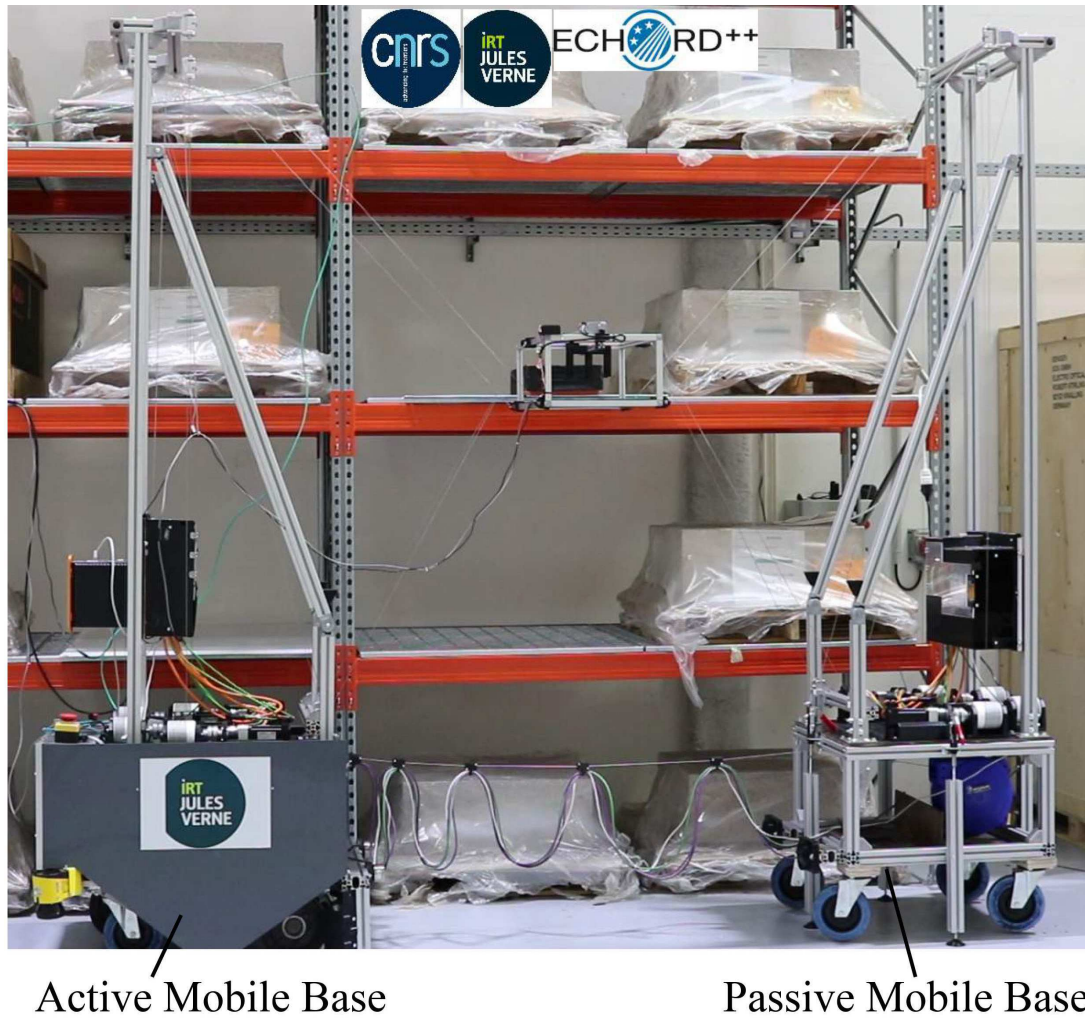
Figure 1.11: A mobile cable-driven parallel robot for logistics [Ped+19]

some DoFs cannot be controlled by the cables and the moving-platform can go through stable or unstable equilibrium state in presence of applied wrench.

Fully-constrained CDPRs have controllable *n*-DoF of the moving- platform and the force equilibrium is dependent on the external wrench applied onto the moving-platform. Since this group of CDPRs are dependent on the external wrench, they can be classified as *Incompletely Restrained Positioning Mechanism* (IRPM) according to Ming et al. in [Min94]. In fully-constrained CDPRs like DeltaBot [Beh+03], NeReBot [Ros+05], number of cable is equal to the number of Dof, i.e., $n = m$.

The moving-platform of a CDPR manipulator is denoted as *over-constrained* while $m > n$. In this family of CDPRs they are called Completely/Over Redundantly Restrained Positioning Mechanisms (CRPM/RRPM). They are not kinematically redundant since they have one solution to their inverse geometric problem but redundant in actuation, e.g. CaTraSys [OCP10] and Cogiro [LG13]. Therefore, generally, there exist more than one solution to their static equilibrium and the domain of the solutions depends on the admissible cable tensions. A CDPR depending on its moving-platform pose and applied external wrench may undergo slack cable(s).

Furthermore, CDPRs can be classified based on their cable arrangement. A *suspended* configuration refers to a CDPR whose all exit-points are fixed above its

Figure 1.12: IPAnema 2 measurement device: Cable sensor based 6-DoF pose measurement system applied to measure the pose of an industrial robot, [Pot+13]
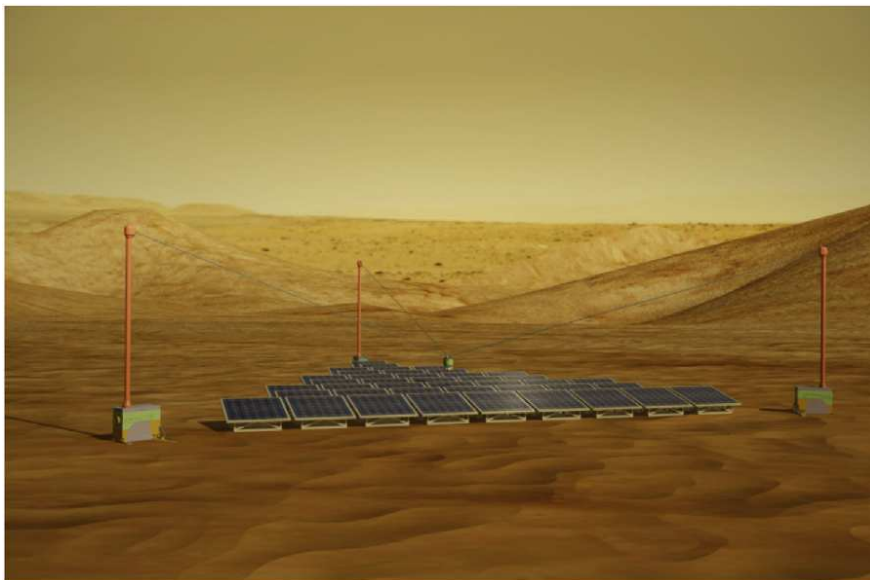
Figure 1.13: A modular CDPR for the maintenance of a large solar array, [SGW16]

moving-platform, e.g, Skycam [Con85]. In this configuration, the gravity force exerted on the moving-platform can be assumed as a virtual cable with a constant tension along the gravity direction and the static equilibrium is dependent on the mass of the moving-platform. Suspended CDPRs have advantages over non-suspended ones in terms of interference of cables with objects and their environment. Moreover, the suspended CDPRs over-perform non-suspended ones regarding maximum admissible payload. On the other hand, in non-suspended configurations, the moving-platform obtains a better stiffness and dynamic performance and as a consequence, less instability and vibration of the moving-platform.

1.4 CDPRs with Large Translation Workspaces

CDPRs are well-known for their large translation workspace thanks to the flexible nature of cables. Few CDPRs with drastically large translation workspace are enumerated in the previous section, e.g., FAST with a suspended moving-platform over 520 meter diameter telescope aperture and Skycam with a suspended camera and a stadium-sized translation workspace.

Geometry selection and cable arrangement are crucial parameters involved in the workspace size of CDPRs. M. Gouttefarde et al. in [Gou+15b] developed a new suspended CDPR geometry with large workspace to footprint ratio. The study is carried out in the context of CoGiRo project with the demonstrator shown in Fig. 1.14. CableRobot is a large scale motion simulator with a workspace size of 100 cubic meter introduced in [Mie+16]. The CableRobot simulator developed at the Max Planck institute is one of the first CDPRs capable of human transport and motion simulation as shown in Fig. 1.15

Figure 1.14: Prototype of the CDPR with large translation worksapce in the context of the CoGiRo project, [Gou+15b]

Figure 1.15: The CableRobot motion simulator with a large translation workspace, [Mie+16]

Reconfigurability, one of the main features of CDPRs, can be used to extend their workspace. In [Gag+16b], the authors studied the importance of the geometry determination of the CDPRs with respect to the sizes of their workspaces. These authors proposed a methodology for the planning reconfiguration of CDPRs from a discrete set of possible exit-points unlike conventional CDPRs. Figure 1.16 demonstrates the concept of a reconfigurable CDPR.
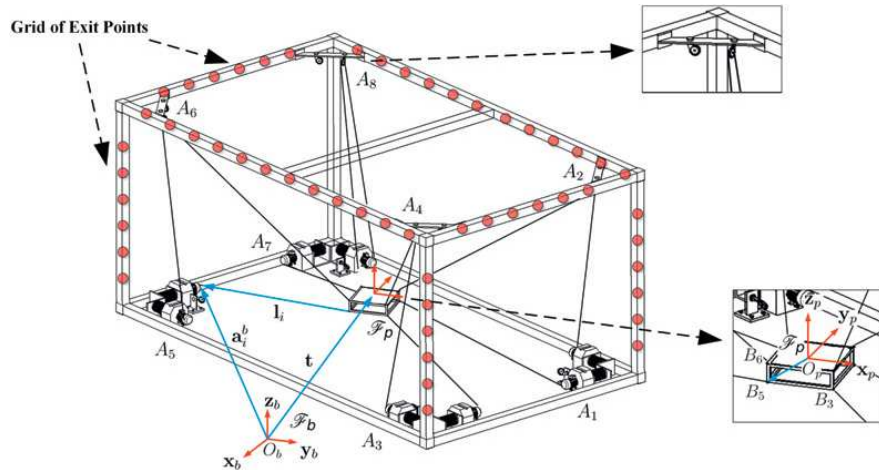
Figure 1.16: Schematic of the concept of a reconfigurable CDPR in [Gag+16b]

1.5   CDPRs with Large Orientation Workspaces

There are varieties of tasks and applications requiring CDPRs with large orientation workspace, e.g., camera surveillance, inspection, 3D object scanning, entertainment. Despite their large translation workspaces, CDPRs are generally unable to provide large amplitudes of rotation of their moving-platform due to collisions between their moving parts. For instance, the large cable-suspended parallel robot of the project CoGiRo in [Gou+15b], can only provide a limitted range of orientation, i.e., $\pm40°$ about its horizontal axes and $105°$ $(-70° \, to + 35°)$ about its vertical axis. In general, the workspace of parallel robots can be increased by combining them with other parallel or serial mechanisms and constructing hybrid mechanisms. To the best of the authors' knowledge, there is but a limited number of research-works addressing the question of extending the rotation workspaces of CDPRs. In [Pla+18], a parallel spherical wrist was introduced into the design of a CDPR to obtain large rotation and translation workspaces. The authors showed that the workspace of CDPRs can be enlarged by combining the advantages of the parallel spherical wrist in terms of rotation amplitudes with those of CDPRs in terms of large translation workspace. Miermeister et al. in [MP15; Rei+19] introduced a new hybrid design for CDPRs with coupled platforms while enabling them for an endless rotatable axis. In Fig. 1.17a a moving-platform with thirteen as the minimal number of required cables for a spatial CDPR with the geometry of a crankshaft, is proposed to achieve an endless rotatable axis. Furthermore, a planar manipulator with eight cables was presented with an unlimited orientation DoF as depicted in Fig. 1.17b. Moreover, a cable structure for haptic interface and cable robots with large orientation workspace were patented by Gosselin in [Gos07]. The mechanism is claimed to provide at least one large rotational DoF.

(a) A spatial CDPR with a crankshaft geometry   **(b)** A planar CDPR with two platforms
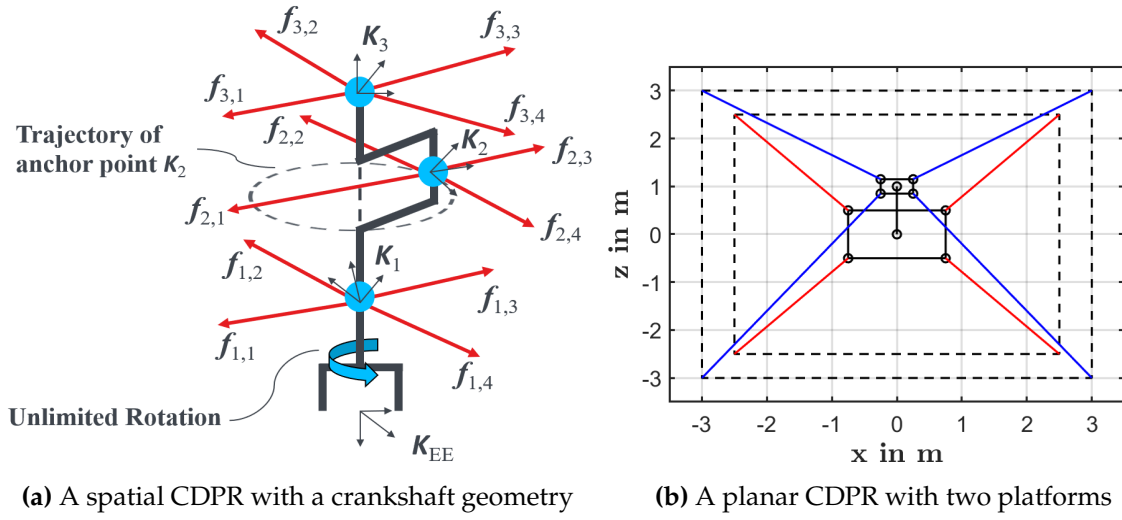
Figure 1.17: Concepts of CDPRs each with an unlimited rotatable axis [MP15; Rei+19]

1.6 Hybrid CDPRs

Serial manipulators exhibit characteristics that are often opposite to those of parallel manipulators. Serial robots have a large workspace while that of parallel manipulators is usually smaller and more complex. In general, the payload, speed, acceleration, stiffness and accuracy of serial robots are lower than those of parallel robots [PD14]. The combination of a parallel and a serial manipulator or at least two parallel manipulators forms a hybrid manipulator. The goal is generally to exploit the advantages of their parallel and serial kinematic chains to improve their overall performance in given tasks. They are generally designed to extend the workspaces of parallel robots.

Macro-micro manipulators are made up of a large (macro) robot carrying a small (micro) robot with high performance in order to improve the functionality of the overall manipulator [SHH93]. Macro-micro manipulators are often known as hybrid robots. A micro manipulator is called active wrist on condition that its orientation DoFs replace those of the macro robot [Mer06]. This architecture enhances the overall manipulator workspace size while imposing mass and size constraints on the manipulator.

Similar to hybrid parallel robots, the combination of CDPRs with serial and parallel mechanisms form hybrid CDPRs. In [BG15], a large-scale cable-suspended 3D foam printer was introduced. The proposed manipulator is an hybrid robot, i.e., a serial end-effector (foam gun mechanism with one-DoF) connected to the moving-platform of the CDPR as shown in Fig. 1.18. This hybrid CDPR employs motorization on the moving-platform and as a consequence on-board motor requires cable routing, which increases the chance of interferences with the CDPR cables. CAT4 is a hybrid cable actuated truss with 4-DoF presented in [KN02]. This hybrid manipulator, namely, a combination of two parallel kinematic chains, consists in a central mechanism while its end-effector is constrained to three translational and one rotational motions as depicted in Fig. 1.19. In [Che+13], the authors presented a hybrid

(parallel-serial kinematic structure) CDPR as a 7-DoF humanoid arm. Figure 1.20 illustrates the hybrid robot with a passive spherical wrist.
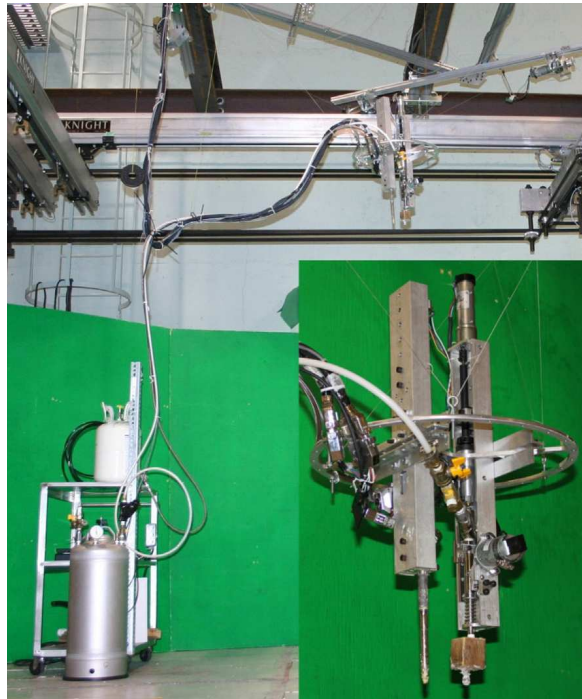
Figure 1.18: Hybrid cable suspended 3D foam printer, [BG15]

The synthesis of CDPRs with complementary mechanisms to design hybrid CD-PRs can be realized through bi-actuated cables, i.e, cable-loops. One advantage of cable-driven parallel robots that has not yet been fully exploited is the possibility of using the cables to transmit power directly from motor fixed to the frame to the moving-platform. This power can then be used to actuate a tool or to control additional degrees of freedom such as rotations over wide ranges [Pla+18], for example. There has been a few research conducted on the modeling of cable-loops. In [Nag+12], a cable-loop is denoted as a Double Actuator Module (DAM). Moreover, cable-loops were developed and studied in context of different types of manipulators. Antagonistic cable pairs accompanied with multi-radius pulleys are presented in [RSBT17] to consolidate the actuation of multiple links of a snake robot. Nagai K. et al. in [Nag+11] proposed a cable-loop-powered mechanism for producing motions with high acceleration of the moving-platform in the global frame by the total force of cable-loop exerted on the moving platform. Besides, it leads to precise motion of the end-effector in its local frame by induced moment of cable-loops. A hybrid CDPR employing cable-loops is presented in [LDN16]. The proposed concept of the hybrid robot by employing seven cable-loops (and fourteen actuators) for producing fast and precise motions is shown in Fig 1.21.

A cable-loop forms a cable circuit by connecting two actuators while passing through two anchor points on the moving-platform and coiling about a drum as shown in Fig. 1.21. This arrangement of cables is used for two distinct purposes. The former is to locate the moving-platform within its workspace and the latter is to actuate the drum. In other words, two motions can be induced by the cable-loop depending on the relative rotation of its two actuators. The first one is the
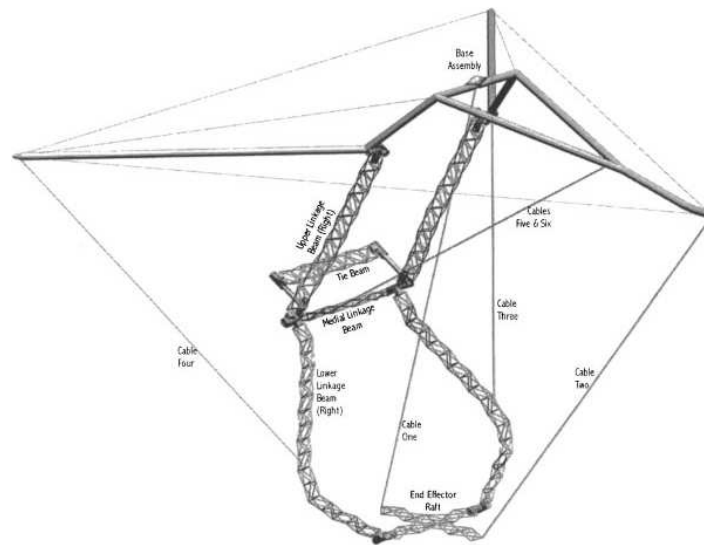
Figure 1.19: CAT4, 4-DOF cable actuated parallel manipulator, [KN02]
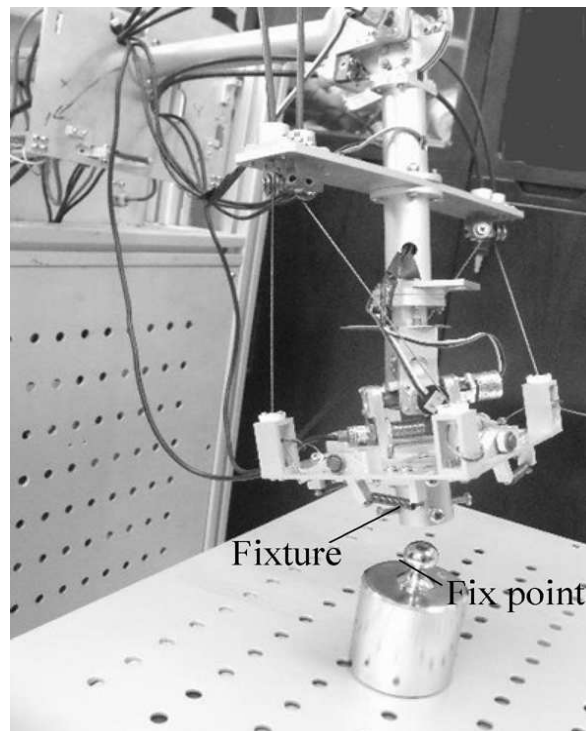
Figure 1.20: Cable-driven humanoid arm, [Che+13]

displacement of the moving-platform and extension of the loop for identical inputs of the two motors. The second motion is circulation of the loop which results into rotation of the drum, when the two actuators rotate in opposite directions. This convention leads to a very large amplitude of rotation of the drum. The cable-loop system provides a vast orientation of its drum, which can be employed whether for enlarging the orientation workspace or for actuating an embedded mechanism on the body of the moving-platform.
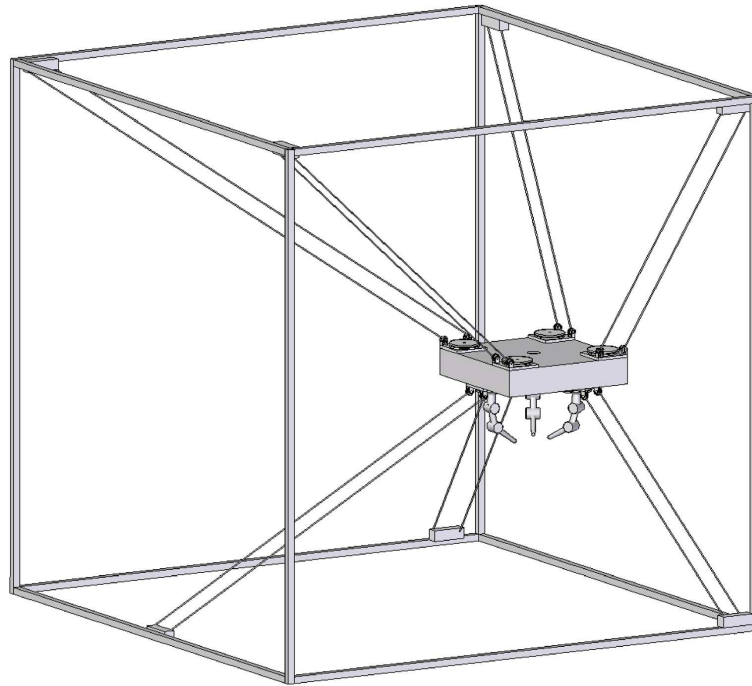
Figure 1.21: Concept of a hybrid CDPR with remote actuation of the end-effector, [LDN16]

Khakpour et al. ([KB14], [KBT14] and [KBT15]) introduced differentially driven cable parallel robots using cable differentials. This idea focuses on replacing actuated cables with two or more cables while connected to one actuator through a differential mechanism. They proved that, by replacing single-actuated cables with differential cables the static and wrench feasible workspaces of CDPRs can be extended while keeping the same number of actuators. The schematic of the proposed deferentially driven planar CDPR is presented in Fig.1.22. Similarly, many tendon-driven robotic hands with hybrid structure have employed differential mechanisms for power transmission. The authors in [BG04; BG06] address kinetostatic and force analysis of tendon-driven mechanisms. In [OHK09], Ozawa et al. enumerate different types of tendon-driven mechanisms, namely Tendon-Controllable mechanisms (TC) capable of generating any joint torque, under-actuated Hybrid Tendon-driven mechanisms (HT) with unique solutions to their associated inverse kinematic problems and finally Under-Tendon driven mechanisms (UT) are the under-actuated systems with multiple solutions for their inverse kinematic problems as shown in Fig. 1.23
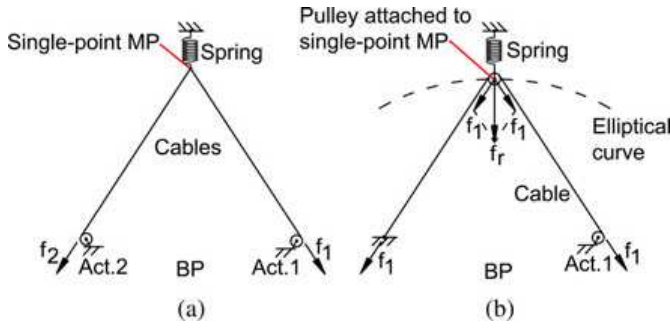
Figure 1.22: A planar CDPR with a point mass moving-platform with (a) two single-actuated cables (b) a differentially driven cable, [KBT14]
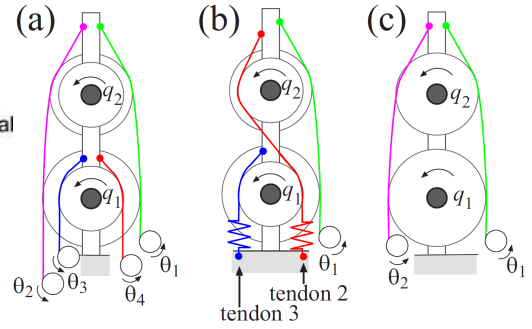
Figure 1.23: Tendon-driven mechanism types, (a) TC (b) HT (c) UT, [OHK09]

1.7 CREATOR Project

The CREATOR (robot parallèle à Câbles ayant un gRand Espace de trAvail en Translation et en ORientation) project aimed to design a hybrid robot with a large workspace in translation and orientation. The CREATOR project, funded by Atlanstic 2020 programme (link [1]), started in 2016 and ended in 2020. The task coordination of the project in illustrated in Fig. 1.24.

The robot is hybrid because it combines advantages of a CDPR in terms of a large translation workspace and pros of spherical wrists with large rotational amplitudes to form CDPRs with large translation and orientation workspaces.

1.8 Contribution and Thesis Organization

Generally, CDPRs have large translation workspace, however, most of them provide only limited rotations of the moving-platform due to the collision between the cables. The objective of this research-work is to design hybrid robots with both large translation and orientation workspaces. Those robots are hybrid because they combine the advantages of cable-driven parallel robots in terms of large translation workspace and the pros of the parallel spherical wrists in terms of large rotational amplitudes. The main contributions of the thesis are highlighted in the following.

1.8.1 A Planar Hybrid Cable-Driven Parallel Crane

This manuscript introduces the concept of a new planar Cable-Driven Parallel Crane (CDPC) for lifting and carrying payloads with a moving hoist mechanism connected in parallel to the ceiling. In the context of our research work. The main objective of this manipulator is to provide underlying foundation for realizing hybrid CDPRs using cable loops. Therefore, the simplest form of a hybrid robot, i.e., one-DoF articulated moving-platform, is considered for further investigation regarding hybrid CDPRs with large translation and orientation workspaces. In contrast to bridge-crane, CDPC is inexpensive and practicable for diverse tasks with simple assembly setup. The hoist mechanism is an under-constrained moving-platform articulated

---

[1] http://tiny.cc/9mjkjz
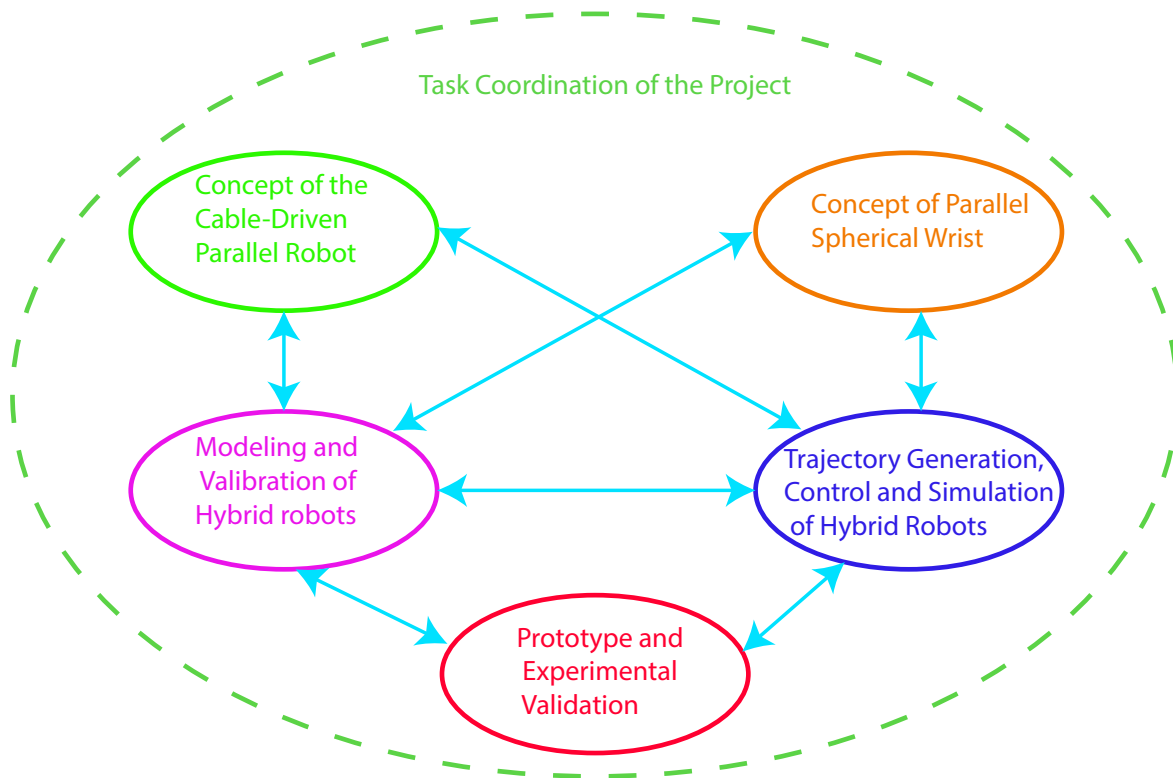
Figure 1.24: Task coordination of the CREATOR project

through a bi-actuated cable circuit, namely, a cable-loop. The hoist is connected to a suspended moving-platform with four DoF. The power is transmitted directly from the motors, mounted to the ground, to the hoist through the cable loop. There-fore, the dynamic performance of the robot is increased due to lower inertia of the moving-platform. However, the moving-platform undergoes some parasitic incli-nations because of the cable-loop for remote actuation of the moving-platform in the CDPC. In the second chapter, we investigate these unwanted rotational motions of the moving-platform. Parasitic inclination as a property of lower mobility parallel mechanisms leads to inaccuracy in positioning. Finally, those parasitic inclinations are modeled and assessed for the mechanism at hand.

This manuscript investigates the parasitic inclination and its effect on the sys-tem. The workspace of the proposed CDPC is studied in terms of static and kine-matic performances. Moreover, the kinetostatic model, optimum design, control and demonstration of the CDPC are presented in Chapter 2.

1.8.2   Hybrid CDPR with an Embedded Tilt-Roll Wrist

The development of a novel CDPR with an embedded tilt-roll wrist is addressed in the framework of the thesis. The manipulator consists of a tilt-roll wrist mounted on the moving-platform of a suspended CDPR. The embedded wrist provides large amplitudes of tilt and roll rotations and a large translational workspace obtained by the CDPR. This manipulator is suitable for tasks requiring large rotation and translation workspaces like tomography scanning, camera-orienting devices and vi-sual surveillance. The moving-platform is an eight-DoF articulated mechanism with

large translation and orientation workspaces and it is suspended from a fixed frame by six cables. The manipulator employs two bi-actuated cables, i.e., cable-loops to transmit the power from motors fixed on the ground to the tilt-roll wrist. Therefore, the manipulator achieves better dynamic performances due to a lower inertia of its moving-platform. Furthermore, the kinetostatic model, optimum design, configuration, prototyping, workspace analysis and control of the proposed CDPR with an embedded tilt-roll wrist are elaborated in Chapter 3.

1.8.3   Hybrid CDPR with an Embedded Parallel Spherical Wrist

The concept of a hybrid CDPR with an embedded parallel spherical wrist is studied and implemented in the context of the manuscript. This manipulator employs the similar kinematic architecture as the CDPR with an embedded tilt-roll wrist but with an additional DoF. The proposed manipulator has nine-DoF while its parallel spherical wrist provides three drastically large orientations DoF of its end-effector beside six DoF of the moving-platform. The hybrid manipulator employs three cable-loops for remote actuation of its active wrist. The kinetostatic model, static workspace, design and experimental demonstration of the proposed manipulator are detailed in Chapter 4.

1.8.4   Twist Feasible Workspace

Although several papers addressed the wrench capabilities of cable-driven parallel robots, few have tackled the dual question of their twist capabilities. In the context of this thesis, these twist capabilities are evaluated by means of the specific concept of twist feasibility, which was defined in [Gag+16b]. A CDPR posture is called twist-feasible if all the twists (point-velocity and angular-velocity combinations), within a given set, can be produced at the CDPR mobile-platform, within given actuator speed limits. Two problems are solved in this manuscript: (1) determining the set of required cable winding speeds at the CDPR winches being given a prescribed set of required mobile platform twists; and (2) determining the set of available twists at the CDPR mobile platform from the available cable winding speeds. Then, twist feasibility is investigated for the proposed hybrid CDPRs.

Chapter 2

Planar Cable-Driven Parallel Robot with an Embedded Crane

Contents

The motivation of this chapter is to analyze, build and prototype a simple hybrid manipulator with large translational and rotational workspace. The strategy followed for realizing hybrid CDPRs with large orientation workspaces is to combine manipulators with large orientation workspaces with CDPRs with large translational workspace. This chapter investigates an innovative approach for the construction of such hybrid robots. The basis of the manuscript i.e., CDPRs with large translation and orientation workspace is formed by studying and realizing one of the earliest type of hybrid CDPRs through remote actuation of the moving-platform through cable-loops. To the best of the author's knowledge, there have been a few research proposing the idea of the remote actuation for CDPRs without practical implementation. A cable-loop or bi-actuated cable circuit is detailed in the context of this chapter.

In order to design the simplest form of a hybrid CDPR compatible with one cable-loop, we introduce the concept of a new planar Cable-Driven Parallel Crane (CDPC) with an embedded hoist mechanism within the moving-platform of the

CDPR. The proposed hoist mechanism is embedded into the CDPR and has one DoF. Figure 2.1 shows the prototype of the proposed manipulator consisting of a moving-platform with an embedded hoist mechanism, two cables (shown in red) which connect the moving-platform to the actuators and a third cable (shown in yellow) which connects the hoist to a payload and adjusts its height. The target applications of the proposed hybrid robot is lifting and carrying payloads indoors with a moving hoist mechanism connected in parallel to the ceiling. The proposed concept of the CDPC does not require its moving-platform to approach the payload. This design improves the CDPR capabilities for carrying payloads while reducing interferences between cables and objects on the ground. The concept of embedding the hoist into the moving-platform is sensible as long as the hoist mechanism does not require actuation on the moving-platform. Actuators on the moving-platform lead to lower-level dynamic performance due to the higher inertia and interference between motor wires and cables of the CDPR. The issue is overcome by employing a cable loop in order to articulate the moving-platform remotely.

Nowadays, overhead cranes or bridge-cranes are widely used in industry. They usually consist in runways fixed to a ceiling which accommodates a hoist mechanism for lifting or lowering payloads throughout its workspace. They are applicable for heavy-payload tasks. However, the bridge-cranes have some drawbacks that reduce their utilization, i.e., they are bulky, expensive and should adapt to the structure of the buildings. In contrast to bridge-crane, the CDPC is inexpensive and practicable for diverse tasks with simple assembly setup. On the other hand, CDPRs may seem sound alternatives for bridge cranes as they can overcome the above-mentioned issues. A CDPR consists of a base frame, a moving-platform and a set of cables connecting in parallel the moving-platform to the base frame. CD-PRs have some advantages over bridge cranes. Indeed, they are easy to reconfigure [Gag+16c], easy to assemble and comparatively inexpensive. Nevertheless, they suffer from cable interferences with the surrounding environment and requires a mounting structure. Therefore with these advantages and drawbacks in mind, we hypothesize that in same situations the capabilities of the bridge cranes can be extended by exploiting the advantageous features of CDPRs.

The hoist mechanism is an under-constrained moving-platform actuated through a bi-actuated cable circuit, namely, a cable loop. The hoist is connected to a suspended moving-platform with four degrees of freedom. The power is transmitted directly from the motors fixed on frames to the hoist through the cable loop. Therefore, the dynamic performance of the manipulator is increased due to lower inertia of the moving-platform.

Overall, this chapter is divided into six sections. Concept and design of the CDPC with an under-constrained mobile hoist, the cable-loop model, kinetostatic model and following the latter models the elasto-static of the manipulator are presented in Sec. 2.1. The analysis of the CDPC in terms of the workspace and parasitic inclinations is carried out in Section 2.2. Section 2.3 studies the optimum design of the manipulator. In addition, the validation of the proposed concept is realized in Sec. 2.4. Finally, conclusions are drawn and future work is presented in the last section of the chapter.
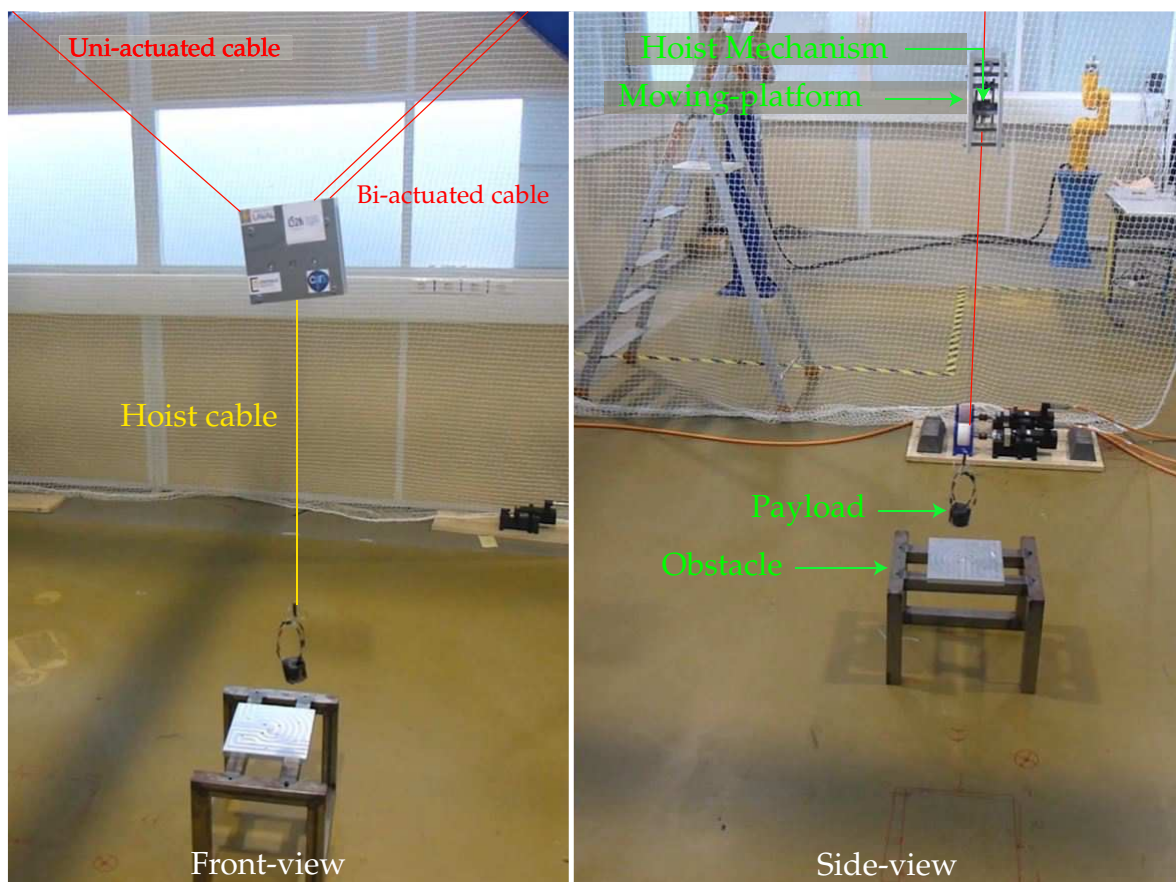
Figure 2.1: Planar Cable-Driven Parallel Crane

2.1   Modeling

This section deals with the model of a simple CDPR with an embedded hoist mechanism and its remote actuation through a cable-loop. Therefore, the cable-loop is introduced as well as kinetostatic and elastostatic models of the hybrid robot.

2.1.1   Cable Loop (bi-actuated cable)

In Fig. 2.2, a schematic represents a simplified form of a cable-loop system actuated by two motors while passing through exit-points, namely, A_1, A_2, and anchor-points, namely, B_1, B_2. The cable-loop is coiled up around a drum on the moving-platform. The cable-loop drum then acquires one rotational DoF with respect to the moving-platform used to actuate a tool or to control additional degrees of freedom such as rotations over wide ranges.

For the sake of the simplicity in modeling, one virtual uni-actuated cables can substitute cable-loops. The latter virtual cable replace the cable-loop with A_{12} and B_{12}, as their exit point and anchor point, respectively. As long as the moving-platform is far from points A_1 and A_2, then A_1B_1 and A_2B_2 can be assumed parallel and the virtual cable model replaces the cable-loop. The main geometrical characteristic of the manipulator is expressed as points A_i and B_i, which stand for the ith exit point and anchor point, respectively. $\mathbf{a}_i = [a_{ix},\ a_{iy}]^T$, $\mathbf{b}_i = [b_{ix},\ b_{iy}]^T$ are the respective Cartesian coordinate vectors of points A_i and B_i. The former point is the location of ith pulley fixed to the ceiling and the latter point is ith cable associated anchor point located on the moving-platform.

$$\mathbf{a}_{12} = (\mathbf{a}_1 + \mathbf{a}_2)/2 \tag{2.1}$$

and,

$$\mathbf{b}_{12} = (\mathbf{b}_1 + \mathbf{b}_2)/2 \tag{2.2}$$

Hereafter, the effect of the cable loop tension onto the moving-platform is the force passing through the midpoint B_{12} between B_1 and B_2 along the unit vector $\mathbf{u}_{12}$ of segment $A_{12}B_{12}$,

$$\mathbf{t}_{12} = \mathbf{t}_1 + \mathbf{t}_2 \tag{2.3}$$

and a moment generated about rotational axis of the drum,

$$\mathbf{m}_{cl} = r_d(t_1 - t_2), \tag{2.4}$$

where r_d is the radius of the cable-loop drum.

2.1.2   Kinetostatic Model of the CDPC

This section deals with the kinetostatic modeling of a simple hybrid CDPR with an embedded one DoF mechanism. The proposed manipulator consists in an articulated moving-platform actuated by three motors through two cables. The moving-platform accommodates a hoist mechanism, which is coupled with a cable loop. The cable loop has two distinct purposes. The first is to position the moving-platform and the second is to actuate the hoist. The hoist consists in a triple-stage reducer that
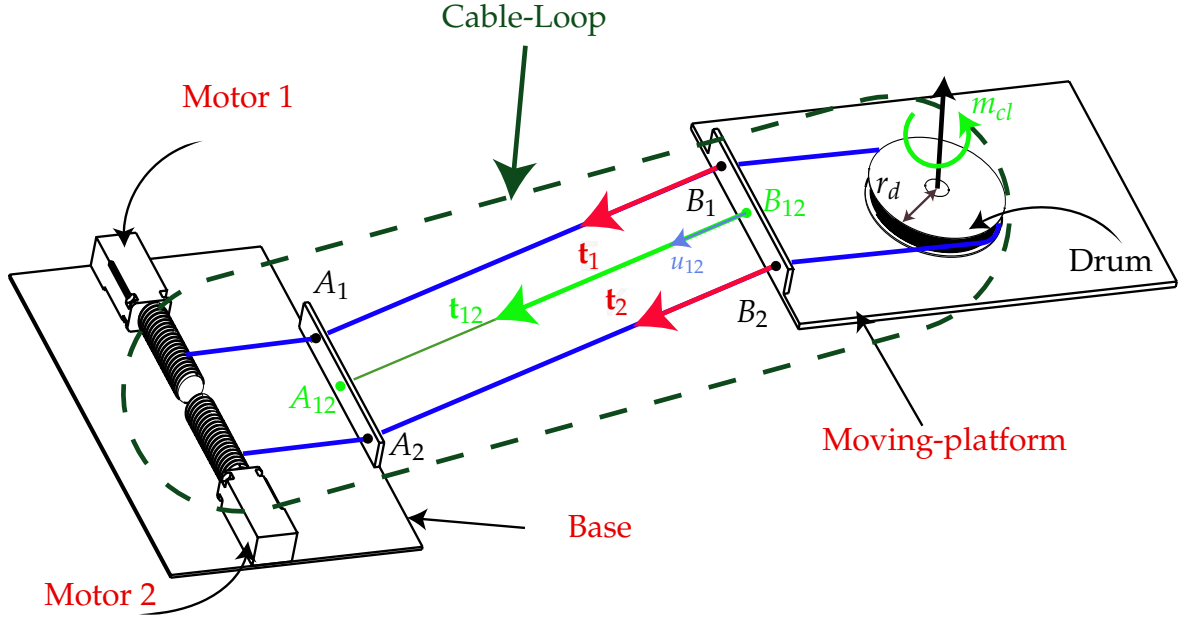
Figure 2.2: Representation of a simple cable-loop system for the moving-platform of a CDPR

increases the input torque generated by the cable loop and transmits it to a cable, $\mathscr{C}_h$, that is wound onto a drum. Therefore, the relative height between the given payload and the moving-platform can be adjusted within the workspace of the CDPC. As the proposed application of the CDPC does not require its moving-platform to approach the payload, the risk of collision between objects on the ground with cables of the manipulator is eliminated.

Architecture of the Manipulator

Here, we discuss the architecture of the CDPC. The overall manipulator consists in a base frame and a moving-platform connected in parallel by two actuated cables as shown in Fig. 2.3. The under-actuated moving-platform possesses four DoF within a planar workspace. The moving-platform has two translational DoF in the $\mathbf{x}O\mathbf{y}$ plane, one rotational DoF of axis normal to its translation plane. The actuation of the additional degree of freedom on the moving-platform is done through a cable loop and a drum, so that no motor needs to be mounted on the moving-platform for actuation of the end-effector.

Figure 2.4 illustrates the overall schematic of the moving-platform of the CDPC. The moving-platform is suspended by two cables, i.e., a cable loop ($\mathscr{C}_1$ and $\mathscr{C}_2$) that are actuated by two motors and another cable, $\mathscr{C}_3$, that connects the support of the moving-platform to the third motor. The cables are directly connected to the support of the moving-platform and the hoist mechanism is accommodated within the support. The hoist is outlined in the figure and its main task is to transmit the power from input shaft, $\mathscr{S}_I$, to the second shaft, $\mathscr{S}_O$. The input shaft is actuated by two motors fixed to the ground and through the cable loop. The gear train, which is inspired from the one in link [1], increases the input torque and transfers it to $\mathscr{S}_O$. The second

---

[1] https://youtu.be/ZAOizXvmzMg
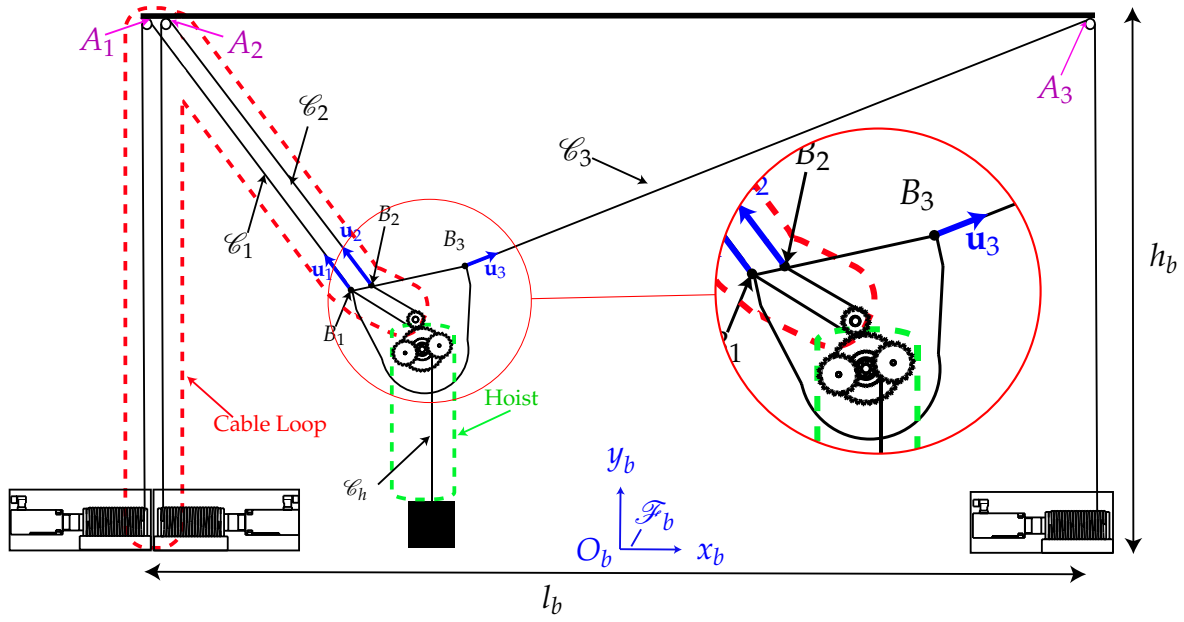
Figure 2.3: A four-DoF planar cable-driven parallel robot with a cable loop

shaft, transmits the power to the hoist drum, $\mathscr{D}_h$, through a gear train. Consequently, $\mathscr{C}_h$, is wound onto $\mathscr{D}_h$. $\mathscr{S}_O$ and $\mathscr{D}_h$ are concentric but are not in contact.

The cable loop connected to two actuators, which are shown in Fig. 2.5, is coiled about, $\mathscr{D}_d$ to make the latter rotate about its own axis. The left side of this cable loop is denoted by $\mathscr{C}_1$ whereas its right side is denoted by $\mathscr{C}_2$. Another cable, identified by $\mathscr{C}_3$, is connected to both the support of the articulated moving-platform and a third actuator. The cable loop consists in two segments each with independent cable tensions t_1 and t_2. Segment $\mathscr{C}_1$, is composed of the part of the cable-loop, which connects the first motor to the drum through points A_1 and B_1. The second segment is denoted as $\mathscr{C}_2$ and connects the second motor to the drum through points A_2 and B_2. Two motions can be induced by the cable-loop depending on the relative rotation of two actuators connected to the cable-loop. The first one is the translation of point D (the center of $\mathscr{D}_d$ shown in Fig. 2.4) for identical inputs to the two motors and the second motion is a rotation about point C when the two actuators rotate in opposite directions.

Figure 2.5 shows the geometry of the moving-platform of the CDPC. The moving-platform frame, $\mathscr{F}_p$, is located on the top of the moving-platform and belongs to its vertical center-line, $\mathcal{L}_v$. The overall dimension of the moving-platform is specified by h_p and l_p that denote the height and length of the moving-platform, respectively. The radius of $\mathscr{D}_d$ is denoted as r_d. Anchor-points B_1 and B_3 are located on the top corners of the moving-platform, so that the width of the moving-platform is computed as $l_p = b_{3x} - b_{1x}$. Finally, the height of the moving-platform is denoted as h_p.

(a) Front view **(b)** Side view
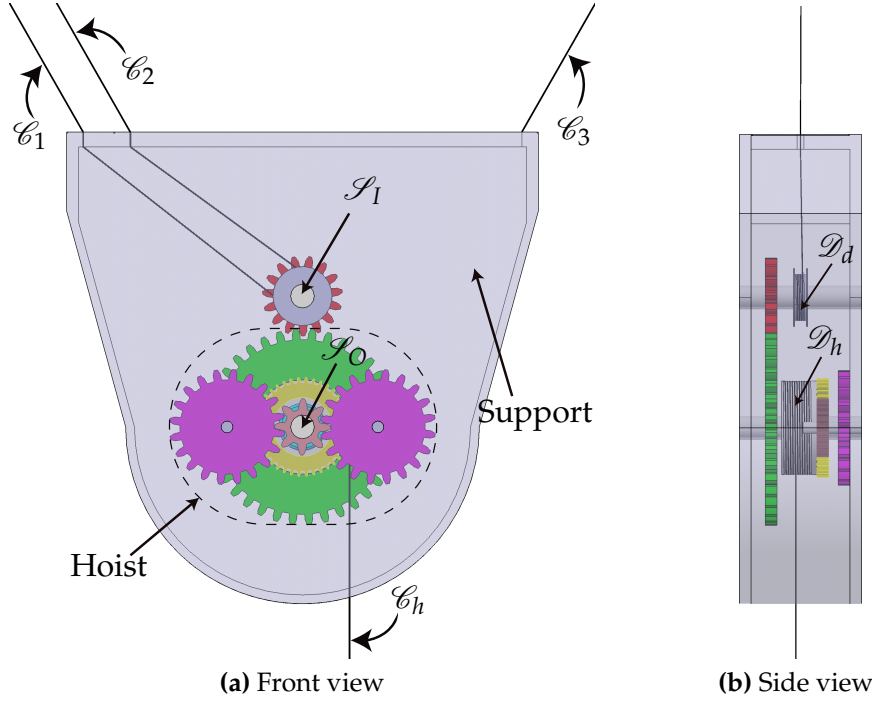
Figure 2.4: Moving-platform of cable-driven parallel crane

Table 2.1: Radius of the main components of the hoist mechanism

Parameter	r_{G1}	r_{G2}	r_{G3}	r_{G4}	r_{G5}	r_{G6}	r_{G7}	r_{G8}	r_h
Value [mm]	17	42	12	25	25	12	12	21	20

Hoist mechanism

The hoist consists of a triple-stage reducer that increases the input torque generated by the cable loop and transmits it to a cable, $\mathscr{C}_h$, that is wound onto a drum. Therefore, the relative height between the given payload and the moving-platform can be adjusted within the workspace of the CDPC. The hoist is outlined in Fig. 2.6 and its main task is to transmit the power from input shaft, $\mathscr{S}_d$, to the second shaft, $\mathscr{S}_h$. The input shaft is actuated by two motors fixed to the ground and through the cable-loop. The cable-loop rotates the input shaft ($\mathscr{S}_d$), which leads to the rotation of the first gear, namely, G_1 and second gear G_2. Next, the power is transmitted to the third gear G_3 through $\mathscr{S}_O$. It should be noted that the rotation of the $\mathscr{S}_I$ does not affect the rotation of $\mathscr{D}_h$ as the drum is connected to $\mathscr{S}_h$ through a bearing. Then, gears G_4 and G_5 rotate the left and right shafts $\mathscr{S}_r$ and $\mathscr{S}_l$, respectively. The last gear, namely, G_8 is actuated through G_6 and G_7. The hoist drum, namely, $\mathscr{D}_h$ is attached to G_8 and coils up $\mathscr{C}_h$. Table 2.1 expresses the radii of the main parts of the hoist components, r_i being the radius of part i of the hoist.
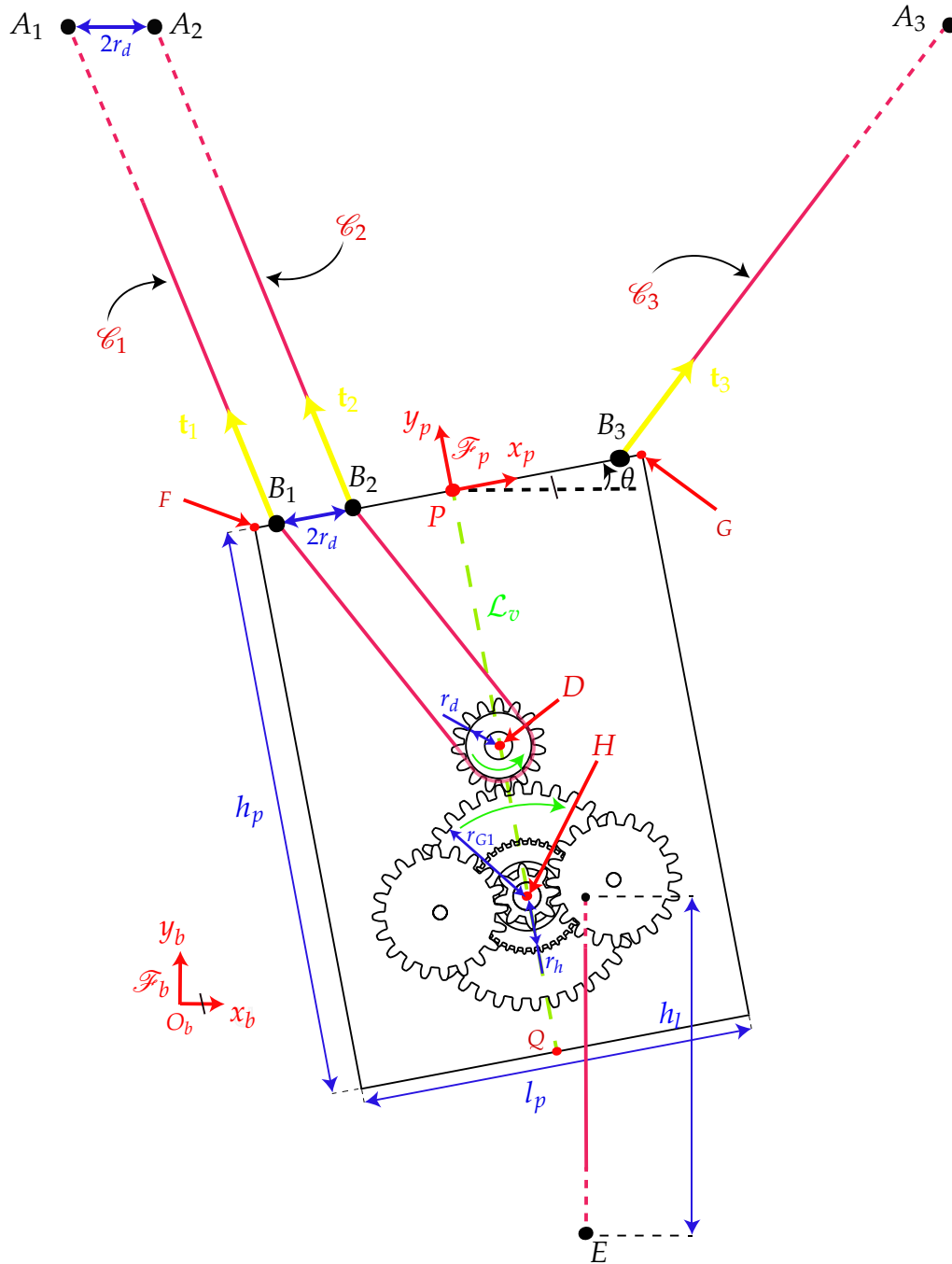
Figure 2.5: Moving-platform of the four-DoF planar under-constrained cable-driven parallel crane
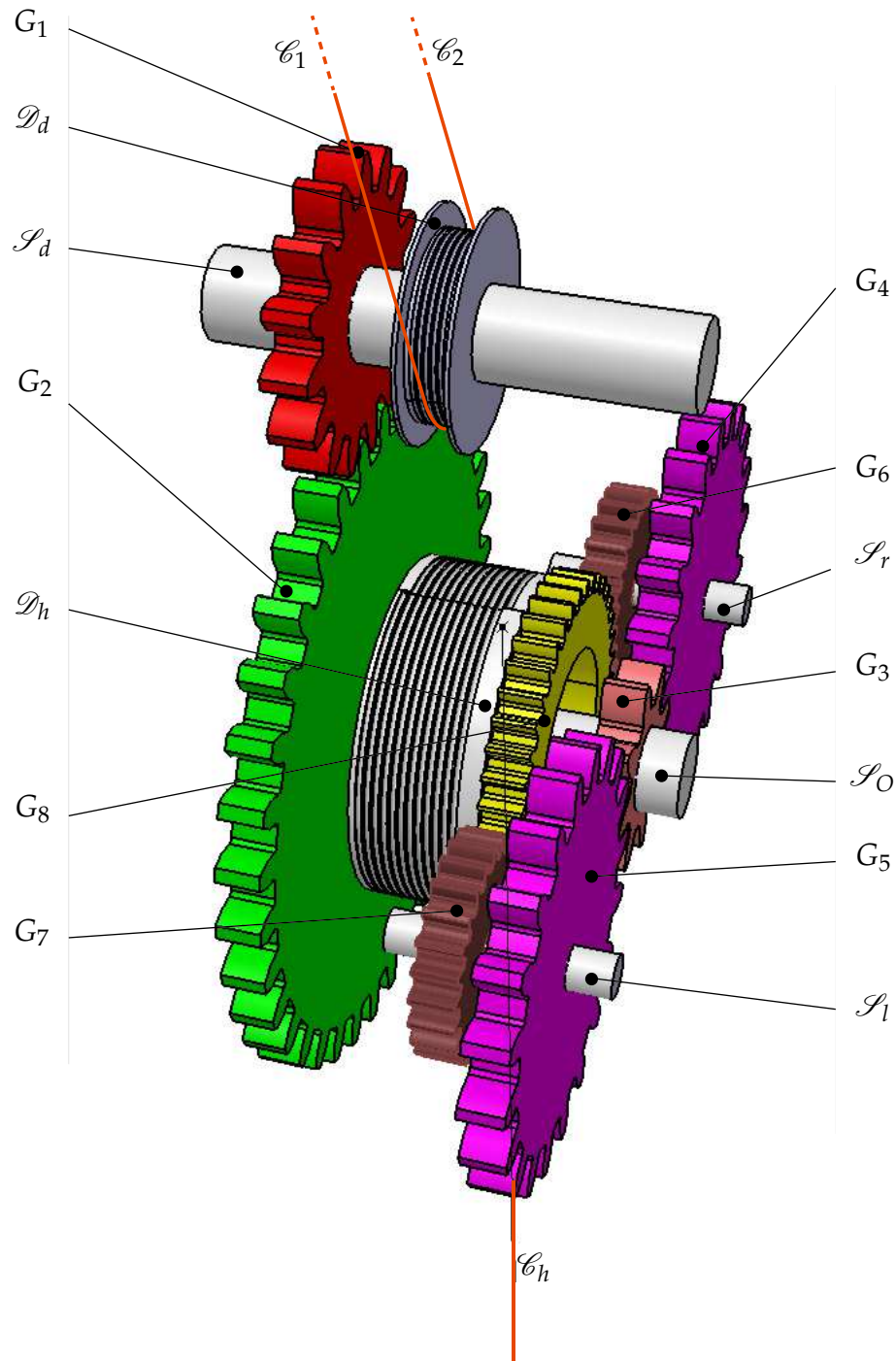
Figure 2.6: Hoist mechanism

Mathematical Modeling

The kinetostatic model consists of geometric model and static model of the CDPC. The model assumes linear cables with no elasticity. Furthermore, the exit-points are assumed to be fixed points without considering pulleys. The geometric model expresses the relation between the cable lengths and the pose of the moving-platform. Static model of the manipulator states the static equilibrium of the wrench applied on the moving-platform. Carricato [Car13] studied an analogous problem, namely, the inverse geometrico-static problem of under-constrained CDPRs which poses major challenges due to the coupling between geometry and static-equilibrium of under-constrained CDPRs. Loop-closure equations of the CDPC are given by:

$$^b\mathbf{l}_i = {}^b\mathbf{a}_i - {}^b\mathbf{p} - {}^b\mathbf{R}_p{}^p\mathbf{b}_i, \quad i = 1, 2, 3 \tag{2.5}$$

where $^b\mathbf{l}_i$ is the ith cable vector, i.e., the Cartesian coordinate vectors pointing from point B_i to points A_i. Point A_i and B_i stand for the ith cable exit point and anchor point, respectively. The former point is the location of i-th pulley fixed to the ceiling and the latter point is the connection between i-th cable and the moving-platform. $^b\mathbf{a}_i = [a_{ix}, a_{iy}]^T$, $^p\mathbf{b}_i = [b_{ix}, b_{iy}]^T$ and $^b\mathbf{p} = [p_x, p_y]^T$ are the Cartesian coordinate vector of points A_i, B_i and P, respectively, expressed in frame $\mathscr{F}_b$. $^b\mathbf{R}_p$ is the rotation matrix from frame $\mathscr{F}_b$ to frame $\mathscr{F}_p$ as follows:

$$^b\mathbf{R}_p = \begin{bmatrix} \cos\theta & -\sin\theta \\ \sin\theta & \cos\theta \end{bmatrix} \tag{2.6}$$

$\theta = \angle(\mathbf{x}_b, \mathbf{x}_p)$ is the rotation angle of the moving-platform. $\mathbf{t}_i$, $i = 1, 2, 3$ is the ith cable tension vector and it is directed from B_i toward A_i. $\mathbf{t}_i = t_i{}^b\mathbf{u}_i$ and its magnitude is expressed as $t_i = \|\mathbf{t}_i\|_2$, $i = 1, 2, 3$ and $^b\mathbf{u}_i$ is denoted as the ith cable unit vector. In order to compute the unit cable vector, $^b\mathbf{u}_i$, we normalize, $^b\mathbf{l}_i$ as follows:

$$\mathbf{u}_i = \frac{\mathbf{l}_i}{l_i}, \quad i = 1, 2, 3, \tag{2.7}$$

l_i being the ith cable length. The wrench exerted on the moving-platform are cable tensions, $\mathbf{t}_i$, $i = 1, 2, 3$, the mass for the moving-platform, $m\mathbf{g}$, and the frictional moment or the resistance to relative motions between $\mathscr{D}_p$ and the hoist that is denoted as m_{fr}. The equilibrium of the external forces applied onto the moving-platform, is expressed as follows:

$$\sum_{i=1}^{3} t_i{}^b\mathbf{u}_i + m\mathbf{g} = 0 \tag{2.8}$$

In Eq. (2.8), m is the mass of the moving-platform and $\mathbf{g} = [0, -g]^T$ is the gravity acceleration with $g = 9.81 \ m.s^{-2}$. The equilibrium of moments about point P in frame $\mathscr{F}_b$ is expressed as follows:

$$\sum_{i=1}^{3} \left(\left(^b\mathbf{b}_i - {}^b\mathbf{p}\right)^T \mathbf{E}^T\mathbf{t}_i \right) + \left(^b\mathbf{c} - {}^b\mathbf{p}\right)^T \mathbf{E}^T m\mathbf{g} = 0 \tag{2.9}$$

with,

$$\mathbf{E} = \begin{bmatrix} 0 & -1 \\ 1 & 0 \end{bmatrix} \tag{2.10}$$

and ${}^{b}\mathbf{c}$ being the Cartesian coordinate vector of the moving-platform Center of Mass (CoM) in $\mathscr{F}_b$, given by:

$${}^{b}\mathbf{c} = {}^{b}\mathbf{p} + {}^{b}\mathbf{R}_p\, {}^{p}\mathbf{c} \tag{2.11}$$

${}^{p}\mathbf{c} = \begin{bmatrix} c_x, & c_y \end{bmatrix}^{T}$ is the Cartesian coordinate vector of the CoM expressed in $\mathscr{F}_p$.
By considering $({}^{b}\mathbf{b}_i - {}^{b}\mathbf{p}) = {}^{b}\mathbf{R}_p\, {}^{p}\mathbf{b}_i$, $i = 1,\ 2,\ 3$, and $({}^{b}\mathbf{c} - {}^{b}\mathbf{p}) = {}^{b}\mathbf{R}_p\, {}^{p}\mathbf{c}$ we can rewrite
Eq. (2.9) as follows:

$$\sum_{i=1}^{3} \left({}^{p}\mathbf{b}_i^{T\,b}\mathbf{R}_p^{T}\mathbf{E}^{T}\mathbf{t}_i \right) + {}^{p}\mathbf{c}^{T\,b}\mathbf{R}_p^{T}\mathbf{E}^{T}m\mathbf{g} = 0 \tag{2.12}$$

Finally, we write the equilibrium of the moments generated by the cable-loop about point P, the latter is the moment that drives $\mathscr{D}_d$ and consequently actuates $\mathscr{D}_h$ and is formulated as follows:

$$r_d \delta t + m_{fr} = 0 \tag{2.13}$$

The cable-loop tension difference is expressed as:

$$\delta t = t_2 - t_1 \tag{2.14}$$

From Eqs. (2.8), (2.12) and (2.13), the static equilibrium equation of the moving-platform is expressed as:

$$\mathbf{W}\mathbf{t} + \mathbf{w}_e = \mathbf{0}_4 \tag{2.15}$$

where $\mathbf{W}$ is the wrench matrix of the CDPC under study

$$\mathbf{W} = \begin{bmatrix} {}^{b}\mathbf{u}_1 & {}^{b}\mathbf{u}_2 & {}^{b}\mathbf{u}_3 \\ {}^{p}\mathbf{b}_1^{T\,b}\mathbf{R}_p^{T}\mathbf{E}^{T\,b}\mathbf{u}_1 & {}^{p}\mathbf{b}_2^{T\,b}\mathbf{R}_p^{T}\mathbf{E}^{T\,b}\mathbf{u}_2 & {}^{p}\mathbf{b}_3^{T\,b}\mathbf{R}_p^{T}\mathbf{E}^{T\,b}\mathbf{u}_3 \\ -r_d & r_d & 0 \end{bmatrix} \tag{2.16}$$

$\mathbf{w}_e$ is the external wrench applied onto the moving-platform

$$\mathbf{w}_e = \begin{bmatrix} 0 & -mg & {}^{p}\mathbf{c}^{T\,b}\mathbf{R}_p^{T}\mathbf{E}^{T}m\mathbf{g} & m_{fr} \end{bmatrix}^{T} \tag{2.17}$$

$\mathbf{0}_4$ is a four-dimension zero vector and the three-dimension cable tension vector $\mathbf{t}$ is expressed as follows:

$$\mathbf{t} = \begin{bmatrix} t_1 & t_2 & t_3 \end{bmatrix}^{T} \tag{2.18}$$

2.1.3 Elasto-static Model of the CDPC

In order to study the manipulator stiffness, the elasto-static model of the CDPC is given by,

$$\delta\mathbf{w}_e = \begin{bmatrix} \delta\mathbf{f}_p \\ \delta m_p \\ \delta m_d \end{bmatrix} = \mathbf{K}\delta\mathbf{r} = \mathbf{K} \begin{bmatrix} \delta\mathbf{p} \\ \delta o_p \\ \delta o_d \end{bmatrix} \tag{2.19}$$

In Equation (2.19), $\delta\mathbf{w}_e$ is denoted as the infinitesimal change in the external wrench. $\mathbf{K}$ and $\delta\mathbf{r}$ stand for the stiffness matrix and small displacement screw of the moving-platform. The vectors of infinitesimal change in the force and displacement are denoted as $\delta\mathbf{f}_p = [\delta f_x, \delta f_y]^T$ and $\delta\mathbf{p} = [\delta p_x, \delta p_y]^T$, respectively. δm_p and δm_d are denoted for infinitesimal variations in applied moments onto the moving-platform and $\mathscr{D}_I$ about $\mathbf{z}_b$. o_p and o_d correspond to the infinitesimal changes in rotation of the moving-platform and drum about $\mathbf{z}_b$.

In [BK06; Gag+16b], the elasto-static model of CDPRs with classical moving-platform is investigated while in this section based on the already-developed models we derive the elasto-static model for the hybrid CDPRs. Hereafter, the stiffness matrix of the moving-platform is expressed as follows:

$$\mathbf{K} = \frac{d\mathbf{w}_e}{d\mathbf{r}} \tag{2.20}$$

The following equation is achieved by substituting Eq. (2.15) into Eq. (2.20)

$$\mathbf{K} = -\frac{d\mathbf{W}\mathbf{t}}{d\mathbf{r}} = \mathbf{K}_a + \mathbf{K}_p = -\frac{d\mathbf{W}}{d\mathbf{r}}\mathbf{t} - \mathbf{W}\frac{d\mathbf{t}}{d\mathbf{r}} \tag{2.21}$$

Passive stiffness matrix, $\mathbf{K}_p$, depends on the cable properties and active stiffness matrix, $\mathbf{K}_a$, depends on the cable tension, $\mathbf{t}$.

Passive Stiffness Matrix

Under the assumption of the linear spring model for cables, the following equation represents the cable elasticity, where i-th cable elasticity coefficient and length variations are denoted as k_i and δl_i, respectively.

$$t_i = k_i \delta l_i \tag{2.22}$$

Equation (2.22) is rewritten for all the cables in the following closed form.

$$\mathbf{t} = \mathbf{K}_l \delta\mathbf{l} \tag{2.23}$$

where, $\delta \mathbf{l} = [\delta l_1, \delta l_2, \delta l_3]^T$ is the vector of infinitesimal variation in cable length and the cable stiffness matrix $\mathbf{K}_l$, is defined as follows:

$$\mathbf{K}_l = \begin{bmatrix} k_1 & 0 & 0 \\ 0 & k_2 & 0 \\ 0 & 0 & k_3 \end{bmatrix} \tag{2.24}$$

The wrench matrix, $\mathbf{W}$ is defined as:

$$\mathbf{W}^T = -\frac{\mathrm{d}\mathbf{l}}{\mathrm{d}\mathbf{r}} \tag{2.25}$$

where, $\mathbf{l} = [l_1, l_2, l_3]^T$ is cable length vector. From Eq. (2.23) and Eq. (2.25) we rewrite the passive stiffness matrix as:

$$\mathbf{K}_p = -\mathbf{W}\mathbf{K}\frac{\mathrm{d}\mathbf{l}}{\mathrm{d}\mathbf{r}} = \mathbf{W}\mathbf{K}_l\mathbf{W}^T \tag{2.26}$$

Upon substituting Eqs. (3.28, 2.24 and 2.25) into Eq (2.26), we can formulate the passive stiffness matrix as follows:

$$\mathbf{K}_p = \sum_{i=1}^{3} k_i \begin{bmatrix} {}^b\mathbf{u}_i{}^b\mathbf{u}_i{}^T & {}^b\mathbf{u}_i{}^b\mathbf{u}_i{}^T\mathbf{E}^r\mathbf{b}_i & w_{3,i}\,{}^b\mathbf{u}_i \\ {}^r\mathbf{b}_i{}^T\mathbf{E}^{Tb}\mathbf{u}_i{}^b\mathbf{u}_i{}^T & {}^r\mathbf{b}_i{}^T\mathbf{E}^{Tb}\mathbf{u}_i{}^b\mathbf{u}_i{}^T\mathbf{E}^r\mathbf{b}_i & w_{3,i}\,{}^r\mathbf{b}_i{}^T\mathbf{E}^{Tb}\mathbf{u}_i \\ w_{3,i}\,{}^b\mathbf{u}_i{}^T & w_{3,i}\,{}^b\mathbf{u}_i{}^T\mathbf{E}^r\mathbf{b}_i & w_{3,i}{}^2 \end{bmatrix} \tag{2.27}$$

where, ${}^r\mathbf{b}_i = {}^b\mathbf{r}_d{}^p\mathbf{b}_i$ and $w_{3,i}$ refers to the third row and the ith column of $\mathbf{W}$.

Active Stiffness Matrix

From Eq. (2.21) the active stiffness matrix can be rewritten as follows:

$$\mathbf{K}_a = -\frac{\mathrm{d}\mathbf{W}}{\mathrm{d}\mathbf{r}}\mathbf{t} = -\sum_{i=1}^{3}\frac{\mathrm{d}\mathbf{w}_i}{\mathrm{d}\mathbf{r}}t_i \tag{2.28}$$

where the differential of the wrench matrix associated to the ith cable with respect to the infinitesimal screw, $\delta\mathbf{r}$ is given by:

$$\frac{\mathrm{d}\mathbf{w}_i}{\mathrm{d}\mathbf{r}} = \begin{bmatrix} \dfrac{\mathrm{d}^b\mathbf{u}_i}{\mathrm{d}\mathbf{p}} & \dfrac{\mathrm{d}^b\mathbf{u}_i}{\mathrm{d}o_p} & \dfrac{\mathrm{d}^b\mathbf{u}_i}{\mathrm{d}o_d} \\ \dfrac{\mathrm{d}\left({}^r\mathbf{b}_i{}^T\mathbf{E}^{Tb}\mathbf{u}_i\right)}{\mathrm{d}\mathbf{p}} & \dfrac{\mathrm{d}\left({}^r\mathbf{b}_i{}^T\mathbf{E}^{Tb}\mathbf{u}_i\right)}{\mathrm{d}o_p} & \dfrac{\mathrm{d}\left({}^r\mathbf{b}_i{}^T\mathbf{E}^{Tb}\mathbf{u}_i\right)}{\mathrm{d}o_d} \\ \dfrac{\mathrm{d}w_{3,i}}{\mathrm{d}\mathbf{p}} & \dfrac{\mathrm{d}w_{3,i}}{\mathrm{d}o_p} & \dfrac{\mathrm{d}w_{3,i}}{\mathrm{d}o_d} \end{bmatrix} \tag{2.29}$$

The differential form of ${}^b\mathbf{u}_i$ is derived from Eq. (2.5) in the following

$$\mathrm{d}^b\mathbf{u}_i = -\frac{1}{l_i}(\mathbf{I}_{2,2} - {}^b\mathbf{u}_i{}^b\mathbf{u}_i{}^T)(\mathrm{d}\mathbf{p} - {}^b\mathbf{r}_d\mathbf{E}^p\mathbf{b}_i\mathrm{d}o_p) \tag{2.30}$$

and the differential term in the second row of Eq. (2.29) is determined as follows:

$$\mathrm{d}\left({}^{r}\mathbf{b}_{i}{}^{T}\mathbf{E}^{T\,b}\mathbf{u}_{i}\right) = -{}^{p}\mathbf{b}_{i}{}^{T\,b}\mathbf{r}_{d}{}^{b}\mathbf{u}_{i} + {}^{r}\mathbf{b}_{i}{}^{T}\mathbf{E}^{T}\mathrm{d}^{b}\mathbf{u}_{i} \tag{2.31}$$

Therefore, the active stiffness matrix of the CDPC is reformulated in Eq. (2.32).

$$\mathbf{K}_{a} = -\sum_{i=1}^{m} t_{i} \begin{bmatrix} \dfrac{\mathrm{d}^{b}\mathbf{u}_{i}}{\mathrm{d}\mathbf{p}} & \dfrac{\mathrm{d}^{b}\mathbf{u}_{i}}{\mathrm{d}o_{p}} & \dfrac{\mathrm{d}^{b}\mathbf{u}_{i}}{\mathrm{d}o_{d}} \\ \dfrac{\mathrm{d}\left({}^{r}\mathbf{b}_{i}{}^{T}\mathbf{E}^{T\,b}\mathbf{u}_{i}\right)}{\mathrm{d}\mathbf{p}} & \dfrac{\mathrm{d}\left({}^{r}\mathbf{b}_{i}{}^{T}\mathbf{E}^{T\,b}\mathbf{u}_{i}\right)}{\mathrm{d}o_{p}} & \dfrac{\mathrm{d}\left({}^{r}\mathbf{b}_{i}{}^{T}\mathbf{E}^{T\,b}\mathbf{u}_{i}\right)}{\mathrm{d}o_{d}} \\ \dfrac{\mathrm{d}w_{3,i}}{\mathrm{d}\mathbf{p}} & \dfrac{\mathrm{d}w_{3,i}}{\mathrm{d}o_{p}} & \dfrac{\mathrm{d}w_{3,i}}{\mathrm{d}o_{d}} \end{bmatrix} \tag{2.32}$$

where,

$$\frac{\mathrm{d}^{b}\mathbf{u}_{i}}{\mathrm{d}\mathbf{p}} = -\frac{1}{l_{i}}(\mathbf{I}_{2,2} - {}^{b}\mathbf{u}_{i}{}^{b}\mathbf{u}_{i}{}^{T}) \tag{2.33}$$

$$\frac{\mathrm{d}^{b}\mathbf{u}_{i}}{\mathrm{d}o_{p}} = \frac{1}{l_{i}}(\mathbf{I}_{2,2} - {}^{b}\mathbf{u}_{i}{}^{b}\mathbf{u}_{i}{}^{T}){}^{b}\mathbf{r}_{d}\mathbf{E}^{p}\mathbf{b}_{i} \tag{2.34}$$

$$\frac{\mathrm{d}^{b}\mathbf{u}_{i}}{\mathrm{d}o_{d}} = \mathbf{0}_{2,1} \tag{2.35}$$

$$\frac{\mathrm{d}\left({}^{r}\mathbf{b}_{i}{}^{T}\mathbf{E}^{T\,b}\mathbf{u}_{i}\right)}{\mathrm{d}\mathbf{d}} = -\frac{1}{l_{i}}{}^{r}\mathbf{b}_{i}^{T}\mathbf{E}^{T}(\mathbf{I}_{2,2} - {}^{b}\mathbf{u}_{i}{}^{b}\mathbf{u}_{i}{}^{T}) \tag{2.36}$$

$$\frac{\mathrm{d}\left({}^{r}\mathbf{b}_{i}{}^{T}\mathbf{E}^{T\,b}\mathbf{u}_{i}\right)}{\mathrm{d}o_{p}} = \frac{1}{l_{i}}{}^{r}\mathbf{b}_{i}^{T}\mathbf{E}^{T}(\mathbf{I}_{2,2} - {}^{b}\mathbf{u}_{i}{}^{b}\mathbf{u}_{i}{}^{T}){}^{b}\mathbf{r}_{d}\mathbf{E}^{p}\mathbf{b}_{i} - {}^{p}\mathbf{b}_{i}{}^{T\,b}\mathbf{r}_{d}{}^{b}\mathbf{u}_{i} \tag{2.37}$$

$$\frac{\mathrm{d}\left({}^{r}\mathbf{b}_{i}{}^{T}\mathbf{E}^{T\,b}\mathbf{u}_{i}\right)}{\mathrm{d}o_{d}} = 0 \tag{2.38}$$

$$\frac{\mathrm{d}w_{3,i}}{\mathrm{d}\mathbf{p}} = \mathbf{0}_{1,2} \tag{2.39}$$

$$\frac{\mathrm{d}w_{3,i}}{\mathrm{d}o_{p}} = 0 \tag{2.40}$$

$$\frac{\mathrm{d}w_{3,i}}{\mathrm{d}o_{d}} = 0 \tag{2.41}$$

The translational displacement of the CDPC is plotted in Fig. 2.7. The contours of the calculated displacement due to the weight of the payload are illustrated along the horizontal axis in Fig. 2.7a and along vertical axis in Fig. 2.7b.

2.2 Analysis

Hybrid CDPRs differ from classical CDPRs and also hybrid robots. The study and analysis of CDPRs diverges from that of classical parallel robots as the non-rigid nature of cables cannot apply bi-directional forces as can rigid links in classical parallel robots. Moreover, CDPRs cable interferences and cable collisions with the
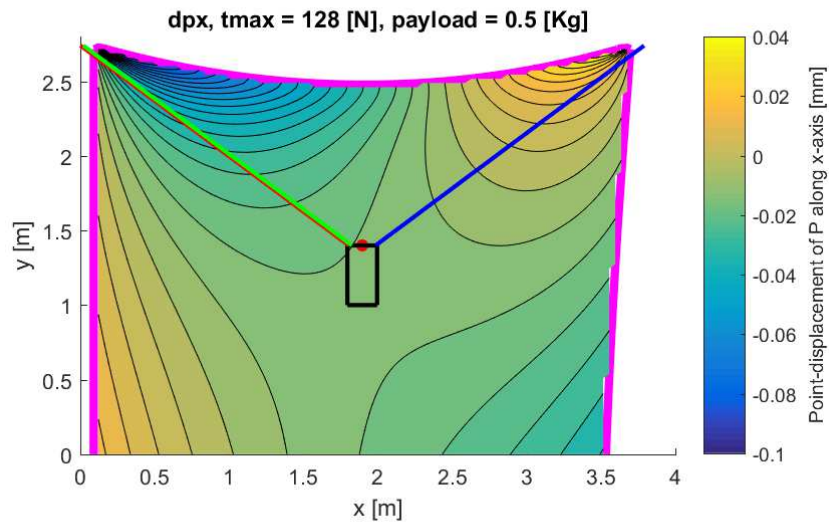
(a) Translation of point P along x-axis
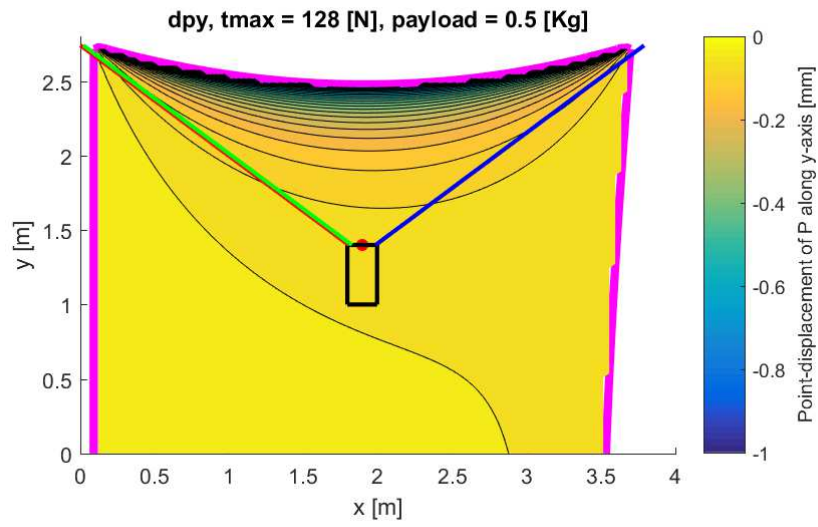
(b) Translation of point P along y-axis

Figure 2.7: Displacement of the moving-platform based on the elastic model for given m = 0.5 kg

surrounding environment are more vulnerable to internal collisions (cable-cable or cable-moving platform) than classical parallel robots. The mentioned problem is of a crucial concern for obtaining large orientation workspace since, interferences of cable with one another and also with the moving-platform usually constrain the size of the workspace. Additionally, the analysis of hybrid CDPRs and their remote actuation through cable loops have not been sufficiently addressed elsewhere, making this investigation relevant to assess the benefit of cable loops. The main motivation of this section is to analyze the benefit of CDPCs and the challenges in order to realize the first remotely actuated CDPR as well as the performance evaluation of the CDPC in terms of workspace size and positioning accuracy.

Several types of workspaces have been proposed and used for the design of CD-PRs, e.g., the Wrench Closure Workspace (WCW), the Wrench Feasible Workspace (WFW), the Twist Feasible Workspace (TFW) and static workspace. WFW is the set of all moving platform poses where it can sustain predefined external wrenches exerted onto the moving-platform. In general, the workspace analysis can be performed in terms of static, kinematic, dynamic, cable-interferences, collision and etc which has been studied thoroughly in the literature. One of the motivation for this section is to investigate the capabilities of the proposed CDPC in terms of the workspace and more specifically twist and wrench feasible workspaces. The WFW branches into two subdivisions, namely, static workspace and WCW. They are particular cases of the WFW, in the former the gravitational wrench is considered as external wrench and in the latter there is no upper-bound for the admissible cable tensions.

In addition to the workspace analysis, the study of the performance of the manipulator in terms of parasitic inclination and required height of the CDPC for a given payload are carried out in the context of this section.

2.2.1   Twist Feasible Workspace (TFW)

A CDPR posture is called twist-feasible if all the twists (point-velocity and angular-velocity combinations), within a given set, can be produced at the CDPR mobile platform, within given actuator speed limits. Two problems were discussed in the previous work: (1) determining the set of required cable winding speeds at the CDPR winches being given a prescribed set of required mobile platform twists; and (2) determining the set of available twists at the CDPR mobile platform from the available cable winding speeds at its winches. The solutions to both problems can be used to determine the twist feasibility of n-degree-of-freedom (DOF) CDPRs driven by $m \geq n$ cables. Therefore, the mentioned problems are expressed as follows:

1. For a given pose of the mobile platform of a CDPR and being given a set $[\mathbf{t}_w]_r$ of required mobile platform twists, determine the corresponding set of cable velocities $\dot{\mathbf{l}}$. The set of cable velocities to be determined is called the *Required Cable Velocity Set* (RCVS) and is denoted $\left[\dot{\mathbf{l}}\right]_r$. The set $[\mathbf{t}_w]_r$ is called the *Required Twist Set* (RTS).

2. For a given pose of the mobile platform of a CDPR and being given a set $\left[\dot{\mathbf{l}}\right]_a$ of available (admissible) cable velocities, determine the corresponding set of mobile platform twists $\mathbf{t}_w$. The former set, $\left[\dot{\mathbf{l}}\right]_a$, is called the *Available Cable*

Velocity Set (ACVS) while the latter is denoted $[\mathbf{t}_w]_a$ and called the *Available Twist Set* (ATS).

The differential kinematics of the CDPR establishes the relationship between the twist $\mathbf{t}_w$ of the mobile platform and the time derivatives of the cable lengths $\dot{\mathbf{l}}$

$$\mathbf{J}\mathbf{t}_w = \dot{\mathbf{l}} \tag{2.42}$$

where $\mathbf{J}$ is the $m \times n$ Jacobian matrix and $\dot{\mathbf{l}} = \left[\dot{l}_1, \ldots, \dot{l}_m \right]^T$. The twist $\mathbf{t}_w = [\dot{\mathbf{p}}, \boldsymbol{\omega}]^T$ is composed of the velocity $\dot{\mathbf{p}}$ of the origin of frame $\mathscr{F}_p$ with respect to $\mathscr{F}_b$ and of the angular velocity $\boldsymbol{\omega}$ of the mobile platform with respect to $\mathscr{F}_b$.

As the main contribution of this thesis is considered to extend the size of the workspace of the CDPRs, we require a tool to determine the workspace of a robot in terms of static, kinematics and dynamics. This is also helpful for measuring how well a CDPR performs a specified task within its workspace and the robustness of that. TFW could be determined either by adopting from three different approaches.

The relationship between the mobile platform twist $\mathbf{t}_w$ and the cable velocities $\dot{\mathbf{l}}$ is the differential kinematics in Eq. (2.42). According to this equation, the RCVS $[\dot{\mathbf{l}}]_r$ is defined as the image of the convex polytope $[\mathbf{t}]_r$ under the linear map $\mathbf{J}$. Consequently, $[\dot{\mathbf{l}}]_r$ is also a convex polytope [Zie94].

Moreover, if $[\mathbf{t}_w]_r$ is a box, the RCVS $[\dot{\mathbf{l}}]_r$ is a particular type of polytope called a zonotope. Such a transformation of a box into a zonotope has previously been studied in CDPR wrench feasibility analysis [BGM10a; GRR01; GK10]. Indeed, a box of admissible cable tensions is mapped by the wrench matrix $\mathbf{W}$ into a zonotope in the space of platform wrenches. However, a difference lies in the dimensions of the matrices $\mathbf{J}$ and $\mathbf{W}$, $\mathbf{J}$ being of dimensions $m \times n$ while $\mathbf{W}$ is an $n \times m$ matrix, where $n \leq m$. When $n < m$, on the one hand, $\mathbf{W}$ maps the m-dimensional box of admissible cable tensions into the n-dimensional space of platform wrenches. On the other hand, $\mathbf{J}$ maps n-dimensional twists into its range space which is a linear subspace of the m-dimensional space of cable velocities $\dot{\mathbf{l}}$. Hence, when $\mathbf{J}$ is not singular, the n-dimensional box $[\mathbf{t}_w]_r$ is mapped into the zonotope $[\dot{\mathbf{l}}]_r$ which lies into the n-dimensional range space of $\mathbf{J}$. When $\mathbf{J}$ is singular and has rank r, $r < n$, the n-dimensional box $[\mathbf{t}_w]_r$ is mapped into a zonotope of dimension r.

When an ACVS $[\dot{\mathbf{l}}]_a$ is given, a pose of the mobile platform of a CDPR is twist feasible if

$$[\dot{\mathbf{l}}]_r \subseteq [\dot{\mathbf{l}}]_a \tag{2.43}$$

Since $[\dot{\mathbf{l}}]_a$ is a convex polytope, (2.43) is verified whenever all the vertices of $[\dot{\mathbf{l}}]_r$ are included in $[\dot{\mathbf{l}}]_a$. Moreover, it is not difficult to prove that $[\dot{\mathbf{l}}]_r$ is the convex hull of the images under $\mathbf{J}$ of the vertices of $[\mathbf{t}_w]_r$. Hence, a simple method to verify if a CDPR pose is twist feasible consists in verifying whether the images of the vertices of $[\mathbf{t}]_r$ are all included into $[\dot{\mathbf{l}}]_a$.

The problem is to determine the ATS $[\mathbf{t}_w]_a$ corresponding to a given ACVS $[\dot{\mathbf{l}}]_a$.

In the most general case considered in this paper, $[\dot{\mathbf{l}}]_a$ is a convex polytope. By the Minkowski-Weyl's Theorem, a polytope can be represented as the solution set of a finite set of linear inequalities, the so-called (halfspace) *H-representation* of the polytope [Fuk; Zie94], i.e.

$$[\dot{\mathbf{l}}]_a = \{ \dot{\mathbf{l}} \mid \mathbf{C}\dot{\mathbf{l}} \leq \mathbf{d} \} \tag{2.44}$$

where matrix $\mathbf{C}$ and vector $\mathbf{d}$ are assumed to be known.

According to (2.42), the ATS is defined as

$$[\mathbf{t}_w]_a = \{\ \mathbf{t}_w \mid \mathbf{J}\mathbf{t}_w \in \left[\dot{\mathbf{l}}\right]_a\ \} \tag{2.45}$$

which, using (2.44), implies that

$$[\mathbf{t}_w]_a = \{\ \mathbf{t}_w \mid \mathbf{C}\mathbf{J}\mathbf{t}_w \le \mathbf{d}\ \} \tag{2.46}$$

The latter equation provides an H-representation of the ATS $[\mathbf{t}_w]_a$.

In practice, when the characteristics of the winches of a CDPR are known, the motor maximum speeds limit the set of possible cable velocities as follows

$$\dot{l}_{i,min} \le \dot{l}_i \le \dot{l}_{i,max} \tag{2.47}$$

where $\dot{l}_{i,min}$ and $\dot{l}_{i,max}$ are the minimum and maximum cable velocities. Note that, usually, $\dot{l}_{i,min} = -\dot{l}_{i,max}$, $\dot{l}_{1,min} = \dot{l}_{2,min} = \ldots = \dot{l}_{m,min}$, and $\dot{l}_{1,max} = \dot{l}_{2,max} = \ldots = \dot{l}_{m,max}$. In other words, $\mathbf{C}$ and $\mathbf{d}$ in (2.44) are defined as

$$\mathbf{C} = \begin{bmatrix} \mathbf{1} \\ -\mathbf{1} \end{bmatrix} \quad \text{and} \quad \mathbf{d} = \begin{bmatrix} \dot{l}_{1,max}, & \ldots, & \dot{l}_{m,max}, & -\dot{l}_{1,min}, & \ldots, & -\dot{l}_{m,min} \end{bmatrix}^T \tag{2.48}$$

where $\mathbf{1}$ is the $m \times m$ identity matrix. Eq. (2.46) can then be written as follows

$$[\mathbf{t}_w]_a = \{\ \mathbf{t}_w \mid \dot{\mathbf{l}}_{min} \le \mathbf{J}\mathbf{t}_w \le \dot{\mathbf{l}}_{max}\ \} \tag{2.49}$$

where $\dot{\mathbf{l}}_{min} = \begin{bmatrix} \dot{l}_{1,min}, & \ldots, & \dot{l}_{m,min} \end{bmatrix}^T$ and $\dot{\mathbf{l}}_{max} = \begin{bmatrix} \dot{l}_{1,max}, & \ldots, & \dot{l}_{m,max} \end{bmatrix}^T$.

When a RTS $[\mathbf{t}_w]_r$ is given, a pose of the mobile platform of a CDPR is twist feasible if

$$[\mathbf{t}_w]_r \subseteq [\mathbf{t}_w]_a \tag{2.50}$$

In this thesis, $[\mathbf{t}_w]_r$ is assumed to be a convex polytope. Hence, (2.50) is verified whenever all the vertices of $[\mathbf{t}_w]_r$ are included in $[\mathbf{t}_w]_a$. With the H-representation of $[\mathbf{t}_w]_a$ in (2.46) (or in (2.49)), testing if a pose is twist feasible amounts to verifying if all the vertices of $[\mathbf{t}_w]_r$ satisfy the inequality system in (2.46) (or in (2.49)). Testing twist feasibility thereby becomes a simple task as soon as the vertices of $[\mathbf{t}_w]_r$ are known.

Finally, let the twist feasible workspace (TFW) of a CDPR be the set of twist feasible poses of its mobile platform. It is worth noting that the boundaries of the TFW are directly available in closed form from (2.46) or (2.49). If the vertices of the (convex) RTS are denoted $\mathbf{t}_{w,j}$, $j = 1, \ldots, k$, and the rows of the Jacobian matrix are $-\mathbf{w}_i^T$, according to (2.49), the TFW is defined by $\dot{l}_{i,min} \le -\mathbf{w}_i^T \mathbf{t}_{w,j}$ and $-\mathbf{w}_i^T \mathbf{t}_{w,j} \le \dot{l}_{i,max}$, for all possible combinations of i and j. Since $\mathbf{w}_i$ contains the only variables in these inequalities that depend on the mobile platform pose, and because the closed-form expression of $\mathbf{w}_i$ as a function of the pose is known, the expressions of the boundaries of the TFW are directly obtained.

Minimum Degree of Twist Feasibility Satisfaction

One needs to measure the capabilities of a robot against the twist applied on the moving-platform and the effect of admissible cable velocities on the robustness of the CDPR in terms of kinematics. In [Gua+14] a concept is introduced that quantifies the robustness of the equilibrium of an object with an index. The latter index is defined under the assumption that the object is supported by forces of known lines of action and bounded amplitudes, and that the external perturbation forces and moments vary within a known set of possibilities. In the latter paper, a method is implemented to compute the Minimum Degree of Constraint Satisfaction (MDCS) by employing *quickhull* algorithm.

For the moving-platform of the CDPR to be twist feasible, it must hold the following conditions; To have cable velocities within the admissible threshold for the predefined twist of the moving-platform for a given pose or RTS being within ATS as expressed in Eq. (2.50).

1. Computation of polytope vertices of the required twist in the moving-platform twist space with $\mathscr{T}$ being the required twist polytope in moving-platform twist space.

$$\mathbf{t}_{r,k} = (\mathbf{1}_{m \times m} - diag(\boldsymbol{\beta}_k))t_{r,min} + diag(\boldsymbol{\beta}_k))t_{r,max} \quad k = 1, ..., q \qquad (2.51)$$

2. Mapping all the vertices, $\mathscr{T}$, onto the cable velocity space from the moving-platform twist space.

$$\dot{\mathbf{l}}_{r,k} = \mathbf{J}\mathbf{t}_{r,k} \quad k = 1, ..., q \qquad (2.52)$$

3. Computation of polytope vertices of the available (admissible) cable velocities, $\mathscr{V}$, in the cable velocity space based on the maximum admissible cable velocity, $\dot{\mathbf{l}}_{max}$ and the minimum available cable velocity, $\dot{\mathbf{l}}_{min}$.

$$\mathbf{v}_k = (\mathbf{1}_{m \times m} - diag(\boldsymbol{\beta}_k))\dot{\mathbf{l}}_{min} + diag(\boldsymbol{\beta}_k))\dot{\mathbf{l}}_{max} \quad k = 1, ..., q \qquad (2.53)$$

Where, $\boldsymbol{\beta}_k$ is a binary representation of k and consists of m (number of cables) bits. k stands for the number of the vertices of available cable tension polytope in cable tension space and it consists of $q = 2^m$ vertices.

4. Computation of convex hull of the required cable velocity polytope, $\mathscr{L}$ by Matlab *convhulln* function and computation of the facets equations.

$$\mathscr{L} = \{\dot{\mathbf{l}}_r \in \mathbb{R}^m : \quad \mathbf{a}_l^T \dot{\mathbf{l}}_r \leq b_l \quad l = 1, ..., p\} \qquad (2.54)$$

where, p expresses the number of the facet of the convex hull calculated in the latter step.

5. Calculation of the degree of twist feasibility satisfaction between j^{th} vertex of $\mathscr{V}$ and l^{th} facet of $\mathscr{L}$ as follows:

$$s_{j,l} = (b_l - \dot{\mathbf{l}}_j^T \mathbf{a}_l)/\|\mathbf{a}_l\|_2 \qquad (2.55)$$

where the degree of constraint satisfaction $s_{j,l}$ is the signed distance from vertex $\mathbf{t}_{r,j}$ of $\mathscr{V}$ to the l th face of $\mathscr{T}$.

6. Computation of the minimum degree of constraint satisfaction index.

$$s = \min_{j=1,\dots,n} \left(\min_{l=1,\dots,p} s_{j,l} \right) \tag{2.56}$$

In order to trace the TFW of a cable-driven parallel robot we need to compute the MDCS in advance. The procedure of computation of this index is implemented based on the described algorithm detailed in this section and similar to one presented in [Gua+14] for wrench feasible workspace. The negative MDCS is associated to a case study, when at least one of the vertices of $\mathscr{V}$ placed outside of $\mathscr{L}$ as depicted in Fig. B.1. In the latter case, $[\mathbf{t}_w]_r$ is not fully inside $[\mathbf{t}_w]_a$ and consequently not twist feasible.

In this section, the overall procedure of determining twist feasible workspace using MDCS index is elaborated. By adopting this approach, the intermediate step (Step 2.), determining the available twist, is accomplished by taking advantage of *convexhull* function of Matlab. The advantage of this approach is providing the visual representation of available twist set by employing the concept of V-representation. The latter is simply expressing the coordinates of all the vertices of available twist set and storing them in a matrix. The following equation expresses the required twist induced on the moving-platform by the cables.

$$\dot{\mathbf{p}} = \begin{bmatrix} \dot{p}_x & \dot{p}_y & \dot{p}_z & \omega_z & \omega_d \end{bmatrix}^T \tag{2.57}$$

ω_z and ω_d are the angular velocities of the moving-platform and cable-loop drum, respectively. Cable velocity boundaries are as follows:

$$\dot{l}_{i,min} \leq \dot{l}_i \leq \dot{l}_{i,max}, \quad i = 1,\ 2,\ 3 \tag{2.58}$$

with $\dot{l}_{i,max} = -\dot{l}_{i,min} = 3.92\ m, s^{-1}$ and $i = 1,\ 2,\ 3$.

The workspaces shown in Fig. 2.8 are associated to a required twist set with only the linear velocity components of the moving-platform in Euclidean space. By increasing the amplitudes of linear twist ($\dot{p}_x$, $\dot{p}_y$) the TFW sizes shrink from Fig. 2.8a to Fig. 2.8d, respectively. The void space inside the TFWs are triangular and they join two opposite corners of the rectangle of the manipulator frame. The evolution of the TFW size is analogous to those mention in Appendix B.2.

The evolution of the TFW due to variation of the hoist required angular velocity (ω_d) is depicted in Fig. 2.9. While the twist set of the moving-platform, namely, [$\dot{p}_x$, $\dot{p}_y$], is kept fixed. The figure clearly shows the reduction in size of workspace by increasing the required twist of the hoist mechanism. The void space within the workspace expands along the cable-loop as the required twist of the hoist is a function of the cable-loop available velocity.

2.2.2 Wrench Feasible Workspace (WFW)

Initially, the WFW of CDPRs was investigated in [VH00; EUV04; GMD07]. WFW is defined as the set of wrench feasible poses. The wrench feasible pose is defined in [EUV04]: the pose of a cable robot is said to be wrench feasible in a particular configuration and for a specified set of wrenches, if the tension forces in the cables

(a) $-2.77\ m.s^{-1} \leq \dot{p}_x,\ \dot{p}_y \leq 2.77\ m.s^{-1}$

(b) $-2.8\ m.s^{-1} \leq \dot{p}_x,\ \dot{p}_y \leq 2.8\ m.s^{-1}$

(c) $-2.9\ m.s^{-1} \leq \dot{p}_x,\ \dot{p}_y \leq 2.9\ m.s^{-1}$

(d) $-3\ m.s^{-1} \leq \dot{p}_x,\ \dot{p}_y \leq 3\ m.s^{-1}$
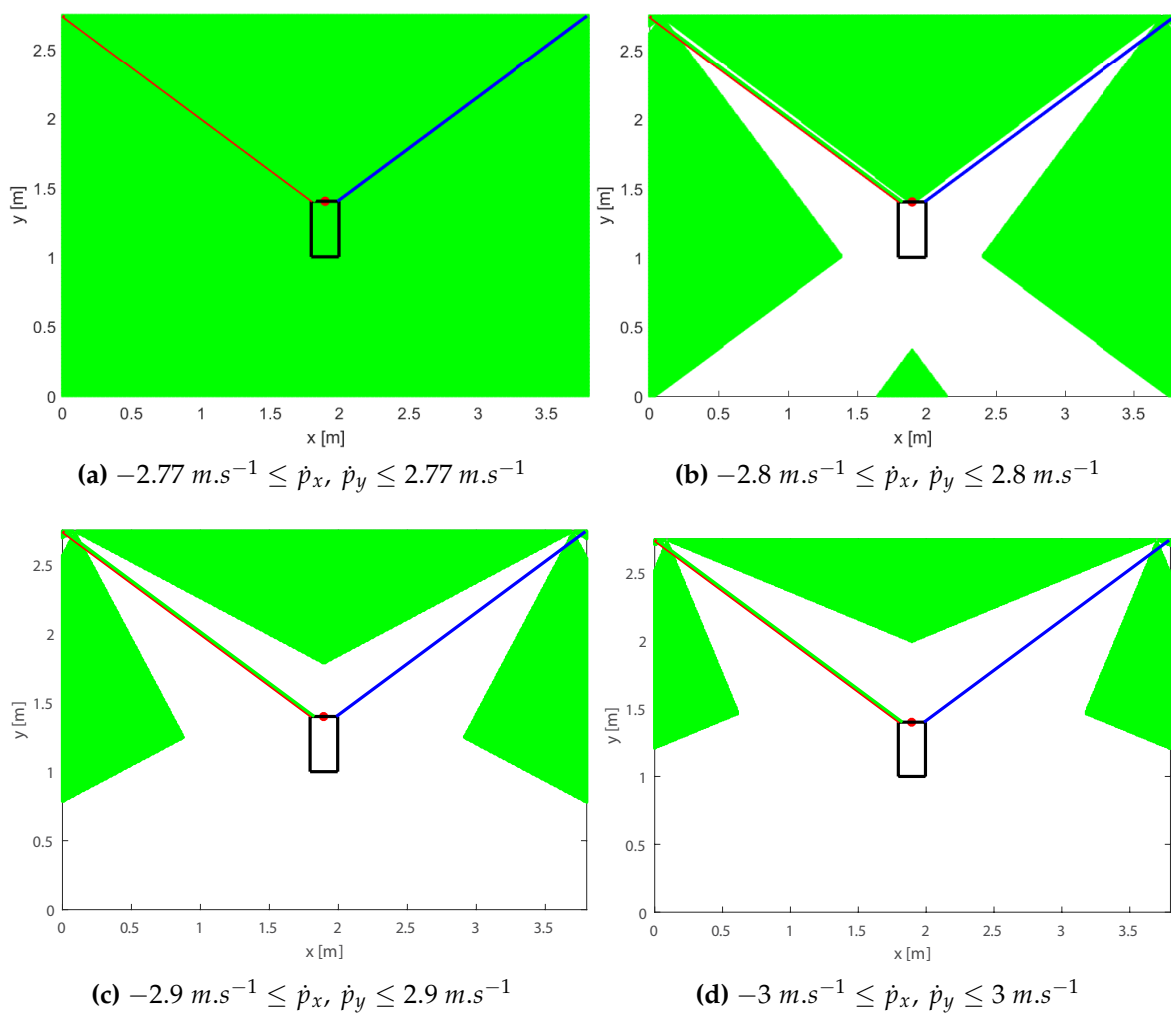
Figure 2.8: TFW of CDPC with $\omega_d = 0\ rad.s^{-1}$

(a) $\omega_d = 0\ rad.s^{-1}$

(b) $-1\ rad.s^{-1} \leq \omega_d \leq 1\ rad.s^{-1}$

(c) $-2\ rad.s^{-1} \leq \omega_d \leq 2\ rad.s^{-1}$

(d) $-6\ rad.s^{-1} \leq \omega_d \leq 6\ rad.s^{-1}$
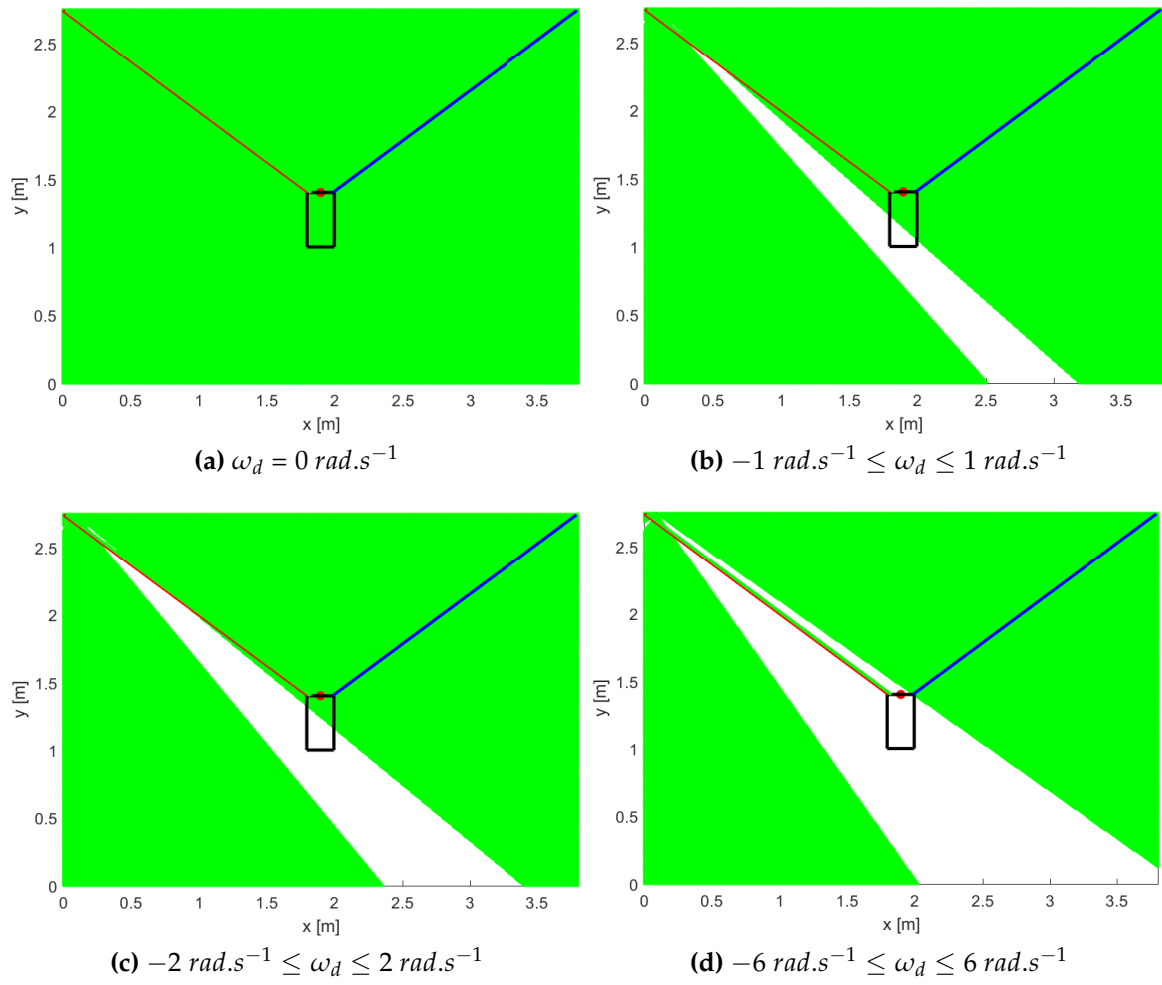
Figure 2.9: TFW of the CDPC with $-2.77\ m.s^{-1} \leq \dot{p}_x,\ \dot{p}_y \leq 2.77\ m.s^{-1}$

can counteract any external wrench of the specified set applied at a specific frame of the moving-platform.

In this section we compute the wrench-feasible workspace of a CDPR based on the state of the art of already-existing approaches. Furthermore, it determines the amplitudes of the orientation and translation of CDPRs while the robot remains in a static equilibrium. The WFW is an important means of estimating the CDPR capabilities and applications especially in the design and planning stage. Moreover, wrench closure workspace and static workspace can be considered as subdivisions of WFW. In [GG06; Gua+14; Rui+15], determination of WFW is detailed through different approaches.

Admissible Cable Tension and Minimum Degree of Constraint Satisfaction

For the moving-platform of the CDPC to remain in static equilibrium, it should satisfy the following two conditions. The first is that of static equilibrium expressed in Eq. (2.15). The second is to have cable tensions within the admissible bounds for any predefined external wrench, $\mathbf{w}_e$. Guay et al. in [Gua+14] introduced an index for evaluation of the latter conditions, namely, the Minimum Degree of Constraint Satisfaction (MDCS) which determines the degree of inclusion of $\mathscr{T}$ within $\mathscr{W}$.

$$\mathscr{T} = \left\{ \mathbf{t} \in \mathbb{R}^m \ : \mathbf{t}_{min} \le \mathbf{t} \le \mathbf{t}_{max} \right\} \tag{2.59}$$

where, $\mathscr{T}$ expresses the feasible tension and m and,

$$\mathscr{W} = \left\{ \mathbf{w}_e \in \mathbb{R}^n : \mathbf{w}_e = \sum_{j=1}^{n} \alpha_j \mathbf{w}_{e,j}, \ \sum_{j=1}^{n} \alpha_j = 1, \ \alpha_j \ge 0 \ \ j = 1, ..., n \right\} \tag{2.60}$$

$\mathscr{W}$ is the set of n-dimensional external wrench applied onto the moving-platform. The following steps express the evaluation of the MDCS:

1. Computing of the polytope vertices of the available cable tensions, $\mathscr{F}$, in the cable tension Space based on the maximum admissible cable tension, t_{max} and the minimum available cable tension, t_{min}.

$$\mathbf{t}_k = (\mathbf{1}_{m \times m} - \text{diag}(\boldsymbol{\beta}_k)) t_{min} + \text{diag}(\boldsymbol{\beta}_k)) t_{max} \quad k = 1, ..., q$$

Where, $\boldsymbol{\beta}_k$ is a binary representation of k and consists of m (number of cables) bits. k stands for the number of the vertices of available cable tension polytope in cable tension space and it consists of $q = 2^m$ vertices.

2. Mapping all the vertices, $\mathbf{t}_k$, onto the moving-platform wrench space from cable tension space.

$$\mathbf{w}_k = -\mathbf{W} \mathbf{t}_k \quad k = 1, ..., q$$

3. Computing of the polytope vertices of the required wrench (task wrench) in the wrench space.

$$\mathbf{j}_k = (\mathbf{1}_{m \times m} - \text{diag}(\beta_k)) \underline{\mathbf{w}} + \text{diag}(\beta_k)) \overline{\mathbf{w}} \quad k = 1, ..., q$$

4. Computing of the convex hull of the available wrench polytope, $\mathscr{W}$ by the Matlab *convhulln* function and computing of the facet equations:

$$\mathscr{W} = \{\mathbf{w} \in \mathbb{R}^n : \quad \mathbf{a}_l^T \mathbf{w} \le b_l \quad l = 1, ..., p\}$$

where, p is the number of facets of the convex hull,

5. Computing the degree of constraint satisfaction between j^{th} vertex of , $\mathbf{w}_{e,j}$, and l^{th} facet of , $\mathbf{a}_l^T \mathbf{w} = b_l$

$$s_{j,l} = (b_l - \mathbf{w}_{e,j}^T \mathbf{a}_l)/\|\mathbf{a}_l\|_2$$

where the degree of constraint satisfaction $s_{j,l}$ is the signed distance from vertex $\mathbf{w}_{e,j}$ of $\mathscr{F}$ to the l th face of $\mathscr{W}$.

6. Computation of the minimum degree of constraint satisfaction index.

$$s = \min_{j=1,...,n} (\min_{l=1,...,p} s_{j,l}) \tag{2.61}$$

The static workspace of the CDPC is illustrated for different cases of the payload of the moving-platform and maximum available cable tension in Fig. 2.10. The workspace analysis is carried out for the given specification of the CREATOR prototype, e.g., 4 m long and 2.75 m high of the fixed structure and 3.25 kg as the mass of the moving-platform. The boundaries of the static workspace is highlighted by the magenta lines and the other lines indicates the amplitude of the MDCS index.

2.2.3 Parasitic Inclinations

Parasitic inclination is defined as undesired orientation of the moving-platform that leads to inaccuracy in manipulation and positioning. Parasitic inclination is described as a property of lower mobility parallel mechanisms in [LGG16]. This kinematic situation is introduced due to use of cable-loop for remote actuation of the moving-platform in CDPRs. In general, by using a cable-loop in a CDPR, the pure translation of the moving-platform requires equal cable tensions on both sides of the drum of the cable-loop. Furthermore, the pure rotation of the end-effector is a result of the different tensions generated by two actuators. The cable-loop allows us to enlarge the orientation workspace of the manipulator at hand, but there exists an undesired rotation associated to the rotation of the moving-platform while different tensions applied on the cable-loops by the two actuators. Since parasitic inclination decreases the accuracy of the manipulator, its investigation is crucial and can be employed to minimize the parasitic inclination by optimizing the design parameters in the design stage. In this section, parasitic inclination is generically investigated for planar CDPRs with an articulated moving-platform through the cable-loop. Therefore, a simplified mock-up of CDPC moving-platform without the hoist mechanism (as shown in Fig. 2.11) is taken into account for the investigation of the parasitic inclinations.
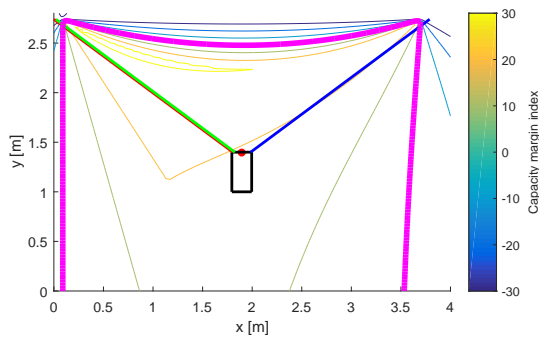
(a) Paylod mass= 0.5 Kg and t_{max} = 128 N
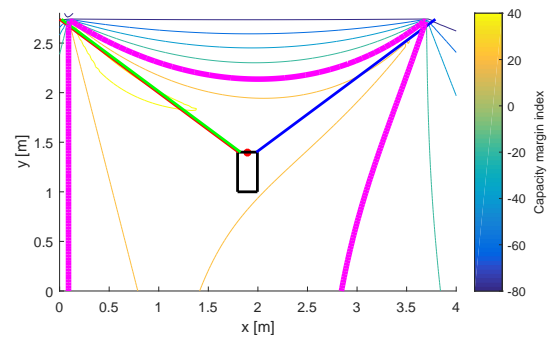
(b) Paylod mass= 5 Kg and t_{max} = 128 N
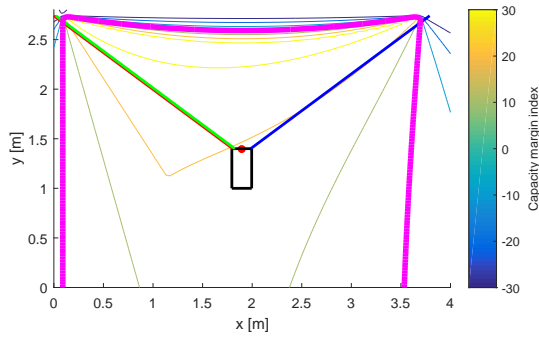
(c) Paylod mass= 0.5 Kg and t_{max} = 224 N
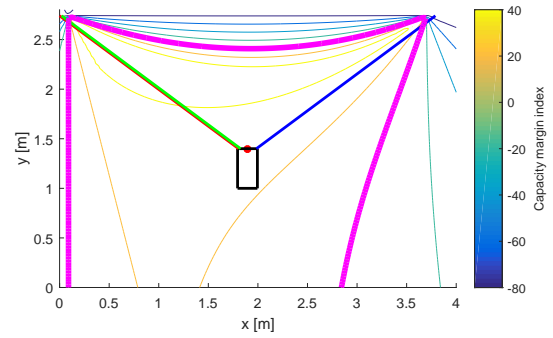
(d) Paylod mass= 5 Kg and t_{max} = 224 N

Figure 2.10: Boundary of the static workspace (magenta contours) of the CDPC for different payloads and maximum cable tensions
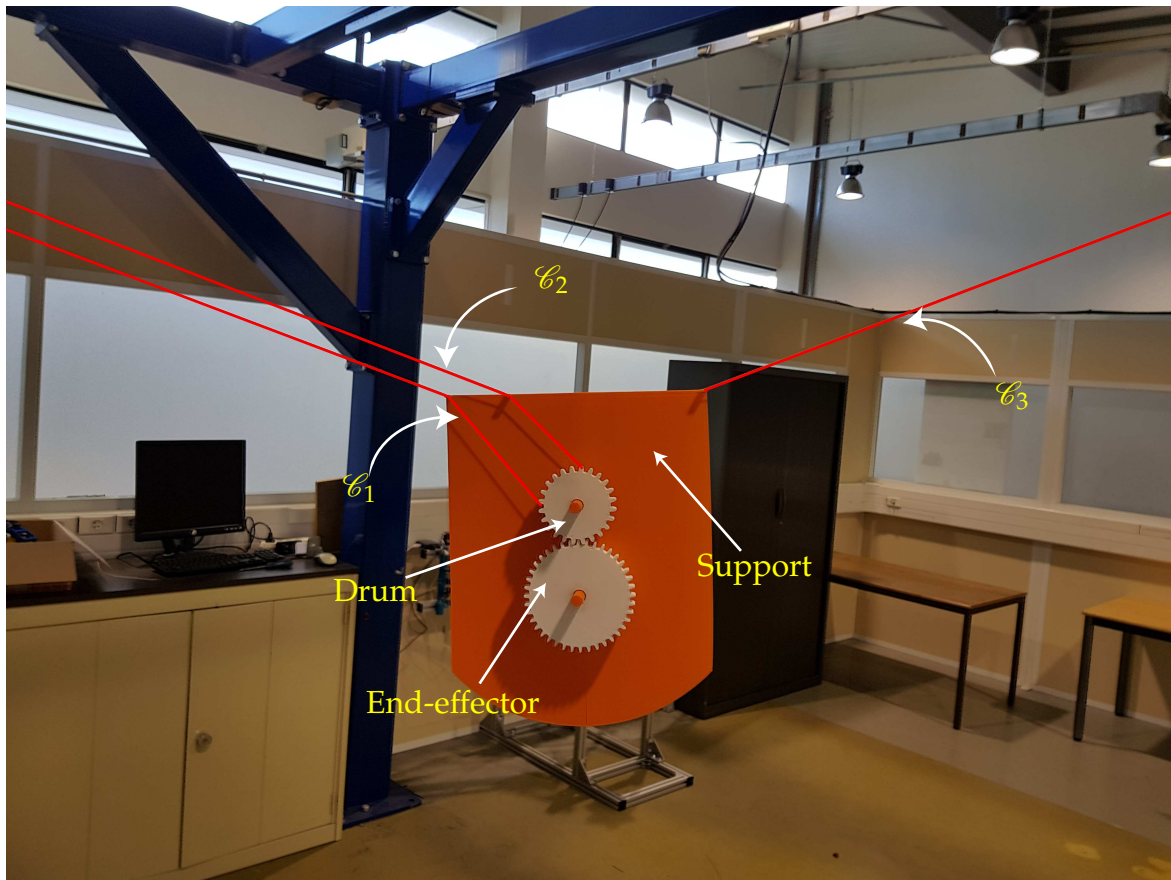
Figure 2.11: Articulated MP of a planar CDPR containing a cable loop

Two approaches are described in the section to determine the orientation of the articulated moving-platform and as a consequence its parasitic inclinations. The first approach aims at solving the kinetostatic model of the CDPR at hand, to find the orientation of the moving-platform for a given position of its geometric center. The second approach aims at approximating the orientation of the moving-platform without considering the kinetostatic model of the manipulator, but by using some geometric properties of the cable loop and the articulated moving-platform. Finally, the results obtained by the two approaches for a planar hybrid CDPR with one cable-loop system are compared.

Employing cable-loops in the design of the CDPRs has been the subject of some previous works, e.g. [KBR16; LDN16; Nag+12]. Nevertheless, to the best of the authors' knowledge, the parasitic inclination induced by cable-loops has not been addressed up to now. Hence, a planar four-DoF under-constrained CDPR with an articulated moving-platform is introduced and studied. The end-effector is actuated through a cable-loop, which enables the robot to obtain a modular pose determination, namely orientation and positioning. As a result, the mechanism under study has a drastically large orientation workspace in addition to the large translation workspace. It should be noted that some unwanted rotational motions of the moving-platform, namely, parasitic inclinations, arise due to the cable-loop. Finally, those parasitic inclinations are modeled and assessed for the mechanism at hand.

Description of the Manipulator under Study

The manipulator under study is similar to the CDPC up to some differences in its end-effector. The manipulator has a planar workspace with an articulated moving-platform which can host different types of end-effectors with one DoF as shown in Fig. 2.12. The planar manipulator possesses four-DoF while it is actuated by three motors through two cables. A cable (cable-loop) connected to two actuators as shown in the figure, is wound about the drum to make the latter rotate about its own axis. The cable-loop consists in two segments each with independent cable tension (t_1 and t_2). First segment, $\mathscr{C}_1$, is composed of the part of the cable-loop which connects the first motor to the drum through points A_1 and B_1. The second segment is denoted as $\mathscr{C}_2$ and connects the second motor to the drum through points A_2 and B_2.

The objective of this manipulator is to provide the underlying foundation for investigating the parasitic inclinations induced by cable-loops in CDPRs. Figure 2.13 illustrates the articulated moving-platform of the CDPR under study. This moving-platform is composed of a support, a drum and an end-effector. The support forms the overall body of the moving-platform and accommodates cable anchor points (B_1, B_2, B_3) and other components. The drum operates the end-effector through the cable-loop. Both the drum and the end-effector are gears such that the rotational motion of the end-effector is provided by the rotational motion of the drum.

Orientation of the moving-platform

Here, two methodologies for finding the orientation of the under-actuated moving-platform, e.g., θ (depicted in Fig. 2.13), for the given position of the moving-platform, namely, point D. In the first approach, the orientation angle θ is computed based on
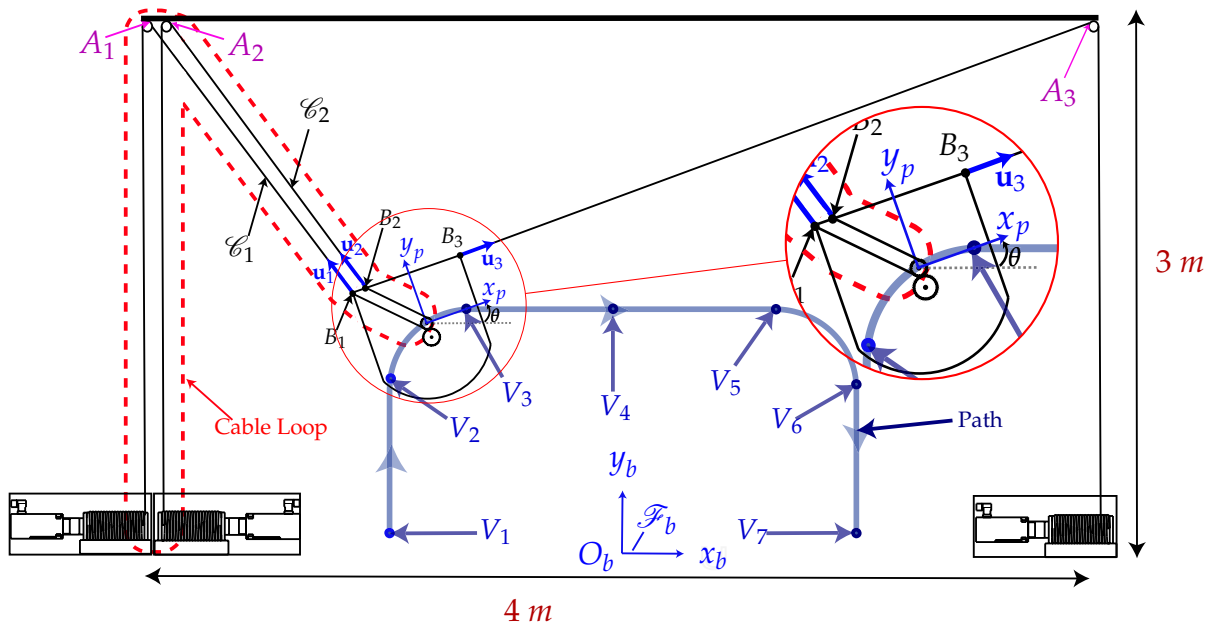
Figure 2.12: A four-DoF planar hybrid cable-driven parallel robot with a cable-loop system

loop closure equations (2.5) and static-equilibrium equation (2.15). The second approach aims at finding the orientation angle θ knowing the cable tension difference δt, and the Cartesian position coordinates of point P expressed in $\mathscr{F}_b$.

Orientation of the moving-platform obtained by Approach 1

In this section, the rotation angle θ of the moving-platform is obtained while considering the three loop-closure equations defined by Eq. (2.5) and the static-equilibrium equations of the moving-platform defined by Eq. (2.15). Accordingly, the following system of seven non-linear equations with nine unknowns, i.e., θ, t_1, t_2, t_3, l_1, l_2, l_3, d_x and d_y is expressed:

$$\begin{cases} f_1\left(\theta,\ t_1,\ t_2,\ t_3,\ l_1,\ l_2,\ l_3,\ d_x,\ d_y\right) & = 0 \\ f_2\left(\theta,\ t_1,\ t_2,\ t_3,\ l_1,\ l_2,\ l_3,\ d_x,\ d_y\right) & = 0 \\ f_3\left(\theta,\ t_1,\ t_2,\ t_3,\ l_1,\ l_2,\ l_3,\ d_x,\ d_y\right) & = 0 \\ f_4\left(\theta,\ t_1,\ t_2,\ t_3,\ l_1,\ l_2,\ l_3,\ d_x,\ d_y\right) & = 0 \\ \qquad f_5\left(\theta,\ d_x,\ d_y\right) & = 0 \\ \qquad f_6\left(\theta,\ d_x,\ d_y\right) & = 0 \\ \qquad f_7\left(\theta,\ d_x,\ d_y\right) & = 0 \end{cases} \tag{2.62}$$

f_1, f_2, f_3 and f_4 are obtained from Eq. (2.15) and they are functions of variables θ, t_1, t_2, t_3, l_1, l_2, l_3, d_x and d_y. The latter equations are expressed analytically as follows:

$$\begin{aligned} f_1 = {} & t_1 l_2 l_3 \left(a_{1x} - d_x - c_\theta b_{1x} + s_\theta b_{1y}\right) + t_2 l_1 l_3 \left(a_{2x} - d_x - c_\theta b_{2x} + s_\theta b_{2y}\right) \\ & + t_3 l_1 l_2 \left(a_{3x} - d_x - c_\theta b_{3x} + s_\theta b_{3y}\right) \end{aligned} \tag{2.63a}$$
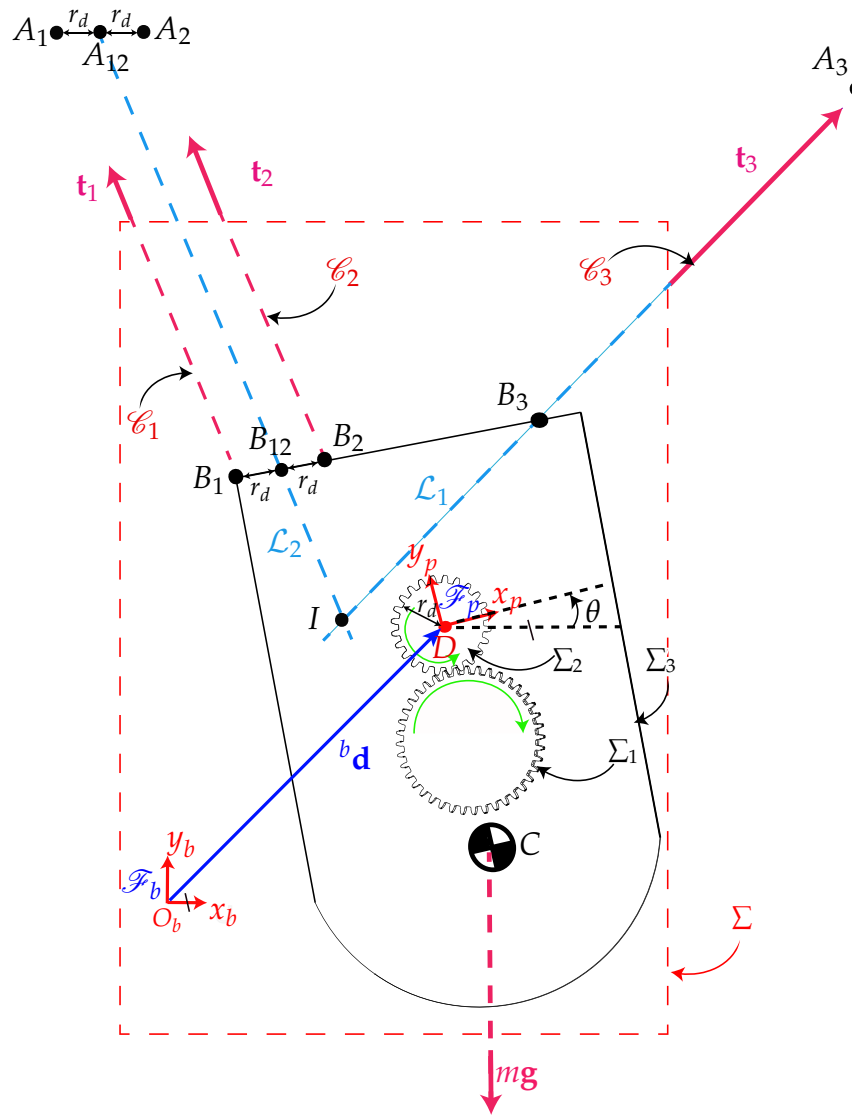
Figure 2.13: Moving-platform of the four-DoF planar under-constrained CDPR

$$f_2 = t_1 l_2 l_3 \left(a_{1y} - d_y - s_\theta b_{1x} - c_\theta b_{1y} \right) + t_2 l_1 l_3 \left(a_{2y} - d_y - s_\theta b_{2x} - c_\theta b_{2y} \right)$$
$$+ t_3 l_1 l_2 \left(a_{3y} - d_y - s_\theta b_{3x} - c_\theta b_{3y} \right) - l_1 l_2 l_3 \ mg \quad\quad\text{(2.63b)}$$

$$f_3 = t_1 l_2 l_3 \left(-s_\theta b_{1x} - c_\theta b_{1y} \right) \left(a_{1x} - d_x - c_\theta b_{1x} + s_\theta b_{1y} \right)$$
$$+ t_1 l_2 l_3 \left(c_\theta b_{1x} - s_\theta b_{1y} \right) \left(a_{1y} - d_y - s_\theta b_{1x} - c_\theta b_{1y} \right)$$
$$+ t_2 \, l_1 l_3 \left(-s_\theta b_{2x} - c_\theta b_{2y} \right) \left(a_{2x} - d_x - c_\theta b_{2x} + s_\theta b_{2y} \right)$$
$$+ t_2 \, l_1 l_3 \left(c_\theta b_{2x} - s_\theta b_{2y} \right) \left(a_{2y} - d_y - s_\theta b_{2x} - c_\theta b_{2y} \right)$$
$$+ t_3 l_1 l_2 \left(-s_\theta b_{3x} - c_\theta b_{3y} \right) \left(a_{3x} - d_x - c_\theta b_{3x} + s_\theta b_{3y} \right)$$
$$+ t_3 l_1 l_2 \left(c_\theta b_{3x} - s_\theta b_{3y} \right) \left(a_{3y} - d_y - s_\theta b_{3x} - c_\theta b_{3y} \right) - l_1 l_2 l_3 \ mg \left(c_x \, c_\theta - c_y \, s_\theta \right)$$
$$\text{(2.63c)}$$

$$f_4 = (t_2 - t_1) r_d + m_{fr} \quad\quad\text{(2.63d)}$$

where $s_\theta = \sin(\theta)$ and $c_\theta = \cos(\theta)$ and $^p\mathbf{c} = \begin{bmatrix} c_x, & c_y \end{bmatrix}^T$ is the Cartesian coordinate vector of the CoM expressed in $\mathscr{F}_p$. f_5, f_6 and f_7 are obtained from Eq. (2.5) and they are functions of variables θ, d_x and d_y. These equations are expressed analytically as follows:

$$f_5 = l_1^2 - \left(a_{1x} - d_x - c_\theta b_{1x} + s_\theta b_{1y} \right)^2 - \left(a_{1y} - d_y - s_\theta b_{1x} - c_\theta b_{1y} \right)^2 \quad\text{(2.64a)}$$

$$f_6 = l_2^2 - \left(a_{2x} - d_x - c_\theta b_{2x} + s_\theta b_{2y} \right)^2 - \left(a_{2y} - d_y - s_\theta b_{2x} - c_\theta b_{2y} \right)^2 \quad\text{(2.64b)}$$

$$f_7 = l_3^2 - \left(a_{3x} - d_x - c_\theta b_{3x} + s_\theta b_{3y} \right)^2 - \left(a_{3y} - d_y - s_\theta b_{3x} - c_\theta b_{3y} \right)^2 \quad\text{(2.64c)}$$

The under-determined system of non-linear equations (2.62) is studied for a given $^b\mathbf{d}$. As a result, a system consisting in seven equations and seven unknowns is obtained. The *lsqnonlin* ©Matlab function is used to solve this system of seven non-linear equations. It should be noted that the following constraints are taken into account for solving the system of equations in order to make sure that cable tensions are positive:

$$t_i > 0 \quad i = 1, \ 2, \ 3 \quad\quad\text{(2.65)}$$

Orientation of the moving-platform obtained by Approach 2

The second method presents a straightforward approach that enables us to obtain a sound approximation of the orientation of the moving-platform without considering the kinetostatic model expressed in Eq. (2.15). This approach takes into account only the equilibrium of the moments applied or sustained about the Instantaneous Center of Rotation (ICR) point regardless of the cables tensions (t_1, t_2, t_3), but the difference of cable-loop tensions, namely, δt. In Fig. 2.13, all the relevant notations are illustrated. The ICR point, I, is a function of θ, $^b\mathbf{d}$, $^b\mathbf{a}_i$ and $^p\mathbf{b}_i$, $i = 1, \ 2, \ 3$. The following equation expresses the equilibrium of the moments applied or sustained about the ICR, point I, expressed in $\mathscr{F}_b$.

$$m_{12} + m_w = 0 \qu\quad\text{(2.66)}$$

m_{12} is the moment applied onto the moving-platform at point I due to cable tension difference δt in the cable-loop. Then, moment m_{12} can be expressed as follows:

$$m_{12} = r_d \delta t \tag{2.67}$$

m_w is the moment applied onto the moving-platform expressed at point I due to the moving-platform weight, which is passing through point H.

$$m_w = (^b\mathbf{c} - {}^b\mathbf{i})^T \mathbf{E}^T m\mathbf{g} \tag{2.68}$$

under the assumption that segments A_1B_1 and A_2B_2 are parallel, which is valid as long as the moving-platform is far from the points A_1 and A_2. In this approach the Cartesian coordinate vector point I, $^b\mathbf{i}$, is computed to formulate the pure rotation of the moving-platform about this point.

ICR is the intersection point between the line $\mathcal{L}_{12}$ passing through points A_{12} and B_{12} and the line $\mathcal{L}_3$ passing through points A_3 and B_3. The equations of lines $\mathcal{L}_{12}$ and $\mathcal{L}_3$ are expressed as:

$$\mathcal{L}_{12}: \quad x(b_{12y} - a_{12y}) + y(a_{12x} - b_{12x}) - a_{12x}b_{12y} + a_{12y}b_{12x} = 0 \tag{2.69}$$

$$\mathcal{L}_3: \quad x(b_{3y} - a_{3y}) + y(a_{3x} - b_{3x}) - a_{3x}b_{3y} + a_{3y}b_{3x} = 0 \tag{2.70}$$

The Cartesian coordinate vectors of points A_{12} and B_{12}, namely, $^b\mathbf{a}_{12} = [a_{12x},\ a_{12y}]^T$ and $^b\mathbf{b}_{12} = [b_{12x},\ b_{12y}]^T$ are the followings:

$$^b\mathbf{a}_{12} = \frac{1}{2}(^b\mathbf{a}_1 + {}^b\mathbf{a}_2) \tag{2.71}$$

$$^b\mathbf{b}_{12} = \frac{1}{2}(^b\mathbf{b}_1 + {}^b\mathbf{b}_2) = {}^b\mathbf{d} + \frac{1}{2}{}^b\mathbf{R}_p(^p\mathbf{b}_1 + {}^p\mathbf{b}_2) \tag{2.72}$$

$^b\mathbf{i}$ being the Cartesian coordinate vector of the intersection point of lines $\mathcal{L}_{12}$ and $\mathcal{L}_3$, i.e., $^b\mathbf{i} \equiv \mathcal{L}_{12} \cap \mathcal{L}_3$, the components of its Cartesian coordinate vector take the form:

$$^b\mathbf{i} = [i_x,\ i_y]^T \tag{2.73}$$

with i_x and i_y being expressed as:

$$i_x = \frac{\mu_1 \nu_2 - \mu_2 \nu_1}{\lambda_1 \mu_2 - \lambda_2 \mu_1}, \quad i_y = \frac{-\nu_1 - \lambda_1 i_x}{\mu_1} \tag{2.74}$$

with

$$
\begin{aligned}
\lambda_1 &= \frac{1}{2}c_\theta(b_{1y} + b_{2y}) + \frac{1}{2}s_\theta(b_{1x} + b_{2x}) - \frac{1}{2}(a_{1y} - a_{2y}) + d_y \\
\lambda_2 &= b_{3x}s_\theta + b_{3y} - a_{3y}c_\theta - a_{3y} + d_y \\
\mu_1 &= -\frac{1}{2}c_\theta(b_{1x} + b_{2x}) + \frac{1}{2}s_\theta(b_{1y} + b_{2y}) + \frac{1}{2}(a_{1x} + a_{2x}) - d_x \\
\mu_2 &= b_{3y}s_\theta - b_{3x}c_\theta + a_{3x} - d_x \\
\nu_1 &= \frac{1}{4}c_\theta[(-a_{1x} - a_{2x})(b_{1y} + b_{2y}) + (b_{1x} + b_{2x})(a_{1y} + a_{2y})] \\
&\quad + \frac{1}{4}s_\theta[(-a_{1x} - a_{2x})(b_{1x} + b_{2x}) - (b_{1y} + b_{2y})(a_{1y} + a_{2y})] \\
&\quad - \frac{1}{2}d_y(a_{1x} - a_{2x}) + \frac{1}{2}d_x(a_{1y} - a_{2y}) \\
\nu_2 &= (a_{3y}b_{3x} - a_{3x}b_{3y})c_\theta - (a_{3x}b_{3x} + a_{3y}b_{3y})s_\theta - a_{3x}d_y + a_{3y}d_x
\end{aligned}
\tag{2.75}
$$

The Weierstrass substitution in Eq. (2.76) is employed in order to obtain an algebraic expression of the θ.

$$
\sin\theta = \frac{2t_\theta}{1 + t_\theta^2}, \quad \cos\theta = \frac{1 - t_\theta^2}{1 + t_\theta^2}
\tag{2.76}
$$

and,

$$
t_\theta = \tan\frac{\theta}{2}
\tag{2.77}
$$

from Eqs. (2.73)-(2.77) we can rewrite Eq. (2.66) as follows:

$$
C_6 t_\theta^6 + C_5 t_\theta^5 + C_4 t_\theta^4 + C_3 t_\theta^3 + C_2 t_\theta^2 + C_1 t_\theta + C_0 = 0
\tag{2.78}
$$

The resulting *6th* order univariate polynomial is a function of t_θ and it is solved numerically to find t_θ. θ can then be substituted with t_θ based on Eq. (2.97). The coefficients of the latter polynomial, $C_0, C_1, ..., C_6$, are detailed in link [2]. Equation (2.78) is solved in order to find the possible inclination(s) θ of the moving-platform for the given position of the moving-platform, namely, point D.

Formulation of the Parasitic Inclinations

This section deals with the determination of the parasitic inclination, θ_p, of the moving-platform due to cable tension differences, δt, into the cable-loop. Accordingly, the following methodology is defined:

1. In order to determine the natural inclination θ_n of the moving-platform. θ_n amounts to the rotation angle θ of the moving-platform obtained with both Approaches 1 and 2 described in Secs. 4.1 and 4.2, resp., for the same tensions in both strands $\mathscr{C}_1$ and $\mathscr{C}_2$ of the cable-loop, i.e., $\delta t = 0$.

---

[2]http://tiny.cc/c8muez

Table 2.2: Design parameters of the CDPC

Anchor point coordinates [m]	Other parameters
${}^{b}\mathbf{a}_2 = [-1.97,\ 3]^T$	$r_d = 0.03$ [m]
${}^{b}\mathbf{a}_3 = [2,\ 3]^T$	${}^{p}\mathbf{c} = [0,\ -0.3]^T$ [m]
${}^{p}\mathbf{b}_1 = [-0.28,\ 0.25]^T$	
${}^{p}\mathbf{b}_2 = [-0.22,\ 0.25]^T$	
${}^{p}\mathbf{b}_3 = [0.25,\ 0.25]^T$	

2. To determine the inclination θ_m of the moving-platform when tensions in both strands of the cable-loop are not the same, i.e., $\delta t \neq 0$. θ_m can be also computed with Approaches 1 and 2 in this section.

3. To determine the parasitic inclination, θ_p of the moving-platform. θ_p is the difference between θ_m and θ_n, i.e.,

$$\theta_p = \theta_m - \theta_n \tag{2.79}$$

Case study

The rotation angle θ and the parasitic inclination θ_p are computed in this section along a given path for the design parameters given in Tab. 2.2 of the four-DoF planar cable-driven parallel robot with a cable loop shown in Fig. 2.12. Eq. (2.80) expresses the Cartesian coordinates vector of seven via-points, namely, $V_1,...,V_7$, on the prescribed path (blue path in Fig. 2.12).

$$
{}^{b}\mathbf{v}_1 = \begin{bmatrix} -1 \\ 0 \end{bmatrix}, \qquad
{}^{b}\mathbf{v}_2 = \begin{bmatrix} -1 \\ 0.65 \end{bmatrix}, {}^{b}\mathbf{v}_3 = \begin{bmatrix} -0.65 \\ +1 \end{bmatrix}, \qquad
{}^{b}\mathbf{v}_4 = \begin{bmatrix} 0 \\ +1 \end{bmatrix}
$$

$$
{}^{b}\mathbf{v}_5 = \begin{bmatrix} 0.65 \\ +1 \end{bmatrix}, \qquad
{}^{b}\mathbf{v}_6 = \begin{bmatrix} +1 \\ 0.65 \end{bmatrix}, {}^{b}\mathbf{v}_7 = \begin{bmatrix} +1 \\ 0 \end{bmatrix} \tag{2.80}
$$

Figure 2.14 shows the natural inclinations θ_{n1} and θ_{n2} of the previous case study obtained with approaches 1 and 2 along the prescribed path, respectively. The difference between θ_{n2} and θ_{n1} along the prescribed path is also depicted in Fig. 2.14. It appears that both approaches 1 and 2 give similar results, which confirms the soundness of the assumption made in approach 2. Figure 2.15 shows the rotation angle θ_{m1} and θ_{m2} of the moving-platform obtained with approaches 1 and 2, respectively, along the prescribed path, for $\delta t = 20$ N. Finally, Fig. 2.16 illustrates the
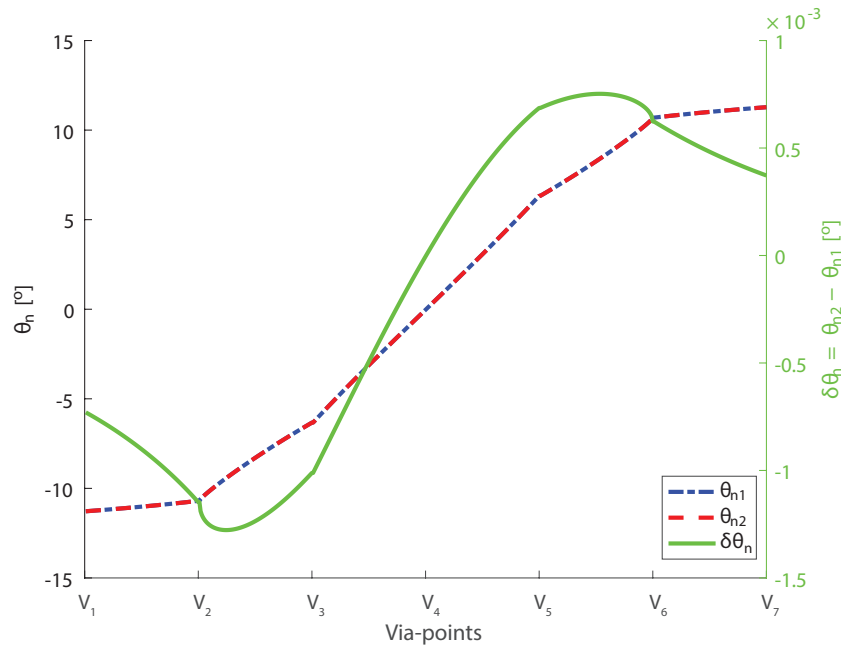
Figure 2.14: Natural inclinations θ_{n1} and θ_{n2} of the moving-platform obtained with Approaches 1 and 2 along a prescribed path

parasitic inclination θ_p of the moving-platform for different values of the cable tension difference δt into the cable-loop. It should be noted that θ_p increases with δt. This confirms the link between δt in the cable loop and the parasitic inclination of the moving-platform.

Overall, the approach proposed in section 2.2.3 yields consistent results and can be applied to determine the parasitic inclination. Furthermore, this approach can be used to design the robot with respect to its parasitic inclination. This contributes to better control and more accurate positioning.

The simulation results of CDPC is presented in Fig. 2.17 for the given position of point P. Figure 2.17 illustrates the inclination of the moving-platform with and without applied moment on the hoist. Moreover, the parasitic inclinations and the cable tensions are depicted in the figure.

We showed that the moving-platform undergoes some parasitic inclinations that are due to the presence of a cable-loop. Moreover, an analytical method to find the orientation of the moving-platform is presented. This method is validated by comparing its results with the solution to the kinetostatic equations of the robot. Then, an approach was established to isolate the parasitic inclination induced by the cable loop only from the natural inclination of the moving-platform.

Modified Parasitic inclinations

This section presents a generic analytical approach towards calculation of parasitic inclination for under-constrained CDPRs. Therefore, the investigation on the undesired orientation of the moving-platform in presence of a pure moment applied on the end-effector is studied. Figure 2.18 shows the schematic model of a generic planar suspended CDPR with all the required notations. The angles between the
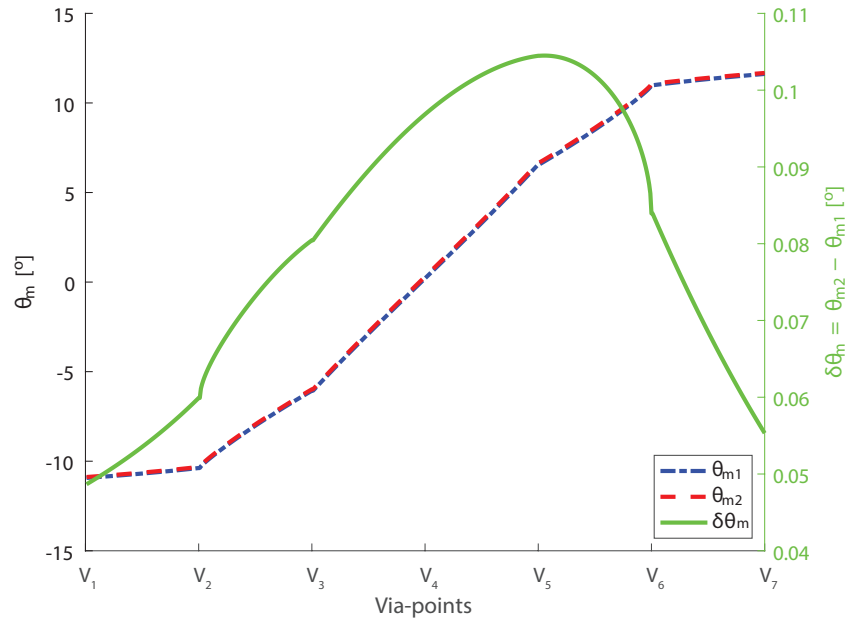
Figure 2.15: Rotation angle θ_{m1} and θ_{m2} of the moving-platform obtained with Approaches 1 and 2 for $\delta t = 20$ N.
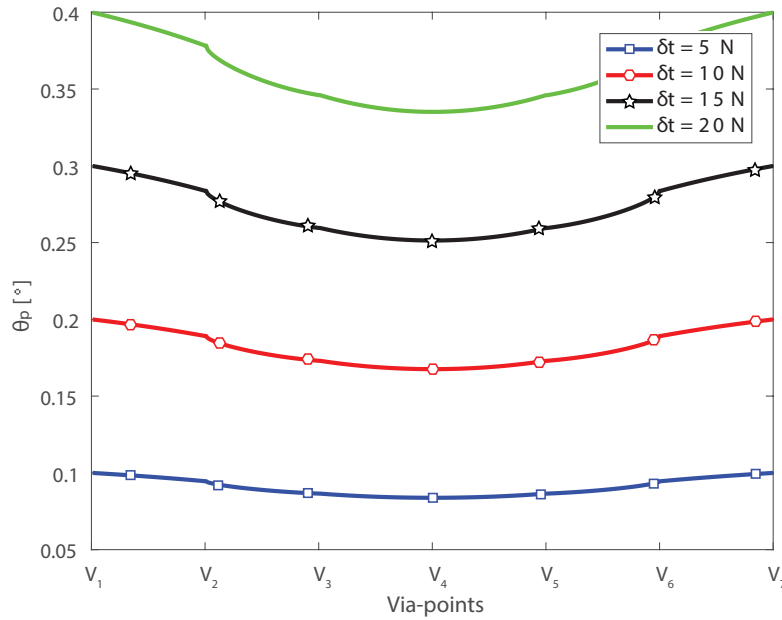
Figure 2.16: Parasitic inclination θ_p of the moving-platform for different values of the cable tension difference δt into the cable-loop

ceiling and both cables, namely, θ_1 and θ_2, are calculated as follows while assuming that the size of the moving-platform is much smaller than the overall dimensions of
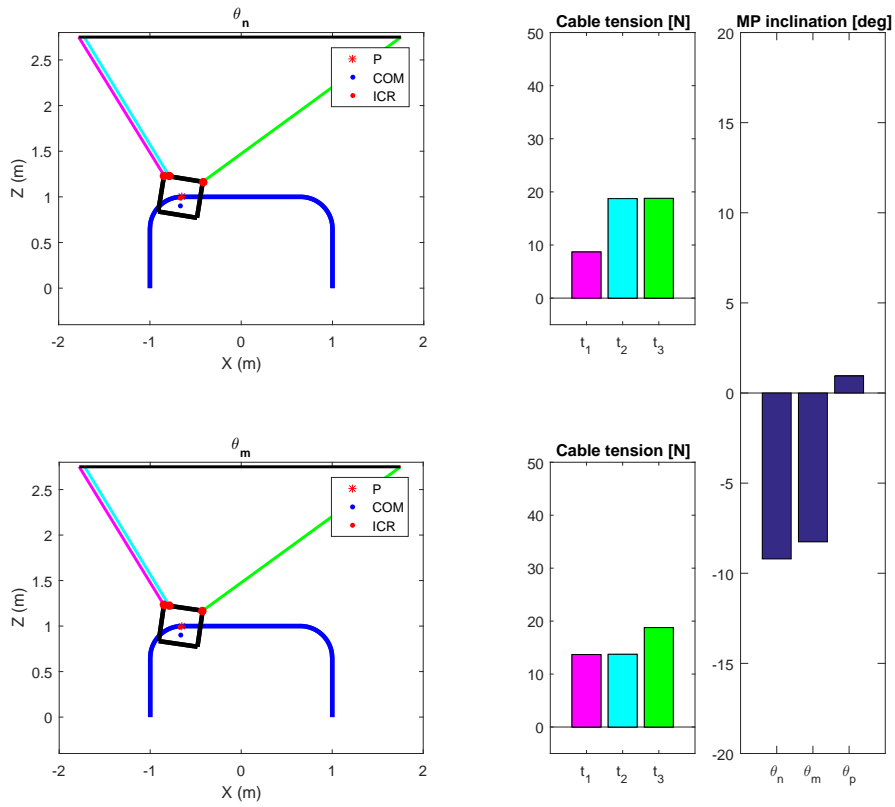
(a) $P=V_3$
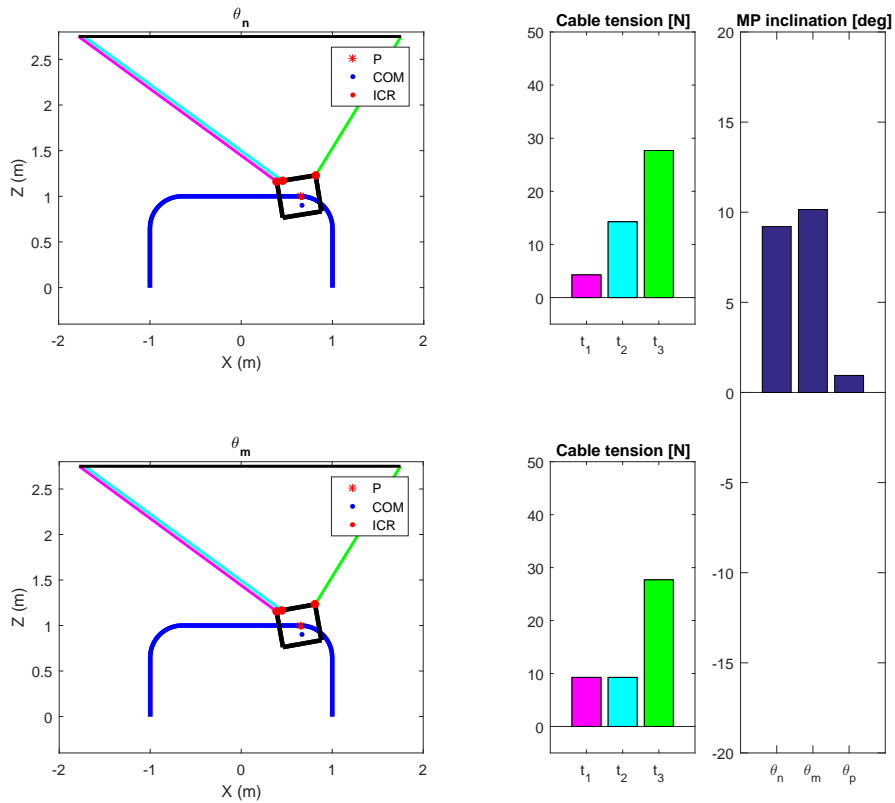
(b) $P=V_5$

Figure 2.17: Parasitic inclination of the moving-platform along the test path

(a) Manipulator   **(b)** Moving-platform
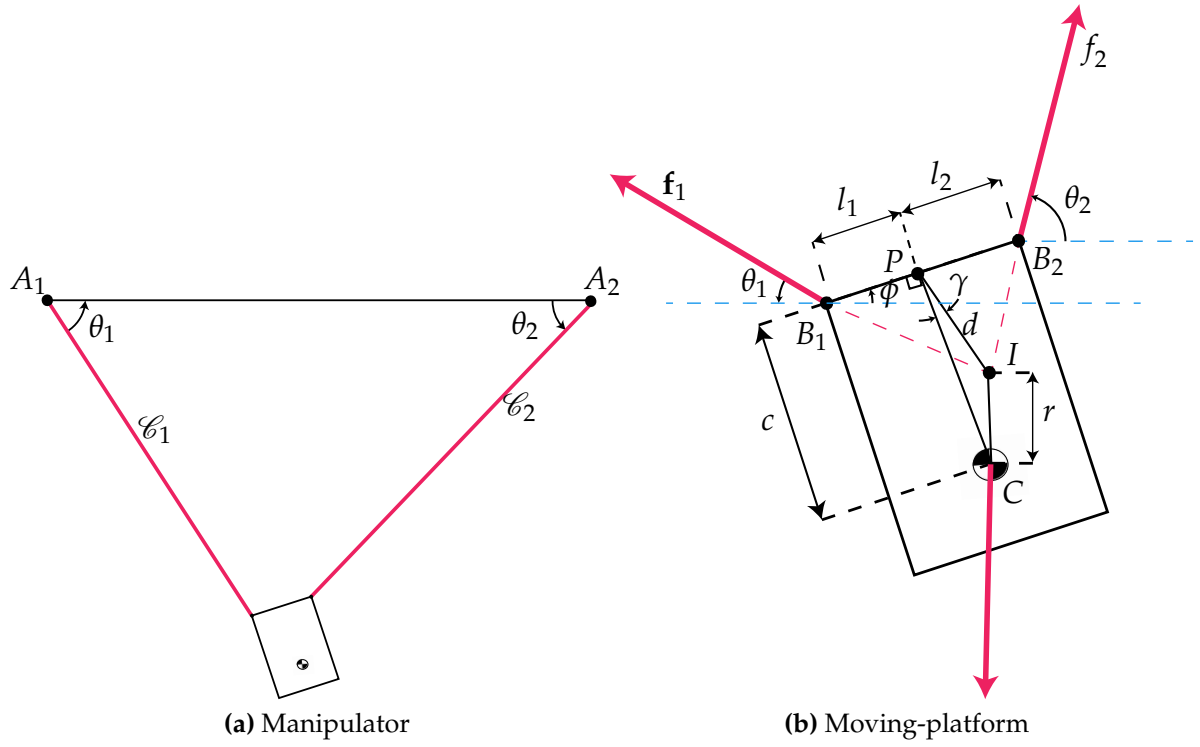
Figure 2.18: Schematics of a planar suspended under-constrained CDPR

the cable suspended manipulator.

$$\tan \theta_1 + \frac{y}{\frac{w}{2} + x} = 0 \tag{2.81}$$

$$\tan \theta_2 + \frac{y}{\frac{w}{2} - x} = 0 \tag{2.82}$$

Eqs. (2.81 and 2.82) are rewritten as follows:

$$\tan \theta_1 = \frac{2y}{w + 2x} \tag{2.83}$$

$$\tan \theta_2 = -\frac{2y}{w - 2x} \tag{2.84}$$

In order to perform a generic calculation of the parasitic inclination regardless of the moving-platform Cartesian coordinates, we normalize the previous equations according to the followings substitutions.

$$x = \tilde{\zeta} w \tag{2.85}$$

$$y = \psi w \tag{2.86}$$

Hereafter, Eqs. (2.83) and (2.84) are rewritten as below:

$$\tan \theta_1 = -\frac{2\psi}{2\tilde{\zeta} + 1} \tag{2.87}$$

$$\tan \theta_2 = \frac{2\psi}{2\xi - 1} \tag{2.88}$$

We then proceed with the computation of ϕ from the equation of the equilibrium. Figure 2.18b illustrates the free body diagram of the moving-platform with all the forces applied on it. The equilibrium of those forces are expressed in the following.

$$\mathbf{t} + m\mathbf{g} = 0 \tag{2.89}$$

with $\mathbf{t} = [t_1, \ t_2]^T$, m being the mass of the moving-platform and $\mathbf{g} = [0, \ -g]^T$ is the gravity acceleration with $g = 9.81 \ m.s^{-2}$. The equilibrium of forces applied onto the moving-platform in the x direction can be extracted from Eq. (2.89) as follows:

$$- t_1 \cos \theta_1 + t_2 \cos \theta_2 = 0. \tag{2.90}$$

We then formulate the equilibrium of the moments about point D,

$$\sum_{i=1}^{2} \left(({}^p b_i - {}^p c)^T \mathbf{E}^{Tp} \mathbf{t}_i \right) = 0. \tag{2.91}$$

We can eliminate the cable tensions t_1 and t_2 from Eqs. (2.90) and (2.91) as follows:

$$h \cos \theta_1 \cos(\phi - \theta_2) + l_2 \cos \theta_1 \sin(\phi - \theta_2) - h \cos \theta_2 \cos(\phi + \theta_1)$$
$$+ l_1 \cos \theta_2 \sin(\phi + \theta_1) = 0. \tag{2.92}$$

Let us perform the following substitution in order to deal with non-dimensional variables.

$$\eta = \frac{c}{l}, \quad \lambda_1 = \frac{l_1}{l}, \quad \lambda_2 = \frac{l_2}{l}, \tag{2.93}$$

where, $l = l_1 + l_2$. Then, Eq. (2.92) is rewritten as follows:

$$\eta \cos \theta_1 \cos(\phi - \theta_2) + \lambda_2 \cos \theta_1 \sin(\phi - \theta_2) - \eta \cos \theta_2 \cos(\phi + \theta_1)$$
$$+ \lambda_1 \cos \theta_2 \sin(\phi + \theta_1) = 0 \tag{2.94}$$

By substituting the tangent half-angle substitution expressed in Eq. (2.95) into Eq. (2.94), the angle $u(\phi)$ is formulated as mentioned in Eq. (2.75).

$$\sin \phi = \frac{2u}{1 + u^2}, \quad \cos \phi = \frac{1 - u^2}{1 + u^2} \tag{2.95}$$

$$u = \pm [-4\xi^2 \lambda_1 - 4\xi^2 \lambda_2 - 4\eta\psi + \lambda_1 + \lambda_2 - ((\lambda_1 + \lambda_2^2)(16\xi^4 + 16\xi^2\psi^2 - 8\xi^2 + 1)$$
$$+ (\lambda_1 + \lambda_2)(\eta\psi\xi^2 - 8\eta\psi) - 16\psi^2\xi(\lambda_1^2 - \lambda_2^2) + 4\psi^2(\lambda_1 - \lambda_2)^2)^{\frac{1}{2}}] \tag{2.96}$$
$$(2\psi(2\xi\lambda_1 + 2\xi\lambda_2 - \lambda_1 + \lambda_2))^{-1}$$

Equation (2.96) above yields the solutions for u while, $\xi > -0.5$ and $\xi < 0.5$. The relation between angle ϕ and its substitution is expressed as follows:

$$u = \tan \frac{\phi}{2}. \tag{2.97}$$
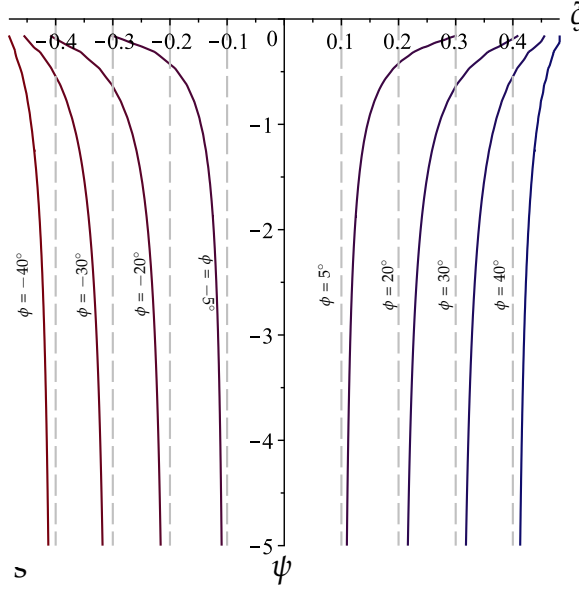
Figure 2.19: Contour-plot and asymptote of ϕ as a function of ξ and ψ

For further investigation we define a numerical example and trace the angle ϕ over a reasonable interval as follows:

$$\eta = \frac{1}{2}, \quad \lambda_1 = \frac{1}{2}, \quad \lambda_2 = \frac{1}{2} \tag{2.98}$$

We trace the contours of ϕ calculated as functions of ξ and ϕ in Eq. (2.96). The dash-lines are the asymptotes corresponding to each contour shown in Fig. 2.19. Apparently, below a certain height, i.e., below a certain value of ψ, the angle ϕ becomes independent of ψ. By substituting $\psi = -\infty$ into Eq. (2.96), ϕ follows the curve shown in Fig. 2.20

Parasitic inclination when a parasitic pure moment is applied on the end-effector

The sine law is applied to the triangles B_1PI and B_2PI, which yields

$$\frac{l_1}{\cos(\phi + \gamma + \theta_1)} - \frac{d}{\sin(\phi + \theta_1)} = 0 \tag{2.99}$$

and

$$\frac{l_2}{\cos(\phi + \gamma - \theta_2)} + \frac{d}{\sin(\phi - \theta_2)} = 0. \tag{2.100}$$

The sine law is applied to triangle CDI as follows:

$$\frac{r}{\sin \gamma} - \frac{c}{\sin \gamma + \phi} = 0. \tag{2.101}$$

Let us eliminate d from the Eqs. (2.99) and (2.100):

$$\frac{l_1 \sin(\phi - \theta_1)}{\cos(\phi + \gamma - \theta_1)} + \frac{l_2 \sin(\phi - \theta_2)}{\cos(\phi + \gamma - \theta_2)} = 0, \tag{2.102}$$
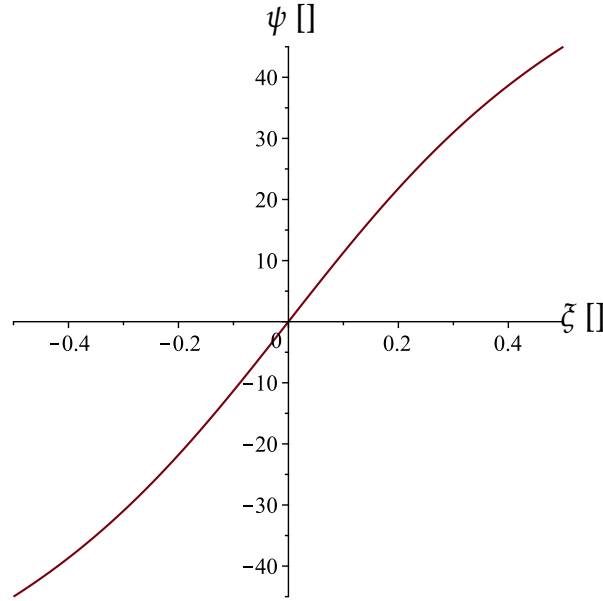
Figure 2.20: Contour-plot of ϕ as a function of ξ and ψ

$$l_2 \sin\left(-\theta_2 + \phi\right) \cos\left(-\theta_1 + \phi + \gamma\right) + l_1 \sin\left(-\theta_1 + \phi\right) \cos\left(-\theta_2 + \phi + \gamma\right) = 0. \quad (2.103)$$

We perform the half-tangent substitution for γ into Eq. (2.100) as follows:

$$\sin\gamma = \frac{2s}{1+s^2}, \quad \cos\gamma = \frac{1-s^2}{1+s^2}, \quad (2.104)$$

and Eq. (2.100) is rewritten as follows:

$$\cos\phi^2(\sin\theta_2 l_2(s-1)(s+1)\cos\theta_1 + \sin\theta_1((s^2 l_1 - l_1)\cos\theta_2 - 2\,s\sin\theta_2(l_1 + l_2)))$$
$$- (l_1 + l_2)\sin(\phi)((s^2\cos\theta_2 - 2\,s\sin\theta_2 - \cos\theta_2)\cos\theta_1 - \sin(\theta_1)(2\,s\cos\theta_2$$
$$+ \sin\theta_2(s^2 - 1)))\cos\phi - ((2\,s(l_1 + l_2)\cos\theta_2 + \sin\theta_2 l_1(s-1)(s+1))\cos\theta_1$$
$$+ \cos\theta_2 \sin\theta_1 l_2(s-1)(s+1))(\sin\phi)^2 = 0.$$

$$(2.105)$$

By applying the latter half-tangent substitution into Eq. (2.101), we obtain:

$$2rs\cos\phi - rt^2\sin\phi - 2ht + r\sin\phi = 0. \quad (2.106)$$

We can generate two new equations by multiplying Eqs. (2.105) and (2.106) with s as follows:

$$s(\cos\phi^2(\sin\theta_2 l_2(s-1)(s+1)\cos\theta_1 + \sin\theta_1((s^2 l_1 - l_1)\cos\theta_2 - 2\,s\sin\theta_2(l_1 + l_2)))$$
$$- (l_1 + l_2)\sin(\phi)((s^2\cos\theta_2 - 2\,s\sin\theta_2 - \cos\theta_2)\cos\theta_1 - \sin(\theta_1)(2\,s\cos\theta_2$$
$$+ \sin\theta_2(s^2 - 1)))\cos\phi - ((2\,s(l_1 + l_2)\cos\theta_2 + \sin\theta_2 l_1(s-1)(s+1))\cos\theta_1$$
$$+ \cos\theta_2 \sin\theta_1 l_2(s-1)(s+1))(\sin\phi)^2) = 0,$$

$$(2.107)$$
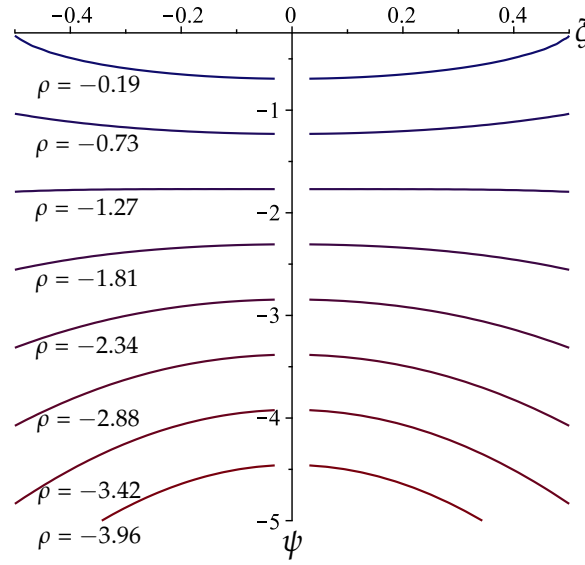
Figure 2.21: Contours of ρ over ξ and ψ

and

$$2srs\cos\phi - rt^2\sin\phi - 2ht + r\sin\phi = 0. \tag{2.108}$$

We then write the system of equations in matrix form, which gives

$$\mathbf{A}_m\mathbf{t}_v = \mathbf{0}_4, \tag{2.109}$$

where $\mathbf{A}_m$ is a 4×4 matrix of coefficients, its rows corresponding to Eqs. (2.105-2.108), and

$$\mathbf{t}_v = \begin{bmatrix} s^3 & s^2 & s & 1. \end{bmatrix}^T \tag{2.110}$$

By solving Eq. (2.109), we obtain the following solution:

$$\begin{aligned}
&2\,c((l_1 + l_2)\,(\sin(\theta_1)\cos(\theta_2) - \sin(\theta_2)\cos(\theta_1))\,(\cos(\phi))^2 + \sin(\phi)\,(l_1 + l_2) \\
&(\cos(\theta_2)\cos(\theta_1) + \sin(\theta_1)\sin(\theta_2))\cos(\phi) - l_2\cos(\theta_2)\sin(\theta_1) \\
&+ l_1\cos(\theta_1)\sin(\theta_2)) = 0
\end{aligned} \tag{2.111}$$

For the numerical example expressed in Eq. (2.98), the contours of ρ over ξ and ψ are plotted in Fig. 2.21. The normalized form of r (distance between points I and C) is defined as:

$$\rho = \frac{r}{l}, \tag{2.112}$$

where $l = l_1 + l_2$.

2.2.4   Required Height of the Ceiling for a Given Payload

The geometry parameters and the fixed structure of CDPCs have an important influences on the performance and workspace size of these manipulators. Therefore, an analysis is proposed to calculate the minimum height of anchor points based on the task requirements. This analysis provides a relation between task specification

and the geometry of the manipulator structure. It should provide insight at early design stages.

In this section, we study the minimum required height of the CDPC for manipulating a given payload. In general, suspended CDPRs are incapable of performing tasks close to their exit points, i.e., the larger part of their workspace is usually closer to the ground for a given external wrench. Here, we elaborate a method that approximates the required height of the CDPC for lifting a given payload within its workspace. The analytical results are based on the hypothesis of a constant orientation ($\theta = 0$) within its workspace. If the input torques to the two ends of the cable loop ($\mathscr{C}_1$, $\mathscr{C}_2$) are equal, then the cable-loop will behave as a single cable, $\mathscr{C}_{12}$, connecting points A_{12} to B_{12} as depicted in Fig. 2.13.

The set $\mathscr{T}$ forms the feasible tension box in the two-dimensional space as follows:

$$\mathscr{T} = \{\mathbf{t} \in \mathbb{R}^2 : \mathbf{t}_{min} \le \mathbf{t} \le \mathbf{t}_{max}\}. \tag{2.113}$$

The static workspace of the CDPC is defined as the set of all the positions of the moving-platform point P where the corresponding cable tensions are within the specified cable limits while satisfying the static equilibrium of the CDPC. Equation (2.114) formulates the static equilibrium.

$$\mathscr{S}_{CDPC} = \{^0\mathbf{p} \in \mathbb{R}^2 \,|\, {}^b\mathbf{R}_p = \mathbf{I}_2 \ : \exists \mathbf{t} \in \mathscr{T}, \ \mathbf{W}\mathbf{t} + \mathbf{w}_g = \mathbf{0}_4\} \tag{2.114}$$

where, minimum and maximum cable tensions are denoted as t_{min} and t_{max}, respectively. The tension vector associated to the described model of CDPC with two cables is given by

$$\mathbf{t}_m = \begin{bmatrix} t_{12} & t_3. \end{bmatrix}^T \tag{2.115}$$

$\mathbf{W}_m$ is the wrench matrix of the considered model and is expressed as follows:

$$\mathbf{W}_m = \begin{bmatrix} {}^b\mathbf{u}_{12} & {}^b\mathbf{u}_3 \end{bmatrix} \tag{2.116}$$

From Eqs. (2.114-2.116), the equilibrium of the external forces applied onto the moving-platform is reformulated as follows:

$$t_{12}{}^b\mathbf{u}_{12} + t_3{}^b\mathbf{u}_3 + m\mathbf{g} = \mathbf{0}_2 \tag{2.117}$$

Let us compute $\mathbf{v}_{12}$ and $\mathbf{v}_3$, the unit vector orthogonal to ${}^b\mathbf{u}_{12}$ and ${}^b\mathbf{u}_{12}$, respectively.

$$\mathbf{v}_i = \mathbf{E}^b\mathbf{u}_i, \quad i = (12), \ 3 \tag{2.118}$$

The following equation is derived from Eq. (2.117) by replacing t_{12} with $2t_{max}$, and eliminating t_3 by a dot product:

$$\mathbf{v}_3^T \left(2t_{max}{}^b\mathbf{u}_{12} + t_3{}^b\mathbf{u}_3 + m\mathbf{g}\right) = 0. \tag{2.119}$$

Similarly, the following equation is obtained by replacing t_3 with t_{max} and eliminating t_1.

$$\mathbf{v}_{12}^T \left(t_{12}{}^b\mathbf{u}_{12} + t_{max}{}^b\mathbf{u}_3 + m\mathbf{g}\right) = 0 \tag{2.120}$$

Upon solving Eqs. (2.119) and (2.120) for p_y, we obtain

$$y_i = \zeta_i \, mg \left(l_b l_p - \frac{1}{2} l_p^2 + 2x^2 - \frac{1}{2} l_b^2 \right) + h_b \quad i = (12), \, 3 \qquad (2.121)$$

where, y_{12} and y_3 stand for the y_p loci whose associated cable tension is considered as the maximum allowed tension for cables $\mathscr{C}_{12}$ and $\mathscr{C}_3$, respectively, and ζ_{12} and ζ_3 are defined as:

$$\zeta_{12} = \frac{1}{\sqrt{16 \, t_{max}^2 (l_b - l_p)^2 - m^2 g^2 (l_b - l_p - 2x)^2}} \qquad (2.122)$$

$$\zeta_3 = \frac{1}{\sqrt{4 \, t_{max}^2 (l_b - l_p)^2 - m^2 g^2 (l_b - l_p + 2x)^2}} \qquad (2.123)$$

Equations (2.122) and (2.123) imply the validity domain of Eq. (2.121) as formulated in the following equations.

$$x_{lb,12} = \frac{(l_b - l_p)(mg - 4t_{max})}{2mg} \qquad (2.124)$$

$$x_{ub,12} = \frac{(l_b - l_p)(mg + 4t_{max})}{2mg} \qquad (2.125)$$

The valid domain for y_3 is expressed in the following equations:

$$x_{lb,3} = \frac{(l_p - l_b)(mg + 2t_{max})}{2mg} \qquad (2.126)$$

$$x_{ub,3} = \frac{(l_p - l_b)(mg - 2t_{max})}{2mg} \qquad (2.127)$$

Therefore, the domain, $\mathbf{x}_i = [x_{lb,i}, \, x_{ub,i}]$, $i = (12), \, 3$, is defined for the boundary equations, y_i. From Eq. (2.121), we hint that there is always a minimum point on the upper-boundary equations, namely, $\mathbf{m}_i = [\underline{x_i}, \underline{y_i}]^T$, $i = (12), \, 3$. This point is associated to the minimum of the upper-boundary equations and thus satisfies the condition

$$\frac{d \, y_i(\underline{x_i})}{d \, x} = 0 \qquad i = (12), \, 3. \qquad (2.128)$$

Hereafter, we define the maximum required height of the payload $\bar{h}_l$, and the minimum required height of the building,

$$h_b = h_c + \bar{h}_l \qquad (2.129)$$

In order to calculate the minimum required height for the ceiling, we define h_c in Eq. (2.130). The latter parameter is associated to the minimum required distance from ceiling the moving-platform can support the given payload within the boundary of the cable tensions. It should be noted that h_c depends on the maximum cable

tension, weight and the width of the frame and moving-platform.

$$h_c = h_b - \bar{y}_p \tag{2.130}$$

We define $\bar{y}_p$ as the maximum value of y_p that the moving-platform could obtain for any $p_x \in \left[\frac{l_p - l_b}{2}, \ \frac{l_b - l_p}{2} \right]$. The following equation yields $\bar{y}_p$:

$$\bar{y}_p = \min(\underline{y}_{12}, \ \underline{y}_3) \tag{2.131}$$

In the previous equation, $\underline{y}_{12}$ and $\underline{y}_3$ state the minimum values of y_{12} and y_3, respectively.

Figure 2.22 shows the workspaces of CDPCs, their upper-boundaries and h_c for different masses and ceiling heights. In this examples the maximum cable tension (t_{max}=220 N), height of the moving-platform (h_p=0.5 m) and length of the CDPC frame (l_b=0.5 m) are constant.

2.3   Optimum Design of the CDPC

The previous models and analysis described in the chapter are employed to determine optimal design of the manipulator. The optimal design of CDPRs usually concerns their workspace or task performance. Bruckmann et al. in [Bru+09] called the former as Design-to-Workspace, i.e., calculation of an optimal robot layout for a given workspace and the latter as Design-to-Task, i.e., calculation of the optimal robot for a specific task. Alternatively, Gouttefarde et al. in [Gou+08] introduced an design approach on finding the geometry of fully-constrained CDPRs such that a prescribed workspace belongs to WFW. The study of the optimum design is performed in the context of an optimization problem formulation. Thus we start by introducing the design hypotheses as follows:

1. The moving-platform anchor points B_1, B_2, B_3 and point P, the origin of moving-platform frame, namely, $\mathscr{F}_p$ are located on the top of the moving-platform as shown in Fig. 2.5.

2. The exit points of the CDPC, A_1 and A_3 are fixed to the frame. However, the position of the second exit point A_2 is not predefined and associated to the radius of the drum (r_d) and A_1 (in Fig. 2.5). The following equation expresses the Cartesian coordinate vector of A_2 expressed in the base frame $\mathscr{F}_b$.

$$^b\mathbf{a}_2 = {}^b\mathbf{a}_1 + \mathbf{v}_{12}, \tag{2.132}$$

where vector $\mathbf{v}_{12}$ relates the Cartesian coordinates of exit and anchor points of the cable-loop as follows:

$$\mathbf{v}_{12} = {}^b\mathbf{a}_2 - {}^b\mathbf{a}_1 = {}^p\mathbf{b}_2 - {}^p\mathbf{b}_1 = \begin{bmatrix} 2r_d \\ 0 \end{bmatrix} \tag{2.133}$$

(a) h_b = 3m & m = 10kg

(b) h_b = 3m & m = 20kg

(c) h_b = 4 m & m = 10kg

(d) h_b = 4 m & m = 20kg
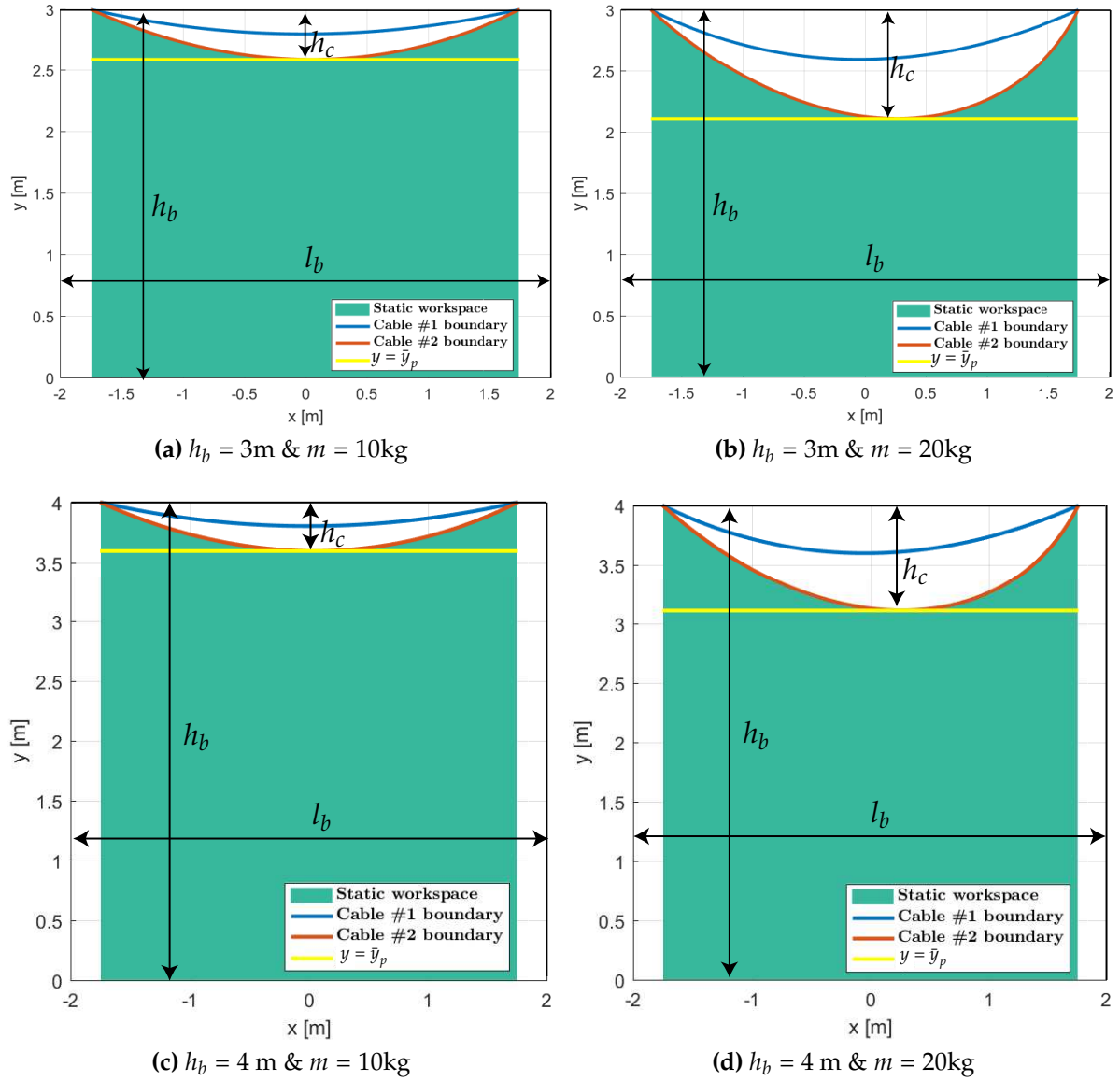
Figure 2.22: Workspace of CDPC for different heights and the overall mass (MP and payload)

3. The anchor points belonging to the cable-loop, namely, B_1 and B_2, are related as follows:

$$^p\mathbf{b}_2 = {^p\mathbf{b}_1} + \mathbf{v}_{12}. \tag{2.134}$$

4. The vertical center-line of the moving-platform, $\mathcal{L}_v$, passes through points P, D and H. Point D stands for the center of the cable-loop drum position on the moving-platform and it is expressed as $^p\mathbf{d} = [d_x, \ d_y]^T$ in $\mathscr{F}_p$. The Cartesian coordinate vector of the hoist center is denoted as $^p\mathbf{h} = [h_x, \ h_y]^T$ expressed in $\mathscr{F}_p$. Knowing that point H belongs to line $\mathcal{L}_v$, we rewrite $^p\mathbf{h}$ as follows:

$$^p\mathbf{h} = \begin{bmatrix} 0 \\ d_y - r_{G1} - r_{G2}. \end{bmatrix} \tag{2.135}$$

   where r_{G1} is the radius of the gear attached to the shaft $\mathscr{S}_1$ and r_{G2} is the radius of the biggest gear attached to shaft $\mathscr{S}_O$ as mentioned in Table 2.1.

5. The Cartesian coordinates of CoM of the moving-platform, namely, point C is expressed as follows:

$$^p\mathbf{c} = \begin{bmatrix} 0 \\ c_y \end{bmatrix} \tag{2.136}$$

   where c_y is formulated as:

$$c_y = \frac{m_h h_y - \frac{m_p h_p}{2}}{m_p + m_h} \tag{2.137}$$

The total mass of the moving platform is given by

$$m = m_p + m_w + m_h, \tag{2.138}$$

where m_p, m_h and m_w are the masses of the support of the moving-platform, the hoist mechanism and the payload, respectively. m_p is calculated as follows:

$$m_p = \rho l_p h_p w_p \tag{2.139}$$

where ρ is the density of the moving-platform material. The maximum allowed mass of the payload (m_w) is indicated as $\bar{m}_w$. The latter variable is associated to the mass of the payload that can be lifted by the hoist for the given tension difference (δt) and $\bar{p}_y$. The following equation expresses the relation between the input torque, τ_d, and the output torque, τ_h.

$$\tau_h = \psi_G \, \tau_d = r_h m_w g \tag{2.140}$$

and,

$$\tau_d = r_d \delta t \tag{2.141}$$

where, the gear ratio of the hoist is calculated as follows:

$$\psi_G = \frac{r_{G2} r_{G4} r_{G8}}{r_{G1} r_{G3} r_{G7}}.$$ (2.142)

Therefore, from Eq. (2.140) and Eq. (2.141), we can extract the mass of the payload m_w as follows:

$$m_w = \frac{\psi_G \, \delta t \, r_d}{r_h \, g}$$ (2.143)

Design Problem and Methodology

An optimization method is proposed to maximize the positioning accuracy of the moving-platform by finding optimal geometrical parameters as well as increasing the moving-platform stiffness along its vertical axis. The purpose of this optimization is to find the optimum geometric values of the moving-platform such that, the manipulator is able to lift a predefined payload for a given ceiling height. The optimization searches the optimal design parameters of the moving-platform regardless of those from the hoist mechanism. Stiffness analysis of CDPRs is crucial since it concerns vibration and positioning accuracy of the moving-platform. Antagonistic tensions can be optimized in order to improve the stiffness [BK06] and consequently the accuracy of the moving-platform positioning. Stiffness of the moving-platform along the vertical axis (y_b) is defined as one of the objective functions of the optimization problem, namely, k_y.

The position of the end-effector for the unactuated hoist is defined as $\mathbf{e}_n$, while the parasitic inclination due to the actuated hoist varies the position $\mathbf{e}_m$ of the end-effector. Finally, the positioning error of the end-effector due to parasitic inclination is defined as

$$e_{er} = \left\| \mathbf{e}_m - \mathbf{e}_{nom} \right\|.$$ (2.144)

Design Variable

The decision variables vector contains the geometric parameters to be optimized as follows:

$$\mathbf{x} = \begin{bmatrix} r_d, & w_p, & l_p, & h_p, & b_{1x}, & b_{3x}, & d_y \end{bmatrix}^T.$$ (2.145)

$\mathbf{x}$ contains the minimum number of geometry variables for the design of the moving-platform regardless of those from the hoist mechanism.

Optimization Constraints

The first linear constraint is the height of the moving-platform and the vertical position of the hoist. The constraint bounds point H between points P and Q, shown in Fig. 2.5.

$$h_p \geq r_{G1} + r_d - d_y$$ (2.146)

Table 2.3: Design variables boundaries

Design variables	r_d	w_p	l_p	h_p	b_{1x}	b_{3x}	d_y
Unit	[mm]	[mm]	[mm]	[mm]	[mm]	[mm]	[mm]
Lower bound	10	40	105	150	-200	-200	-560
Upper bound	50	60	400	600	200	200	-100

The next constraints limit the positions of the anchor points B_1 and B_3 between the points F and G:

$$\frac{-l_p}{2} \le b_{1x} \le \frac{l_p}{2} - 2r_d, \tag{2.147}$$

$$\frac{-l_p}{2} \le b_{3x} \le \frac{l_p}{2}. \tag{2.148}$$

The mass of the payload, m_w is calculated in Eq. (2.143). Since, the task of the CDPC is determined as lifting payloads up to the maximum required mass ($\overline{m}_w$), the following constraint is employed to bound m_w:

$$\overline{m}_w \le \frac{\psi_G \, \delta t \, r_d}{r_h \, g}. \tag{2.149}$$

The fifth non-linear constraint limits the mass of the moving-platform within the admissible bounds according to the maximum cable tension, namely, t_{max}. This constraint guarantees the mass of the moving-platform, m_p not to overload the maximum admissible mass of the manipulator, namely, m.

$$0 \le m_p \le m - m_h - \overline{m}_w \tag{2.150}$$

the lower bound vector, $\mathbf{x}_{lb}$, and upper bound vector, $\mathbf{x}_{ub}$, of the decision variables are detailed in Table 2.3.

Optimization Problem Formulation

In order to reduce the positioning error and increasing the stiffness of the moving-platform along a given direction, the following optimization problem is formulated.

$$\begin{aligned}
&\text{minimize} \quad f_1(\mathbf{x}) = e_{er} \\
&\text{maximize} \quad f_2(\mathbf{x}) = k_y \\
&\quad\text{over} \quad \mathbf{x} = \begin{bmatrix} r_d, \ w_p, \ l_p, \ h_p, \ b_{1x}, \ b_{3x}, \ d_y \end{bmatrix}^T
\end{aligned}$$

subject to:

$$\begin{aligned}
&g_1: \ h_p \geq r_{G1} + r_{G2} - d_y \\
&g_2: \ \frac{-l_p}{2} \leq b_{1x} \leq \frac{l_p}{2} - 2r_d \\
&g_3: \ \frac{-l_p}{2} \leq b_{3x} \leq \frac{l_p}{2} \\
&g_4: \ \overline{m}_w \leq \frac{\psi_G \ \delta t \ r_d}{r_h \ g} \\
&g_5: \ 0 < m_p \leq m - m_h - m_w \\
&\quad\quad \mathbf{x}_{lb} \leq \mathbf{x} \leq \mathbf{x}_{ub}
\end{aligned} \tag{2.151}$$

The optimization of the latter problem is solved by *ga* $^{\copyright}$Matlab function. The optimization is performed for a given position of the moving-platform, namely, point *P* and the optimization inputs are mentioned in Table 2.4. The Pareto frontier amounting to the non-dominated solutions with regard to the two objective functions is shown in Fig. 2.23. The parallel graph in Fig. 2.24 shows seventy sets of optimal design variables.

Results and discussion

The following setting is applied for solving the optimization problem:

- Population size: 200

- Maximum number of generations: 100

- Function tolerance: 1×10^{-5}

- Pareto fraction: 35%

The outputs of the optimization are detailed in this section. Table 2.4 expresses the input of the optimization problem based on the CREATOR prototype hardware and setup. Figure 2.23 illustrates the set of generated solutions consisting in optimal and non-optimal solutions. More than twenty thousands solutions are generated (red dots) with 346 optimal solutions (green dots) which form the Pareto frontier as shown in the figure. The parallel graph in Fig 2.24, illustrates the connection between the optimal decision variables and the objective function. This helps for an in-depth understanding of the relation between selection of design variables and their effect on the positioning error and stiffness of the CDPC. Table 2.5 illustrates
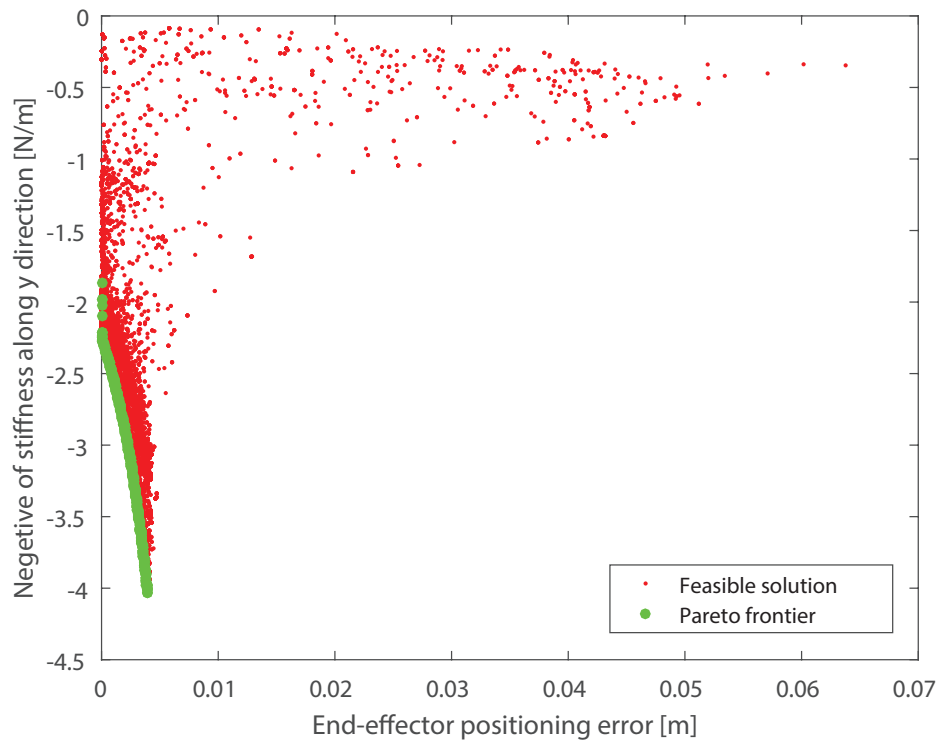
Figure 2.23: Feasible solutions and Pareto frontier of the optimization problem

the minimum and the maximum values for decision variables and objective functions obtained by genetic algorithm.

The parallel graphs shows that, the optimal values of r_d are mostly close to the lower bound. This could be justified as the lower r_d associated to the lower parasitic inclination and consequently lower positioning error. The optimal width of the moving-platform, w_p, is distributed within its upper and lower bounds, while the most of the optimal lengths l_p of the moving-platform are close to their upper-bound. A longer moving-platform is associated with a heavier moving-platform and as a result less parasitic inclination and positioning error. Optimal h_p tends towards the upper-bound and cause higher mass for the moving platform as well as larger values for d_y. According to the results in Table 2.5, the anchor points, b_{1x} and b_{3x} are in the shortest distance from the vertical centerline. This is justified as the closer anchor points yields higher antagonistic forces along cables and consequently, stiffer moving-platform in horizontal direction for the given pose of the moving-platform, namely, P. The last decision variable, r_d is optimal for the values close to the lower-bound which brings the CoM of the moving-platform towards anchor point p. The latter leads to larger distance between point D and CoM that is associated to higher moments of the moving-platform weight about point D and lower parasitic inclination and as a result lower positioning error. The variation of the optimal objective functions, e_{er} and $k_{dr,x}$ are shown in the last two columns of the parallel graphs, respectively.

Table 2.4: Input parameters of the optimization problem

Parameter	abbreviation	Value
Gear ratio of hoist	ψ_G	9
Density [kg/m^3]	ρ	1.21
Radius of the hoist drum [mm]	r_h	30
Free length of the hoist cable [m]	h_l	5
Stiffness of the cables [N/m]	k	6.5×10^5
Mass of the hoist [kg]	m_h	3.25
Total mass of the manipulator [kg]	m	20
Maximum mass of the Payload [kg]	$\overline{m}_w$	4
Tension difference in cable loop [N]	δt	10
Cartesian Coordinate vector of the first exit point [m]	$\mathbf{a}_1$	$[-2\ 3]^T$
Cartesian Coordinate vector of the third exit point [m]	$\mathbf{a}_3$	$[2\ 3]^T$
Cartesian coordinate vector of point P [m]	$\mathbf{p}$	$[0\ 2]^T$
Maximum allowed height of the MP [m]	$\bar{y}_p$	1.75
Maximum admissible cable tension [N]	t_{max}	220
Minimum admissible cable tension [N]	t_{min}	10

	r_d [mm]	w_p [mm]	l_p [mm]	h_p [mm]	b_{1x} [mm]	b_{3x} [mm]	d_y [mm]	e_{er} [mm]	$-k_y$ [N/mm]
Minimum value	12	45.9	324.5	421	-27.3	-0.95	-148	0	-40.4
Maximum value	13.9	59.4	397.2	598.5	-23.2	8.71	-100	3.93	-18.7

Table 2.5: Boundary of optimal design variables and objective functions
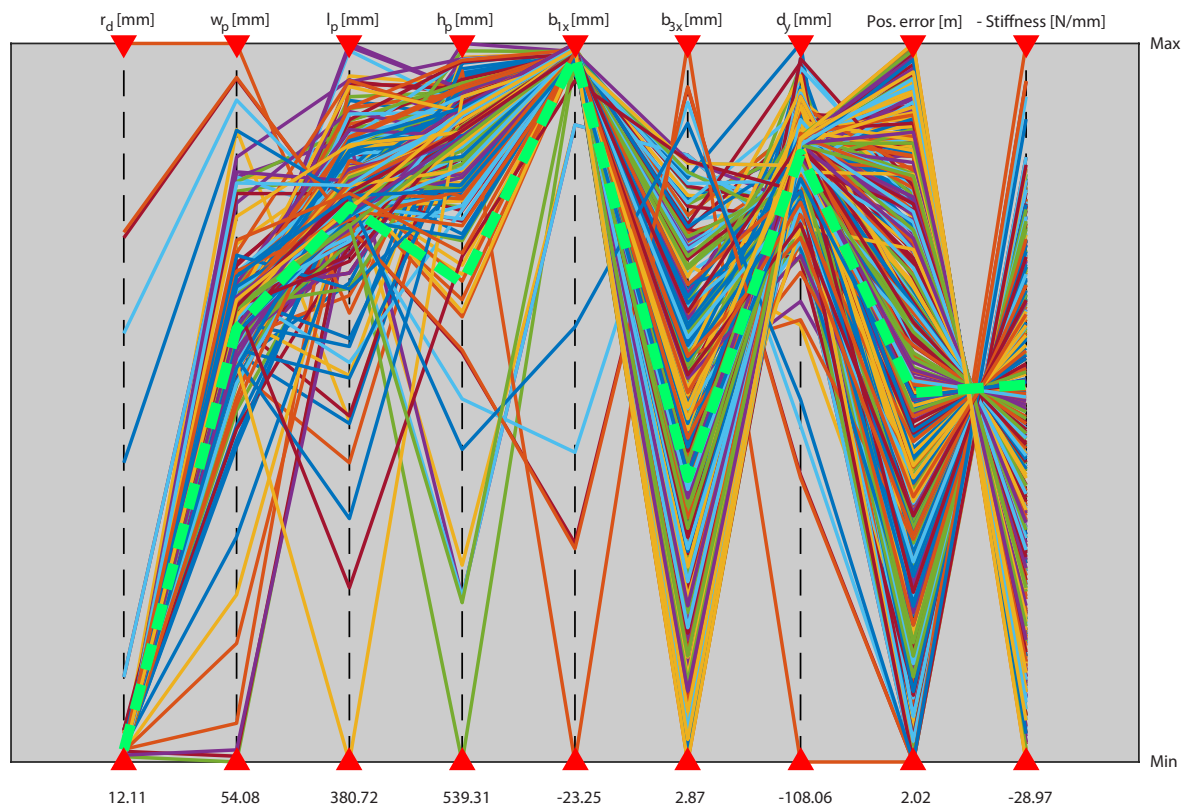
Figure 2.24: Parallel graphs corresponding to the optimal design variables and objective functions. As an instance, the optimal values of a solution is expressed on the horizontal axis for the highlighted graph in green dash-line

2.4 Prototyping and Experimentation

This section deals with the practical aspects of the planar CDPC with an embedded hoist. The ultimate goal of the prototyping is firstly to take an initial step towards CDPRs with large translational and rotational workspaces and secondly to validate the concept of hybrid CDPRs by means of bi-actuated cables. These objectives are attained by obtaining demonstration of this novel manipulator and justification by experimentation on the presented analysis. This research work is in the framework of the CREATOR project. The originality of the CREATOR project aims to design hybrid robots with both large translational and orientation workspaces. Those robots are hybrid because they combine the advantages of cable-driven parallel robots in terms of large translational workspace and the advantages of other mechanisms in terms of large rotational amplitudes. The first goal is to set-up the CREATOR demonstrator and to obtain a demonstration of a planar CDPC. Therefore, the design and prototyping of the demonstrator started with the design of actuator units, control unit and mechanical set-up which is elaborated thoroughly in Appendix A.

The prototyping of the CDPC moving-platform is also outlined hereafter. The hoist mechanism is composed of commercial gears in steel and the moving-platform is made of steel and aluminum. The overall mass of the moving platform is 3.25 kg. Mechanical drawings of the moving-platform are illustrated in Fig. 2.25 demonstrating all the mechanical components used in the manufacturing. Figure 2.26 shows the assembly of the moving-platform with the embedded hoist mechanism.

2.4.1 CREATOR Demonstrator

The main framework of the CREATOR prototype in terms of actuation and geometry is discussed in this section. The equivalent architecture of the CREATOR demonstrator is presented in Fig. 2.27. The fundamental units are expressed in the figure and are elaborated in the following:

- PC with ©Matlab 2016a and ©ControlDesk software: The respective models of the manipulator are implemented into a graphical programming environment of ©Matlab 2016a, namely, *Simulink*. Hereafter, by *ControlDesk* one can access to the manipulator connected bus in through *dSpace* controller for performing the manipulator task, measurement, calibration and etc.

- dSpace controller: This unit is an intermediary hardware which provides the communication between motor drivers and CREATOR PC through *ControlDesk* software.

- ^{TM}Parker motor drivers: This unit communicates current and break signals between *dSpace* and the motors. CREATOR has four ^{TM}Parker drivers that suffice to control eight motors.

- Actuation unit: Each unit consists of a motor, a reducer and a winch. The winch adjusts the cable length by its rotary motion induced by its motor.

- Moving- platform: Depending on the manipulator and task, different moving-platforms and actuation units can be employed.

(a) Side-view (Top) and cross section view (Bottom)

(b) Top-view (Top) and cross section view (Bottom)
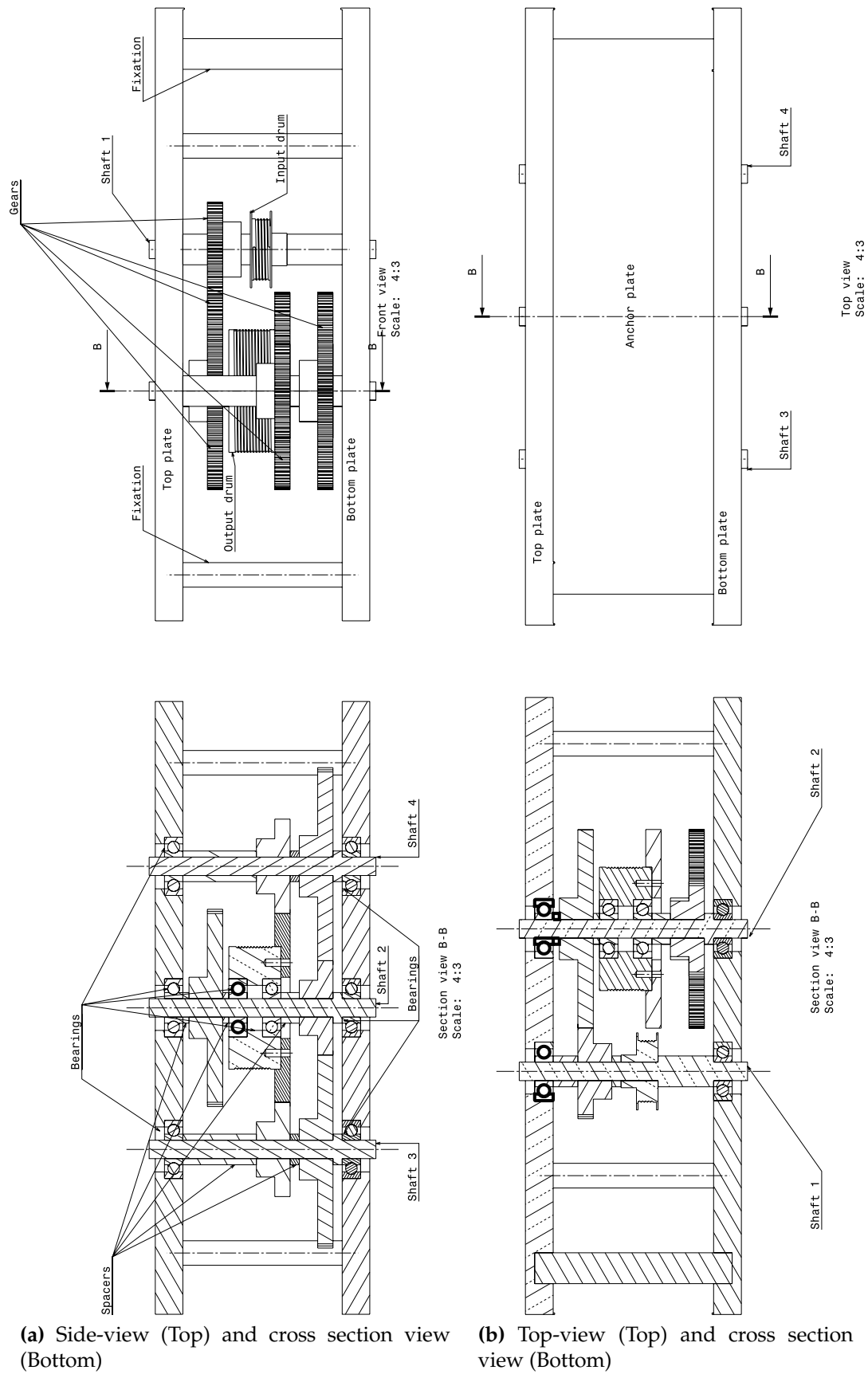
Figure 2.25: Design drawings of the moving-platform of the CDPC
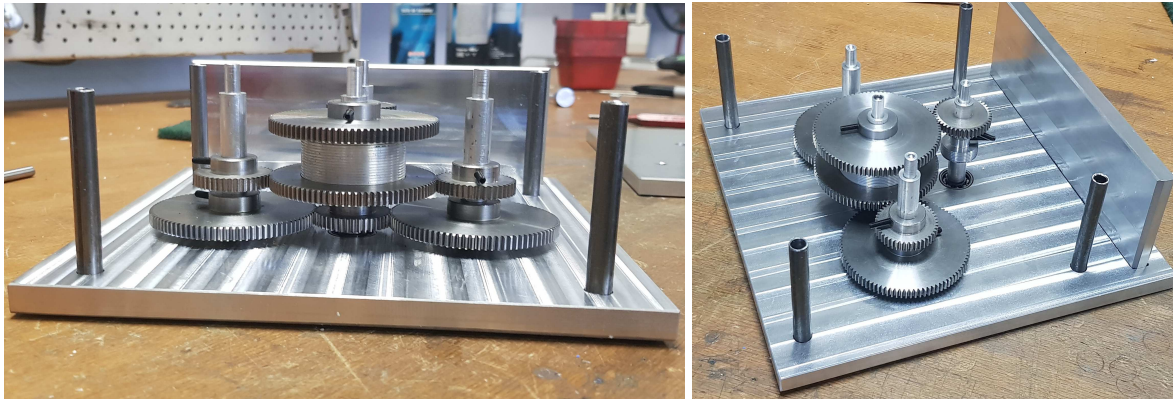
Figure 2.26: Assembly of the manufactured moving-platform of the CDPC
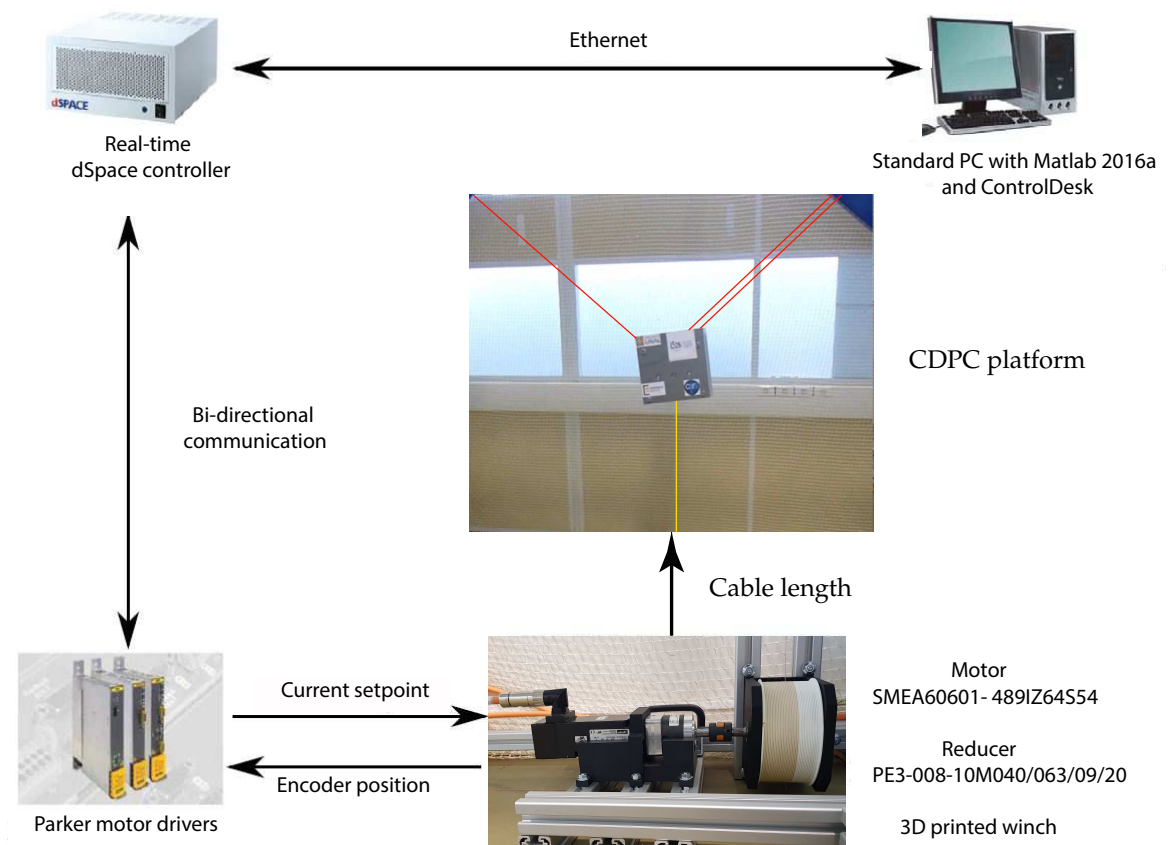
Figure 2.27: Equivalent architecture of the CREATOR prototype, [Bak+19]

The prototype parameters are detailed in Table 2.6. The second stage is devoted to the manufacturing and prototyping of the moving-platform of the CDPC. Figure 2.26 depicts two instances of the prototype of the CDPC moving-platform and the embedded hoist mechanism.

2.4.2 Control

The proposed control of the planar CDPC is based on a computed torque controller elaborated in [Bak+19; Lam13] and shown in Fig. 2.28. The control utilizes a priori knowledge of the dynamics of the CDPC in order to compensate the friction effects for enhancing trajectory tracking. The friction compensation is a feed-forward block, which contributes to the reduction of vibrations of the moving-platform so the accuracy of the trajectory tracking improves. The following details the signal used in the scheme.

- $\mathbf{q}_d \in \mathbb{R}^m$: Vector of the desired joints angular positions

- $\dot{\mathbf{q}}_d \in \mathbb{R}^m$: Vector of the desired joint angular velocities

- $\mathbf{q}_m \in \mathbb{R}^m$: Vector of the measured joint's angular positions

- $\dot{\mathbf{q}}_m \in \mathbb{R}^m$: Vector of the measured joint angular velocities

- $\mathbf{e}_q = \mathbf{q}_d - \mathbf{q}_m$: Vector of the error in the angular positions

- $\dot{\mathbf{e}}_q = \dot{\mathbf{q}}_d - \dot{\mathbf{q}}_m$: Vector of the error in the angular velocities

- $\mathbf{K}_p \in \mathbb{R}^{m \times m}$: Diagonal matrix of the proportional gain

- $\mathbf{K}_i \in \mathbb{R}^{m \times m}$: Diagonal matrix of the integral gain

- $\mathbf{K}_d \in \mathbb{R}^{m \times m}$: Diagonal matrix of the derivative gain

The output torque of the controller $\boldsymbol{\tau}_m$, is sent to the motors and its computations is detailed as follows:

$$\boldsymbol{\tau}_m = \boldsymbol{\tau}_{PID} + \ddot{\mathbf{q}}_d \mathbf{I}_m + \boldsymbol{\tau}_{FF} + \boldsymbol{\tau}_f \tag{2.152}$$

with $\boldsymbol{\tau}_f$ being the friction compensation torque. This torque is a function of static and viscous frictions of the motors, namely, $\mathbf{F}_s$ and $\mathbf{F}_v$, respectively.

$$\boldsymbol{\tau}_f = \mathbf{F}_s \tanh \dot{\mathbf{q}}_d + \mathbf{F}_v \dot{\mathbf{q}}_d \tag{2.153}$$

the well-known PID torque is denoted as $\boldsymbol{\tau}_{PID}$ and computed as follow:

$$\boldsymbol{\tau}_{PID} = \mathbf{K}_p \mathbf{e}_q(t) + \mathbf{K}_d \dot{\mathbf{e}}_q(t) + \int_{t_0}^{t} \mathbf{K}_i \mathbf{e}_q(t') dt' \tag{2.154}$$

The feed-forward torque is expressed as follows:

$$\boldsymbol{\tau}_{FF} = \frac{-m \mathbf{R}_w \mathbf{W}^+ [\ddot{\mathbf{X}} + \mathbf{g}]}{r_g} \tag{2.155}$$

Table 2.6: Design parameters of CREATOR prototype

Efforts	Abbreviation	Value
Nominal torque of motor [N.m]	τ_M	0.8
Peak torque of motor [N.m]	τ_{Mpic}	1.4
Nominal torque of reducer [N.m]	τ_R	6.4
Peak torque reducer [N.m]	τ_{Rpic}	11.2
Nominal tension of cable [N]	T_C	128
Peak tension of cable [N]	T_{Cpic}	224
Speeds	**Abbreviation**	**Value**
Motor angular velocity [rpm]	V_M	6000
Angular velocity of reducer [rpm]	V_R	750
Linear velocity of cable [m/s]	V_C	3.92
Geometric parameters	**Abbreviation**	**Valeur**
Reducer ratio [ ]	μ_r	8
Drum radius [m]	R_E	0.05
Cable length [m]	L_C	6.72
Cable diameter (+ winch groove radius) [m]	D_C	0.005
Drum length [m]	L_E	0.01
Number of drum turns [ ]	N_T	23
Length of fixed frame [m]	L_b	4.5
Width of fixed frame [m]	l_b	4
Height of fixed frame [m]	H_b	3
Length motor + reducer [m]	L_{MT}	0.4
External width of drum [m]	L_{Ex}	0.1
Length motor + reducer + drum [m]	L_{MRE}	0.6
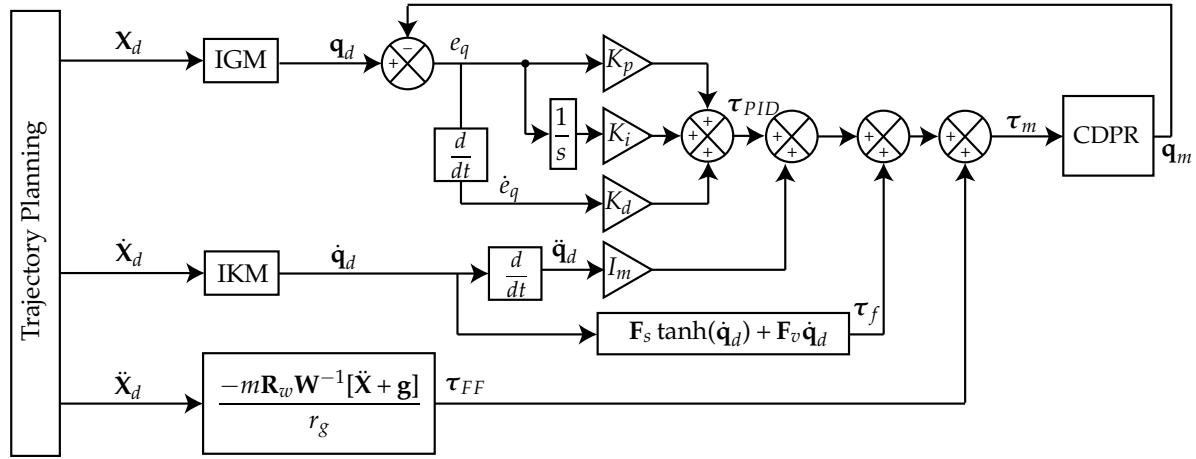
Figure 2.28: computed torque control scheme

with m being the mass of the moving-platform, r_g as the reducer ratio, $\ddot{\mathbf{X}} \in \mathbb{R}^2$ is the acceleration vector of the moving-platform and $\mathbf{R}_w$ being an identity matrix of the radius of the motor winches as:

$$\mathbf{R}_w = r_w \mathbf{1}_{2 \times 2}. \tag{2.156}$$

It is noteworthy that the moment of inertia of the moving-platform is not taken into account since the orientation of the moving-platform is not controlled. This is due to the under-actuation of the CDPC.

Finally, the video in link [3] refers to the preliminary demonstration of the hybrid CDPC. The video shows the concept of a four-DoF moving-platform that adjusts the height of a payload with 0.5 kg mass while avoiding an obstacle while translating from an initial point to a final point.

2.4.3 Measurement of the Natural Inclinations

The magnitude of θ_m is very close to that of θ_n, i.e., less than one degree for the CDPC at hand. Hence, it is not possible to detect the parasitic inclination is not possible with the accuracy of the accelerometer used in the experiments. Moreover, the perturbations on the prototype complicates the determination of small-scale parasitic inclinations. Therefore, the computation of the negligible parasitic inclinations is excluded from these trials.

The inclination of the moving-platform of the CDPC was measured with the accelerometer of a mobile phone as shown in Fig. 2.29. The measurement aims at evaluating the natural inclination of the moving-platform along three horizontal paths with different heights, i.e., from point V_3 to point V_5, shown in Fig. 2.12. The measurement of the natural inclination, θ_n, of the moving-platform along the test paths was repeated five times.

The accuracy of the sensor is approximately 0.2 degree. The mean and standard deviation (STD) values of the natural inclination θ_n of the moving-platform along the test paths are traced in Fig. 2.30. From Fig. 2.30a to Fig. 2.30c, it is apparent

---

[3]http://tiny.cc/snwhkz

Figure 2.29: Measurement of the inclination θ_n of the CDPC moving-platform with the accelerometer of a mobile phone

that the higher the height of the moving-platform, the lower the absolute value of the inclination of the moving-platform. Besides, the measured inclinations of the moving-platform are close to the theoretical values shown in Fig. 2.14.

2.5 Summary of the Chapter

In this chapter, we introduced a novel four-DoF planar under-constrained cable-driven parallel robot connected to a hoist mechanism for lifting payloads. The robot utilizes a bi-actuated cable-loop system, which provides large amplitudes to its rotating end-effector. The manipulator exploits cables to transmit power directly from fixed motors to the moving-platform. Thanks to the mentioned novelty, the proposed concept is less at risk of interfering with obstacles within the workspace, as the moving platform can remain higher above the ground. In comparison with conventional cable-driven parallel robots and cable-driven suspended robots. The proposed cable-driven cranes are inexpensive and could be an potential alternative to bridge-crane mechanisms.

The required models for such a manipulator were studied. Moreover, capabilities and deficiencies of such a manipulator were elaborated through studying the CPDC. The architecture and kineto-static models of the manipulator were detailed in this chapter. The investigation of the static workspace and maximum required height for the robot were carried out. The effect of hoisting torque on the moving-platform inclination was also investigated. It was shown that the angle of inclination can be computed efficiently and reliably. The optimal design of the moving-platform in terms of stiffness and positioning error of the end-effector was detailed in this chapter. Beside the conceptual and detailed designs, we elaborated an approach for obtaining an optimal design to search for the design parameters based

(a) Height=1 m

(b) Height=1.5 m

(c) Height=2 m
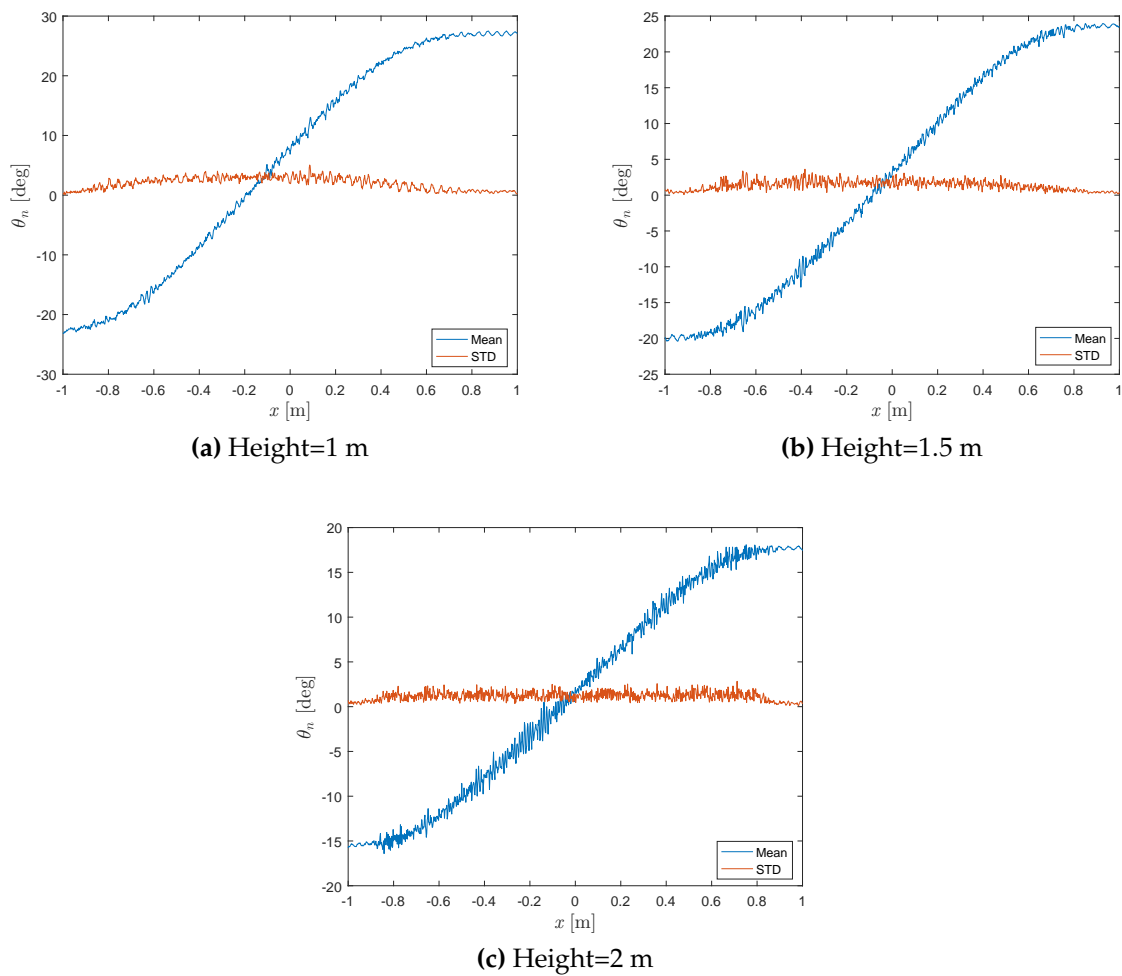
Figure 2.30: Measured inclination of the CDPC moving-platform along a test path with three different heights

on the detailed models and the previous investigations.

The practical aspects of the cable-driven parallel robots with an embedded crane was included within the chapter for further clarification and proof of the concept. This was done through a demonstration of the manipulator and the measurement of the inclination of its moving-platform. Nevertheless, further experimentations on the static workspace and elasticity analysis are left for future contributions.

Chapter 3

Cable-Driven Parallel Robot with an Embedded Tilt-Roll Wrist

Contents

There exists a wide variety of applications requiring large rotation workspace, e.g., search and rescue, motion simulation and entertainment. CDPRs have drawn their interest of industry thanks to their fundamental advantages and capabilities, such as high payload-to-weight ratios, large translational workspaces and high-speed motions. They generally cannot cover large rotation workspaces due to collisions between their moving parts, i.e., cable/cable, cable/moving-platform, cable/environment collisions.

Cable-loops as the fundamental components in the synthesis of CDPRs with large translational and rotational workspaces have been addressed in the previous chapter besides its modeling. A cable loop was employed for the actuation of a hoist mechanism embedded in the moving-platform which shows its reliability for further investigation on CDPRs with lare orientation workspace. In the CDPC, the large rotational amplitudes provided by a cable loop was used to actuate a one Degree of Freedom (DoF) mechanism, while here we employ two cable loops to actuate a tilt-roll wrist having a large rotational workspace.

A hybrid robot with a large translational and rotational workspace consisting of a CDPR connected to a tilt-roll wrist mechanism is introduced here. The manipulator combines the advantages of CDPRs, i.e., a large translational workspace, with

Figure 3.1: Prototype of the CDPR with an embedded tilt-roll wrist

those of tilt-roll wrists, namely, large amplitudes of rotation one. Solution to overcome the limited rotation workspace of CDPRs could consist in mounting a standard tilt-roll wrist on the moving-platform of a CDPR, but actuation of the tilt-roll wrist could be a challenge. Adding motors to the moving-platform for actuating the wrist increases the weight of the moving-platform and reduces the dynamic performance of the manipulator. Therefore, a pair of bi-actuated cable circuits, namely, cable loops are employed in the design of the CDPR in order to transmit the power from the motors fixed on the frame to the tilt-roll wrist. In general, the workspace of parallel robots can expand by connecting other parallel or serial mechanisms and constructing hybrid mechanisms. This usually complicates the design and reduces the dynamic performance of the manipulator unless, the power is transmitted directly to the end-effector without locating motors on the moving-platform. By employing remote actuation, we avoid mass and entanglement of a long power line tethering the moving-platform to the ground. Moreover, because of the mentioned reasons, remote actuation minimizes the size of the moving-platform. This leads to a better dynamic performance due to the lower inertia of the moving-platform. Hence, coupling two parallel mechanisms is proposed in order to exploit their combined workspaces through cable loops. Many applications require pointing the end-effector over a wide range of directions such as, camera surveillance, laser scanning, tomographic imaging and etc.

Tilt-roll wrist (also known as pitch-roll wrist) is a mechanism providing singularity-free rotation DoFs about two axes and in large amplitudes. The two-DoF tilt-roll wrist has been addressed in literature, e.g., in [HBA06] the design of a gear-less pitch-roll wrist with spherical cam-roller are presented equivalent to a bevel-gear differential mechanism. The input and output rotary shafts of the tilt-roll wrist are perpendicular to one another. Therefore, straight-tooth bevel gears were used as the
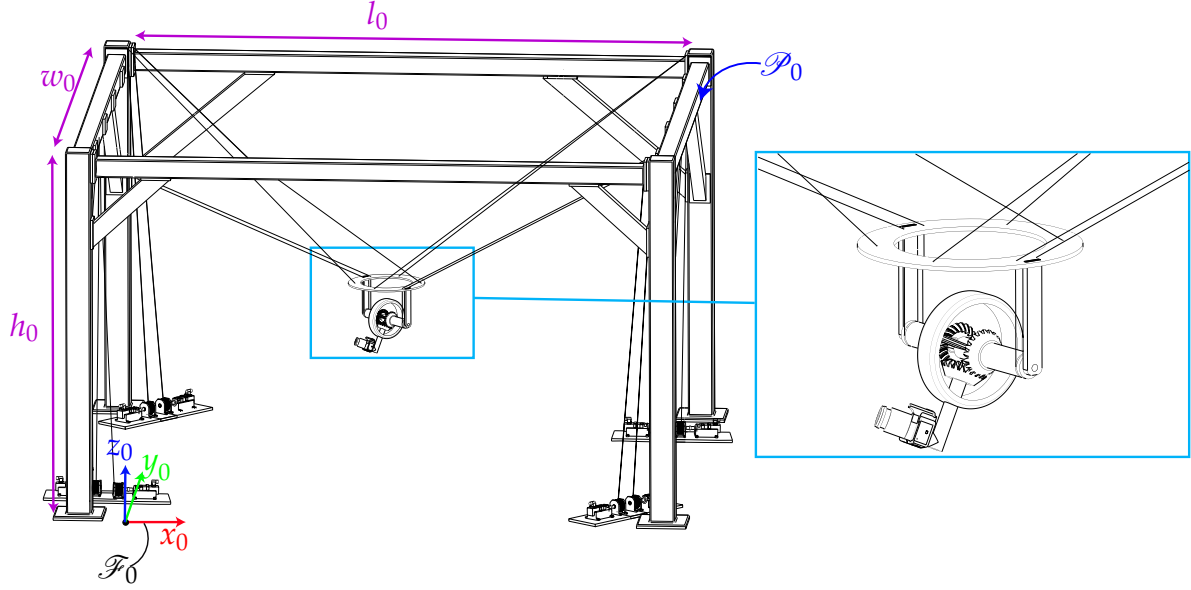
Figure 3.2: Schematic of the CDPR with an embedded tilt-roll wrist

simplest motion transmission mechanism between intersecting shafts [Shi11] and also they have low manufacturing cost. Bevel gears are used in automotive differential, marine, aviation applications and etc.

The study of the concept of the hybrid CDPR is organized into four sections. Section 3.1 introduces the architecture of the proposed under-constrained manipulator with eight DoF beside its modeling. The manipulator is analyzed in terms of workspaces, cable-interferences and sensitivity in Sec.3.3. Section 3.2 studies the optimal design of the moving-platform and cable arrangement of the manipulator. The prototype of the CDPR with an embedded tilt-roll wrist is presented in Sec. 3.3 and Sec. 3.4 concludes the chapter by highlighting the main contributions of the chapter.

3.1 Modeling

Figure 3.2 shows the overall schematic of the manipulator and Fig. 3.3 represents the schematic of the moving-platform with the embedded tilt-roll wrist with their main components as $\mathscr{P}_i$, $i = 1, ..., 5$. The proposed manipulator consists of the base frame, namely, $\mathscr{P}_0$, an under-constrained moving-platform, $\mathscr{P}_1$, which is suspended by six cables. Two bi-actuated cables and four uni-actuated cables are illustrated in Fig. 3.2. Each cable loop forms a circuit by connecting two actuators while passing through two anchor points on the moving-platform and coiling about a gear on the tilt-roll wrist. Two motions can be induced by the cable-loop depending on the relative rotation of its two actuators. The first one is the displacement of the moving-platform for identical inputs to the two motors. The second motion is the rotation of the gears $\mathscr{P}_3$ and $\mathscr{P}_4$ about their respective axes (z_3 and z_4) as shown in Fig. 3.3, when the two actuators rotate in opposite directions.

Here, we present the architecture of the manipulator, which is a hybrid robot consisting of a base frame and a tilt-roll wrist connected to the moving-platform of a CDPR. The moving-platform is suspended by six cables, i.e., two bi-actuated

cable circuits, also named cable loops, and four uni-actuated cables as illustrated in Fig. 3.2.

A cable loop forms a circuit by connecting two actuators while passing through two anchor points on the moving-platform and coiling about a gear on the tilt-roll wrist. This arrangement of cables is used for two distinct purposes. The former is to locate the moving-platform within its workspcae and the latter is to actuate the tilt-roll wrist connected in series to the moving-platform. In other words, two motions can be induced by the cable loop depending on the relative rotation of its two actuators. The first one is the displacement of the moving-platform for identical inputs to the two motors. The second motion is the rotation of gears $\mathscr{P}_3$ and $\mathscr{P}_4$ about their axes (z_3 and z_4), shown in Fig. 3.4, when the two actuators rotate in opposite directions. This leads to an unlimited rotation of $\mathscr{P}_3$ and $\mathscr{P}_4$ about their respective rotation axes. Figure 3.4 describes the main geometrical parameters of the moving-platform as well as the tilt-roll wrist. A cable-loop connected to two motors and drums is highlighted in the figure. Cable-loop consists of two segments each connecting the drums to their anchor points on the moving-platform with independent tensions and velocities.

The moving-platform frame $\mathscr{F}_1$ is located on the top of the moving-platform at point P. $^0\mathbf{p}$ is the vector pointing from the origin of $\mathscr{F}_0$ to the origin of $\mathscr{F}_1$. $^0\mathbf{R}_1$ is the rotation matrix from frame $\mathscr{F}_0$ to frame $\mathscr{F}_1$ and it is expressed as three sequence of rotations, α and β, shown in Fig. 3.5, are the tilt and roll angles of the tilt-roll wrist..

3.1.1 Kinetostatic Model of the Tilt-Roll Wrist

Kinetostatic model of the tilt-roll wrist is investigated in this section. The section-view of the moving-platform and the wrist is shown in Fig. 2. Their main components are denoted as $\mathscr{P}_i$, $i = 1, ..., 5$. The moving-platform is represented with $\mathscr{P}_1$, carrier of the wrist is denoted as $\mathscr{P}_2$, input gears connected to the cable loops $\mathscr{C}_{12}$ and $\mathscr{C}_{56}$ being $\mathscr{P}_3$ and $\mathscr{P}_4$, respectively. $\mathscr{P}_5$ is the end-effector.

Figure 3.5 shows the parametrization of the tilt-roll wrist in terms of angles. The rotation angles of $\mathscr{P}_2$, $\mathscr{P}_3$ and $\mathscr{P}_4$ about z_2-axis are denoted as $\alpha = \angle(z_2, \ x_5)$, $\theta_3 = \angle(y_1, \ x_3)$ and $\theta_4 = \angle(y_1, \ x_4)$, respectively. Its roll angle of the end-effector is defined as $\beta = \angle(z_2, \ x_5)$. The gear train ratio, μ is expressed as:

$$\mu = \frac{r_5}{r_3} = \frac{N_5}{N_3} \tag{3.1}$$

where N_3 and N_5 are the number of teeth of gears $\mathscr{P}_3$ and $\mathscr{P}_5$. The pitch radius of ith gear is denoted as r_i and $i = 3, \ 4, \ 5$. It should be noted that $r_3 = r_4$. The linear velocities at gear contact points C_{35} and C_{45} are expressed as follows:

$$^1\mathbf{v}_{c35} = -\dot{\theta}_3 r_3 \, ^1\mathbf{y}_2 \tag{3.2}$$

$$^1\mathbf{v}_{c34} = -\dot{\theta}_4 r_4 \, ^1\mathbf{y}_2 \tag{3.3}$$

with $\dot{\theta}_3$ and $\dot{\theta}_4$ being the angular velocities of $\mathscr{P}_3$ and $\mathscr{P}_4$, respectively.

$$^1\mathbf{v}_{H5} = -r_3 \dot{\alpha} \, ^1\mathbf{y}_2 \tag{3.4}$$
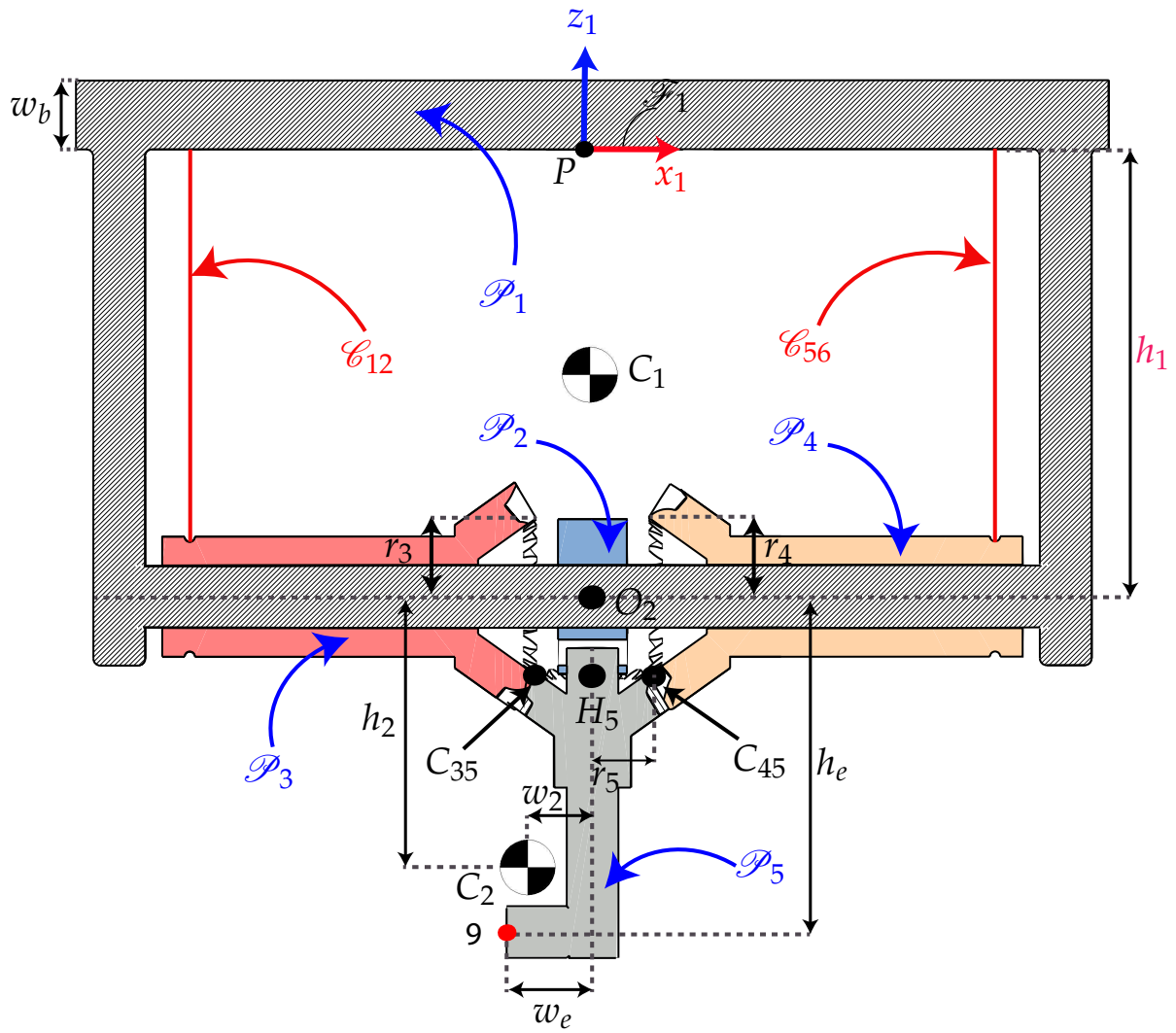
Figure 3.3: Section-view of the moving-platform and tilt-roll wrist

Figure 3.4: Schematic of the moving-platform with an embedded camera

Figure 3.5: Angles α, β, θ_3 and θ_4
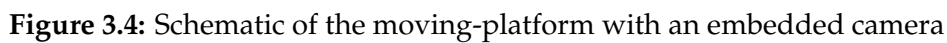
$^1\mathbf{v}_{H5}$ is the linear velocity of point H_5 which belongs to $\mathscr{P}_5$ expressed in $\mathscr{F}_1$. Furthermore, the angular velocity of the end-effector $\mathscr{P}_5$ with respect to $\mathscr{F}_1$ and expressed in $\mathscr{F}_1$ takes the form:

$$^1\omega_{5/1} = \dot{\alpha}\,^1\mathbf{z}_2 - \dot{\beta}\,^1\mathbf{x}_2 \tag{3.5}$$

Knowing the linear velocity $^1\mathbf{v}_{H5}$ of point H_5 in $\mathscr{F}_1$, the linear velocities $^1\mathbf{v}_{c35}$ and $^1\mathbf{v}_{c45}$ of points $\mathbf{c}_{35}$ and $\mathbf{c}_{45}$ in $\mathscr{F}_1$ can be expressed as:

$$^1\mathbf{v}_{c35} = {}^1\mathbf{v}_{H5} + \left({}^1\mathbf{h}_5 - {}^1\mathbf{c}_{35}\right) \times {}^1\omega_{5/1} \tag{3.6}$$

$$^1\mathbf{v}_{c45} = {}^1\mathbf{v}_{H5} + \left({}^1\mathbf{h}_5 - {}^1\mathbf{c}_{45}\right) \times {}^1\omega_{5/1} \tag{3.7}$$

From Eqs. (3.2)-(3.5) and Eqs. (3.6)-(3.7):

$$-\dot{\theta}_3 r_3\,^1\mathbf{y}_2 = -r_3\dot{\alpha}\,^1\mathbf{y}_2 + r_5\,^1\mathbf{z}_2 \times (\dot{\alpha}\,^1\mathbf{z}_2 - \dot{\beta}\,^1\mathbf{x}_2) \tag{3.8}$$
$$-\dot{\theta}_4 r_4\,^1\mathbf{y}_2 = -r_4\dot{\alpha}\,^1\mathbf{y}_2 - r_5\,^1\mathbf{z}_2 \times (\dot{\alpha}\,^1\mathbf{z}_2 - \dot{\beta}\,^1\mathbf{x}_2) \tag{3.9}$$

Upon simplification of Eqs. (3.8) and (3.9), we obtain:

$$\dot{\theta}_3 = \dot{\alpha} + \mu\dot{\beta} \tag{3.10}$$
$$\dot{\theta}_4 = \dot{\alpha} - \mu\dot{\beta} \tag{3.11}$$

As a result, the output rotational velocity vector $\dot{\mathbf{q}}_{TR}$ of the tilt-roll wrist is expressed as a function of its input velocity vector $\dot{\boldsymbol{\theta}}$ in a matrix form as follows:

$$\dot{\mathbf{q}}_{TR} = \mathbf{J}_{TR}\dot{\boldsymbol{\theta}} \tag{3.12}$$

with $\mathbf{J}_{TR}$ is the kinematic Jacobian matrix of the wrist expressed as:

$$\mathbf{J}_{TR} = \begin{bmatrix} 1/2 & 1/2 \\ 1/2\mu & -1/2\mu \end{bmatrix} \tag{3.13}$$

$\dot{\mathbf{q}}_{TR} = [\dot{\alpha},\ \dot{\beta}]^T$ and $\dot{\boldsymbol{\theta}} = [\dot{\theta}_3,\ \dot{\theta}_4]^T$.
Let $\mathbf{m} = [m_\alpha,\ m_\beta]^T$ be the output moments of the tilt-roll wrist and $\boldsymbol{\tau} = [\tau_3,\ \tau_4]^T$ be the input torque vector of the wrist. From Eq. (3.12),

$$\boldsymbol{\tau} = -\mathbf{J}_{TR}^T\mathbf{m}_e \tag{3.14}$$

with $\mathbf{m}_e = -\mathbf{m}$ being the external moments applied by environment to the tilt-roll wrist. By rewriting Eq. (3.14) we can express the static equilibrium of the tilt-roll wrist as follows:

$$\mathbf{m}_e = \mathbf{W}_{TR}\boldsymbol{\tau} \tag{3.15}$$

with $\mathbf{W}_{TR}$ being the wrench matrix of the wrist:

$$\mathbf{W}_{TR} = -\mathbf{J}_{TR}^{-T} \tag{3.16}$$

Besides $\mathbf{m}_e$ is expressed as:

$$\mathbf{m}_e = \begin{bmatrix} m_2 g h_2 \cos\alpha & m_2 g w_5 \cos\alpha \sin\beta \end{bmatrix}^T \tag{3.17}$$

m_2 indicates the mass of $\mathscr{P}_5$ and $\mathbf{g} = [0,\ 0,\ -g]^T$ is the gravity acceleration with $g = 9.81\ m.s^{-2}$. As shown in Fig. 3.3, h_2 and w_5 denotes the distances between O_2 and C_2 along z_5 and y_5, respectively. C_2 is the Center of Mass (CoM) of the end-effector.

3.1.2 Kinetostatic Model of the Overall Manipulator

In this section we present the kinetostatic model of the overall manipulator. In order to define the manipulator Jacobian and its wrench matrix, we first introduce the loop-closure equations of the CDPR, which are given by

$$^0\mathbf{l}_i = {}^0\mathbf{a}_i - {}^0\mathbf{p} - {}^0\mathbf{R}_1\,{}^1\mathbf{b}_i, \quad i = 1,\ 2,\ ...,\ 8 \tag{3.18}$$

where $^0\mathbf{l}_i$ is the ith cable vector, i.e., the Cartesian coordinate vector pointing from point B_i to point A_i. Points A_i and B_i stand for the ith cable exit point and anchor point, respectively. The former point is the location of the ith pulley fixed to the ceiling and the latter is the connection point between the cable and the moving-platform. $^0\mathbf{a}_i = [a_{ix},\ a_{iy},\ a_{iz}]^T$, $^1\mathbf{b}_i = [b_{ix},\ b_{iy},\ b_{iz}]^T$ and $^0\mathbf{p} = [p_x,\ p_y,\ p_z]^T$ are the Cartesian coordinate vector of points A_i, B_i and P, respectively. $\mathbf{t}_i$, $i = 1,\ 2,\ ...,\ 8$, stands for the ith cable tension vector. $\mathbf{t}_i = t_i\,{}^0\mathbf{u}_i$ and its magnitude is expressed as $t_i = \|\mathbf{t}_i\|_2$, $i = 1, ..., 8$. $^0\mathbf{u}_i$ denotes the ith cable unit vector namely,

$$^0\mathbf{u}_i = \frac{^0\mathbf{l}_i}{l_i}, \quad i = 1,\ 2,\ ...,\ 8 \tag{3.19}$$

l_i being the ith cable length. The equilibrium of the external forces applied on the moving-platform, is formulated as follows:

$$\sum t_i\,{}^0\mathbf{u}_i + m\mathbf{g} = 0, \quad i = 12,\ 3,\ 4,\ 56,\ 7,\ 8 \tag{3.20}$$

$m\mathbf{g}$ is the weight of the moving-platform. m denotes total mass of the moving-platform and the spherical wrist. The equilibrium of moments applied onto the moving-platform about point P expressed in frame $\mathscr{F}_0$ takes the form:

$$\sum t_i \left({}^0\mathbf{R}_1\,{}^1\mathbf{b}_i \times {}^0\mathbf{u}_i \right) + m({}^0\mathbf{c} - {}^0\mathbf{p}) \times {}^0\mathbf{g} = 0, \quad i = 1, ..., 8 \tag{3.21}$$

with $\mathbf{c}$ being the Cartesian coordinates vector of the CoM of moving-platform:

$$\mathbf{c} = \frac{m_1 \mathbf{c}_1 + m_2 \mathbf{c}_2}{m_1 + m_2} \tag{3.22}$$

$\mathbf{c}_1$ is the Cartesian coordinates vector of the CoM of components $\mathscr{P}_1$ to $\mathscr{P}_4$ with mass of m_1 defined as:

$$m_1 = m_b + 2m_c + m_s + m_{\mathscr{P}_2} + m_{\mathscr{P}_3} + m_{\mathscr{P}_4} \tag{3.23}$$

m_b, m_c and m_s being the masses of the moving-platform components i.e., its base, columns and shaft, respectively. $\mathbf{c}_2$ is the Cartesian coordinates vector of the CoM of the terminal link $\mathscr{P}_5$, its mass being equal to m_2. Therefore, the total mass of the moving-platform is expressed as follows:

$$m = m_1 + m_2 \tag{3.24}$$

The input tilt-roll wrist torques τ_3 and τ_4 are a function of the cable tension difference in cable loops $\mathscr{C}_{12}$ and $\mathscr{C}_{56}$, respectively:

$$\tau_3 = r_c\,(t_1 - t_2) \tag{3.25}$$
$$\tau_4 = r_c\,(t_6 - t_5) \tag{3.26}$$

r_c being the radius of the groove made in $\mathscr{P}_3$ and $\mathscr{P}_4$ to house the two cable loops. From Eq. (3.15) and Eqs. (3.20) to (3.26) the static equilibrium model of the manipulator is expressed in a matrix form as:

$$\mathbf{W}\mathbf{t} + \mathbf{w}_g = \mathbf{0}_8 \tag{3.27}$$

where $\mathbf{0}_8$ is the eight-dimensional zero vector and the wrench matrix $\mathbf{W}$ takes the following form:

$$\mathbf{W} = \begin{bmatrix} {}^0\mathbf{u}_1 & {}^0\mathbf{u}_2 & {}^0\mathbf{u}_3 & {}^0\mathbf{u}_4 & {}^0\mathbf{u}_5 & {}^0\mathbf{u}_6 & {}^0\mathbf{u}_7 & {}^0\mathbf{u}_8 \\ {}^0\mathbf{d}_1 & {}^0\mathbf{d}_2 & {}^0\mathbf{d}_3 & {}^0\mathbf{d}_4 & {}^0\mathbf{d}_5 & {}^0\mathbf{d}_6 & {}^0\mathbf{d}_7 & {}^0\mathbf{d}_8 \\ r_c & -r_c & 0 & 0 & -r_c & r_c & 0 & 0 \\ \mu r_c & -\mu r_c & 0 & 0 & \mu r_c & -\mu r_c & 0 & 0 \end{bmatrix} \tag{3.28}$$

with,

$$ {}^0\mathbf{d}_i = {}^0\mathbf{R}_1\,{}^1\mathbf{b}_i \times {}^0\mathbf{u}_i, \quad i = 1, \ldots, 8. \tag{3.29}$$

$\mathbf{t}$ is the vector containing the tensions exerted by the eight actuators to the cables.

$$\mathbf{t} = [t_1 \quad t_2 \quad t_3 \quad t_4 \quad t_5 \quad t_6 \quad t_7 \quad t_8]^T \tag{3.30}$$

$\mathbf{w}_g$ is the eight-dimensional gravity wrench vector applied on the moving-platform and the tilt-roll wrist, namely,

$$\mathbf{w}_g = [m\,{}^0\mathbf{g}^T \quad m({}^0\mathbf{R}_1\,{}^1\mathbf{c} \times {}^0\mathbf{g})^T \quad \mathbf{m}_{\alpha,\beta}^T]^T \tag{3.31}$$

The Cartesian coordinates vector of C_1 expressed in $\mathscr{F}_1$ is denoted as:

$$ {}^1\mathbf{c}_1 = [0,\ 0,\ c_{1z}]^T \tag{3.32}$$

with,

$$c_{1z} = \frac{-h_1(m_c + m_s + m_{\mathscr{P}_2} + m_{\mathscr{P}_3} + m_{\mathscr{P}_4})}{m_1} \tag{3.33}$$

and variable Cartesian coordinates vector of CoM, namely, C_2 is a function of α and β as follows:

$$
{}^1\mathbf{c}_2 = \begin{bmatrix} -w_2 \sin \beta \\ -h_2 \cos \alpha - w_2 \sin \alpha \cos \beta \\ -h_2 \sin \alpha + w_2 \cos \alpha \cos \beta - h_1 \end{bmatrix}
\tag{3.34}
$$

The tilt angle of the end-effector is denoted as $\alpha = \angle(y_1, \ x_2)$ and its roll angle is defined as $\beta = \angle(z_2, \ x_5)$. $\mathbf{m}_{\alpha, \beta}$ is the array of the moments applied by gravity onto the tilt-roll wrist about axes z_2 and z_5, respectively:

$$
\mathbf{m}_{\alpha, \beta} = [m_\alpha, \ m_\beta]^T
\tag{3.35}
$$

with $m_\alpha = m_{g_z}$ and $m_\beta = -m_{g_x}$. The moment due to the weight of $\mathscr{P}_5$ exerted on the tilt-roll wrist expressed in $\mathscr{F}_2$ is denoted as

$$
{}^2\mathbf{m}_g = m_2 \left({}^2\mathbf{c_2} \times {}^2\mathbf{R}_0 {}^0\mathbf{g} \right) = m_2 g \begin{bmatrix} -w_2 \sin \beta \cos \alpha \\ w_2 \sin \beta \sin \alpha \\ h_2 \cos \alpha + w_2 \cos \beta \sin \alpha \end{bmatrix}
\tag{3.36}
$$

It should be noted that, in Eq. (3.27) the friction between cable-loops and $\mathscr{P}_3$ and $\mathscr{P}_4$ is neglected. Hereafter, we can express the differential kinematics of the manipulator that formulates the relation between the output twist $\dot{\mathbf{q}} = \begin{bmatrix} \dot{\mathbf{p}}^T, & \boldsymbol{\omega}^T, & \dot{\mathbf{q}}_{TR}^T \end{bmatrix}^T$ of the manipulator and the cable vector $\dot{\mathbf{l}} = \begin{bmatrix} \dot{l}_1, & ..., & \dot{l}_8 \end{bmatrix}^T$:

$$
\mathbf{J}\dot{\mathbf{q}} = \dot{\mathbf{l}}
\tag{3.37}
$$

Velocity of the origin of frame $\mathscr{F}_1$ with respect to $\mathscr{F}_0$ is defined as $\dot{\mathbf{p}}$ and the angular velocity of the moving-platform with respect to $\mathscr{F}_0$ is defined as $\boldsymbol{\omega}$. Jacobian matrix $\mathbf{J}$ is calculated based on the well-known kineto-static duality:

$$
\mathbf{J} = -\mathbf{W}^T
\tag{3.38}
$$

3.1.3   Wrench Feasible Workspace

In this section, we introduce the static workspace of the CDPR with an embedded tilt-roll wrist. In general, the static workspace of the eight-DoF CDPR with embedded tilt-roll wrist consist of set of positions and orientation of the moving platform and the orientation of the end-effector, namely, ${}^0\mathbf{p}$ and ${}^0\mathbf{R}_1$ and $\mathbf{q}_{TR}$ which satisfies the static equilibrium of the manipulator. The set $\mathscr{T}$ forms the feasible cable tensions as a box in eight-dimensional space:

$$
\mathscr{T} = \{\mathbf{t} \in \mathbb{R}^8 : \ \mathbf{t}_{min} \le \mathbf{t} \le \mathbf{t}_{max}\}.
\tag{3.39}
$$

where, $\mathbf{t}_{min}$ and $\mathbf{t}_{max}$ are the lower and upper bounds of admissible cable tensions. Static Workspace (SW), namely, $\mathscr{S}$ is set of moving-platform poses and tilt-roll wrist

configurations satisfying the static equilibrium of the manipulator with admissible cable tensions.

$$\mathscr{S} = \{(^0\mathbf{p}, {}^0\mathbf{R}_1, \mathbf{q}_{_{TR}}) \in \mathbb{R}^3 \times SO(3) \times \in \mathbb{R}^2 : \exists \mathbf{t} \in \mathscr{T}, \mathbf{Wt} + \mathbf{w}_g = \mathbf{0}_8\} \qquad (3.40)$$

where $SO(3)$ is the group of proper rotation matrices. As the visualization of such an eight-dimensional workspace is impossible with common human perception in 3D, we define the static workspace of the manipulator for two different cases. From Eq. (3.40), we derive two subsets $\mathscr{S}_1$ and $\mathscr{S}_2$ based on the constrained orientations of the moving-platform and the tilt-roll wrist. The former subset, namely, $\mathscr{S}_1$ is a set for a given orientation of the moving-platform and the wrist, i.e., the translational SW of the manipulator with constant orientation of $^0\mathbf{R}_1$ and $\mathbf{q}_{_{TR}}$.

$$\mathscr{S}_1 = \{{}^0\mathbf{p} \in \mathbb{R}^3 \,|\, {}^0\mathbf{R}_1 = \mathbf{I}_3, \; \alpha = \beta = \pi/2 \; : \exists \mathbf{t} \in \mathscr{T}, \mathbf{Wt} + \mathbf{w}_g = \mathbf{0}_8\} \qquad (3.41)$$

The minimum moment due to weight of $\mathscr{P}_5$ exerted on the tilt-roll wrist corresponds to $\alpha = \beta = \pi/2$. Therefore, for largest possible workspace of $\mathscr{S}_1$ we consider those angles for tilt and roll of the wrist. $\mathscr{S}_2$ is defined as the static workspace of the manipulator for a constant orientation of the moving-platform while the tilt and roll angles are free to rotate.

$$\mathscr{S}_2 = \{{}^0\mathbf{p} \in \mathbb{R}^3 \,|\, {}^0\mathbf{R}_1 = \mathbf{I}_3 : -\pi \leq \alpha \;\&\; \beta \leq \pi : \exists \mathbf{t} \in \mathscr{T}, \mathbf{Wt} + \mathbf{w}_g = \mathbf{0}_8\} \qquad (3.42)$$

In order to trace the static workspace, the capacity margin index is employed to determine the static equilibrium of the moving-platform for a given pose. In [Gua+14] and [Rui+15] the capacity margin index was introduced and implemented for tracing wrench feasible workspace and static equilibrium of the CDPRs. In the latter papers the algorithm of calculation of capacity margin is detailed.

Hereafter, the capacity margin index can be checked to indicates whether a pose of the moving-platform belongs to the static workspace or not. By discretizing the Cartesian space and interpolating between the index values, we are able to trace the static workspace. The discretization of Cartesian space is detailed, respectively given by

$$\begin{align}
x_i &= x_0 + i\,\delta \quad (i = 0, \, ..., \, n_x) \tag{3.43}\\
y_j &= y_0 + j\,\delta \quad (j = 0, \, ..., \, n_y) \tag{3.44}\\
z_k &= z_0 + k\,\delta \quad (k = 0, \, ..., \, n_z) \tag{3.45}
\end{align}$$

with δ being the resolution of the discretization and $\mathbf{o}_0 = [x_0, \, y_0, \, z_0]^T$ denoting the origin of frame $\mathscr{F}_0$. The number of discretized points along x, y and z are detailed in the following, respectively.

$$n_x = \left\lfloor \frac{l_0 - x_0}{\delta} \right\rfloor \qquad (3.46)$$

$$n_y = \left\lfloor \frac{w_0 - y_0}{\delta} \right\rfloor \qquad (3.47)$$

$$n_z = \left\lfloor \frac{h_0 - z_0}{\delta} \right\rfloor \qquad (3.48)$$

where, l_0, w_0 and h_0 are the length, width and height of the manipulator frame ($\mathscr{P}_0$), respectively. The number of points found to be inside the static workspace, $\mathscr{S}_1$ and $\mathscr{S}_2$, are denoted as $N_{\mathscr{S}_1}$ and $N_{\mathscr{S}_2}$ as follows:

$$N_{\mathscr{S}_1} = \left| \left\{ \mathbf{p} \left(x_i, \ y_j, \ z_k \right) \in \mathscr{S}_1 \right\} \right| \tag{3.49}$$

$$N_{\mathscr{S}_2} = \left| \left\{ \mathbf{p} \left(x_i, \ y_j, \ z_k \right) \in \mathscr{S}_2 \right\} \right| \tag{3.50}$$

with x_i, y_i and z_i being defined in Eqs. (3.43-3.45). The ratios of static workspace, namely $\mathscr{R}_{\mathscr{S}_i}$, $i = 1, 2$, is introduced to quantify the proportion of $\mathscr{S}_1$ and $\mathscr{S}_2$ to the task space, respectively.

$$\mathscr{R}_{\mathscr{S}_1} = \frac{N_{\mathscr{S}_1}}{(n_x + 1)(n_y + 1)(n_z + 1)} \tag{3.51}$$

$$\mathscr{R}_{\mathscr{S}_2} = \frac{N_{\mathscr{S}_2}}{(n_x + 1)(n_y + 1)(n_z + 1)} \tag{3.52}$$

The section deals with the workspace analysis of the CDPR using a tilt-roll wrist under study.
The set $\mathscr{T}$ represents the feasible cable tensions and takes the shape of a box in eight-dimensional space:

$$\mathscr{T} = \left\{ \mathbf{t} \in \mathbb{R}^8 : \ \mathbf{t}_{min} \leq \mathbf{t} \leq \mathbf{t}_{max} \right\}. \tag{3.53}$$

where, $\mathbf{t}_{min}$ and $\mathbf{t}_{max}$ are the lower and upper bounds of admissible cable tensions. The static Workspace, $\mathscr{S}$ is the set of moving-platform poses and tilt-roll wrist configurations satisfying the static equilibrium of the manipulator under the action of gravity.

Here, we consider the CREATOR prototype setup in order to trace $\mathscr{S}_1$ and $\mathscr{S}_2$ for different orientations of the moving-platform. The main dimensions of the prototype are given in Table 3.2. The specifications listed in Table 3.2 are based on the preliminarily manufactured prototype shown in Fig. 3.1. The weight of the wrist highly depends on the material of the parts $\mathscr{P}_2$, $\mathscr{P}_5$ and the end-effector. Because ABS plastic is employed for $\mathscr{P}_2$, the overall weight of the moving-platform can be significantly reduced by substituting steel bevel gears with nylon ones. The prototype frame is 4 m long (l_0), 3.5 m wide (w_0) and 4 m high (h_0). The moving-platform under study is suspended by six cables as shown in Fig. 3.2. The SW illustrated in Fig. 3.6 refers to constant orientation of the moving-platform for different given orientation of moving-platform. Cable loops are plotted in magenta and single-actuated cables are represented in red. It is apparent that ψ has significant effect on the size of the SW as well as the position of anchor points and exit points. According to the obtained results, the largest SW (fig. 3.10b) is associated with $\psi = 0°$. The gravitational external wrench due to the varying CoM of the wrist, namely C_2 has effect on the SW. Therefore, two cases are considered. The former case (shown with green volume in the figure) considers the minimum external wrench applied onto the moving-platform by the wrist, i.e., the tilt-roll wrist is in home configuration
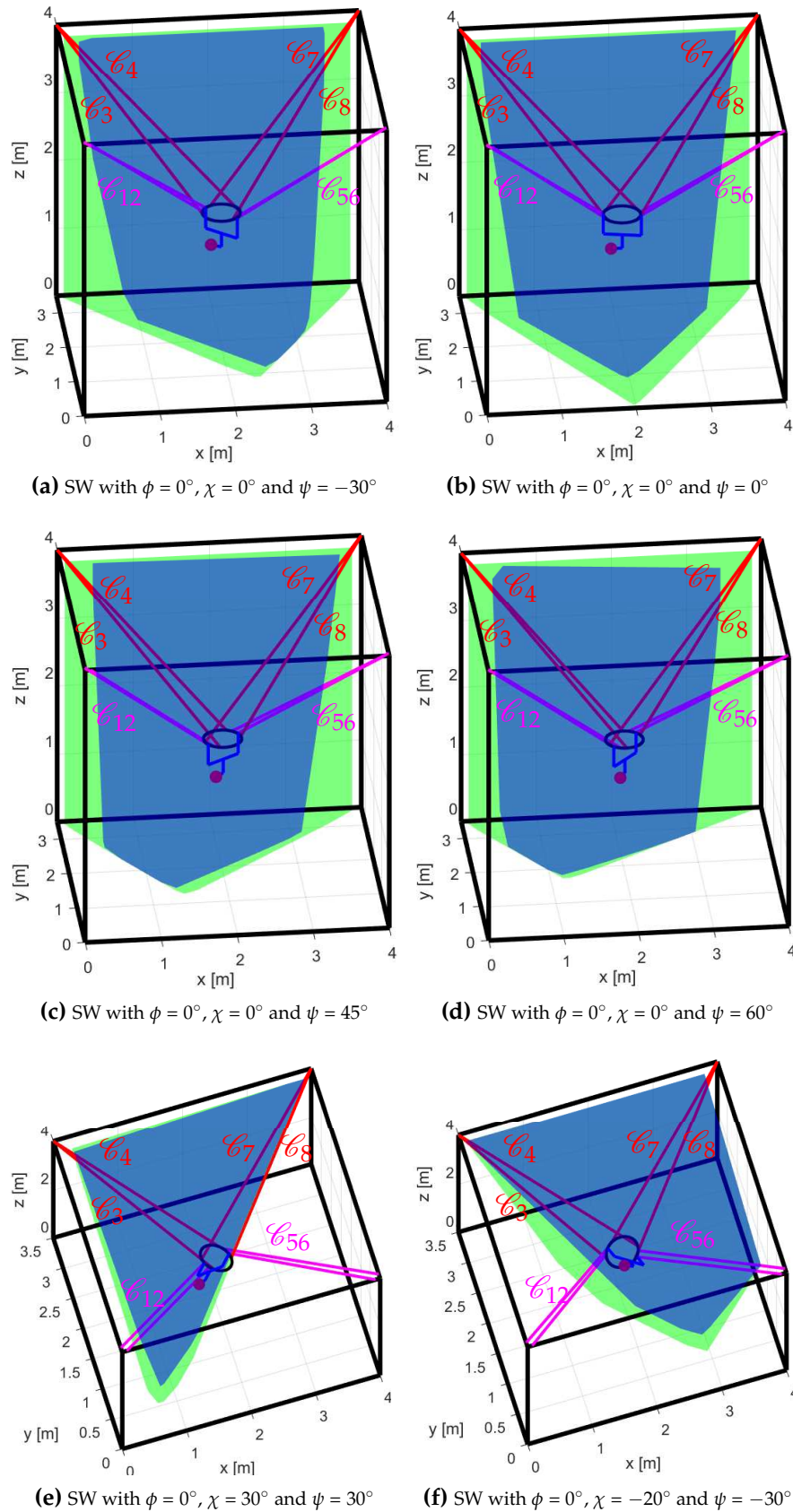
Figure 3.6: $\mathscr{S}_1$ and $\mathscr{S}_2$ for different orientations of the top-plate

Table 3.1: Parameters of the CREATOR prototype

Parameter	Abbreviation	Value
Vector of CoM associated to $\mathscr{P}_1$-$\mathscr{P}_4$ [m]	$^1\mathbf{c}_1$	$[0,\, 0,\, -0.15]^T$
Vector of CoM associated to $\mathscr{P}_5$ [m]	$^2\mathbf{c}_2$	$[-h_2,\, w_5 cos\beta,\, -w_5 sin\beta]^T$
Mass of $\mathscr{P}_1$-$\mathscr{P}_4$ [kg]	m_1	4
Mass of $\mathscr{P}_5$ [kg]	m_2	0.6
Radius of the groove made in $\mathscr{P}_3$ and $\mathscr{P}_4$ [m]	r_c	0.1
Distance between O_2 and C_2 along z_5 [m]	h_2	0.23
Distance between O_2 and C_2 along y_5 [m]	w_5	0.03
Maximum admissible cable tension [N]	t_{max}	128
Minimum admissible cable tension [N]	t_{min}	0

($\alpha = \pi/2$ and $\beta = 0$). The latter case computes the SW while the $\mathscr{P}_5$ exerts the maximum external wrench due to gravity on the moving-platform and the wrist with blue volume in the figure. It should be noted that, the gravitational external wrench of the wrist is a function of α and β. The figure shows the variation of $\mathscr{S}_1$ and $\mathscr{S}_2$ for different orientation of moving-platform. The largest volumes for $\mathscr{S}_1$ and $\mathscr{S}_2$ are 25.3 m^3 and 14.15 m^3, respectively, as shown in Fig. 3.6(b). On the other hand, the smallest volume of SW is associated to Fig. 3.6(d) with 13 m^3 of $\mathscr{S}_1$ and 8.15 m^3 of $\mathscr{S}_2$.

It appears to be a trade-off between translation and large rotation workspaces due to the cable-loops in the fully-actuated CDPR. It is noteworthy that translation and orientation workspaces become larger when employing two additional actuators.

3.1.4 Twist Feasible Workspace

After the wrench feasibility analysis, we proceed with further analysis on the twist feasibility of the CDPR with an embedded tilt-roll wrist. The definition of the workspace is detailed in Sec. 2.2. Figures 3.7 and 3.8 shows the TFW of the 3T2R manipulator for different cases. The following equation expresses the required twist induced on the moving-platform by the cables.

$$\dot{\mathbf{p}} = \begin{bmatrix} \dot{p}_x & \dot{p}_y & \dot{p}_z & \omega_x & \omega_y & \omega_z & \omega_\alpha & \omega_\beta \end{bmatrix}^T \tag{3.54}$$

and cable velocity boundaries are as follows:

$$\dot{l}_{i,min} \leq \dot{l}_i \leq \dot{l}_{i,max}, \quad i = 1, ..., 8 \tag{3.55}$$

with $\dot{l}_{i,max} = -\dot{l}_{i,min} = 2.94 \, m.s^{-1}$ and i=1,...,8. The workspaces shown in Fig. 3.7 are associated to a required twist set with only the linear velocity components of the moving-platform in Euclidean space. By increasing the amplitudes of linear twist ($\dot{p}_x$, $\dot{p}_y$, $\dot{p}_z$) the TFW sizes shrink from Fig. 3.7a to Fig. 3.7d, respectively. The void space inside the TFWs are conic and they join two opposite corners of the cuboid of the manipulator frame. The evolution of the TFW size is analogous to that mention in Fig. B.11 Appendix B.2.

The evolution of the TFW due to variation of the tilt-roll required twist [ω_α, ω_β] is depicted in Fig. 3.8. While the twist set of the moving-platform, namely, [$\dot{p}_x$, $\dot{p}_y$, $\dot{p}_z$, ω_x, ω_y, ω_z], is kept fixed. The figure clearly shows the reduction in size of workspace by increasing the required twist of the tilt-roll wrist. The void spaces within the workspace expand along the cable-loops as the required twist of the tilt-roll wrist is function of the cable-loops available velocity.

3.2 Optimum Design of the Manipulator

The manipulator under study is a hybrid robot consisting in an under-constrained moving-platform accommodating a tilt-roll wrist. The embedded wrist provides large amplitudes of tilt and roll rotations and a large translational workspace obtained by the moving-platform. This manipulator is suitable for tasks requiring

(a) $-1.6 \, m.s^{-1} \leq \dot{p}_x, \dot{p}_y, \dot{p}_z \leq 1.6 \, m.s^{-1}$

(b) $-1.7 \, m.s^{-1} \leq \dot{p}_x, \dot{p}_y, \dot{p}_z \leq 1.7 \, m.s^{-1}$

(c) $-1.75 \, m.s^{-1} \leq \dot{p}_x, \dot{p}_y, \dot{p}_z \leq 1.75 \, m.s^{-1}$

(d) $-1.8 \, m.s^{-1} \leq \dot{p}_x, \dot{p}_y, \dot{p}_z \leq 1.8 \, m.s^{-1}$
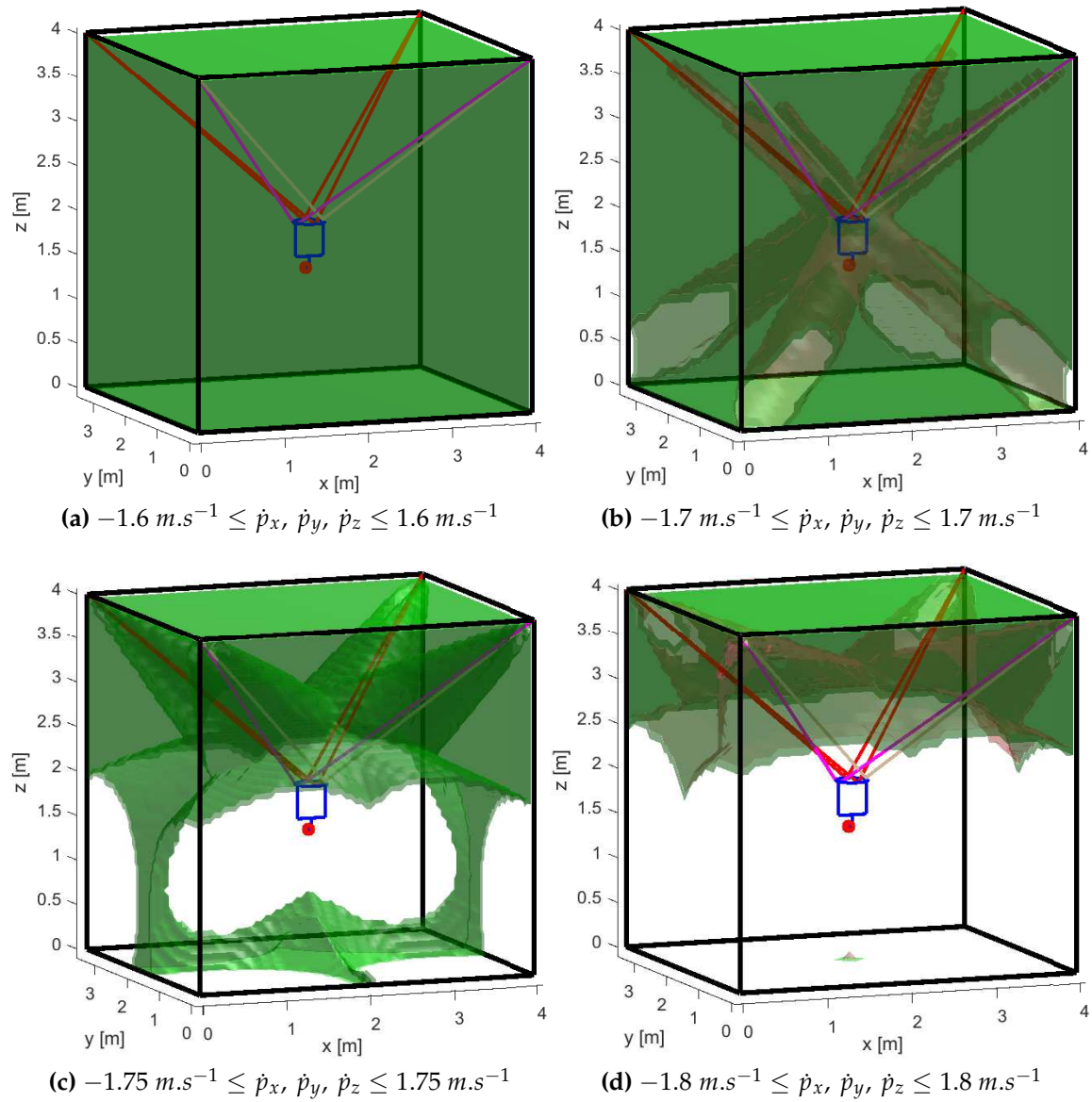
Figure 3.7: Twist feasible workspace of the manipulator with ($\omega_x = \omega_y = \omega_z = \omega_\alpha = \omega_\beta = 0 \, rad.s^{-1}$)

(a) $-1.2\ rad.s^{-1} \leq \omega_\alpha,\ \omega_\beta \leq 1.2\ rad.s^{-1}$

(b) $-1.23\ rad.s^{-1} \leq \omega_\alpha,\ \omega_\beta \leq 1.23\ rad.s^{-1}$

(c) $-1.28\ rad.s^{-1} \leq \omega_\alpha,\ \omega_\beta \leq 1.28\ rad.s^{-1}$

(d) $-1.44\ rad.s^{-1} \leq \omega_\alpha,\ \omega_\beta \leq 1.44\ rad.s^{-1}$

Figure 3.8: Twist feasible workspace of the manipulator with ($-1.6\ m.s^{-1} \leq \dot{p}_x,\ \dot{p}_y,\ \dot{p}_z \leq 1.6\ m.s^{-1}$ & $\omega_x = \omega_y = \omega_z = 0\ rad.s^{-1}$)

large rotation and translation workspaces like tomography scanning, camera-orienting devices and visual surveillance. The moving-platform is an eight-degree-of-freedom articulated mechanism with large translational and rotational workspaces and it is suspended from a fixed frame by six cables. The manipulator employs two bi-actuated cables, i.e., cable loops to transmit the power from motors fixed on the ground to the tilt-roll wrist. Therefore, the manipulator achieves better dynamic performances due to a lower inertia of its moving-platform.

This section deals with the optimization of the CDPR design with an embedded tilt-roll wrist. The investigation of the optimum manipulator focuses on two goals. The first one is to determine the optimum cable arrangement. The second goal is to find the optimum design variables of the moving-platform. The design variables appearing in Table 3.2 are searched for whereas the design parameters given in Table 3.3 are predefined and constant. The optimization problem aims to maximize the volume of the static w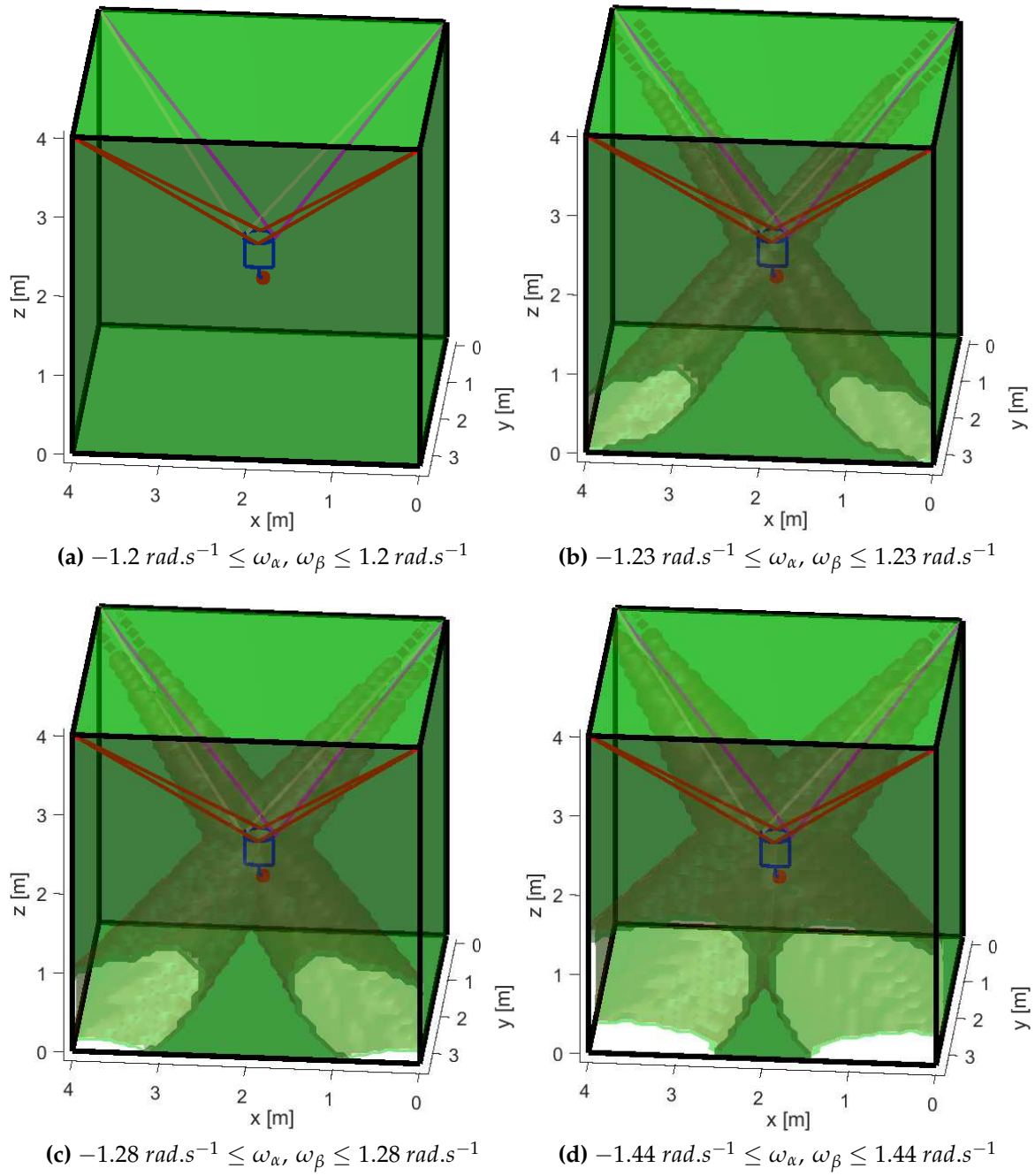orkspace, $\mathscr{R}_{\mathscr{S}_2}$. The decision variables describe the overall dimensions of the moving-platform while those of the tilt-roll wrist are considered as design parameters. The positions of the anchor points B_i, $i = 1, \ldots, 8$ on $\mathscr{P}_1$ are also considered as decision variables in order to determine the optimum cable arrangement of the CDPR.

The design variables appearing in Table 3.2 are searched while the position of the moving-platform, namely, point P and the inputs are mentioned in Table 3.3. This section deals with optimum design of the moving-platform to maximize the volume of the static workspace, $\mathscr{R}_{\mathscr{S}_2}$. The decision variables describe the overall dimensions of the moving-platform while those of tilt-roll wrist are considered as design parameters. The positions of the anchor points on $\mathscr{P}_1$ are also considered as decision variables in order to determine the optimum cable configuration of the CDPR.

Objective Function

The cable-loops and the tilt-roll wrist have significant effects on the size and shape of the static workspace. The main goal of the manipulator is to achieve large amplitudes of rotations α and β of its moving-platform across its workspace. Therefore, maximizing $\mathscr{R}_{\mathscr{S}_2}$ is the objective function considered to improve the performance of the manipulator.

Design variables

All the exit-points of the CDPR, namely, A_i and $i = 1, \ldots, 8$ are located on the top of $\mathscr{P}_0$ and on its rectangle vertices. The vertices, namely, $\mathscr{A}_i$ and $i = 1, 2, 3, 4$ are illustrated in Fig. 3.9. Moreover, we formulate all the combinations of the cable arrangement by assuming that each $\mathscr{A}_i$, $i = 1, 2, 3, 4$ accommodates two exit-points. Therefore, cables $\mathscr{C}_i$ connects A_i to B_i and $i = 1, \ldots, 8$. The total number $\mathcal{N}_a$ of cable arrangements is computed as:

$$\mathcal{N}_a = \frac{P(n, k)}{v_1! \, v_2! \, v_3! \, v_4!} = \frac{8!}{(2!)^4} = 2520 \tag{3.56}$$
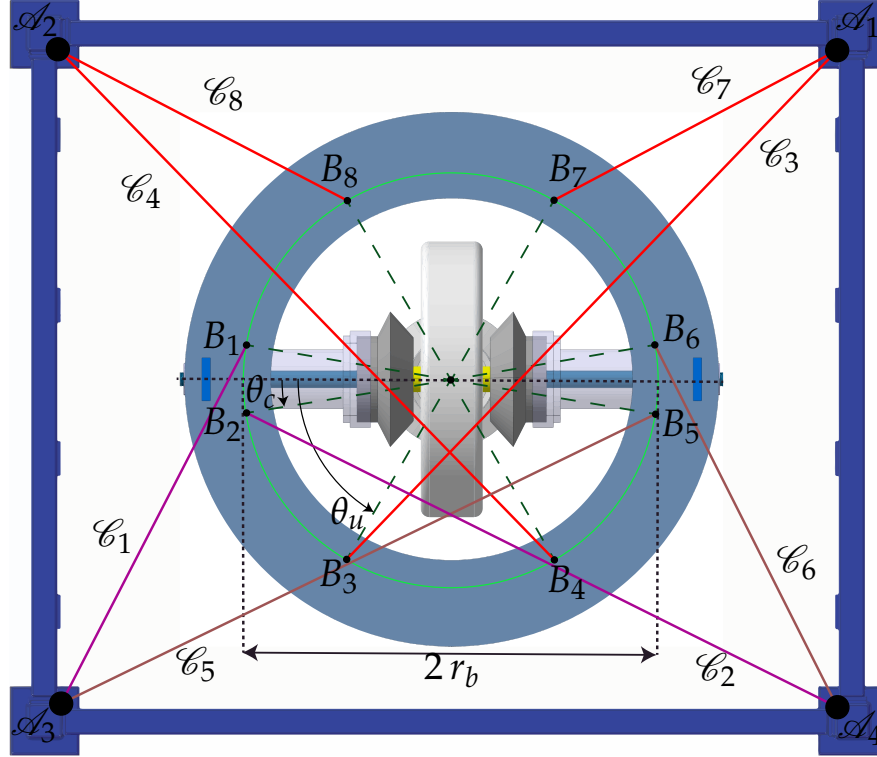
Figure 3.9: Top-view of the base frame and up-scaled moving-platform with the embedded tilt-roll wrist

$P(n, k)$ refers to k-permutations of n with $n = k = 8$. The number of times that $\mathscr{A}_i$, $i = 1, 2, 3, 4$ can be chosen as exit points is noted as $v_i = 2$. From Eq. (3.56), 2520 cable arrangements are considered for the CDPR under study. Decision variable, η is associated to the cable arrangement of the CDPR.

The geometric design variables are shown in Figs. 3.4 and 3.9. The first decision variable, namely, r_b, is the radius of the circle passing through B_i, $i = 1, ..., 8$. h_1 denotes the height of the moving-platform. w_b is the width of the top-plate of the moving-platform. All the anchor points are located on a circle drawn on the top-plate with radius of r_b, as shown in Fig. 3.9. Therefore, the positions of the anchor points $^1\mathbf{b}_i$ are defined in polar coordinates as follows:

$$^1\mathbf{b}_i = -r_b \begin{bmatrix} \cos \theta_i \\ \sin \theta_i \end{bmatrix} \qquad i = 1, ..., 8. \qquad (3.57)$$

The anchor point B_i is connected to the exit point A_i, $i = 1, ..., 8$. The exit points of the manipulator, A_i, are fixed on the top vertices of $\mathscr{P}_0$ as shown in Fig. 3.2.

The anchor points of the cable-loops, namely, B_1, B_2, B_5, B_6 are constrained to be close to x_1-axis in order to facilitate the actuation of $\mathscr{P}_3$ and $\mathscr{P}_4$. This constraint prevents undesired cable-loop routing. Moreover, the anchor points of the cable-loops are dependent on one another to guarantee the symmetric actuation of the tilt-roll wrist as follows:

Table 3.2: Boundaries and optimum values of the design variables

Design variable	r_b	h_1	w_b	θ_c	θ_u	μ
Unit	[mm]	[mm]	[mm]	[deg]	[deg]	[]
Lower-bound (lb)	5	100	3	-45	0	1
Optimum value	183	384	8	45	90	201
Upper-bound (ub)	210	400	10	45	360	2520

$$\theta_1 = -\theta_c \tag{3.58}$$
$$\theta_2 = \theta_c \tag{3.59}$$
$$\theta_5 = \pi - \theta_c \tag{3.60}$$
$$\theta_6 = \pi + \theta_c \tag{3.61}$$

θ_c is the cable loop angle depicted in Fig. 3.9.

Moreover, some constraints are defined to keep a symmetry of the anchor points B_i onto the moving-platform. The following expresses the constraints relating the anchor points of uni-actuated cables to one another:

$$\theta_3 = \theta_u \tag{3.62}$$
$$\theta_4 = \pi - \theta_u \tag{3.63}$$
$$\theta_7 = \pi + \theta_u \tag{3.64}$$
$$\theta_8 = -\theta_u \tag{3.65}$$

θ_u being the angle defining the location of the anchor points of the uni-actuated cables onto the moving-platform. Therefore, the location of anchor points B_i, $i = 1, \ldots, 8$, are function of θ_c or θ_u, and the vector **x** of decision variables becomes

$$\mathbf{x} = [r_b,\ h_1,\ w_b,\ \theta_c,\ \theta_u,\ \mu]^T \tag{3.66}$$

Constraints

The first non-linear constraint prevents collision between the end-effector and the top-plate, $\mathscr{P}_5$ and $\mathscr{P}_1$, respectively. Point E placed on the tip of $\mathscr{P}_5$ is prone to undesired contact with $\mathscr{P}_1$ for some amplitudes of α and β. Hence, the following

Table 3.3: Given design parameters

Parameter	Abbreviation	Value
Mass of $\mathscr{P}_2$ [g]	$m_{\mathscr{P}_2}$	60
Mass of $\mathscr{P}_3$ [g]	$m_{\mathscr{P}_3}$	200
Mass of $\mathscr{P}_4$ [g]	$m_{\mathscr{P}_4}$	200
Mass of the terminal link [g]	m_2	600
Length of the terminal link [mm]	h_e	126
Width of the end-effector [mm]	w_e	20
Maximum admissible cable tension [N]	t_{max}	128
Minimum admissible cable tension [N]	t_{min}	0
Gear ratio of the wrist []	μ	1

constraint is set to prevent any collision.

$$h_e{}^2 + w_e{}^2 < h_1{}^2 \tag{3.67}$$

The actuation of the tilt-roll wrist requires a tension difference between the two ends of a cable-loop. This tension difference is a function of the total mass m of the tilt-roll wrist. The larger m, the higher the tension difference. Therefore, the upper bound m_{max} of m is set to 5 kg, i.e., $m_{max} = 5$ kg. The lower bound vector, $\mathbf{x}_{lb}$, and upper bound vector, $\mathbf{x}_{ub}$, of the decision variable vector $\mathbf{x}$ are given in Table 3.2.

Finally, the optimization problem at hand is formulated as follows:

$$
\begin{aligned}
\text{maximize} \quad & f(\mathbf{x}) = \mathscr{R}_{\mathscr{S}_2} \\
\text{over} \quad & \mathbf{x} = [r_b,\ h_1,\ w_b,\ \theta_c,\ \theta_u,\ \eta]^T \\[6pt]
\text{subject to:} \quad & \\
& g_1 : h_e{}^2 + w_e{}^2 < h_1{}^2 \\
& g_2 : m < m_{max} \\
& \mathbf{x}_{lb} \leq \mathbf{x} \leq \mathbf{x}_{ub}
\end{aligned}
\tag{3.68}
$$

Table 3.4: Tuning parameters of the genetic algorithm

Parameter	Abbreviation	Value
Maximum Number of Generations	MNG	100
Function Tolerance	FT	1×10^{-4}
Population Size	PS	200
Crossover Fraction	CF	0.8
Elite Count	EC	$0.05\times$ PS

Results

The optimization problem is solved by using a genetic algorithm, i.e., with the ©Matlab *ga* function. The algorithm begins by creating a random initial population. The algorithm then creates a sequence of new populations. At each step, the algorithm uses the individuals in the current generation to create the next population. To create the new population, the algorithm performs different steps including: (*i*) scoring each member of the current population by computing its fitness value; (*ii*) selecting members, called parents, based on their fitness value; (*iii*) producing children from the parents, children are produced either by making random changes to a single parent-mutation or by combining the vector entries of a pair of parents-crossover; (*iv*) replacing the current population with the children to form the next generation. Finally, the algorithm stops when one of the stopping criteria is met. The tuning parameters of the algorithm are given in Tab. 3.4.

Figure 3.10a shows the workspaces $\mathcal{W}_1$ and $\mathcal{W}_2$ of the classical CDPR obtained by replacing the two bi-actuated cables (cable-loops) depicted in Fig. 3.10b by four uni-actuated cables. $\mathcal{W}_1$ amounts to the static workspace of the corresponding classical CDPR with the gravity wrench defined as in (3.41). $\mathcal{W}_2$ amounts to the wrench-feasible workspace of the corresponding classical CDPR with the set of external wrenches due the tilt-roll wrist motion defined as in (3.42). From Figs. 3.10b and 3.10a, it should be noted by substituting uni-actuated cables with bi-actuated cables (cable-loops), the size of the static workspace decreases. In spite of that, the moving-platform can reach large amplitudes of the tilt and roll rotations as a result of cable-loops. It appears to be a trade-off between large translation and orientation workspaces due to the cable-loops in the fully-actuated CDPR. It is noteworthy that translation and orientation workspaces are maximal when employing two additional actuators as shown in Fig. 3.11.

The obtained optimum design variable values are given in Tab. 3.2. The optimum design, cable configuration of the overall manipulator and its maximal static workspaces, namely $\mathcal{S}_1$ and $\mathcal{S}_2$, are illustrated in Fig. 3.10b. The optimum design and cable configuration of the moving-platform yield 0.57 and 0.45 for $\mathcal{R}_{\mathcal{S}_1}$ and $\mathcal{R}_{\mathcal{S}_2}$, respectively.

$\mathcal{S}_2$ is the translation static workspace of the moving-platform for all possible

(a) Workspaces $\mathcal{W}_1$ and $\mathcal{W}_2$ of a classical CDPR with design variables values set to the optimum values given in Tab. 1

(b) Workspaces $\mathcal{S}_1$ and $\mathcal{S}_2$ associated with the optimum design of the CDPR with an embedded tilt-roll wrist
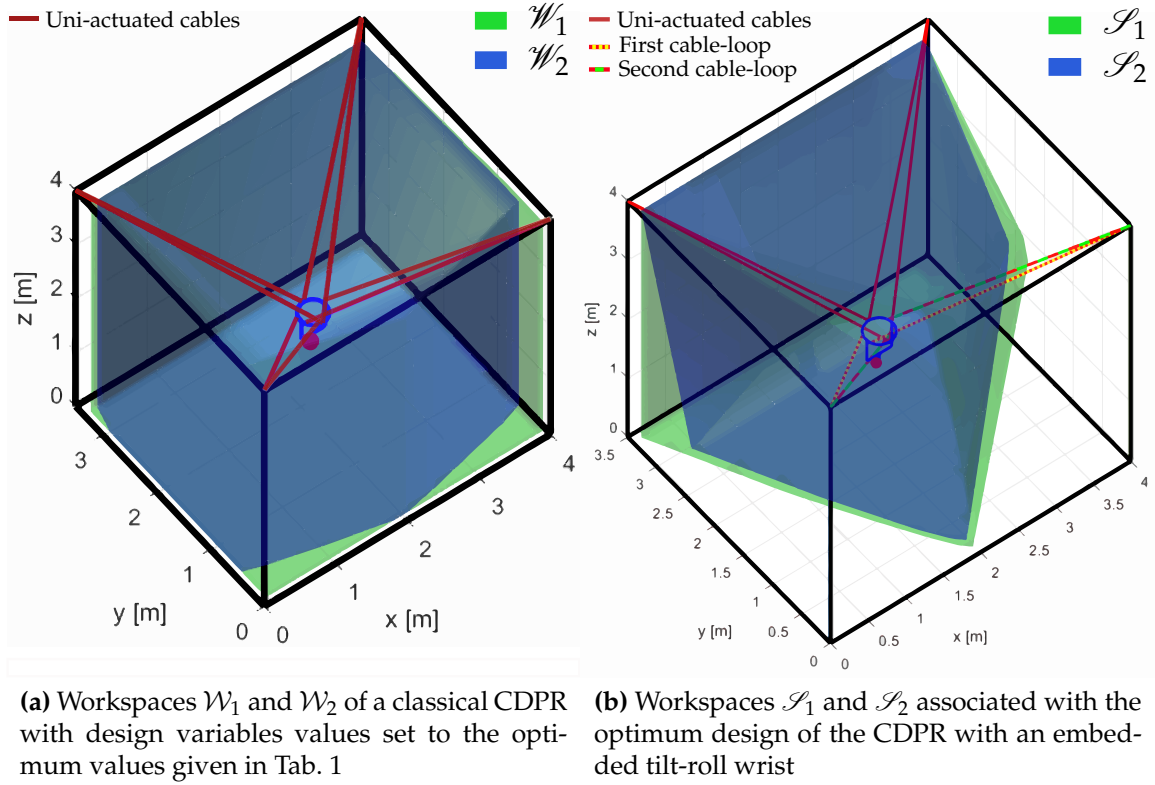
Figure 3.10: Workspace of the CDPR without (Left) and with (Right) an embedded tilt-roll wrist

orientations of the tilt-roll wrist. Figure 3.12a shows the isocontours of ratio $\mathcal{R}_{\mathcal{S}_2}$ as a function of masses m_1 and m_2, with the decision variables set to their optimum values, except r_b and w_b. Note that m_1 depends on r_b, w_b and the material density ρ. $\rho = 7800$ kg/m^3 as the top plate is made up of steel. $\mathcal{R}_{\mathcal{S}_2}$ increases with m_1, while, on the contrary, it decreases with m_2. However, it can be noticed that the effect of m_1 on $\mathcal{R}_{\mathcal{S}_2}$ is negligible compared to that of m_2. The maximum applied moment onto $\mathcal{P}_3$ and $\mathcal{P}_4$ by cable-loops is proportional to the tension difference in the two segments of cable-loops.

It is understood from the obtained results that the variable gravitational wrench onto the moving-platform induced by $\mathcal{P}_5$ mass has a significant impact on the size of the manipulator workspace. Similarly, Figs. 3.12b to 3.12d illustrate the effect of r_b, θ_c and θ_u on $\mathcal{R}_{\mathcal{S}_2}$. From Figs. 3.12c to 3.12d, it is noteworthy that $\mathcal{R}_{\mathcal{S}_2}$ is very sensitive to variations in angle θ_u. Indeed, a small variation in θ_u from its nominal value may lead to a significant decrease of $\mathcal{R}_{\mathcal{S}_2}$.

3.3 Prototyping and Experimentation

The prototyping of the moving-platform with an embedded tilt-roll wrist is presented in this section. The base frame of the CREATOR platform $\mathcal{P}_0$ is 4 m long (l_0), 3.5 m wide (w_0) and 4 m high (h_0) as shown in Fig. 3.2. Steel, aluminum alloys and ABS are used in the manufacturing of the prototype. The prototype of the moving-platform has the overall dimensions of $20 \times 20 \times 25$ cm, as shown in Fig. 3.1. The
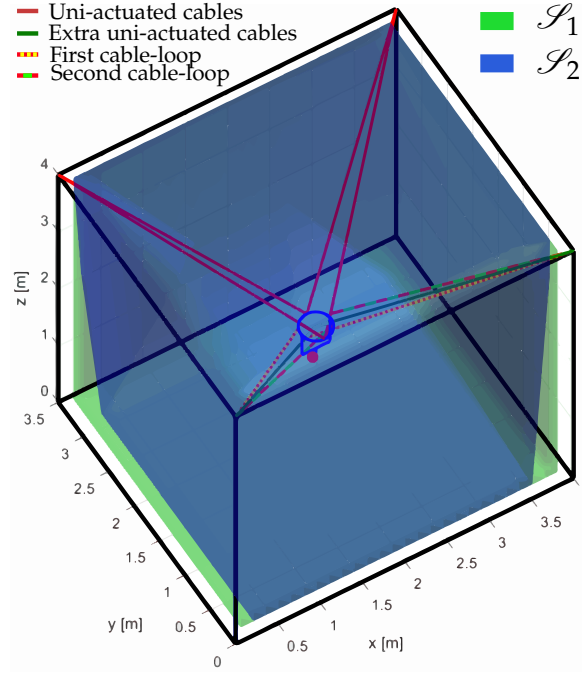
Figure 3.11: Workspaces $\mathscr{S}_1$ and $\mathscr{S}_2$ associated with the optimum design of the CDPR with an embedded tilt-roll wrist with two additional uni-actuated cables

mass of the components of the moving-platform is detailed in Table 3.3, and the overall mass of the moving-platform is 3.5 kg. Figure 3.13 shows the main components and a mechanical drawing of the moving-platform with its embedded tilt-roll wrist.

This section deals with the design of the moving-platform, control and experimentation of the CDPR\TRW. The performance of the manipulator is exhibited in terms of large orientation workspace and precision of the end-effector. The demonstrations are carried out in context of two test-trajectories and the sensitivity analysis of the manipulator is performed for evaluation of the system and further improvements.

3.3.1   Control scheme

The manipulator is controlled with a Proportional– Integral–Derivative (PID) controller as shown in Fig. 3.14. The overall architecture of the controller of the demonstrator is depicted in Fig. 3.15. The PID controller relies on the feedback from motor encoders to correct their positions. The following details the signals used in the control scheme.

  – $\mathbf{q}_d \in \mathbb{R}^m$: Vector of the desired joint's angular positions

  – $\dot{\mathbf{q}}_d \in \mathbb{R}^m$: Vector of the desired joint angular velocities

  – $\mathbf{q}_m \in \mathbb{R}^m$: Vector of the measured joint's angular positions

  – $\dot{\mathbf{q}}_m \in \mathbb{R}^m$: Vector of the measured joint angular velocities

  – $\mathbf{e}_q = \mathbf{q}_d - \mathbf{q}_m$: Vector of the error of the angular positions
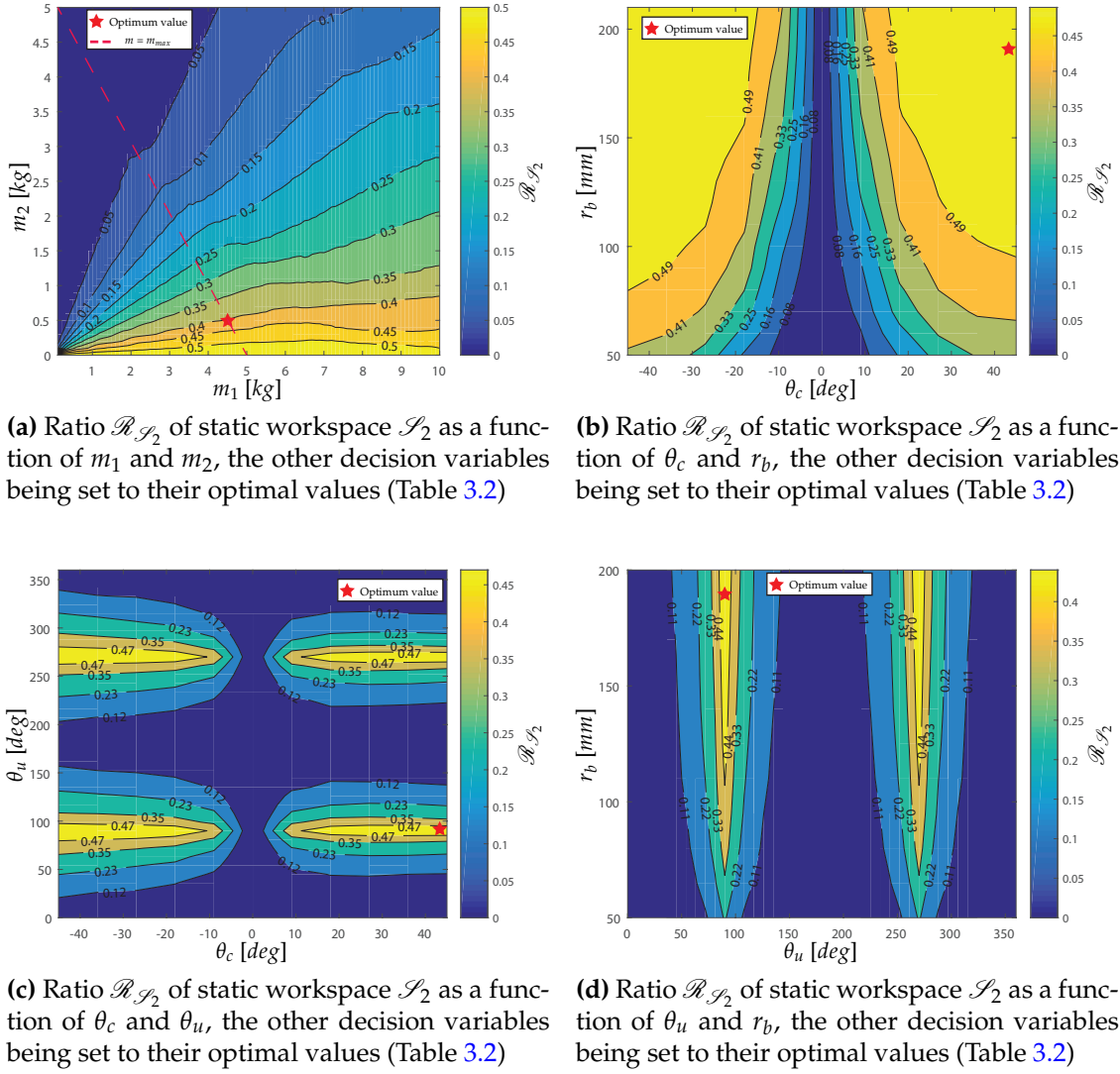
(a) Ratio $\mathscr{R}_{\mathscr{S}_2}$ of static workspace $\mathscr{S}_2$ as a function of m_1 and m_2, the other decision variables being set to their optimal values (Table 3.2)

(b) Ratio $\mathscr{R}_{\mathscr{S}_2}$ of static workspace $\mathscr{S}_2$ as a function of θ_c and r_b, the other decision variables being set to their optimal values (Table 3.2)

(c) Ratio $\mathscr{R}_{\mathscr{S}_2}$ of static workspace $\mathscr{S}_2$ as a function of θ_c and θ_u, the other decision variables being set to their optimal values (Table 3.2)

(d) Ratio $\mathscr{R}_{\mathscr{S}_2}$ of static workspace $\mathscr{S}_2$ as a function of θ_u and r_b, the other decision variables being set to their optimal values (Table 3.2)

Figure 3.12: Evolution of $\mathscr{R}_{\mathscr{S}_2}$ as function of pairs of decision variables
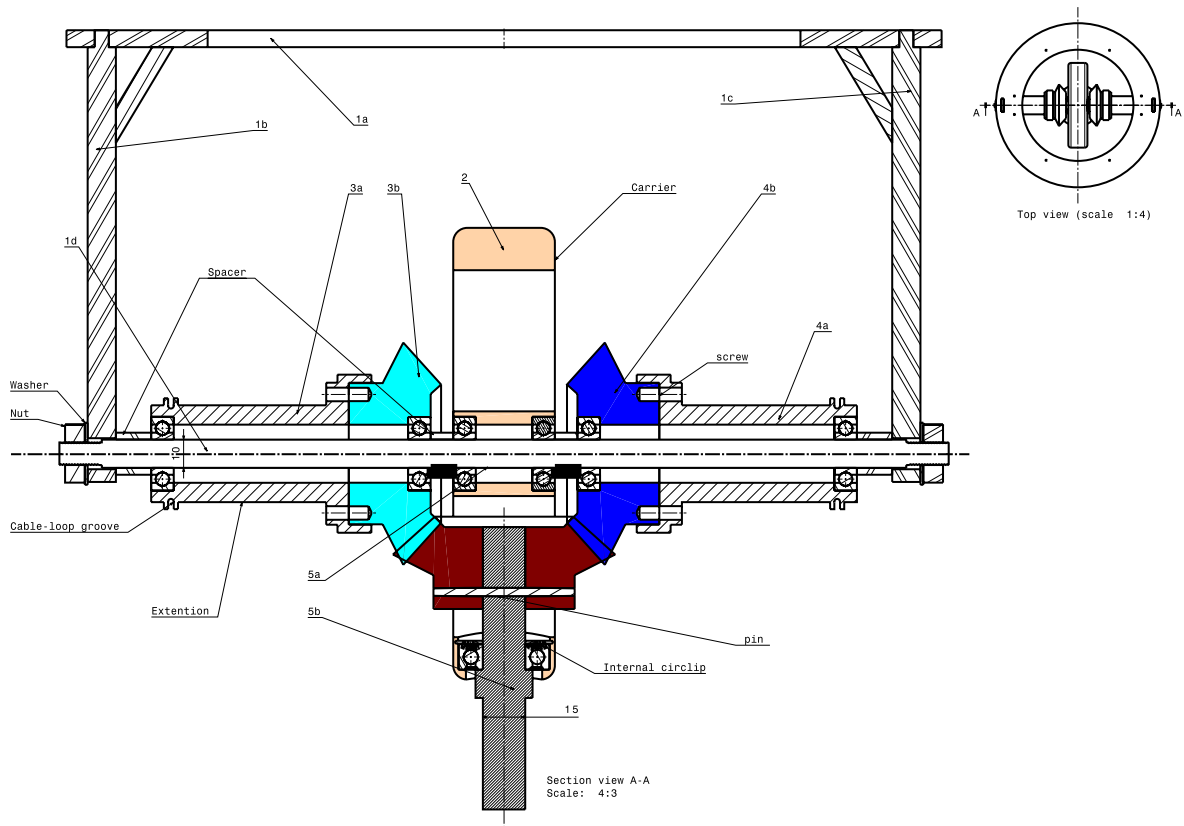
Figure 3.13: Mechanical drawing of the tilt-roll wrist and the moving-platform, section-view(left) top-view (right)
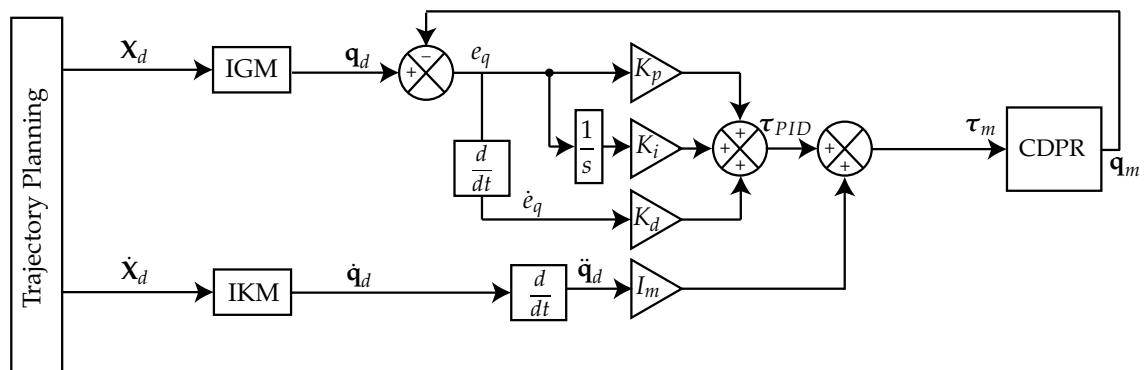

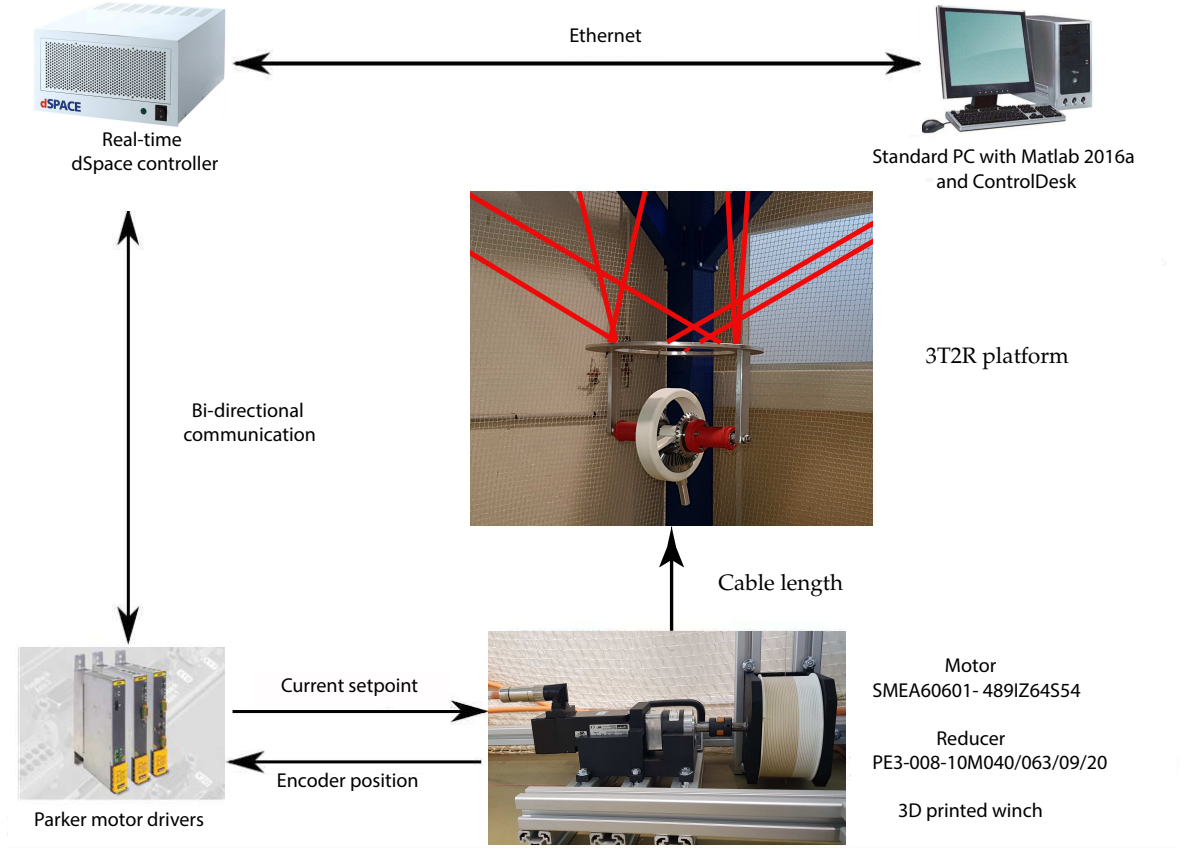**Figure 3.14:** PID control scheme of the 3T2R manipulator

Figure 3.15: Equivalent architecture of the manipulator

- $\dot{\mathbf{e}}_q = \dot{\mathbf{q}}_d - \dot{\mathbf{q}}_m$: Vector of the error of the angular velocities

- $\mathbf{K}_p \in \mathbb{R}^{m \times m}$: Diagonal matrix of the proportional gains

- $\mathbf{K}_i \in \mathbb{R}^{m \times m}$: Diagonal matrix of the integral gains

- $\mathbf{K}_d \in \mathbb{R}^{m \times m}$: Diagonal matrix of the derivative gains

The output torque vector of the controller $\boldsymbol{\tau}_m$, is sent to the motors and its computation is detailed as follows:

$$\boldsymbol{\tau}_m = \boldsymbol{\tau}_{PID} + \ddot{\mathbf{q}}_d \mathbf{I}_m + \boldsymbol{\tau}_{FF} + \boldsymbol{\tau}_f \tag{3.69}$$

the well-known PID torque is denoted as $\boldsymbol{\tau}_{PID}$ and computed as follow:

$$\boldsymbol{\tau}_{PID} = \mathbf{K}_p \mathbf{e}_q(t) + \mathbf{K}_d \dot{\mathbf{e}}_q(t) + \int_{t_0}^{t} \mathbf{K}_i \mathbf{e}_q(t') dt' \tag{3.70}$$

3.3.2 Test-Trajectory

Here, we elaborate one of the essential steps of the demonstration for 3T2R manipulator. In order to demonstrate the capabilities of the manipulator, two different test-trajectories. The first one shows the ability of the manipulator in terms of its

rotational workspace with large amplitudes. While, the second path-trajectory puts emphasize on the accuracy of the moving-platform and its sensitivity for a potential surveillance task.

Test-trajectory 1

The first test-trajectory focuses on the generation of a desired trajectory for the CDPR with tilt-roll wrist. The main aim of this trajectory is a straightforward demonstration of the large rotational workspace capability of the manipulator. Therefore, the following steps construct the different paths of the trajectory. This link [1] refers to a video of the first test-trajectory. The test-trajectory is composed of several via-points such that the moving-platform translates between them based on a fifth-order polynomial profile of motions. Within via-points the tilt-roll wrist performs pure tilt, pure roll and combination of both motions. The amplitude of the rotation for the tilt and roll is 8π radians, i.e., four turns.

Test-trajectory 2

The second test-trajectory is proposed to demonstrate one of the potential tasks of the CDPR with an embedded tilt-roll wrist requiring high precision of the manipulator in position and orientation. For this task, a laser pointer is attached to the end-effector of the moving-platform. Overall, the laser dot aims at a fixed target on the ground while the moving-platform follows a circular path. The trajectory is designed to evaluate the precision and sensitivity of the tilt-roll wrist. The second test-trajectory is shown in this link [2] and it consists of the following steps:

1. Start from the home-configuration of the moving-platform and proceed to the starting configuration of the circular path.

2. Perform the circular path of the end-effector while laser-pointer is aimed at the fixed target on the ground.

3. Return to the home-configuration of the moving-platform.

We employed fifth-order polynomial trajectory planning for the first and the third parts of the trajectory. The initial velocities and acceleration of the via points are set to zero as well as the final ones. The second path of the trajectory uses horizontal coordinate system and more specifically parametrized by azimuth and elevation. Hereafter, we define the described path in the second step of the trajectory. Point O_5 being the laser beam origin and H (Shown in Figure 3.16) being the center of circular path of O_5, then we write:

$$^0HO_5 = \begin{bmatrix} r_T \cos\phi & r_T \sin\phi & 0 \end{bmatrix}^T \tag{3.71}$$

ϕ refers to the azimuth angle. Point I is the point of interest which laser beam is locked on and the following expresses the vector from the object to the laser pointer

---

[1] http://tiny.cc/oaiycz
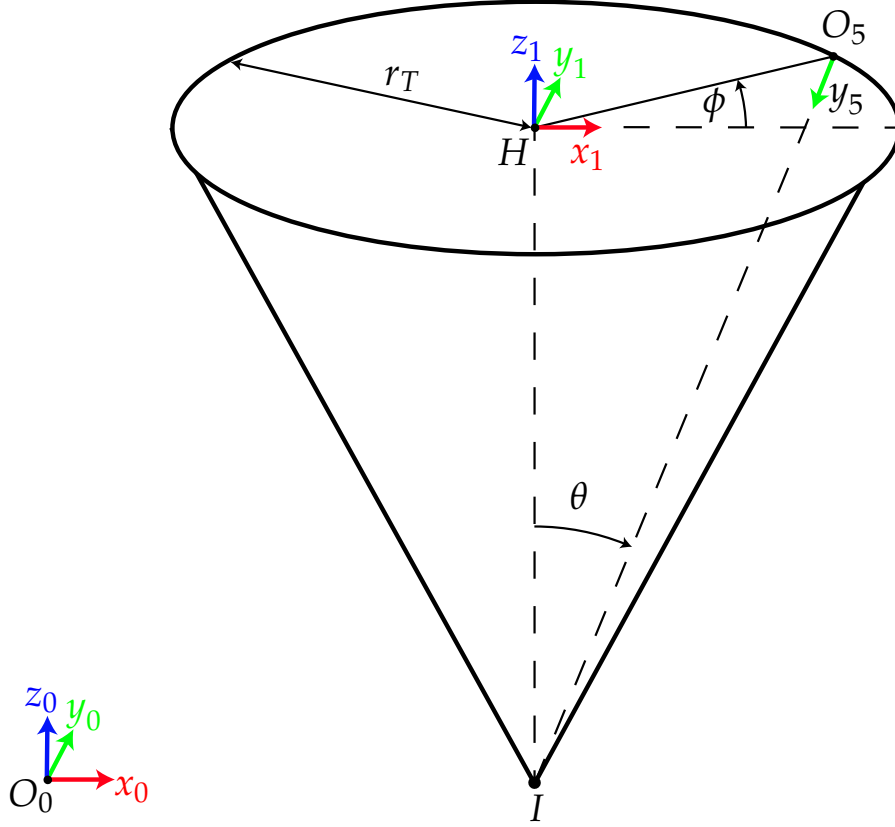[2] http://tiny.cc/cohycz

Figure 3.16: Parameterization of test-trajectory 2

origin.

$$^0IO_5 = {}^0IH + {}^0HO_5 = \begin{bmatrix} r_T \cos \phi & r_T \sin \phi & \dfrac{r_T}{\tan \theta} \end{bmatrix}^T \tag{3.72}$$

angle θ is the elevation angle between z-axis and O_5.

$$^0OO_5 = {}^0OI + {}^0IO_5 = \begin{bmatrix} x_I + h \cos \phi \tan \theta & y_I + h \sin \phi \tan \theta & h \end{bmatrix}^T \tag{3.73}$$

with $h = \|IH\|_2$.

$$^0OO_5 = \begin{bmatrix} x_I + h \cos \phi \tan \theta & y_I + h \sin \phi \tan \theta & z_I + h \end{bmatrix}^T \tag{3.74}$$

$$^0y_5 = - \begin{bmatrix} \cos \phi \tan \theta & \sin \phi \tan \theta & \cos \theta \end{bmatrix}^T \tag{3.75}$$

Transformation matrix from $\mathscr{F}_0$ to $\mathscr{F}_5$ is expressed in the following:

$$^0\mathbf{T}_5 = \begin{bmatrix} \cos \beta & -\sin \beta & 0 & x_p \\ -\sin \alpha \sin \beta & -\sin \alpha \cos \beta & -\cos \alpha & y_p - h_2 \cos \alpha \\ -\cos \alpha \sin \beta & \cos \alpha \cos \beta & -\sin \alpha & z_p - h_1 - h_2 \sin \alpha \\ 0 & 0 & 0 & 1 \end{bmatrix} \tag{3.76}$$

From Eq. 3.76 we extract the following:

$$^{0}OO_5 = \begin{bmatrix} x_p & y_p - h_2 \cos \alpha & z_p - h_1 - h_2 \sin \alpha \end{bmatrix}^{T} \tag{3.77}$$

$$^{0}y_5 = \begin{bmatrix} -\sin \beta & -\sin \alpha \cos \beta & \cos \alpha \cos \beta \end{bmatrix}^{T} \tag{3.78}$$

For the second phase of the path, there are two conditions. The former condition is for O_5 to follow the circular trajectory described by r_T, h and θ. The latter is $^{0}y_5$ to be parallel to the $^{0}IO_5$. Therefore, we solve Eqs. (3.74, 3.75, 3.77, 3.78) to find the desired pose of the moving-platform. Solving the equations yields two solutions for α:

$$\alpha = \arctan(-\sin \phi \tan \theta) \tag{3.79}$$

$$\alpha = \pi + \arctan(-\sin \phi \tan \theta) \tag{3.80}$$

and as consequence four solutions for β:

$$\beta = \arctan(\frac{\cos \phi \sin \theta}{\sqrt{(\cos \theta)^2 + (\sin \phi \sin \theta)^2}}) \tag{3.81}$$

$$\beta = \pi + \arctan(\frac{\cos \phi \sin \theta}{\sqrt{(\cos \theta)^2 + (\sin \phi \sin \theta)^2}}) \tag{3.82}$$

$$\beta = \arctan(-\frac{\cos \phi \sin \theta}{\sqrt{(\cos \theta)^2 + (\sin \phi \sin \theta)^2}}) \tag{3.83}$$

$$\beta = \pi + \arctan(-\frac{\cos \phi \sin \theta}{\sqrt{(\cos \theta)^2 + (\sin \phi \sin \theta)^2}}) \tag{3.84}$$

From the eight combinations of α and β in Eqs. (3.79 - 3.84) we discard four infeasible solutions. The remaining four solutions, two being feasible and two being infeasible, are illustrated for a given configuration of the manipulator in Fig. 3.17.

Sensitivity analysis

There is a disparity between the desired and actual trajectories during the second phase of the second test-trajectory as shown in Fig. 3.19. The figure presents the reconstruction of the laser dot through image processing. The upper-bound of the error in the position of the laser-dot with respect to the center of the target is around 30 cm. There are several factors involved in the orienting error of the wrist, but the most influential seems to be the sensitivity of the tilt-roll wrist inputs. Figure 3.20 presents the variations of the cable lengths as a function of time. More specifically, Fig. 3.20a presents the cable length variations corresponding to all motions involved in the trajectory, while Fig. 3.20b presents cable length variations corresponding only to wrist rotations. The maximum required cable length variation is not more than 15 mm. This sensitivity can be reduced simply by increasing the gear ratio of the
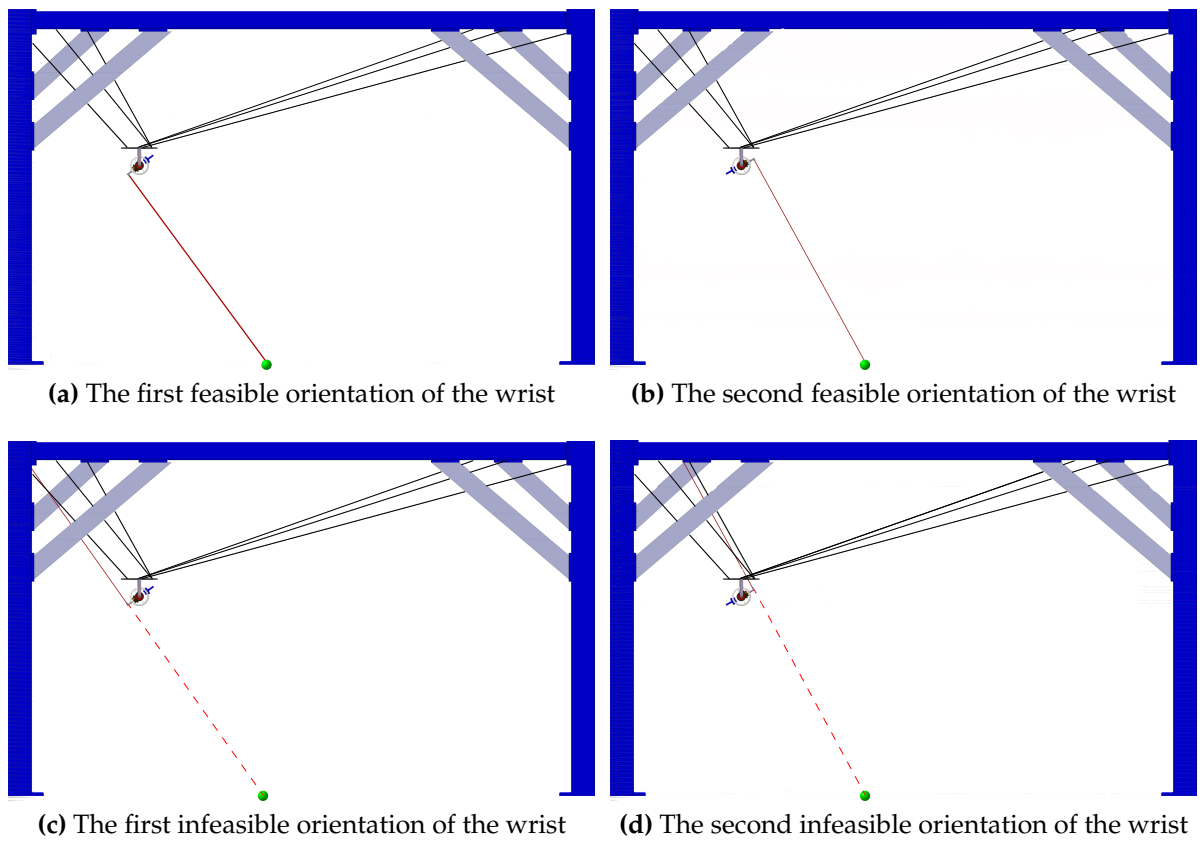
(a) The first feasible orientation of the wrist

(b) The second feasible orientation of the wrist

(c) The first infeasible orientation of the wrist

(d) The second infeasible orientation of the wrist

Figure 3.17: Schematic illustration of the inverse-geometric solutions of the tilt-roll wrist for a given pose of the top-plate related to test-trajectory 2
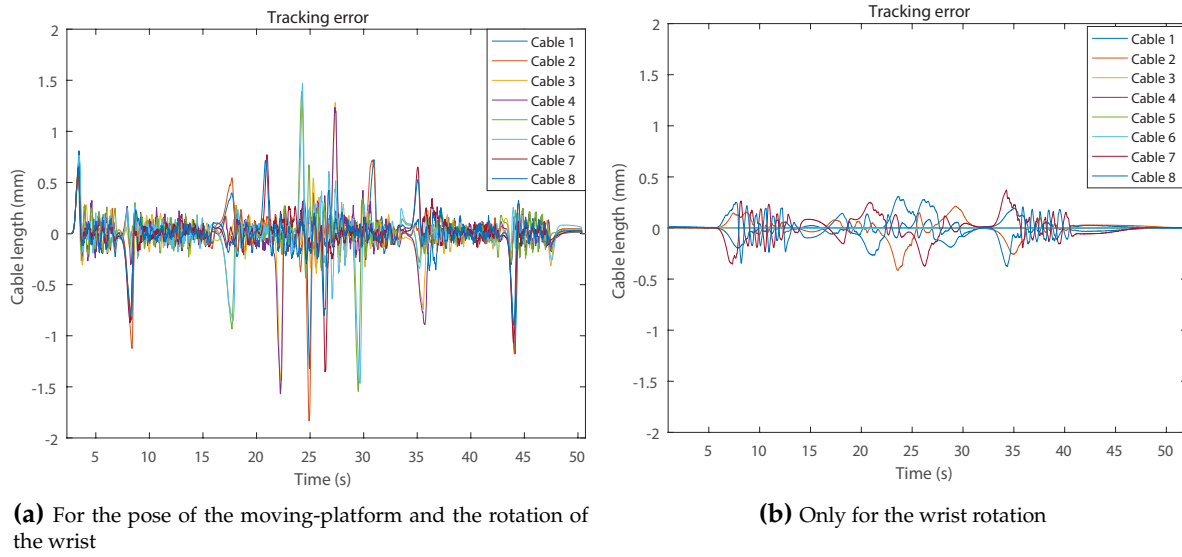
(a) For the pose of the moving-platform and the rotation of the wrist

(b) Only for the wrist rotation

Figure 3.18: Controller tracking error along the test-trajectory 2

wrist, namely, μ, which requires substantial modifications in the wrist design. Another solution to improve accuracy in control of the wrist is to employ more sophisticated cable models, e.g. an elastostatic model and a hysteresis model [Bak+17]. Moreover a better accuracy could be obtained by improving the control system and acquiring visual feedback on the pose of the manipulator [Zak+19; HK92].

Figure 3.21 shows the proportion of the cable loop length variation required for α and β to the maximum cable loop length variation during thorough test-trajectory 2. Clearly, the lengths of the cable loops are not limiting factors in our current design. In general, their lengths can be chosen to be large without affecting other characteristics of the CDPR. We can estimate the robustness of the model due to the uncertainties concerns the sensitivity of the manipulator. The sensitivity analysis requires precise measurement devices to measure the task performance, however we can approximate the sensitivity of the model based on the motor encoders data. The manipulator undergoes positioning and orientation error due to the geometrical ill-identification, gear backlash, tracking error of the controller, elongation of cables, compliance in motor coupling parts and etc. Therefore, the sensitivity analysis is crucial for further improvement of the manipulator especially in the next iteration of the design process. Figure. 3.18 demonstrates the tracking error which is based on the difference between desired and actual encoders displacements. Tracking error is mainly originated from controller and tuning of the PID gains. Figure 3.18a shows the tracking error for the thorough trajectory while, in Fig. 3.18b exclusively wrist rotation of the test-trajectory, namely, $\mathbf{q}_{TR}$ is taken into account. The latter is done in order to demonstrate the sensitivity of the tilt-roll wrist to the cable-loop length variation. Figure 3.20 shows the actual cable lengths based on the encoder measurements for two different cases, namely, thorough test-trajectory 2 and the required cable lengths for the actuation of the tilt-roll wrist. In Fig. 3.20a, the maximum variation of cable lengths is about 15 cm while, the maximum cable-loop displacement for the orientation of the tilt-roll wrist is about 17 mm. Figure 3.21 shows the relative
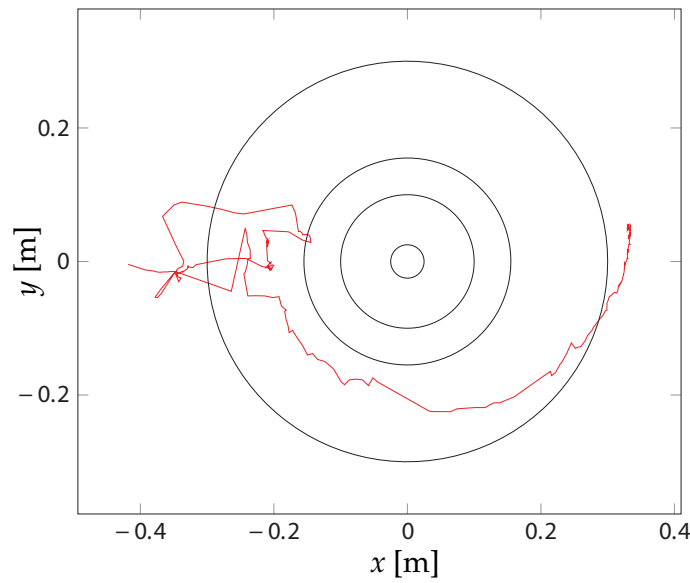
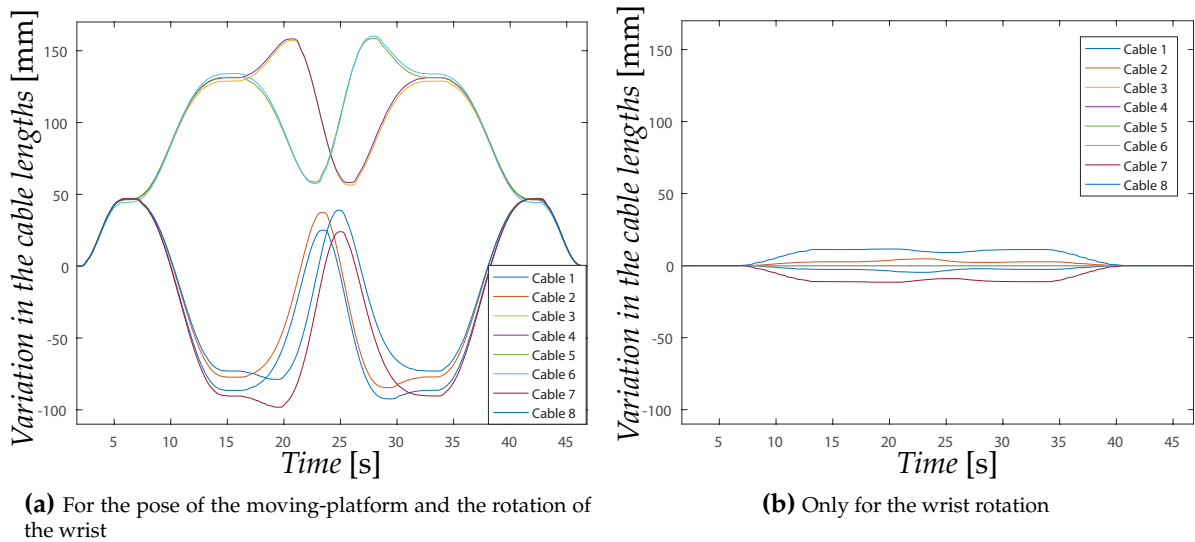**Figure 3.19:** Extracted laser dot trajectory during the second phase of the test-trajectory 2

(a) For the pose of the moving-platform and the rotation of the wrist

(b) Only for the wrist rotation

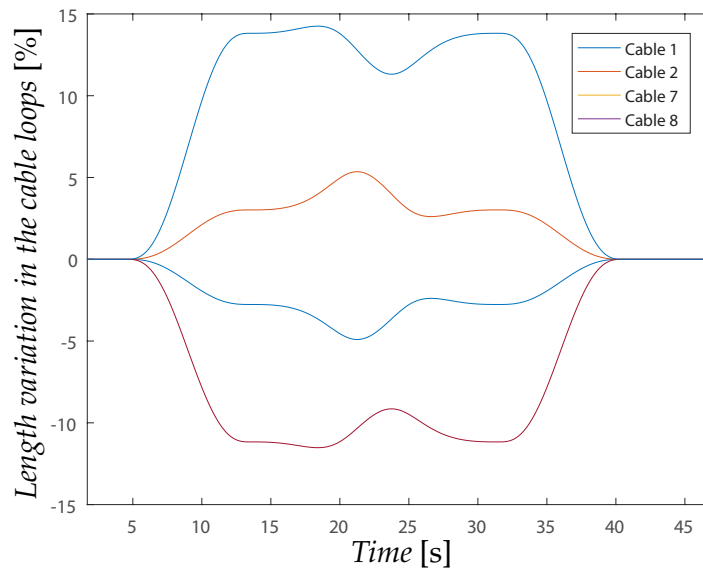**Figure 3.20:** Variation in the cable length during test-trajectory 2

Figure 3.21: Proportion of the cable-loop lengths variation due to the wrist rotations during the test-trajectory 2

cable-loop displacements required only for the wrist actuation.

3.4 Summary of the Chapter

A CDPR using a tilt-roll wrist has been introduced in this chapter. The robot combines the advantages of CDPR in terms of large translational workspace with those of tilt-roll wrist in terms of large rotational amplitudes. The robot uses cables to transmit power directly from fixed motors on the ground to the tilt-roll wrist. In comparison with conventional cable-driven parallel robots and cable-driven suspended robots, the proposed concept adds singularity-free and large tilt-roll motions to the end-effector. This leads to a trade-off, however, between translational and rotational workspaces due to tension coupling in cable-loops for fully-actuated CDPRs. The kinetostatic model of the proposed manipulator was studied. The static workspace of the manipulator was also defined and analyzed. The detailed design, prototyping and dynamic modeling of the cable-driven parallel robot equipped with a tilt-roll wrist are left for future work. Moreover, the study of the over-actuated CD-PRs with the embedded tilt-roll wrist will be carried out in order to maximize their workspaces.

This chapter addresses the optimum design of a CDPR with an embedded tilt-roll wrist for large translational and rotational workspaces. The eight-degree-of-freedom hybrid robot was studied in terms of its kinetostatic workspace. Moreover, design and prototyping of the CDPR with the embedded tilt-roll wrist was presented. The optimization results revealed that, the size of the static workspace highly relies on the specifications of the tilt-roll wrist. That is to say, the variable gravitational moment of the wrist and cable-loops arrangement have crucial effects on the workspace size. It should be noted that, the considered workspace assumes no external forces on the moving-platform, except for gravity, so that the workspace

analysis is relevant to the applications such as, tomography scanning and surveillance.

The moving-platform is suspended by six cables and its embedded tilt-roll wrist is driven through two bi-actuated cable-loops. As a result, the end-effector covers very large rotation amplitudes about two axes without singularities. This leads to a trade-off, however, between translational and rotational workspaces due to tension coupling in cable-loops for fully-actuated CDPRs. Future work will consist in studying other factors influencing the size of the workspace, e.g., orientation of the moving-platform, cable interferences and over-actuation.

Chapter 4

Cable-Driven Parallel Robot with a Parallel Spherical Wrist

Contents

A hybrid CDPR was proposed with a parallel spherical active wrist as its end-effector at LS2N (Laboratoire des Sciences du Numérique de Nantes). The proposed manipulator has 9-DoF with large rotational motions about three axes. The kinematic architecture of the manipulator consists of two parallel manipulators mounted in series. The first mechanism is a CDPR capable of providing a large translation workspace while the second mechanism is a parallel spherical wrist granting 3 rotational DoFs. Thanks to its novel assembly, the hybrid manipulator is able to combine advantages of both mechanisms in terms of large translation and orientation workspaces. Even though the proposed concept has promising contributions to CDPRs with large translation and orientation workspaces, it presents challenges in terms of design, control and kinematic analysis due to its hybrid kinematic architecture. Figure 4.1 illustrates different stages of the design process of the proposed manipulator. All the steps and contributions regarding the CDPRs with an embedded parallel spherical wrist are summarized as follows:

- Earliest step toward the concept : At this stage, augmentation of the orientation workspace of CDPRs was the initiative towards the design and analysis of a hybrid CDPR. This research was conducted in the context of a master thesis in [Ang15]. Figure 4.1a shows the equivalent parallel manipulator proposed in the context of this research work.

- Design and prototyping : The manufacturing of the first mock-up was followed by further investigation and detailed design in [Tah16; Pla+18].

- Optimal design, manufacturing and demonstration : Based on the previously-developed prototype, the second iteration of the design led to the realization of the CDPR with an embedded parallel spherical wrist in the framework of the CREATOR project. This stage is accompanied with demonstrations of the proposed hybrid robot with large orientation workspace in [Mét19] as well as the context of this doctorate thesis.

Even though, the concept of a CDPR with an embedded parallel spherical wrist was initiated earlier, the development and realization of the early-stage concept was one of the primary original contributions of this thesis (CREATOR project), i.e., CDPRs with large rotational magnitudes about three axes. Hence, further investigations are carried out in the framework of Marceau Metillon's master thesis co-advised by the author's of this doctorate thesis, Philippe Cardou, Kévin Subrin and Stéphane Caro. The contributions of [Mét19; Mét+ l] are the complete kinematic model of the manipulator based on the developed cable-loop model, wrench feasible workspace analysis as a main feasibility criterion of the manipulator, optimization of the cable arrangements as the most crucial parameter in the size of the workspace, detailed design and prototyping of the moving-platform based on the correction of the earliest developed mock-up. Moreover, experimental demonstration is carried out as the final contribution.

In the context of this manuscript, CDPR with an embedded parallel spherical wrist is interchangeable with CDPR\PSW.

## 4.1   Description of the Manipulator

Figure 4.2 shows the overall structure of the CDPR\PSW with its main components, namely, winches, exit-points and the moving-platform. The cables connect the moving-platform to the fixed structure of the manipulator by passing through exit and anchor points.

The parallel spherical wrist mechanism is embedded into the moving-platform of the CDPR. The orientation of the sphere is determined by the orientations of its omni-wheels. Three cable-loop systems transmit the required power from motors fixed on the ground to the omni-wheels. Hereafter, the manipulator is detailed in terms of kinetostatic model and static workspace.

4.1.1   Kinetostatic Model of the Parallel Spherical Wrist

The kinetostatic model of the CDPR with an embedded parallel spherical wrist is detailed in the context of this section. The overall kinetostatic model of the manipulator can be divided into two parts, namely, kinetostatic models of the CDPR and parallel spherical wrist. We demonstrate three coordinates frames in order to express all the coordinates in Figs. 4.2-4.3 and they are detailed below:
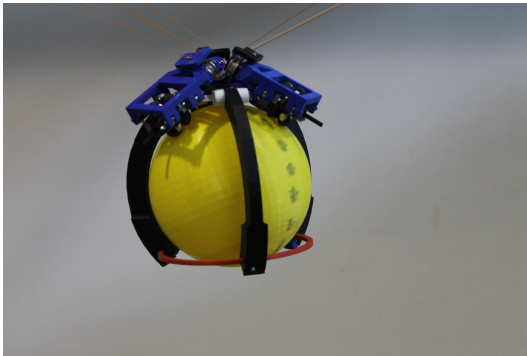
- $\mathscr{F}_0$ is the global frame and its origin is denoted as O_0 with orthogonal axes, namely, x_0, y_0 and z_0.
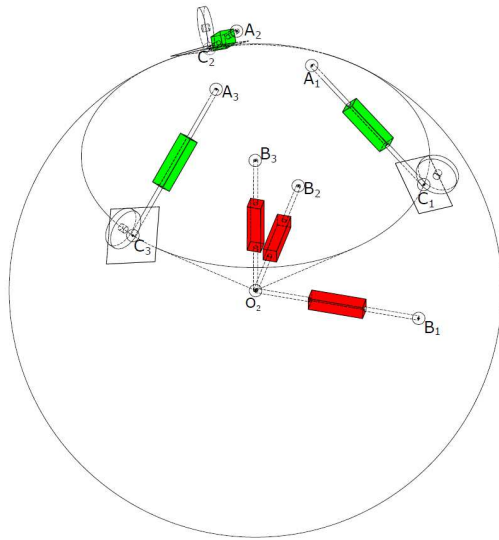
(a) Equivalent 6-SPS parallel manipulator, [Ang15]
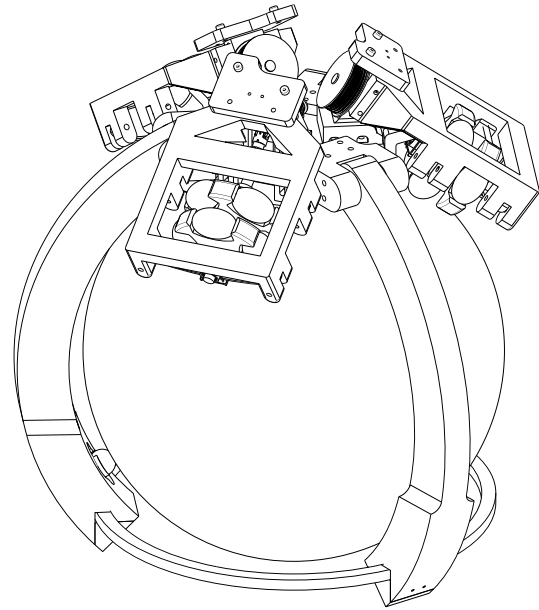
(b) Initial wrist design, [Tah16]

(c) The first prototype, [Tah16]

(d) Manufactured parallel spherical wrist, [Mét19]

Figure 4.1: Design and prototyping process of the concept of CDPRs with an embedded parallel spherical wrist
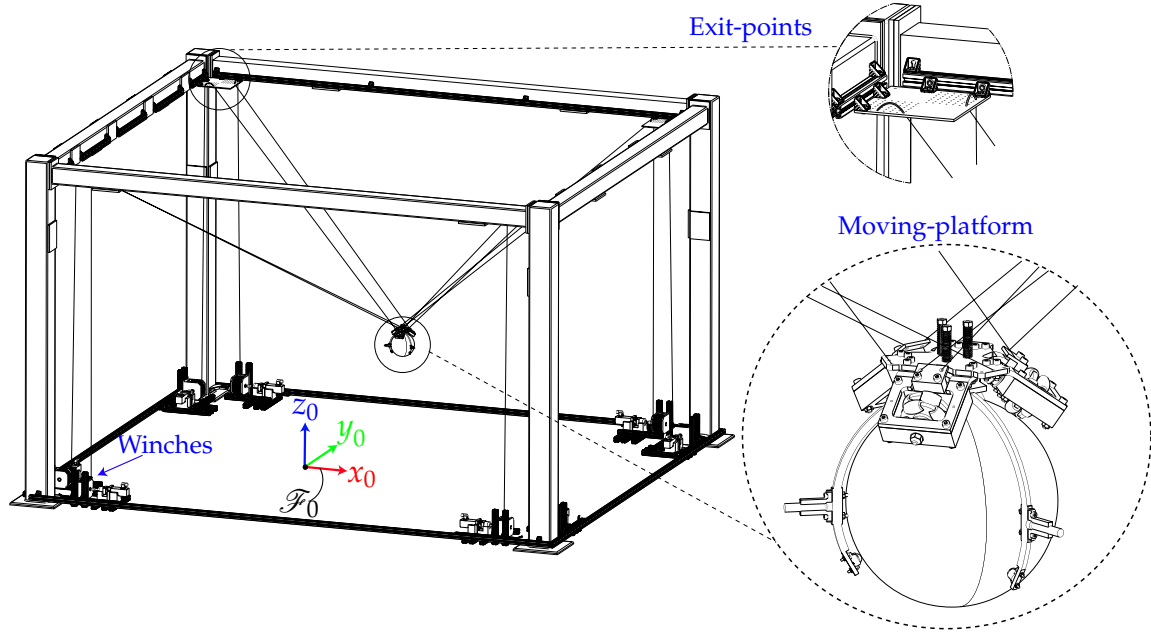
Figure 4.2: Architecture of the CDPR with an embedded parallel spherical wrist, in the framework of the CREATOR project

- $\mathscr{F}_1$ is the frame attached to the top-plate of the moving-platfotm, P, being its origin.

- $\mathscr{F}_2$ is the frame attached to the end-effector (sphere), O_2 being its origin, which coincides with the center of the sphere.

The parameterization of the parallel spherical wrist is shown in Fig. 4.4 and expressed as follows:

C_i : Contact point between the omni-wheel and the sphere

π_i : Plane passing through the contact point C_i and tangent to the sphere

λ_i : Unit normal vector of the i-th omni-wheel

μ_i : Unit tangent vector of i-th omni-wheel

α : Angle associated to the position of the contact points C_i ($\alpha \in [0, \pi]$), on the sphere
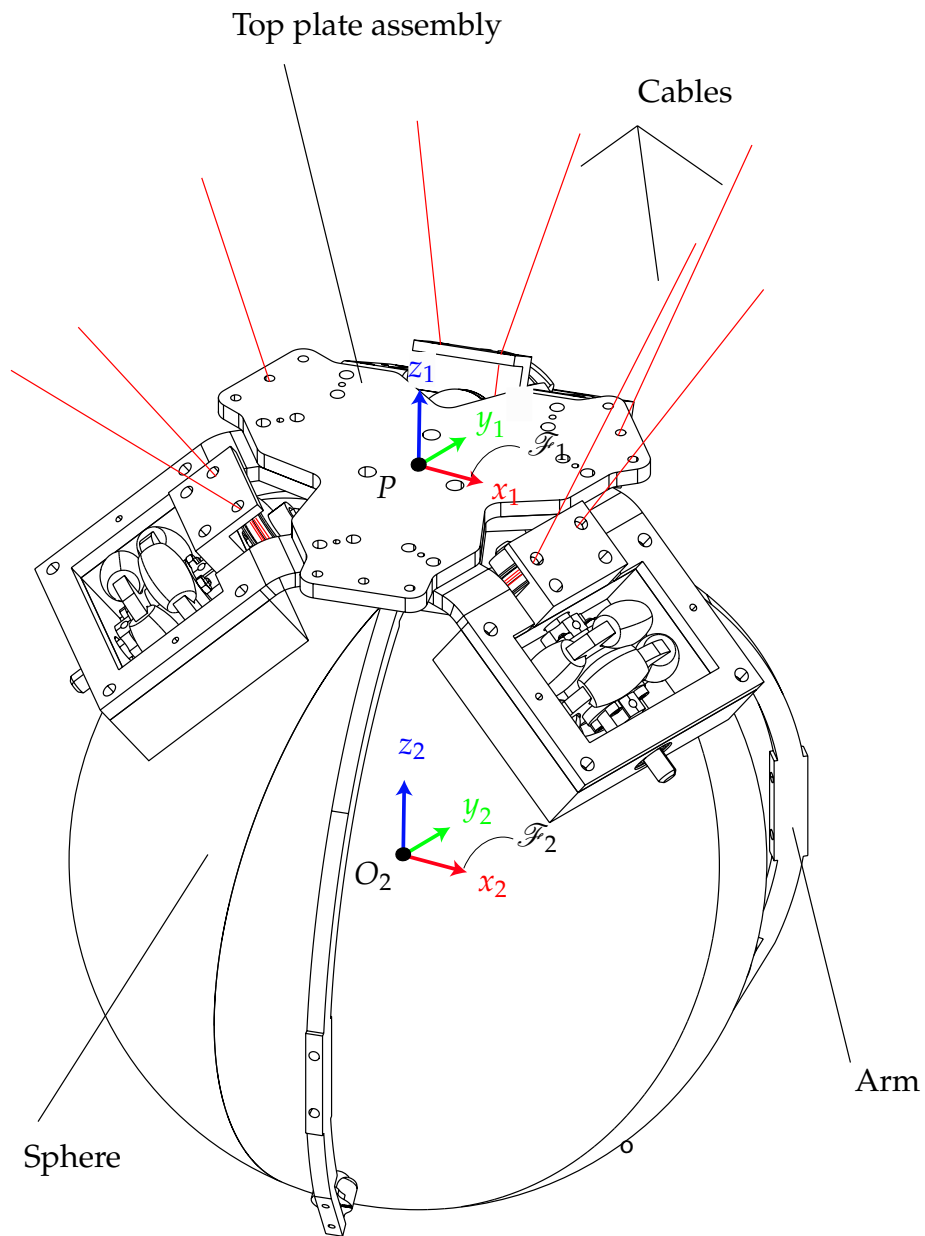
β : Angle between tangent to the sphere and the actuation force of the omni-wheel ($\beta \in [-\frac{\pi}{2}, \frac{\pi}{2}]$)
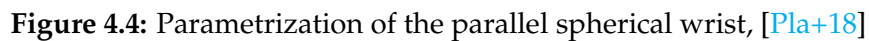
γ_2: Angles between the contact points C_1 and C_2

γ_3: Angles between the contact points C_1 and C_3

r_s : Radius of the sphere

r_o : Radius of the omni-wheels

Figure 4.3: The mobile platform with cables

Figure 4.4: Parametrization of the parallel spherical wrist, [Pla+18]

$\dot{\varphi}_i$: Angular velocity of the i-th omni-wheel

$f_{n\,i}$: Actuation force produced by the i-th omni-wheel on the sphere

The optimal set of the parameters of the wrist was defined in [Pla+18] in order to maximize the amplitudes of the orientation of the wrist as well as the dexterity. The following hypotheses are taken into account for the further analysis and modeling.

- The omni-wheels are normal to the sphere.

- The contact points of the omni-wheels on the sphere belong to the circumference of a circle being the base of an inverted cone the tip of which is the center of the sphere. The angle between the vertical axis and the cone is α.

- In the plane containing the cone base, the three contact points form an equilateral triangle.

By taking into account the hypotheses, α and β are calculated as follows:

$$\alpha = 35.2°$$
$$\beta = 0°$$

$$(4.1)$$

The angular velocity vector of the sphere $\boldsymbol{\omega} = [\omega_x, \omega_y, \omega_z]^T$ is expressed as a function of the angular velocity vector of the omni-wheels $\dot{\boldsymbol{\varphi}} = [\dot{\varphi}_1, \dot{\varphi}_2, \dot{\varphi}_3]^T$, as follows:

$$\mathbf{A}\boldsymbol{\omega} = \mathbf{B}\dot{\boldsymbol{\varphi}} \qquad (4.2)$$

A and **B** are kinematic coefficient matrices of the parallel spherical wrist as formulated below:

$$\mathbf{A} = \frac{r_s}{2} \begin{bmatrix} -2C_\alpha C_\beta & -2S_\beta & 2S_\alpha C_\beta \\ C_\alpha C_\beta + \sqrt{3}S_\beta & S_\beta - \sqrt{3}C_\alpha C_\beta & 2S_\alpha C_\beta \\ C_\alpha C_\beta - \sqrt{3}S_\beta & S_\beta + \sqrt{3}C_\alpha C_\beta & 2S_\alpha C_\beta \end{bmatrix} \tag{4.3}$$

and,

$$\mathbf{B} = r_o \mathbf{1}_{3\times3} \tag{4.4}$$

where, r_s is the sphere radius and r_o is the omni-wheel radius $S_i = \sin(i)$ and $C_i = \cos(i)$, $i = \alpha, \beta$. Notice that the radii of the omni-wheels are identical. Equation (4.2) is then rewritten as follows :

$$\boldsymbol{\omega} = \mathbf{J}_\omega \dot{\boldsymbol{\varphi}} \tag{4.5}$$

where $\mathbf{J}_\omega = \mathbf{A}^{-1}\mathbf{B}$, is the Jacobian matrix of the wrist, i.e., $\mathbf{J}_\omega$ is the mapping from angular velocities of the omni-wheels into the required angular velocity of the end-effector. Based on the reciprocity in screw theory [Bal00], we write:

$$\mathbf{m}^T \boldsymbol{\omega} = \boldsymbol{\tau}^T \dot{\boldsymbol{\varphi}} \tag{4.6}$$

where $\mathbf{m} = [m_x, m_y, m_z]^T$ is the output moment vector of the sphere and $\boldsymbol{\tau} = [\tau_1, \tau_2, \tau_3]^T$ is the input torque vector, namely the omni-wheel torque vector. By substituting Eq. (4.5) into Eq. (4.6), we have:

$$\boldsymbol{\tau} = \mathbf{J}_\omega^T \mathbf{m} \tag{4.7}$$

Hereafter, the wrench matrix of the parallel spherical wrist is defined:

$$\boldsymbol{\tau} = \mathbf{W}_\omega \mathbf{m} \tag{4.8}$$

The wrench matrix $\mathbf{W}_\omega = \mathbf{J}_\omega^T$ maps the output torque of the sphere to the omni-wheels torques. As shown in Fig. 4.5, it is possible to express $\boldsymbol{\tau}$ as a function of cable tension $\mathbf{t}$ so that:

$$\tau_1 = r(t_1 - t_2) \tag{4.9}$$
$$\tau_2 = r(t_3 - t_4) \tag{4.10}$$
$$\tau_3 = r(t_5 - t_6) \tag{4.11}$$

where $\mathbf{t} = [t_1, \ldots, t_8]^T$ is the vector of cable tensions.

$$\boldsymbol{\tau} = \mathbf{W}_c \mathbf{t} \tag{4.12}$$

where:

$$\mathbf{W}_c = \begin{bmatrix} r_o & -r_o & 0 & 0 & 0 & 0 & 0 & 0 \\ 0 & 0 & r_o & -r_o & 0 & 0 & 0 & 0 \\ 0 & 0 & 0 & 0 & r_o & -r_o & 0 & 0 \end{bmatrix} \tag{4.13}$$
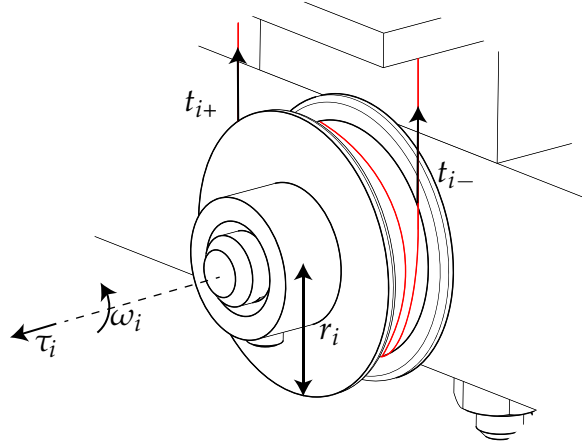
Figure 4.5: Representation of the applied wrench on a drum of a cale-loop

The equilibrium of the wrench applied on the parallel spherical wrist is written in the following:

$$\mathbf{m}_{\text{PSW}} = \mathbf{W}_{\text{PSW}} \mathbf{t} \tag{4.14}$$

with $\mathbf{m}_{\text{PSW}}$ being the external moments applied by environment onto the parallel spherical wrist. The wrench matrix of the parallel spherical wrist expressing the relationship between cable tensions and the wrist moments, is defined as follows:

$$\mathbf{W}_{\text{PSW}} = \mathbf{W}_\omega \mathbf{W}_c \tag{4.15}$$

In Fig. 4.6, the orientation of the camera axis, namely, x_2 is expressed through pitch, yaw and roll in the following:

$$\mathbf{q}_{PSW} = \begin{bmatrix} \theta \\ \psi \\ \chi \end{bmatrix} \tag{4.16}$$

4.1.2 Kinetostatic Model of the Manipulator

After determining the static equilibrium of the parallel sperical wrist, we can proceed with the kinetostatic modeling of the overall manipulator. The loop-closure equation of the CDPR is given by:

$$^0\mathbf{l}_i = {}^0\mathbf{a}_i - {}^0\mathbf{p} - {}^0\mathbf{R}_1 {}^1\mathbf{b}_i, \quad i = 1, 2, ..., 8 \tag{4.17}$$

It should be noted that the modeling is carried out for an under-constrained manipulator suspended by five (three bi-actuated and two uni-actuated) cables and nine DoF. However, the cable-loops are assumed as a pair of uni-actuated cables resulting in eight independent cables in terms of kinetostatic modeling.
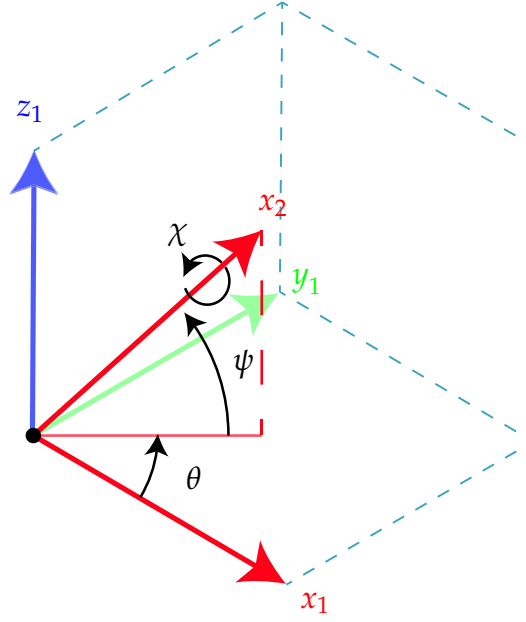
Figure 4.6: Orientation of the camera axis, y_2 with respect to $\mathscr{F}_1$

Similar to the equations (2.8- 3.26), the overall static equation of the manipulator is defined as follows:

$$\mathbf{W}\mathbf{t} + \mathbf{w}_g = \mathbf{0}_9, \tag{4.18}$$

where $\mathbf{0}_9$ is the nine-dimensional zero vector and the wrench matrix $\mathbf{W}$ takes the following form:

$$\mathbf{W} = \begin{bmatrix} \mathbf{W}_{\text{TP}} \\ \mathbf{W}_{\text{PSW}} \end{bmatrix}_{9\times 8}. \tag{4.19}$$

The wrench matrix of the top-plate of the moving-platform is expressed as

$$\mathbf{W}_{TP} = \begin{bmatrix} {}^0\mathbf{u}_{12} & {}^0\mathbf{u}_{12} & {}^0\mathbf{u}_3 & {}^0\mathbf{u}_4 & {}^0\mathbf{u}_{56} & {}^0\mathbf{u}_{56} & {}^0\mathbf{u}_7 & {}^0\mathbf{u}_8 \\ {}^0\mathbf{d}_1 & {}^0\mathbf{d}_2 & {}^0\mathbf{d}_3 & {}^0\mathbf{d}_4 & {}^0\mathbf{d}_5 & {}^0\mathbf{d}_6 & {}^0\mathbf{d}_7 & {}^0\mathbf{d}_8 \end{bmatrix}_{6\times 8}, \tag{4.20}$$

where

$$ {}^0\mathbf{d}_i = {}^0\mathbf{R}_1 {}^1\mathbf{b}_i \times {}^0\mathbf{u}_i, \quad i = 1, ..., 8. \tag{4.21}$$

$\mathbf{t}$ is the vector containing the tensions exerted by the eight actuators to the cables.

$$\mathbf{t} = \begin{bmatrix} t_1 & t_2 & t_3 & t_4 & t_5 & t_6 & t_7 & t_8 \end{bmatrix}^T \tag{4.22}$$

$\mathbf{w}_g$ is the eight-dimensional gravity wrench vector applied on the moving-platform and tilt-roll wrist, namely,

$$\mathbf{w}_g = \begin{bmatrix} m {}^0\mathbf{g}^T & m({}^0\mathbf{R}_1 {}^1\mathbf{c} \times {}^0\mathbf{g})^T & \mathbf{m}_{PSW}^T \end{bmatrix}^T \tag{4.23}$$

with **c** being the Cartesian coordinates vector of the CoM of moving-platform. Hereafter, we can express the differential kinematics of the manipulator as a relation between its output velocity vector $\dot{\mathbf{q}} = \begin{bmatrix} \dot{\mathbf{p}}^T, & \boldsymbol{\omega}^T, & \dot{\mathbf{q}}_{PSW}^T \end{bmatrix}^T$ and the cable velocity vector $\dot{\mathbf{l}} = \begin{bmatrix} \dot{l}_1, & ..., & \dot{l}_8 \end{bmatrix}^T$:

$$\mathbf{J}\dot{\mathbf{q}} = \dot{\mathbf{l}}. \tag{4.24}$$

The velocity of the origin of frame $\mathscr{F}_1$ with respect to $\mathscr{F}_0$ is defined as $\dot{\mathbf{p}}$ and the angular velocity of the moving-platform with respect to $\mathscr{F}_0$ is defined as $\boldsymbol{\omega}$. The Jacobian matrix **J** is calculated based on the well-known kinetostatic duality:

$$\mathbf{J} = -\mathbf{W}^T \tag{4.25}$$

4.1.3   Static Workspace

Here, we introduce the static workspace of the CDPR\PSW manipulator. The static workspace of the nine-DoF CDPR consists of the set of positions and orientations of the moving-platform and the orientations of the end-effector, namely, $^0\mathbf{p}$ and $^0\mathbf{R}_1$ and $\mathbf{q}_{PSW}$, which satisfies the static equilibrium of the manipulator.

The set $\mathscr{T}$ represents the cable tension space and takes the shape of a box in an eight-dimensional space:

$$\mathscr{T} = \left\{ \mathbf{t} \in \mathbb{R}^8 : \mathbf{t}_{min} \leq \mathbf{t} \leq \mathbf{t}_{max} \right\} \tag{4.26}$$

where $\mathbf{t}_{min}$ and $\mathbf{t}_{max}$ are respectively the lower and upper bounds of the feasible tension in cables. Let's define the static workspace of the CDPR\PSWmanipulator as follows:

$$\mathscr{S} = \left\{ (^0\mathbf{p}, {}^0\mathbf{R}_1, \mathbf{q}_{PSW} \in \mathbb{R}^3 \times SO(3) \times \in \mathbb{R}^3 : \exists \mathbf{t} \in \mathscr{T}, \ \mathbf{W}\mathbf{t} + \mathbf{w}_g = \mathbf{0}_8 \right\} \tag{4.27}$$

where $SO(3)$ is the group of proper rotation matrices. Equation (4.27) expresses the static workspace in a nine-dimensional space and as the visualization of such high-dimensional space is impossible with common human perception in 3D, we define the static workspace of the manipulator for a simplified case. We define $\mathscr{S}_{3T3R}$, while constraining the orientations of the top-plate. The former subset, namely, $\mathscr{S}_{AO}$ is a set for a given orientation of the top-plate while the wrist is free to rotate, i.e., the translational static workspace of the manipulator with constant orientation of $^0\mathbf{R}_1$ and all orientations of the parallel spherical wrist.

$$\mathscr{S}_{3T3R} = \left\{ {}^0\mathbf{p} \in \mathbb{R}^3 \mid {}^0\mathbf{R}_1 = \mathbf{I}_3 : -\pi \leq \theta, \ \psi, \ \chi \leq \pi : \exists \mathbf{t} \in \mathscr{T}, \ \mathbf{W}\mathbf{t} + \mathbf{w}_g = \mathbf{0}_8 \right\} \tag{4.28}$$

4.2   Design and Optimal Cable Arrangement

The manipulator is realized in the context of the CREATOR project with already developed setup in terms of hardware and software for the manipulators presented in Chapters 2 and 3. Hence, the main focus of this section is on the design and prototyping of the moving-platform of the manipulator. The moving-platform basically

consists of a top-plate on which the parallel spherical wrist is embedded. The top-plate hosts all the required components of the parallel spherical wrist. Furthermore, an approach for determining the cable arrangement that yields the maximal static workspace is presented.

4.2.1 Design of the Moving-Platform

The Parallel spherical wrist is a parallel mechanism embedded into the moving-platform which drastically expands the orientation workspace of the manipulator. The first mock-up of the concept is depicted in Fig. 4.1c and is made of filament 3D printing. The previous research-work on the CDPR\PSW has not engaged into development of a practicable prototype. In the following, the main issues concerning the mechanical design are listed:

- Compliance of the arm:
  At the connection points between the caster balls of the arm and the sphere, the arms undergoes relatively high amplitudes of displacement resulting in a loose contact with the sphere. The arm however, must always constrain the translation of the sphere with respect to the top-plate, but not its orientation.

- Sphere surface:
  The sphere surface and its finish have a major role on the actuation of the end-effector and consequently on the orientation accuracy. The manufactured sphere in plastic undergoes uneven contact with omni-wheels and caster balls due to its rough surface. This causes slipping, which undermines the accuracy of the system.

- Suspension of the omni-wheels:
  The suspension system should be able to adjust the magnitudes of the forces applied on the sphere. The suspensions employ leaf-springs, which are prone to permanent deformations.

- Double U-joints:
  As the input shaft of the omni-wheel is not aligned with the output shaft of the cable-loop drum, double U-joints were introduced in the design of the carriage. These joints lead to a jerky motion of the omni-wheels and consequently a loss of contact between the sphere and the omni-wheels.

Initially, the design targets in solving the mechanical issues of the previous research work. After a revision of the design, a first prototype was manufactured for further analysis and investigation through experimentations. In the new design as shown in Fig. 4.7, the mobile-platform consists of three main sub-components, namely, a top-plate housing all the anchor points, a sphere and an arm structure to hold the sphere within. Figure 4.8 presents the top-plate sub-assembly. The top-plate is the base of the mobile-platform and it hosts the anchor points as well as three carriages sub-assembly. Every carriage supports an omni-wheel and transmits the torque from cable-loop to the omni-wheel. The arm functions as a fixation between top-plate and the sphere while allowing the relative rotation of the sphere with respect to the top-plate. The arm is connected to the top-plate by bolts and
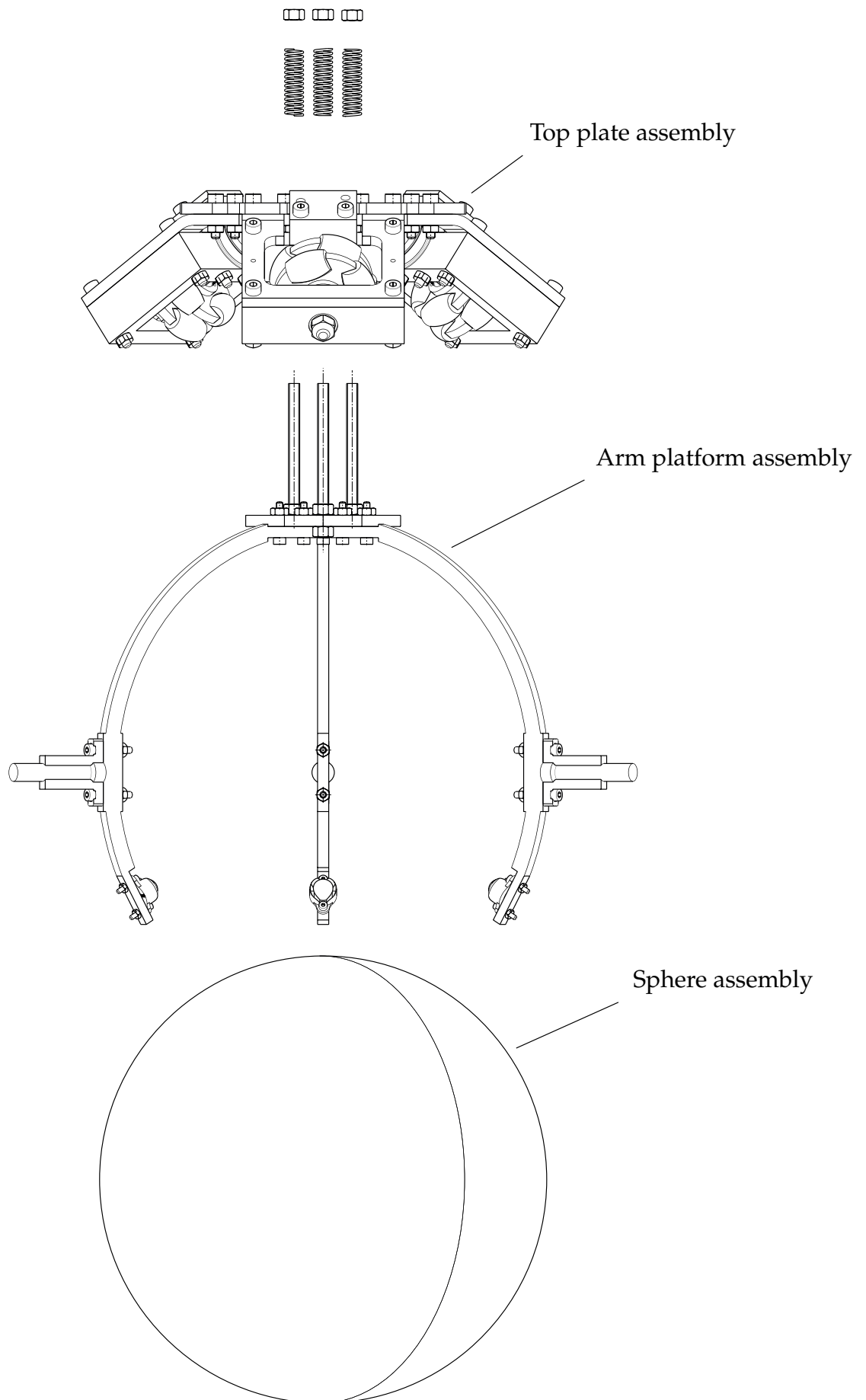
Top plate assembly

Arm platform assembly

Sphere assembly

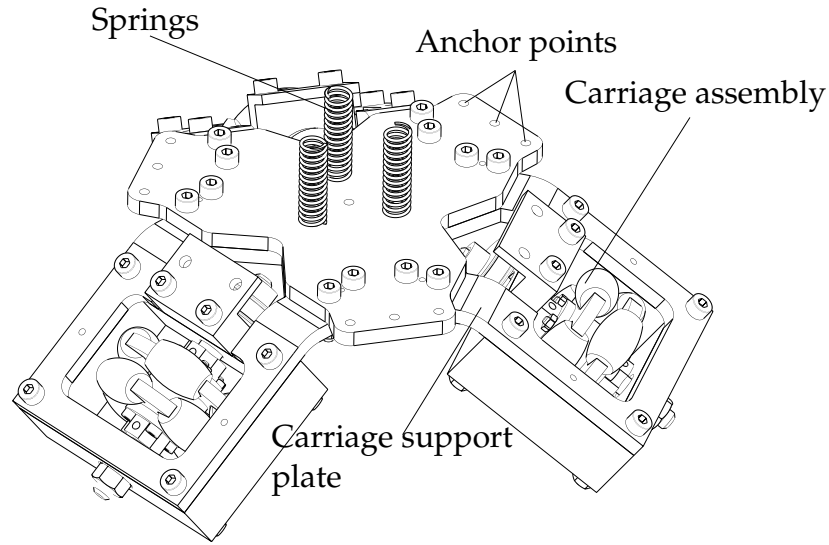**Figure 4.7:** Exploded view of the parallel spherical wrist

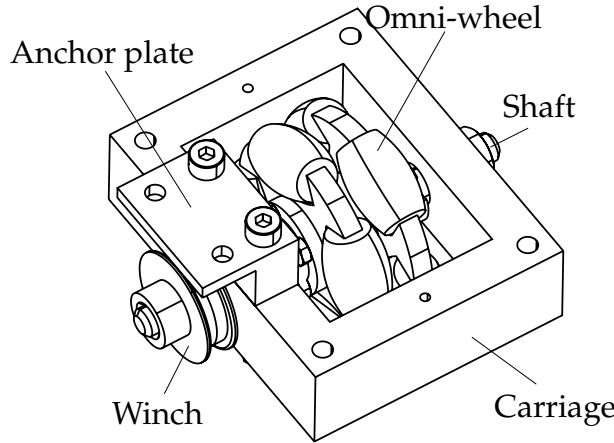**Figure 4.8:** Top plate sub-assembly

Figure 4.9: Carriage assembly

springs to adjust the contact forces between each omni-wheel and the sphere. The top-plate consists of two main components, namely, the carriage and the anchor-plate as shown in Fig. 4.8.

The anchor-plate functions as a plate containing all the anchor points as well as a routing structure for cable-loops. The carriage is the subcomponent of the parallel spherical wrist, which attaches the omni-wheels to the top plate as depicted in Fig. 4.9. The carriage is mounted on the top-plate folded with an angle of $\alpha = 35.6°$ as by Eq. (4.1) and shown in Fig. 4.4.

The friction coefficient between the drum and the cable-loop, i.e., μ, plays an crucial role since, insufficient friction leads to slippage of the cable-loop on the drum. The drums transmit the input torque to the sphere through the omni-wheels. Radii of the cable-loop drums are fixed as $r_d = 5$ mm based on the design parameters and constraints. The friction coefficient varies based on the surface condition including the roughness of the drum surface. Figure 4.10a illustrates a friction model for a cable on the circumference of a circle. In [KS13], the Euler-Eytelwein formula relates
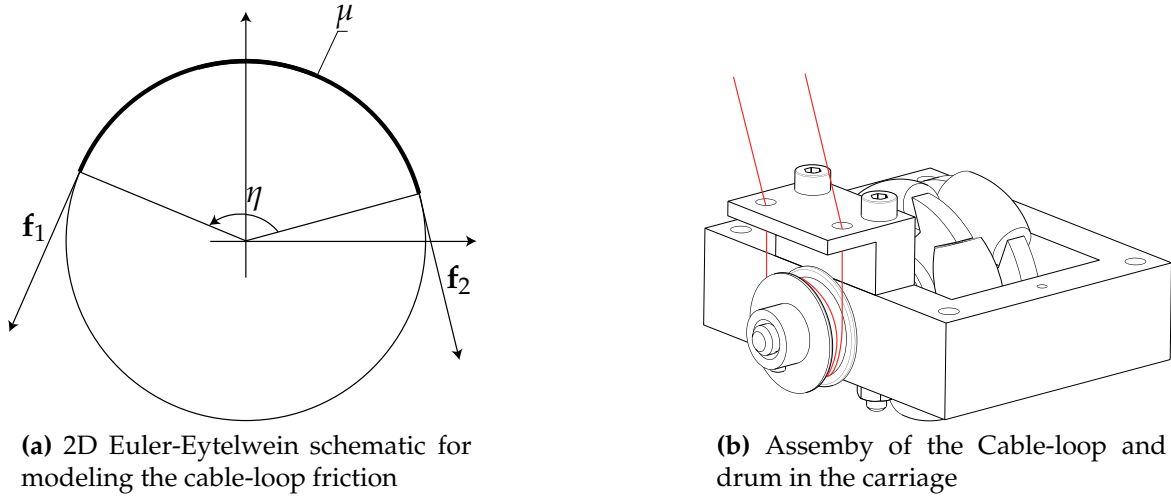
(a) 2D Euler-Eytelwein schematic for modeling the cable-loop friction

(b) Assemby of the Cable-loop and drum in the carriage

Figure 4.10: Schematics of the assembly of cable-loops

the friction force between a cable and a curve on a drum as given by:

$$f_1 = f_2 e^{\mu\eta} \tag{4.29}$$

under the following condition:

$$0 < f_2 < f_1 \tag{4.30}$$

with f_1 and f_2 being the tensions at the two ends of the cable, η being the angle expressed in radian of coiled cable on the circumference of the drum. Equation (4.29) is reformulated as:

$$\eta = \frac{1}{\mu} \left(ln\frac{f_1}{f_2} \right). \tag{4.31}$$

The friction coefficient between the cable and the drum is computed experimentally as $\mu = 0.07$. By taking into account the characteristic of the wrist, the minimum value of η is calculated as follows:

$$\eta \simeq 10\pi \tag{4.32}$$

The value obtained in Eq. (4.32) indicates that at least five turns of cable should be coiled on the drum to avoid cable-loop slippage.

4.2.2   Cable Arrangement

The anchor-plate has fifteen points to be selected as anchor points. Since, the number of actuators of the CREATOR platform is limited to eight, we consider eight out of total fifteen anchor points. The number of exit point combinations, $\mathcal{N}_e$ is expressed as:

$$\mathcal{N}_e = \binom{n_e}{n_c}, \tag{4.33}$$

with n_e and n_c being the numbers of exit-points and cables, respectively. The number of anchor-points combinations, $\mathcal{N}_a$, consists in the number of permutations of

the set of points, which is given by:

$$\mathcal{N}_a = \binom{n_a}{n_c} n_c!, \tag{4.34}$$

n_a being the number of selected anchor-points. The number of possible cable configurations $\mathcal{N}_C = dim(\mathcal{S}_C)$ is thus given by:

$$\mathcal{N}_c = \mathcal{N}_a \mathcal{N}_e = \binom{n_e}{n_c}\binom{n_a}{n_c} n_c!. \tag{4.35}$$

Additionally, anchor points are divided into two groups those associated to cable-loops and those associated to the simple cables. All the cable-loop anchor-points should be picked in order to actuate the wrist. Therefore, the number of the single and bi-actuated cables are denoted as, n_{SC} and n_{CL}, respectively.

$$n_c = n_{SC} + n_{CL} \tag{4.36}$$

We define as well the number of anchor points available for the single and bi-actuated cables, respectively n_{aSC} and n_{aCL}, so that:

$$n_a = n_{aSC} + n_{aCL} \tag{4.37}$$

The number of combinations considering cable-loop, $\mathcal{N}_{CL}$, is given by:

$$\mathcal{N}_{CL} = \binom{n_e}{n_c}\binom{n_{aSC}}{n_{SC}} n_c! \tag{4.38}$$

Figure 4.11 shows all the available anchor points, namely, r_i, $i = 1, 2, \ldots, 15$. Six points are associated to the wrist actuation and consequently to the three cable-loops, $n_{aCL} = 6$. The remaining nine anchor points are nine points to be assigned to simple cables, $n_{aSC} = 9$. Finally, $\mathcal{N}_{CL}$ expressed in Eq. (4.38) is computed for the CDPR\PSW manipulator in the framework of the CREATOR:

$$\mathcal{N}_{CL} = \binom{8}{8}\binom{9}{2} 8! = 1451520 \tag{4.39}$$

Figure 4.12 illustrates the cable arrangement corresponding to the largest possible workspace. Figure 4.12a shows a schematic of the anchor-plate as well as the cable arrangement. Figure 4.12b shows the corresponding static workspace with 65% of the total volume of the manipulator.

4.3 Experimental Demonstration

The architecture of the manipulator with an embedded parallel spherical wrist is presented in Fig. 4.13. The main hardware of the CREATOR demonstrator consists of a PC (equipped with ©MATLAB and ©ControlDesk software), motors and drivers, controller and winches are shown. Moreover, a computed torque control scheme is implemented for the control of the manipulator as depicted in Fig. 2.28.
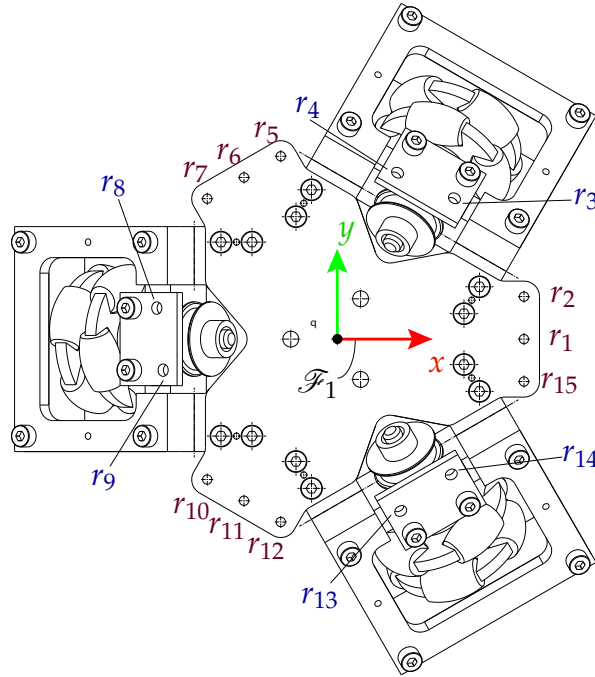
Figure 4.11: Top-plate of the 3T3R manipulator and anchor points

The provided setup enables us to evaluate the capabilities of the manipulator in operation. However, there is one crucial constraint imposed by the demonstrator setup in terms of the number of actuators. Since the manipulator has nine-DoF and the demonstrator is equipped with only eight motors, the manipulator undergoes under-actuation. However, we can estimate the overall performance of the manipulator by considering the following case:

- Case 1: The moving-platform is over-actuated with six controllable DoF of the top-platform. Hence, the desired trajectory includes the translation of the top-plate within the workspace while fixing the orientations of the top-plate as well as the parallel spherical wrist. This link [1] refers to a video of this case.

- Case 2: The pose of the top-plate is mechanically constrained and the orientation of the wrist is controlled. This case is designed just to illustrate the performance of the parallel spherical wrist regardless of the parasitic inclination due to under-actuation. A video is uploaded at link [2] corresponding to this demonstration case.

- Case 3: The control of 8-DoF of the manipulator, i.e., leaving the free rotation of the top-plate about the vertical axis, namely, z_0. As a consequence, the parasitic inclination is introduced to the system. This case demonstrates the under-actuation effects imposed onto the system due to an insufficient number of actuators. The third case of the demonstration is shown in link [3].

---

[1] http://tiny.cc/smcxdz
[2] http://tiny.cc/6icxdz
[3] http://tiny.cc/1ncxdz

(a) Cable configuration
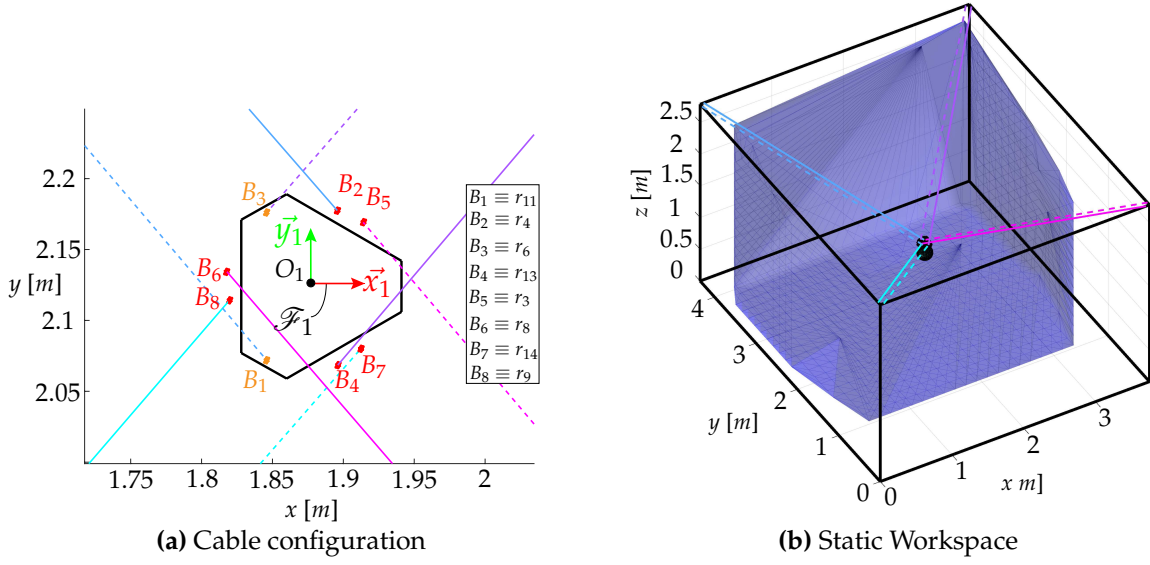
(b) Static Workspace

Figure 4.12: Results of the optimization algorithm

4.4 Conclusions

The chapter detailed the main contributions and results about CDPRs with an embedded parallel spherical wrist in [Mét19]. However, the concept was developed in the framework of [Ang15] and advanced in [Tah16]. Even though promising results have been obtained through preliminary demonstrations, the study and work on CDPRs with augmented large orientation workspace is not complete yet.

This chapter started by presenting the previous research work and contributions. Then, kinetostatic model was detailed for the parallel spherical wrist and the entire manipulator. The static workspace of the manipulator was formulated beside its analysis for different cases. Section 4.2 detailed the previous design challenges and proposed the solutions for realizing the first CDPR with an embedded parallel spherical wrist. Since cable arrangement has a crucial effect on the size of the static workpsace, the investigation of the optimal exit and anchor points was carried out.

4.5 Future Work

Besides all the results obtained regarding CDPRs with large orientation workspaces, there are several improvements to be done in the next design iterations. This modification will concern the precision of the end-effector, the size of its translational workspace and under-actuations as listed below.

Design Improvements

The studied hybrid manipulator has nine DoF, while the demonstrator possesses eight actuators. This under-actuation leads to undesired and parasitic motions of the moving-platform. Since the orientation of the top-plate is always fixed, the orientation DoF of the top-plate could be constrained by employing three parallelograms. This solution theoretically solves the problem of the under-actuations and
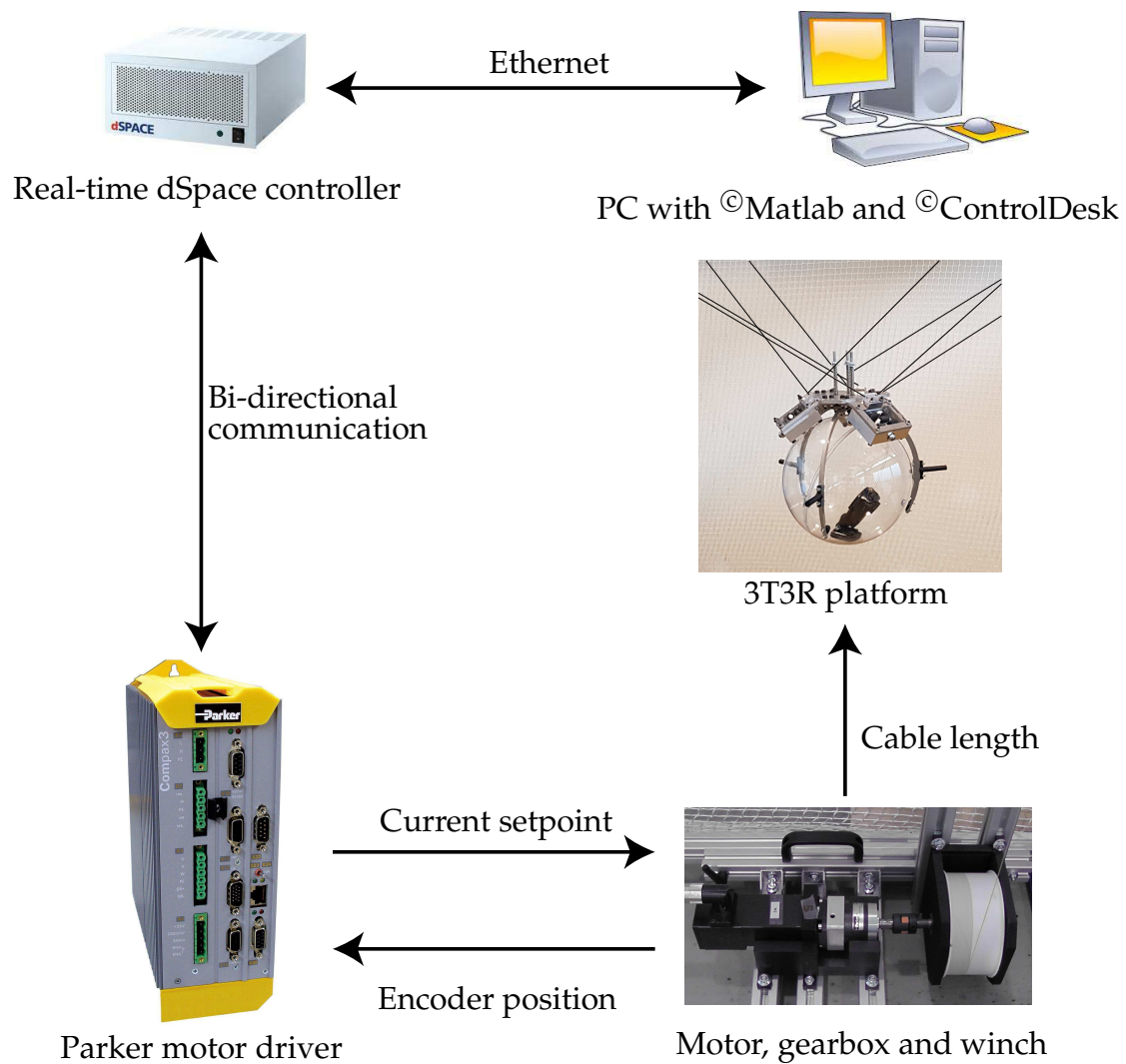
Figure 4.13: Control architecture of *CREATOR*

cable interferences by constraining the robot motion with less actuators. Moreover, cable-loops are one of the fundamental components for hybrid CDPRs with an embedded wrist and there are several challenges to their application. They circulate through drums, anchor points and exit points, leading to higher friction between the cable-loop and the other components. Thus, further investigation is required for cable maintenance and the reduction of friction. Furthermore, modeling of emergency scenarios in case of cable failure will improve the reliability of the manipulator.

Modeling Improvements

To this date, we only have investigated the kinetostatic model of the manipulator with non-elastic cables. Precision and performance are dependent on the modeling of the manipulator and therefore more accurate models could be employed. As an instance, a dynamic model will contribute to the stability of the system especially for the wrist actuation. Hysteresis and elastostatic models of cables are also effective solutions toward precision of the manipulator and substantially constructive to the accuracy of the wrist orientation.

Chapter 5

Conclusions and Perspectives

Contents

5.1 General Conclusions

Cable-Driven Parallel Robots (CDPRs) have been studied and developed for few decades. They are outstanding manipulators in terms of translation workspace size, high payload to weight ratio and reconfigurability. However, CDPRs generally undergo a crucial issue in terms of orientation workspace stemmed by cable collisions and interferences. Hence, analysis, design and prototyping of CDPRs with large translation and orientation workspaces are defined in the scope of this manuscript. The presented research work carries out the development of hybrid CDPRs with augmented orientation workspace.

5.1.1 Analysis and Modeling

The development of hybrid CDPRs with large translation and orientation workspaces was begun by analysis of the workspace of the CDPRs, i.e., Wrench Feasible Workspace (WFW) and Twist Feasible Workspace (TFW). WFW are exhaustively studied in the literature. Therefore, WFW was employed for the proposed hybrid CDPRs in the manuscript. Although several papers addressed the wrench capabilities of CDPRs, few have tackled the dual question of their twist capabilities. In Appendix B we clarify the analysis of twist feasibility by means of the more specific concept of twist feasibility, which was defined by Gagliardini et al. in [GCG15]. Contrary to the latter paper, the twist feasibility analysis proposed here is based on the usual CDPR

differential kinematics where the Jacobian matrix maps the mobile-platform twist into the cable velocities.

Parasitic inclination is defined as undesired orientation of the moving-platform that leads to inaccuracy in manipulation and positioning. Parasitic inclination can be induced by employing cable-loops in the design of CDPRs. This kinematic situation was investigated in detail for the planar Cable-Driven Parallel Crane (CDPC). In spite of the negligible effect of the parasitic inclination on the positioning accuracy of the moving-platform, the parasitic inclination model was employed for lowering its downside through design optimization.

The proposed manipulators were modeled as in kinetostatic, elasto-static and cable-loops. However, there have been similar models developed for CDPRs, the main contribution of this manuscript lies in developing models for hybrid CDPRs with remote actuation system of cables for their active wrists with large orientation workspace.

5.1.2   Design of Hybrid CDPRs

Three hybrid CDPRs were designed and manufactured in the framework of this thesis. The proposed manipulators employed bi-actuated cables, namely, cable-loops in their hybrid kinematic structure. To the best of author's knowledge, Although, few papers proposed the concept of hybrid CDPRs through cable-loops, the ones developed in this research work are the first realized manipulators of the kind. The optimum designs of the three manipulators were conducted in following of the prior analysis results.

5.1.3   Manufacturing and Demonstration

This research work also undertook prototyping, manufacturing and demonstrating of the proposed manipulators to communicate their potential applications as well as the practical challenges. The manufacturing process started with the preparation of CREATOR (robot parallèle à Câbles ayant un gRand Espace de trAvail en Translation et en ORientation) demonstrator located at LS2N (Laboratoire des Sciences du Numérique de Nantes). Firstly, several iterations of design were conducted, in terms of winches, pulleys, reconfigurable systems of actuation units and etc. In following of the prepared structure of the demonstrator, the design and prototyping of the moving-platforms were started.

5.2   Perspectives

In the scope of the thesis, two CDPRs with large translation and orientation workspaces were realized. The CDPR with an embedded tilt-roll wrist is capable of providing large amplitudes of rotations about two axes. Similarly, the CDPR with an embedded parallel spherical wrist with large amplitudes of orientation about three axes. The amplitudes of the rotations are bounded by the length of cable-loops only. With the average-sized winches designed in the framework of the CREATOR, up to $114\,\pi$ radians, i.e., 57 turns are provided for the amplitudes of rotations for the CDPR with an embedded parallel spherical wrist. Since, the lengths of the cable-loops are not

limiting factors in our current design, their lengths can be chosen to be large without affecting other characteristics of the manipulator. In spite of the large obtained orientation workspace, the precision of the manipulator can be subject of further improvements. Therefor, the following perspectives are proposed.

5.2.1 Analysis and Modeling

All the developed models in this thesis were based on the linear model of cables. In spite of the detailed elasto-static model of the CDPC, the elasto-static model of the other hybrid manipulators should be investigated for enhanced stiffness of the moving-platforms. Moreover, a better accuracy especially for active wrist is expected be employing more sophisticated models, e.g., hysteresis of cables and dynamic models of the hybrid manipulators. In addition to the studied workspaces, dynamic and interference-free workspaces should be determined for more rigorous models of the manipulators.

The demonstration and practical implementations unanimously showed high sensitivity of the orientation of the active wrist to the uncertainties arisen by imperfect models. Therefore, the design with the prior sensitivity analysis leads to improved performance of the manipulator.

5.2.2 Design of Hybrid CDPRs

We suggest two perspectives for hybrid CDPRs with large translation and orientation workspaces. The first one is the improvement of the already-proposed manipulators and the latter concerns new concepts of hybrid CDPRs with large workspaces. Further design improvements in the design of the proposed manipulators are listed hereafter:

- Parallelogram joints: In CDPR\TRW and CDPR\PSW, the orientation DoFs of the top-plates are predefined fixed for the potential tasks. Therefore, the higher controllable DoF are required for the restrained orientation of the top-plates. One solution to minimize the number of actuators is to include parallelogram system of cables for restraining orientation of the top-plates. In other words, three actuated cables are discarded and consequently, lower risk of cable interferences. Figure 5.1 illustrates the kinematic structure of the proposed parallelogram system made of a differential mechanism, uni-actuated and bi-actuated cables.

- Design improvement of CDPR\TRW: The tilt-roll wrist has three heavy bevel gears made of steel. Therefore, a counter-balance weight was designed to fix the center of gravity for all orientations of the wrist leading to a higher mass of the moving-platform. The design can be improved by substituting steel gears with nylon gears. The manipulator undergoes backlash due to spur gears embedded in the tilt-roll wrist. However, a spherical cam mechanism appears to be a good alternative as detailed in [BA05].

- Accuracy of orientations : The amplitudes of the rotations are extremely large, e.g., more that $100\,\pi$ in CDPR\PSW about any axis. Even though, the main objective was to augment the size of the orientation workspace, but most of
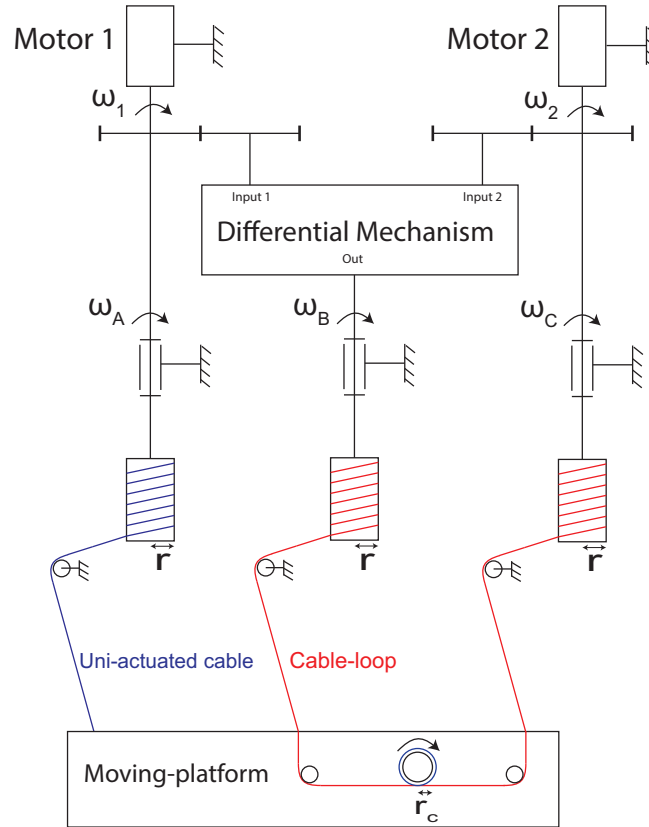
Figure 5.1: Schematic of the proposed parallelogram cable system

the potential applications of the proposed manipulators require considerably smaller orientation workspace. Accordingly, improving the orientation accuracy through altering transmission ratio between the cable-loop displacement and the end-effector of the wrist contributes to the accuracy of the system.

In the context of this manuscript, the concept of hybrid CDPRs established an augmentation of the classical CDPRs functionalities through remote actuation, i.e., all actuators off the moving-platform. Consequently, cable-loops are employed as the most fitting and complementary implementation. Nonetheless, there are other approaches towards the concept of hybrid CDPRs, e.g., actuators on the moving-platform. Besides the proposed embedded mechanisms, other parallel wrists with large orientation workspace can be embedded into the moving-platform of the CDPRs like, agile eye mechanism.

5.2.3   Manufacturing and Experimentation

Further experimentation should be conducted on the parasitic inclinations of the moving-platform with precise pose measurement systems, e.g., laser tracker. Since the beginning of this research work, the provision of the CREATOR demonstrator has been proceeded. Moreover, further improvements like integrating visual pose-feedback with the control system will enhance the precision of the manipulators. Acquiring more actuators will also contribute to the hybrid CDPRs with large translation and orientation workspaces.

Appendix A

Design and Prototyping of the CREATOR Demonstrator

In this appendix, we detail the mechanical design and prototyping of the CREATOR demonstrator since its earliest stage. The first step towards prototyping of the demonstrator is to select and purchase the required hardware consisting of motors, gearboxes, drivers, etc. The next step concerns design and manufacturing of the remaining parts of the CREATOR prototype, e.g., shafts, winches and the base of the actuation system. Setting up and the assembly of all the components are the next steps. Therefore, a preliminary experiment could be conducted after finalizing the prototyping. Hereafter, we are able to realize CDPRs with large orientation and translation workspaces for various designed moving-platforms.

A.1   Overall Architecture

The main framework of the CREATOR prototype in terms of actuation and structure is discussed in this section. The design parameters were detailed earlier in Table 2.6. Figure A.1 illustrates the initial setup for a suspended CDPR with a point-mass as the moving-platform and three cables and Fig. A.2 shows a schematic of the second stage of the development on the architecture of the CREATOR demonstrator. The design is improved mainly regarding the reconfigurability of the exit-points, actuation and winch units as detailed in the following.

A.2   Actuation and Winch Unit

An actuation unit consists of a servomotor, a reducer (gearbox), coupling and a base for fixing the unit on the ground. Figure A.3 shows an exploded view of all the components of the actuation unit. The effort generated by motor is transmitted to a winch after increasing the input torque by the reducer and consequently reduction in the output speed. Hereafter, the output of the reducer is transmitted through a coupling component to the shaft of the winch unit. The coupling is employed for the smooth transmission of the power from reducer shaft to shaft of the winch unit. An exploded view of the winch and its components is shown in Fig A.4.

The winch is a mechanism connected to an actuator to coil a cable onto its drum and consequently to control the cable length. Design of a winch is dependent on the CDPR task and the actuator effort, overall geometry of the manipulator (maximum of possible cable length variation) and the admissible cable tension and velocity.
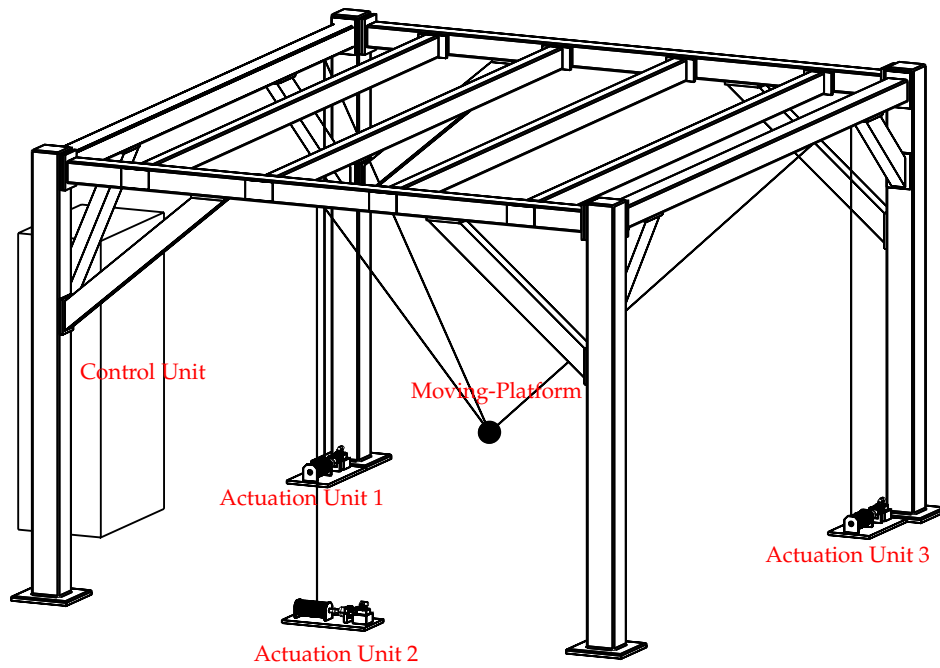
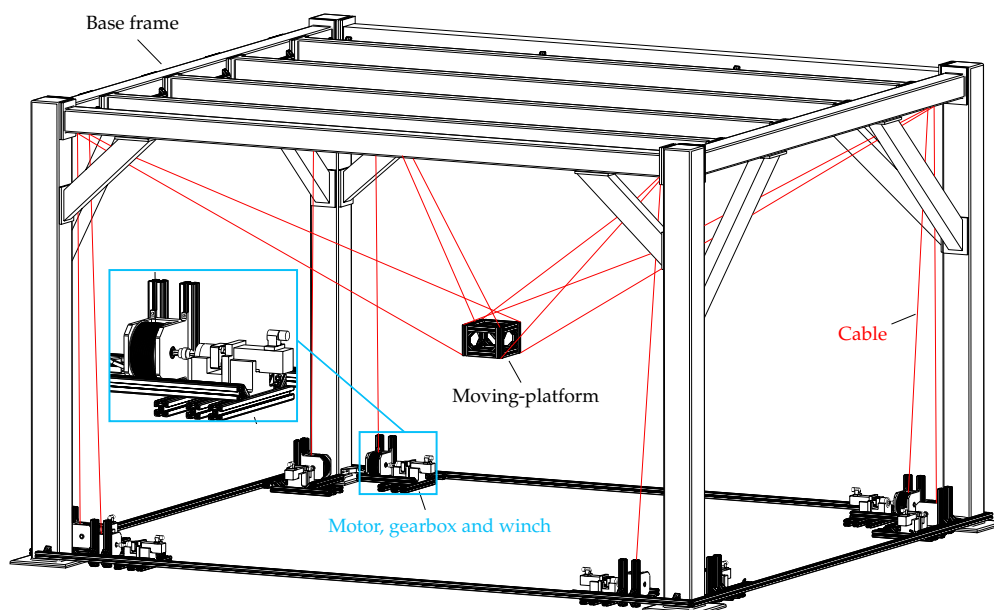**Figure A.1:** Initial architecture of the CREATOR demonstrator

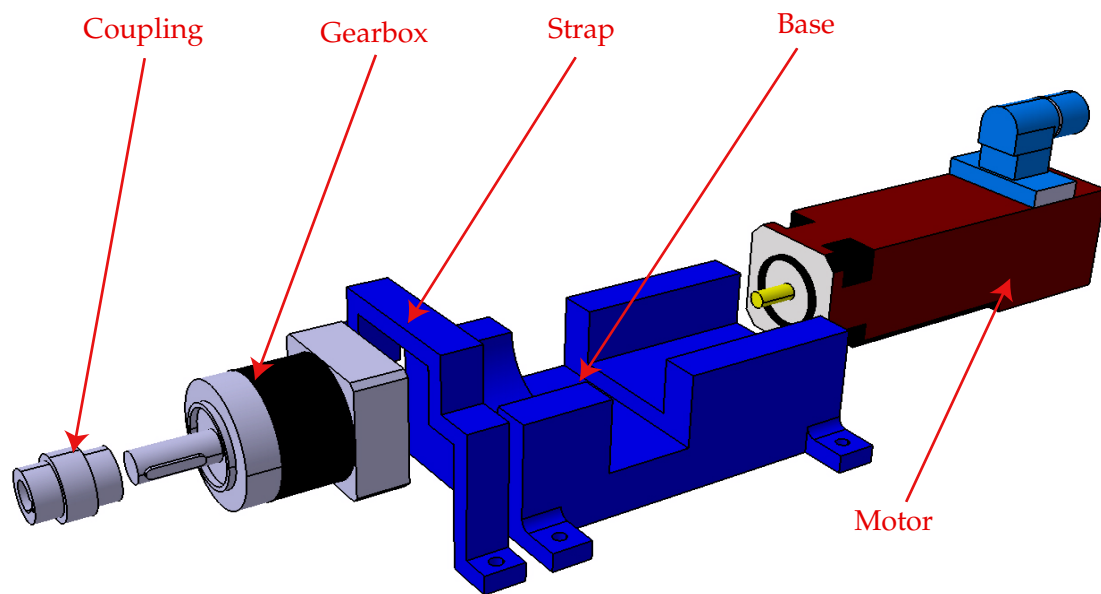**Figure A.2:** Architecture of the Reconfigurable CREATOR demonstrator

Figure A.3: Exploded view of the actuation unit
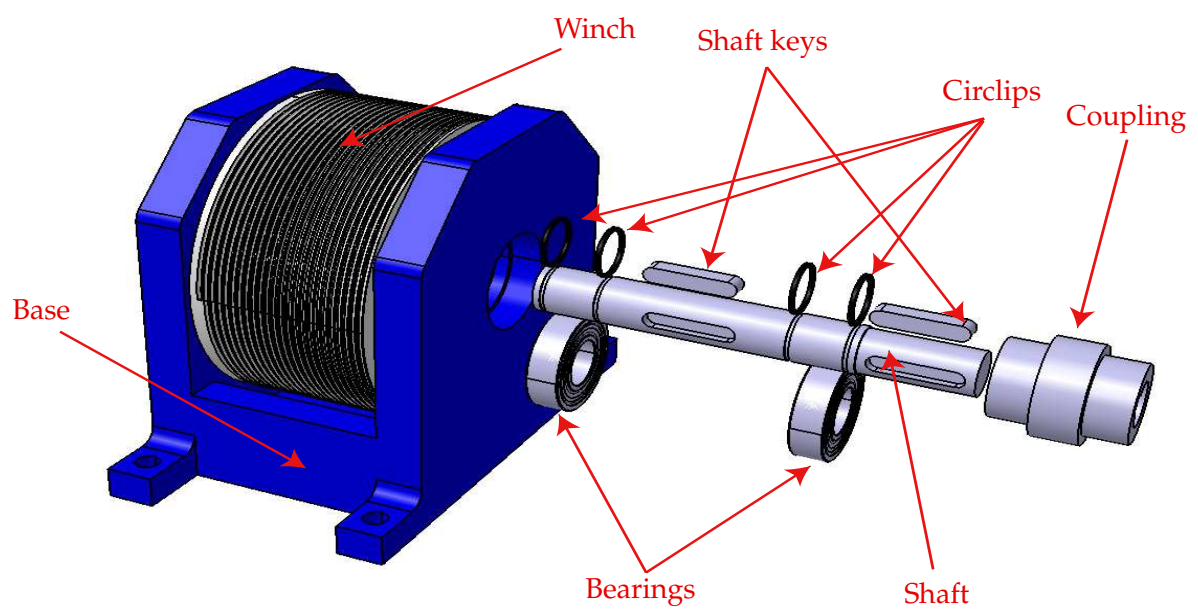

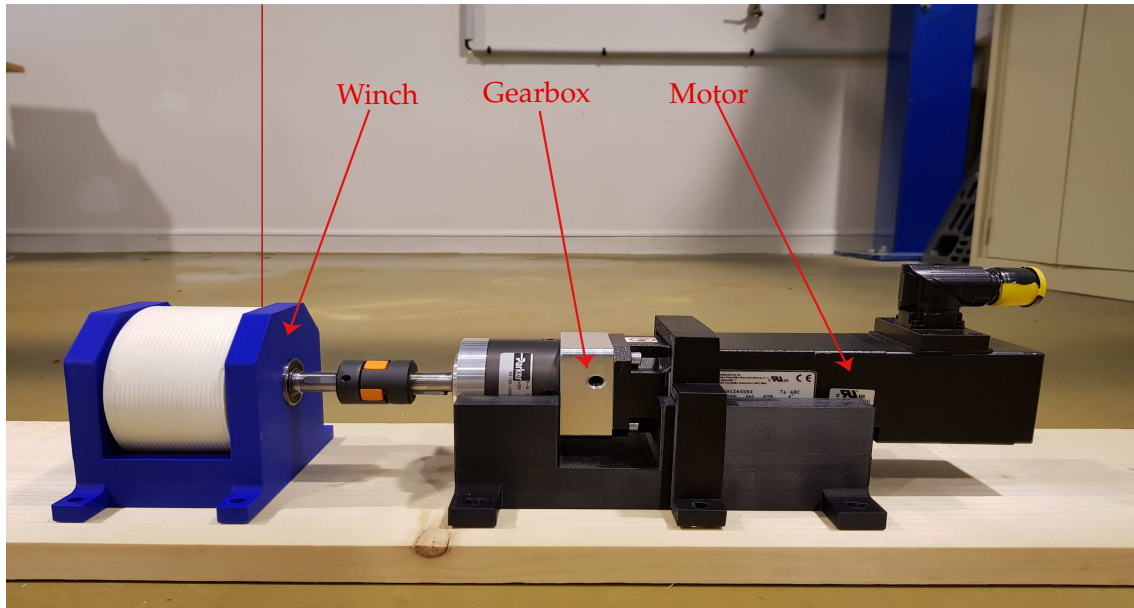**Figure A.4:** Exploded CAD-view of the winch mechanism

Figure A.5: Assembly of the preliminary actuation and winch unit

The design progress of the winch units are shown in Figs. (A.5, A.6). The former figure shows the preliminary setup while the latter one shows the assembled unit granting fast and easy reconfigurability of the CREATOR demonstrator.

A.3   Exit-point

Pulleys are usually used to vary the direction of the force along the cables. The contact point between cable and pulley is denoted as a CDPR exit-point. Three types of exit-points are designed for the CREATOR demonstrator. The first one is a 3D printed eyelet in nylon as shown in Fig. A.7. This preliminary rapid-prototype enables us to obtain a relatively accurate exit-point while generating high amplitudes of friction between cable and the eyelet. Figure A.8 shows a plate containing eyelets made of steel with a high payload capacity suitable for heavy moving-platforms. The CAD design of a 2-DoF pulley is depicted in Fig. A.9 in order to overcome the friction problem with the earlier designs.

Figure A.6: Reconfigurable actuation unit and winch mechanism
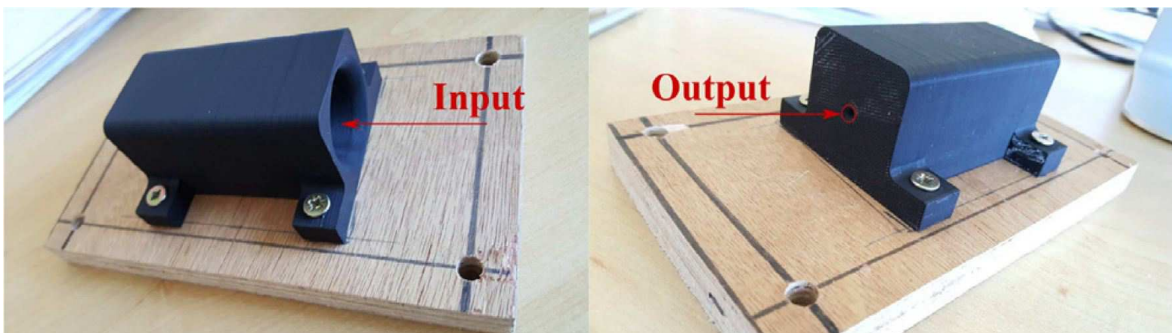
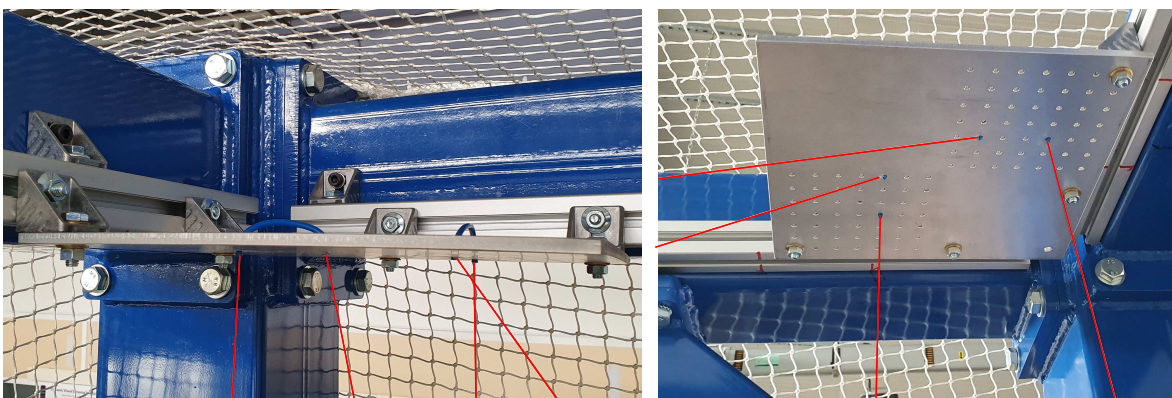**Figure A.7:** Preliminary 3D printed eyelet, [Bak+19]

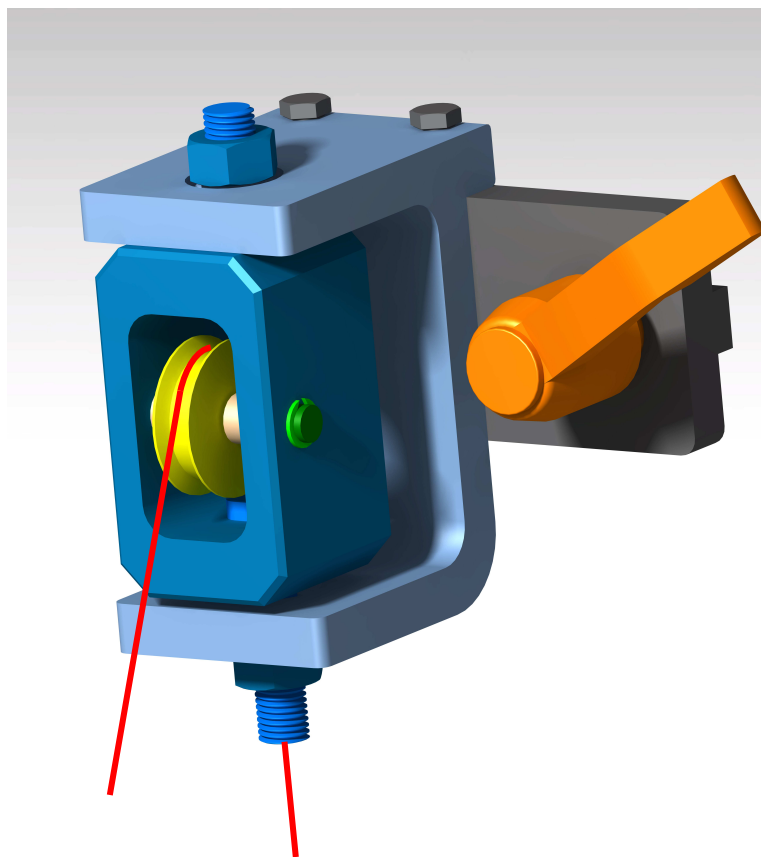**Figure A.8:** Eyelet plate

Figure A.9: CAD design of a 2-DoF pulley

Appendix B

Workspace Analysis

B.1 Wrench-Feasible Workspace

Wrench feasibility of CDPRs are comprehensively addressed in the literature. The first approach employed in this manuscript is called hyperplane Shifting Method (HSM) detailed in [BGM10b]. The HSM takes advantage of H-representation method, which requires a non-iterative approach in order to construct the available wrench set. The second employed approach of WFW calculation is based on the Capacity Margin Index (CMI) detailed in [Gua+14]. Moreover, Cruz Ruiz et al. in [Rui+15] developed the ARACHNIS software for computation of WFW of CDPRs through CMI. The CMI indicates how well moving-platform of CDPRs supports varying external wrench for a given pose and an admissible cable boundary. In other words, CMI quantifies the robustness of the equilibrium of the moving-platform of CDPRs. Since in this approach all the vertices of the wrench exerted on the moving-platform is calculated, the visual representation of available and required wrench set are presented through *convexhull* algorithm as shown in Fig. B.1.

In order to prove the reliability of the implemented algorithm based on the HSM and CMI, we compare the results obtained by our implementation with the ones from ARACHNIS software developed in the context of [Rui13]. The comparison is carried out for two cases, namely, planar and special CDPRs. These two cases are depicted in Fig. B.2.

Case Study 1

The first case study deals with a planar CDPR with four cables. Figure B.2a illustrates the configuration and specification of the CDPR. The demonstration of WFWs obtained by ARACHNIS and developed program are depicted in Fig. B.3.

Case Study 2

A spacial CDPR is studied as the second case study. This case was introduced to analyze the constant-orientation WFW workspace in [Rui13]. The configuration and the specification of the CDPR is detailed in Figure B.2b.

As it is shown in Figs. B.3-B.4, the WFW boundaries obtained by the implemented algorithm and the ARACHNIS ineterface are identical.
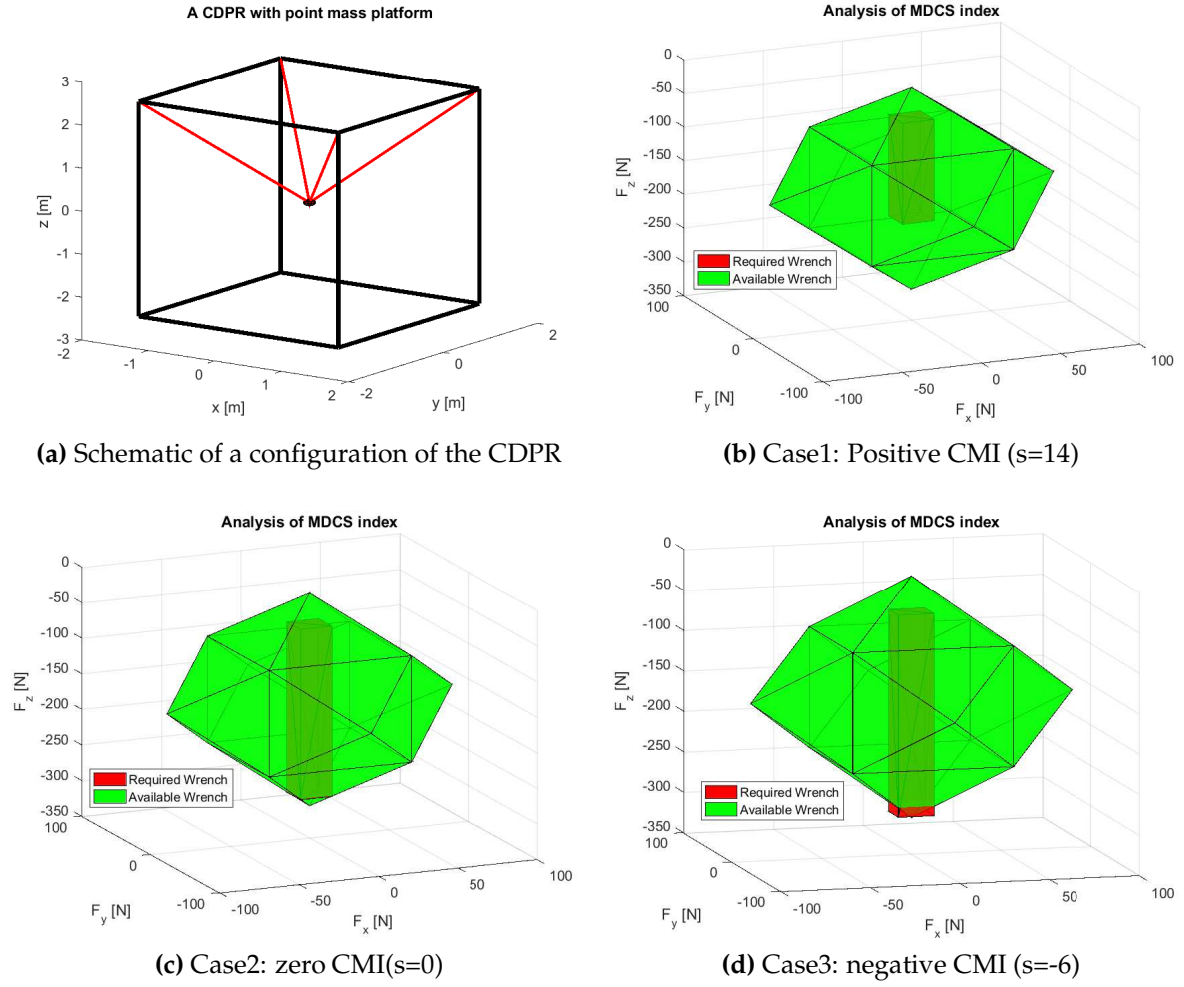
(a) Schematic of a configuration of the CDPR

(b) Case1: Positive CMI (s=14)

(c) Case2: zero CMI(s=0)

(d) Case3: negative CMI (s=-6)

Figure B.1: Analysis of CMI for a given configuration of a CDPR

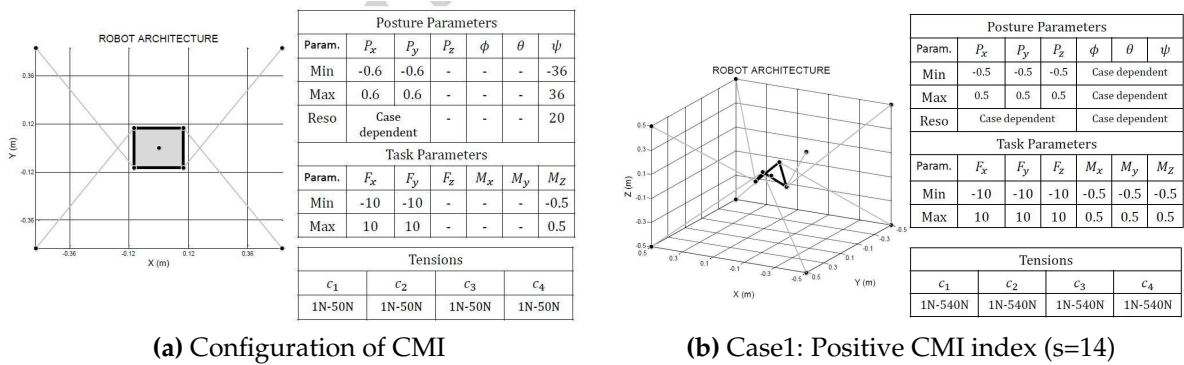**(a)** Configuration of CMI

(b) Case1: Positive CMI index (s=14)

Figure B.2: Analysis of CMI for a given configuration of CDPR, [Rui13]

(a) ARACHNIS: top-view [Rui13]

(b) ARACHNIS: isometric-view [Rui13]

(c) Developed algorithm: top-view

(d) Developed algorithm: isometric-view
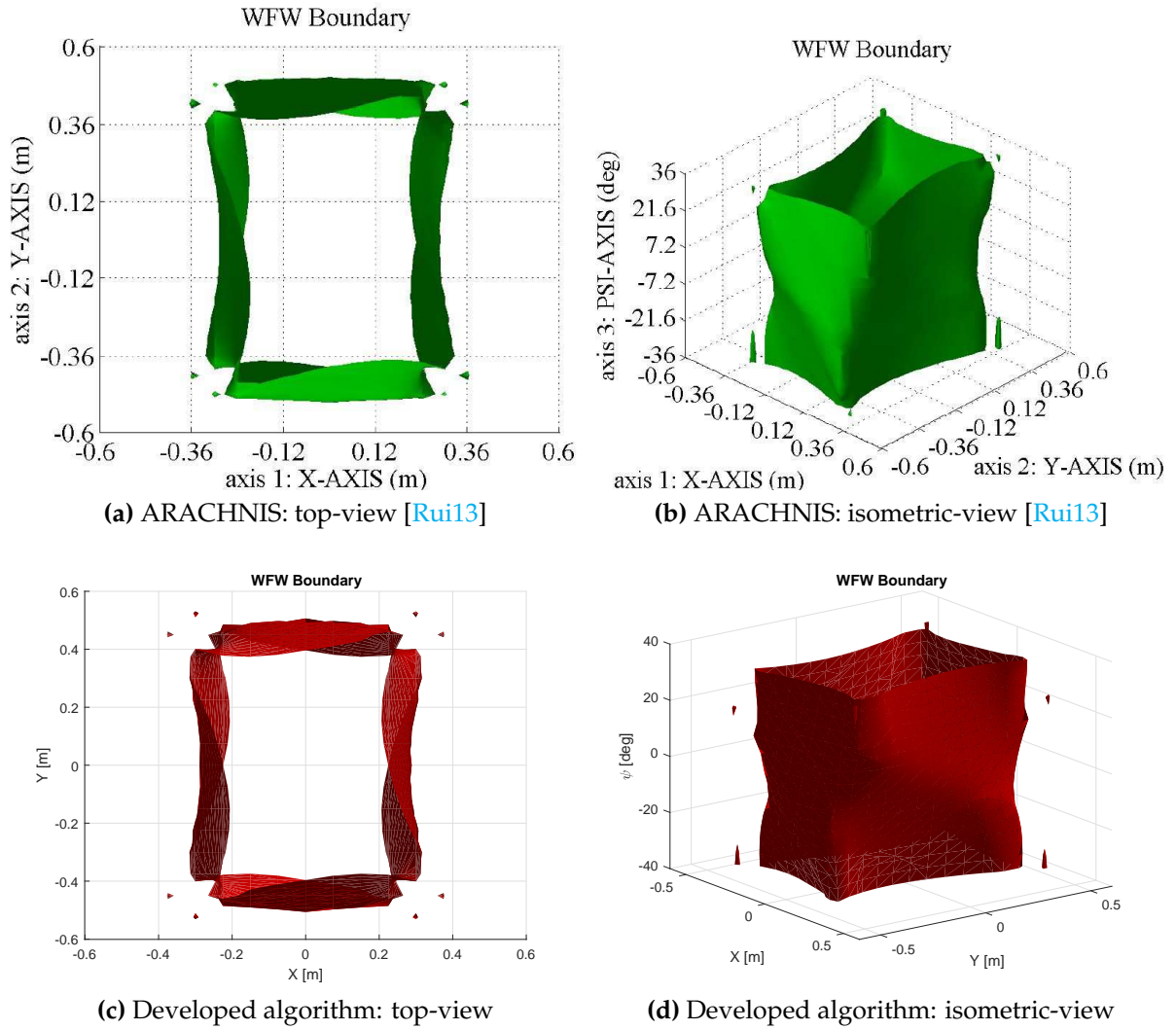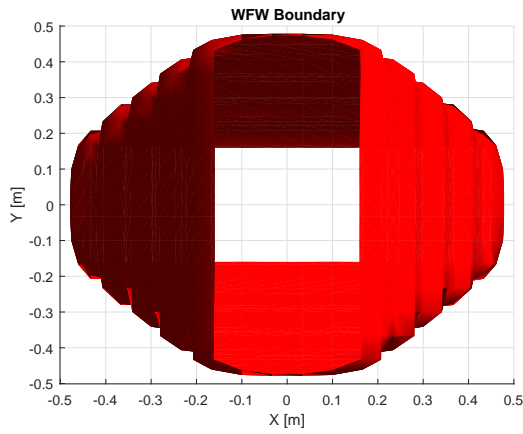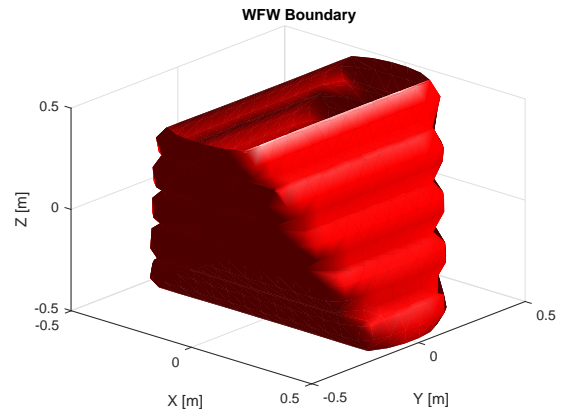
Figure B.3: WFW boundary of the first case study
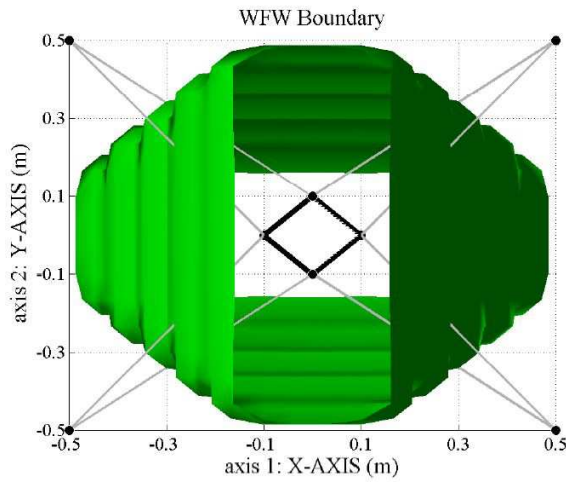
(a) ARACHNIS: top-view [Rui13]
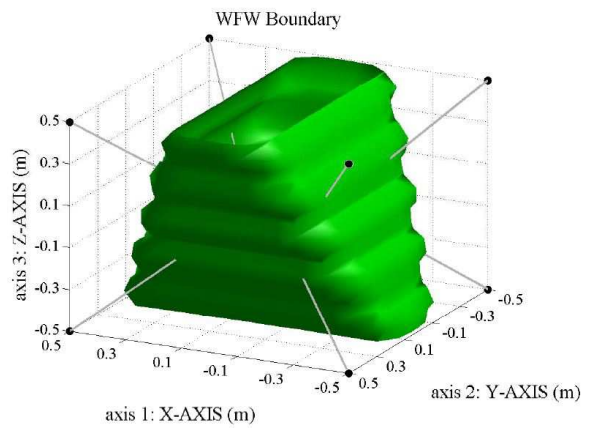
(b) ARACHNIS: isometric-view [Rui13]

(c) Developed algorithm: top-view

(d) Developed algorithm: isometric-view

Figure B.4: WFW boundary of the second case study

B.2 Twist Feasibility Analysis of Cable-Driven Parallel Robots

Although several papers addressed the wrench capabilities of CDPRs, few have tackled the dual question of their twist capabilities. In this chapter, these twist capabilities are evaluated by means of the more specific concept of twist feasibility, which was defined by Gagliardini et al. in a previous work. A CDPR posture is called twist-feasible if all the twists (point-velocity and angular-velocity combinations), within a given set, can be produced at the CDPR mobile platform, within given actuator speed limits. Two problems are solved in this paper: (1) determining the set of required cable winding speeds at the CDPR winches being given a prescribed set of required mobile platform twists; and (2) determining the set of available twists at the CDPR mobile platform from the available cable winding speeds at its winches. The solutions to both problems can be used to determine the twist feasibility of n-degree-of-freedom (DOF) CDPRs driven by $m \geq n$ cables. An example is presented, where the twist-feasible workspace of a simple CDPR with $n = 2$ DOF and driven by $m = 3$ cables is computed to illustrate the proposed method.

A CDPR consists of a base frame, a mobile platform, and a set of cables connecting in parallel the mobile platform to the base frame. The cable lengths or tensions can be adjusted by means of winches and a number of pulleys may be used to route the cables from the winches to the mobile platform. Among other advantages, CDPRs with very large workspaces, e.g. [Gou+15a; LNC07], heavy payloads capabilities [ABD93], or reconfiguration capabilities, e.g. [Gag+16a; RZA11] can be designed. Moreover, the moving parts of CDPRs being relatively light weight, fast motions of the mobile platform can be obtained, e.g. [KKW00a].

The cables of a CDPR can only pull and not push on the mobile platform and their tension shall not become larger than some maximum admissible value. Hence, for a given mobile platform pose, the determination of the feasible wrenches at the platform is a fundamental issue, which has been the subject of several previous works, e.g. [BGM10a; HK11]. A relevant issue is then to determine the set of wrench feasible poses, *i.e.*, the so-called Wrench-Feasible Workspace (WFW) [BREU06; REU04], since the shape and size of the latter highly depends on the cable tension bounds and on the CDPR geometry [Ver04]. Another issue which may strongly restrict the usable workspace of a CDPR or, divide it into several disjoint parts, are cable interferences. Therefore, software tools allowing the determination of the interference-free workspace and of the WFW have been proposed, e.g. [CR+15; Per+10],. Besides, recently, a study on acceleration capabilities was proposed in [Ede+16; GGC16].

As noted in [Gag+15] and as well known, in addition to wrench feasibility, the design of the winches of a CDPR also requires the consideration of cable and mobile platform velocities since the selection of the winch characteristics (motors, gearboxes, and drums) has to deal with a trade-off between torque and speed. Twist feasibility is then the study of the relationship between the feasible mobile platform twists (linear and angular velocities) and the admissible cable coiling/uncoiling speeds. In the following, the cable coiling/uncoiling speeds are loosely referred to as cable velocities. The main purpose of this paper is to clarify the analysis of twist
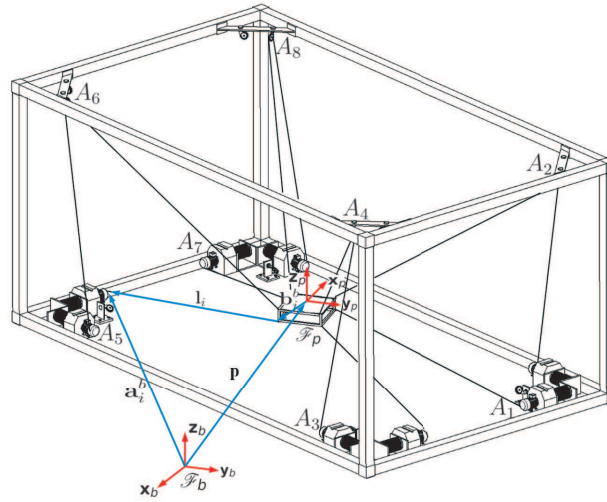
Figure B.5: Geometric description of a fully constrained CDPR

feasibility and of the related twist-feasible workspace proposed in [Gag+15]. Contrary to [Gag+15], the twist feasibility analysis proposed here is based on the usual CDPR differential kinematics where the Jacobian matrix maps the mobile platform twist into the cable velocities. This approach is most important for redundantly actuated CDPRs, whose Jacobian matrix is rectangular.

A number of concepts in this paper are known, notably from manipulability ellipsoids of serial robots, e.g. [Yos90], and from studies on the velocity performance of parallel robots, e.g. [KCP04]. A review of these works is however out of the scope of the present paper whose contribution boils down to a synthetic twist feasibility analysis of n-degrees-of-freedom (DOF) CDPRs driven by m cables, with $m \geq n$. The CDPR can be fully constrained or not, and the cable mass and elasticity are neglected.

The paper is organized as follows. The usual CDPR wrench and Jacobian matrices are defined in Section B.2.1. Section B.2.2 presents the twist feasibility analysis, which consists in solving two problems. The first one is the determination of the set of cable velocities corresponding to a given set of required mobile platform twists (Section B.2.2). The second problem is the opposite since it is defined as the calculation of the set of mobile platform twists corresponding to a given set of cable velocities (Section B.2.2). The twist and cable velocity sets considered in this paper are convex polytopes. In Section B.2.3, a 2-DOF point-mass CDPR driven by 3 cables is considered to illustrate the twist feasibility analysis. Section B.2.4 concludes the paper.

B.2.1   Wrench and Jacobian Matrices

In this section, the well-known wrench matrix and Jacobian matrix of n-DOF m-cable CDPRs are defined. The wrench matrix maps the cable tensions into the wrench applied by the cables on the CDPR mobile platform. The Jacobian matrix relates the time derivatives of the cable lengths to the twist of the mobile platform. These two matrices are essentially the same since one is minus the transpose of the other.

Some notations and definitions are first introduced. As illustrated in Fig. B.5, let us consider a fixed reference frame, $\mathscr{F}_b$, of origin O_b and axes $\mathbf{x}_b$, $\mathbf{y}_b$ and $\mathbf{z}_b$. The coordinate vectors ${}^b\mathbf{a}_i, i = 1, \ldots, m$ define the positions of the exit points, $A_i, i = 1, \ldots, m$, with respect to frame $\mathscr{F}_b$. A_i is the point where the cable exits the base frame and extends toward the mobile platform. In this paper, the exit points A_i are assumed to be fixed, i.e., the motion of the output pulleys is neglected. A frame $\mathscr{F}_p$, of origin O_p and axes $\mathbf{x}_p$, $\mathbf{y}_p$ and $\mathbf{z}_p$, is attached to the mobile platform. The vectors ${}^p\mathbf{b}_i, i = 1, \ldots, m$ are the position vectors of the points B_i in $\mathscr{F}_p$. The cables are attached to the mobile platform at points B_i.

The vector ${}^b\mathbf{l}_i$ from B_i to A_i is given by

$$ {}^b\mathbf{l}_i = {}^b\mathbf{a}_i - \mathbf{p} - \mathbf{R}\,{}^p\mathbf{b}_i, \ i = 1, \ldots, m \tag{B.1} $$

where $\mathbf{R}$ is the rotation matrix defining the orientation of the mobile platform, i.e., the orientation of $\mathscr{F}_p$ in $\mathscr{F}_b$, and $\mathbf{p}$ is the position vector of $\mathscr{F}_p$ in $\mathscr{F}_b$. The length of the straight line segment $A_i B_i$ is $l_i = ||{}^b\mathbf{l}_i||_2$ where $||\cdot||_2$ is the Euclidean norm. Neglecting the cable mass, l_i corresponds to the length of the cable segment from point A_i to point B_i. Moreover, neglecting the cable elasticity, l_i is the "active" length of the cable that should be unwound from the winch drum. The unit vectors along the cable segment $A_i B_i$ is given by

$$ {}^b\mathbf{d}_i = {}^b\mathbf{l}_i / l_i , \ i = 1, \ldots, m \tag{B.2} $$

Since the cable mass is neglected in this paper, the force applied by the cable on the platform is equal to $\tau_i\,{}^b\mathbf{d}_i$, τ_i being the cable tension. The static equilibrium of the CDPR platform can then be written [Hil+05; RG98]

$$ \mathbf{W}\boldsymbol{\tau} + \mathbf{w}_e = 0 \tag{B.3} $$

where $\mathbf{w}_e$ is the external wrench acting on the platform, $\boldsymbol{\tau} = [\tau_1, \ldots, \tau_m]^T$ is the vector of cable tensions, and $\mathbf{W}$ is the wrench matrix. The latter is an $n \times m$ matrix defined as

$$ \mathbf{W} = \begin{bmatrix} {}^b\mathbf{d}_1 & {}^b\mathbf{d}_2 & \ldots & {}^b\mathbf{d}_m \\ \mathbf{R}^p\mathbf{b}_1 \times {}^b\mathbf{d}_1 & \mathbf{R}^p\mathbf{b}_2 \times {}^b\mathbf{d}_2 & \ldots & \mathbf{R}^p\mathbf{b}_m \times {}^b\mathbf{d}_m \end{bmatrix} \tag{B.4} $$

The differential kinematics of the CDPR establishes the relationship between the twist $\mathbf{t}$ of the mobile platform and the time derivatives of the cable lengths $\dot{\mathbf{l}}$

$$ \mathbf{J}\mathbf{t} = \dot{\mathbf{l}} \tag{B.5} $$

where $\mathbf{J}$ is the $m \times n$ Jacobian matrix and $\dot{\mathbf{l}} = [\dot{l}_1, \ldots, \dot{l}_m]^T$. The twist $\mathbf{t} = [\dot{\mathbf{p}}, \boldsymbol{\omega}]^T$ is composed of the velocity $\dot{\mathbf{p}}$ of the origin of frame $\mathscr{F}_p$ with respect to $\mathscr{F}_b$ and of the angular velocity $\boldsymbol{\omega}$ of the mobile platform with respect to $\mathscr{F}_b$. Moreover, the well-known kineto-statics duality leads to

$$ \mathbf{J} = -\mathbf{W}^T \tag{B.6} $$

In the remainder of this paper, $\dot{\mathbf{l}}$ is loosely referred to as cable velocities. The wrench and Jacobian matrices depend on the geometric parameters $\mathbf{a}_i$ and $\mathbf{b}_i$ of the CDPR and on the mobile platform pose, namely on $\mathbf{R}$ and $\mathbf{p}$.

B.2.2 Twist Feasibility Analysis

This section contains the contribution of the paper, namely, a twist feasibility analysis which consists in solving the following two problems.

1. For a given pose of the mobile platform of a CDPR and being given a set $[\mathbf{t}]_r$ of required mobile platform twists, determine the corresponding set of cable velocities $\dot{\mathbf{l}}$. The set of cable velocities to be determined is called the *Required Cable Velocity Set* (RCVS) and is denoted $[\dot{\mathbf{l}}]_r$. The set $[\mathbf{t}]_r$ is called the *Required Twist Set* (RTS).

2. For a given pose of the mobile platform of a CDPR and being given a set $[\dot{\mathbf{l}}]_a$ of available (admissible) cable velocities, determine the corresponding set of mobile platform twists $\mathbf{t}$. The former set, $[\dot{\mathbf{l}}]_a$, is called the *Available Cable Velocity Set* (ACVS) while the latter is denoted $[\mathbf{t}]_a$ and called the *Available Twist Set* (ATS).

In this paper, the discussion is limited to the cases where both the RTS $[\mathbf{t}]_r$ and the ACVS $[\dot{\mathbf{l}}]_a$ are *convex polytopes*.

Solving the first problem provides the RCVS from which the maximum values of the cable velocities required to produce the given RTS $[\mathbf{t}]_r$ can be directly deduced. If the winch characteristics are to be determined, the RCVS allows to determine the required speeds of the CDPR winches. If the winch characteristics are already known, the RCVS allows to test whether or not the given RTS is feasible.

Solving the second problem provides the ATS which is the set of twists that can be produced at the mobile platform. It is thus useful either to determine the velocity capabilities of a CDPR or to check whether or not a given RTS is feasible.

Note that the feasibility of a given RTS can be tested either in the cable velocity space, by solving the first problem, or in the space of platform twists, by solving the second problem. Besides, note also that the twist feasibility analysis described above does not account for the dynamics of the CDPR.

Problem 1: Required Cable Velocity Set (RCVS)

The relationship between the mobile platform twist $\mathbf{t}$ and the cable velocities $\dot{\mathbf{l}}$ is the differential kinematics in (2.42). According to this equation, the RCVS $[\dot{\mathbf{l}}]_r$ is defined as the image of the convex polytope $[\mathbf{t}]_r$ under the linear map $\mathbf{J}$. Consequently, $[\dot{\mathbf{l}}]_r$ is also a convex polytope [Zie94].

Moreover, if $[\mathbf{t}]_r$ is a box, the RCVS $[\dot{\mathbf{l}}]_r$ is a particular type of polytope called a zonotope. Such a transformation of a box into a zonotope has previously been studied in CDPR wrench feasibility analysis [BGM10a; GRR01; GK10]. Indeed, a box of admissible cable tensions is mapped by the wrench matrix $\mathbf{W}$ into a zonotope in the space of platform wrenches. However, a difference lies in the dimensions of the matrices $\mathbf{J}$ and $\mathbf{W}$, $\mathbf{J}$ being of dimensions $m \times n$ while $\mathbf{W}$ is an $n \times m$ matrix, where $n \leq m$. When $n < m$, on the one hand, $\mathbf{W}$ maps the m-dimensional box of

admissible cable tensions into the n-dimensional space of platform wrenches. On the other hand, $\mathbf{J}$ maps n-dimensional twists into its range space which is a linear subspace of the m-dimensional space of cable velocities $\dot{\mathbf{l}}$. Hence, when $\mathbf{J}$ is not singular, the n-dimensional box $[\mathbf{t}]_r$ is mapped into the zonotope $[\dot{\mathbf{l}}]_r$ which lies into the n-dimensional range space of $\mathbf{J}$, as illustrated in Fig. B.7 . When $\mathbf{J}$ is singular and has rank r, $r < n$, the n-dimensional box $[\mathbf{t}]_r$ is mapped into a zonotope of dimension r.

When an ACVS $[\dot{\mathbf{l}}]_a$ is given, a pose of the mobile platform of a CDPR is twist feasible if

$$[\dot{\mathbf{l}}]_r \subseteq [\dot{\mathbf{l}}]_a \tag{B.7}$$

Since $[\dot{\mathbf{l}}]_a$ is a convex polytope, (2.43) is verified whenever all the vertices of $[\dot{\mathbf{l}}]_r$ are included in $[\dot{\mathbf{l}}]_a$. Moreover, it is not difficult to prove that $[\dot{\mathbf{l}}]_r$ is the convex hull of the images under $\mathbf{J}$ of the vertices of $[\mathbf{t}]_r$. Hence, a simple method to verify if a CDPR pose is twist feasible consists in verifying whether the images of the vertices of $[\mathbf{t}]_r$ are all included into $[\dot{\mathbf{l}}]_a$.

Problem 2: Available Twist Set (ATS)

The problem is to determine the ATS $[\mathbf{t}]_a$ corresponding to a given ACVS $[\dot{\mathbf{l}}]_a$.

In the most general case considered in this paper, $[\dot{\mathbf{l}}]_a$ is a convex polytope. By the Minkowski-Weyl's Theorem, a polytope can be represented as the solution set of a finite set of linear inequalities, the so-called (halfspace) *H-representation* of the polytope [Fuk; Zie94], i.e.

$$[\dot{\mathbf{l}}]_a = \{ \dot{\mathbf{l}} \mid \mathbf{C}\dot{\mathbf{l}} \leq \mathbf{d} \} \tag{B.8}$$

where matrix $\mathbf{C}$ and vector $\mathbf{d}$ are assumed to be known.

According to (2.42), the ATS is defined as

$$[\mathbf{t}]_a = \{ \mathbf{t} \mid \mathbf{J}\mathbf{t} \in [\dot{\mathbf{l}}]_a \} \tag{B.9}$$

which, using (2.44), implies that

$$[\mathbf{t}]_a = \{ \mathbf{t} \mid \mathbf{C}\mathbf{J}\mathbf{t} \leq \mathbf{d} \} \tag{B.10}$$

The latter equation provides an H-representation of the ATS $[\mathbf{t}]_a$.

In practice, when the characteristics of the winches of a CDPR are known, the motor maximum speeds limit the set of possible cable velocities as follows

$$\dot{l}_{i,min} \leq \dot{l}_i \leq \dot{l}_{i,max} \tag{B.11}$$

where $\dot{l}_{i,min}$ and $\dot{l}_{i,max}$ are the minimum and maximum cable velocities. Note that, usually, $\dot{l}_{i,min} = -\dot{l}_{i,max}$, $\dot{l}_{1,min} = \dot{l}_{2,min} = \ldots = \dot{l}_{m,min}$, and $\dot{l}_{1,max} = \dot{l}_{2,max} = \ldots = \dot{l}_{m,max}$. In other words, $\mathbf{C}$ and $\mathbf{d}$ in (2.44) are defined as

$$\mathbf{C} = \begin{bmatrix} \mathbf{1} \\ -\mathbf{1} \end{bmatrix} \quad \text{and} \quad \mathbf{d} = \begin{bmatrix} \dot{l}_{1,max}, & \ldots, & \dot{l}_{m,max}, & -\dot{l}_{1,min}, & \ldots, & -\dot{l}_{m,min} \end{bmatrix}^T \tag{B.12}$$

where $\mathbf{1}$ is the $m \times m$ identity matrix. Eq. (2.46) can then be written as follows

$$[\mathbf{t}]_a = \{\ \mathbf{t} \mid \dot{\mathbf{l}}_{min} \leq \mathbf{J}\mathbf{t} \leq \dot{\mathbf{l}}_{max}\ \} \tag{B.13}$$

where $\dot{\mathbf{l}}_{min} = \begin{bmatrix} \dot{l}_{1,min}, \ \ldots, \ \dot{l}_{m,min} \end{bmatrix}^T$ and $\dot{\mathbf{l}}_{max} = \begin{bmatrix} \dot{l}_{1,max}, \ \ldots, \ \dot{l}_{m,max} \end{bmatrix}^T$.

When a RTS $[\mathbf{t}]_r$ is given, a pose of the mobile platform of a CDPR is twist feasible if

$$[\mathbf{t}]_r \subseteq [\mathbf{t}]_a \tag{B.14}$$

In this paper, $[\mathbf{t}]_r$ is assumed to be a convex polytope. Hence, (2.50) is verified whenever all the vertices of $[\mathbf{t}]_r$ are included in $[\mathbf{t}]_a$. With the H-representation of $[\mathbf{t}]_a$ in (2.46) (or in (2.49)), testing if a pose is twist feasible amounts to verifying if all the vertices of $[\mathbf{t}]_r$ satisfy the inequality system in (2.46) (or in (2.49)). Testing twist feasibility thereby becomes a simple task as soon as the vertices of $[\mathbf{t}]_r$ are known.

Finally, let the twist feasible workspace (TFW) of a CDPR be the set of twist feasible poses of its mobile platform. It is worth noting that the boundaries of the TFW are directly available in closed form from (2.46) or (2.49). If the vertices of the (convex) RTS are denoted $\mathbf{t}_j$, $j = 1, \ldots, k$, and the rows of the Jacobian matrix are $-\mathbf{w}_i^T$, according to (2.49), the TFW is defined by $\dot{l}_{i,min} \leq -\mathbf{w}_i^T \mathbf{t}_j$ and $-\mathbf{w}_i^T \mathbf{t}_j \leq \dot{l}_{i,max}$, for all possible combinations of i and j. Since $\mathbf{w}_i$ contains the only variables in these inequalities that depend on the mobile platform pose, and because the closed-form expression of $\mathbf{w}_i$ as a function of the pose is known, the expressions of the boundaries of the TFW are directly obtained.

B.2.3 Case Study

Figure B.6: A two-DOF point-mass planar cable-driven parallel robot driven by three cables

This section deals with the twist feasibility analysis of the two-DOF point-mass planar CDPR driven by three cables shown in Fig.B.6. The robot is 3.5 m long and 2.5 m high. The three exit points of the robot are named A_1, A_2 are A_3, respectively.

The point-mass is denoted P. ${}^b\mathbf{d}_1$, ${}^b\mathbf{d}_2$ and ${}^b\mathbf{d}_3$ are the unit vectors, expressed in frame $\mathscr{F}_b$, of the vectors pointing from point-mass P to cable exit points A_1, A_2 are A_3, respectively. The 3×2 Jacobian matrix $\mathbf{J}$ of this planar CDPR takes the form:

$$\mathbf{J} = - \begin{bmatrix} {}^b\mathbf{d}_1^T \\ {}^b\mathbf{d}_2^T \\ {}^b\mathbf{d}_3^T \end{bmatrix} \tag{B.15}$$

Figure B.7 is obtained by solving the Problem 1 formulated in Sec. B.2.2. For the robot configuration depicted in Fig. B.7a and the given RTS of the point-mass P represented in Fig. B.7b, the RCVS for the three cables of the planar CDPR are illustrated in Figs. B.7c to B.7f. Note that the RTS is defined as:

$$-1 \text{ m.s}^{-1} \le \ \dot{x}_P \ \le 1 \text{ m.s}^{-1} \tag{B.16}$$
$$-1 \text{ m.s}^{-1} \le \ \dot{y}_P \ \le 1 \text{ m.s}^{-1} \tag{B.17}$$

where $[\dot{x}_P, \dot{y}_P]^T$ is the velocity of P in the fixed reference frame $\mathscr{F}_b$.

Figure B.8 demonstrates the available twist set and the required twist set for a given position of the end-effector in the case study. Figure B.9 depicts the isocontours of the Maximum Required Cable Velocity (MRCV) for each cable through the Cartesian space and for the RTS shown in Fig. B.7b. Those results are obtained by solving Problem 1 for all positions of point P. It is apparent that P RTS is satisfied through the Cartesian space as long as the maximum velocity of each cable is higher than $\sqrt{2}$ m.s^{-1}, namely, $\dot{l}_{1,max} = \dot{l}_{2,max} = \dot{l}_{3,max} = \sqrt{2}$ m.s^{-1} with $\dot{l}_{i,min} = -\dot{l}_{i,max}$, $i = 1, 2, 3$.

For the Available Cable Velocity Set (ACVS) defined by inequalities (B.11) with

$$\dot{l}_{i,max} = 1.3 \text{ m.s}^{-1}, \ i = 1, 2, 3 \tag{B.18}$$

Fig. B.10 is obtained by solving the Problem 2 formulated in Sec. B.2.2.

For the two robot configurations illustrated in Fig. B.10a and B.10c, the Available Twist Set (ATS) associated to the foregoing ACVS is determined from Eq. (B.13). It is noteworthy that the ATS in each configuration in delimited by three pairs of lines normal to three cables, respectively. It turns out that the first robot configuration is twist feasible for the RTS defined by Eqs. (B.16) and (B.17) because the latter is included into the ATS as shown Fig. B.10b. Conversely, the second robot configuration is not twist feasible as the RTS is partially outside the ATS as shown Fig. B.10d.

Finally, Fig. B.13 shows the TFW of the planar CDPR for four maximum cable velocity limits and for the RTS shown in Fig. B.7b. It is apparent the all robot poses are twist feasible as soon as the cable velocity limits of the three cables are higher than $\sqrt{2}$ m.s^{-1}.

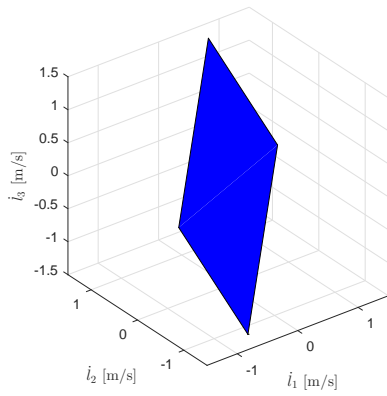## Computation of TFW by Cable Velocity Boundary

Previously, the TFW is obtained by checking the twist feasibility condition expressed in Eq. (B.7) through CMI for the discretized task space. We can also track the TFW
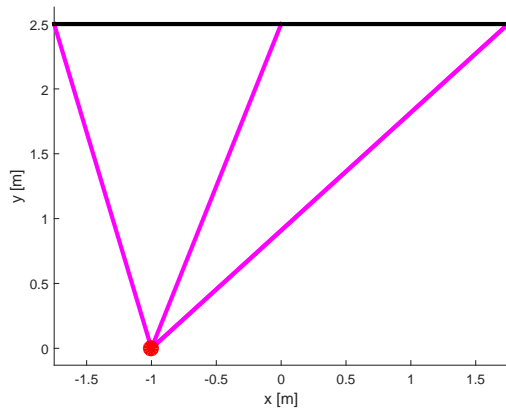
(a) Robot configuration
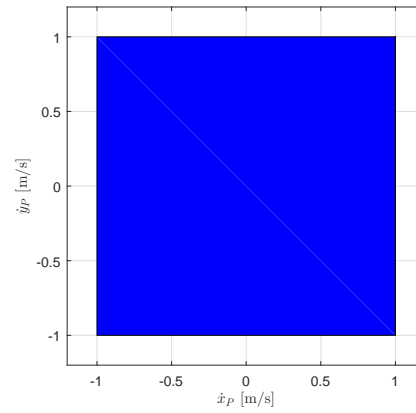
(b) RTS

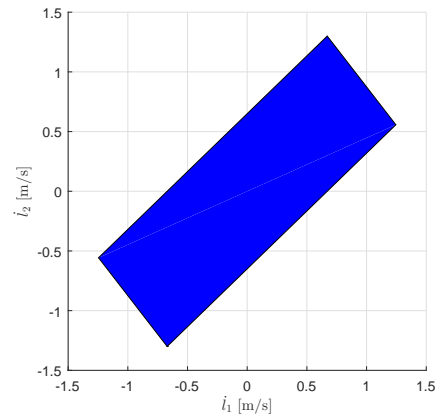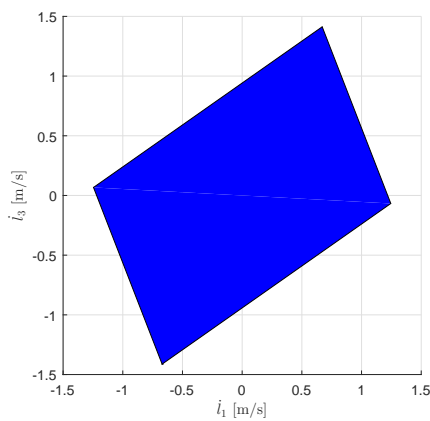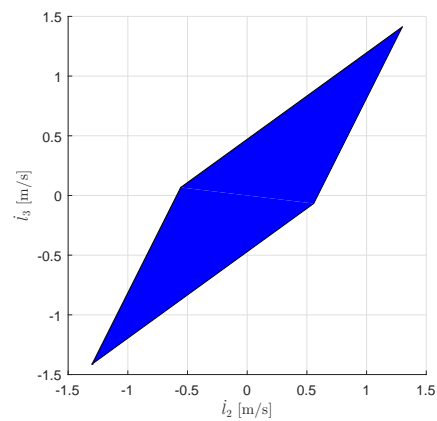**(c)** Image of the RTS into the three-dimensional cable velocity space

(d) Image of the RTS into the $(\dot{l}_1, \dot{l}_2)$-space

(e) Image of the RTS into the $(\dot{l}_1, \dot{l}_3)$-space

(f) Image of the RTS into the $(\dot{l}_2, \dot{l}_3)$-space

Figure B.7: Required Twist Set (RTS) of the point-mass P and corresponding Required Cable Velocity Sets for the three cables of the CDPR in a given robot configuration
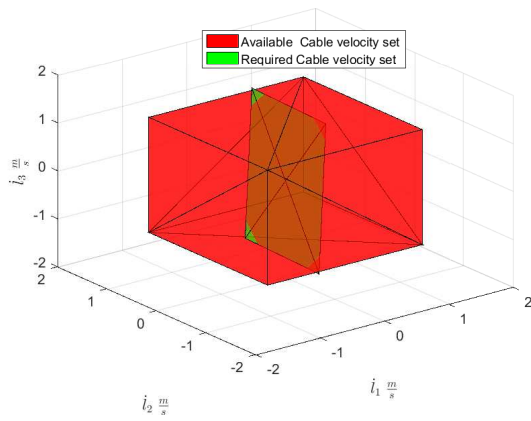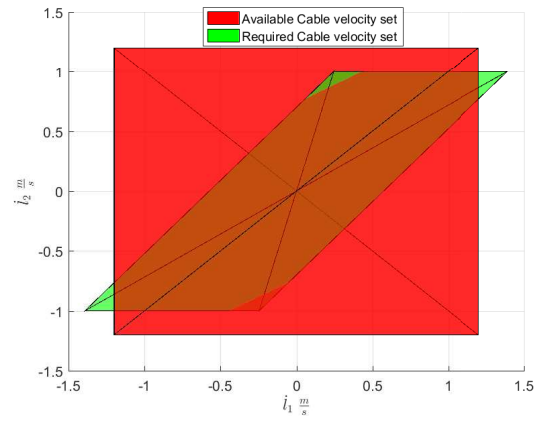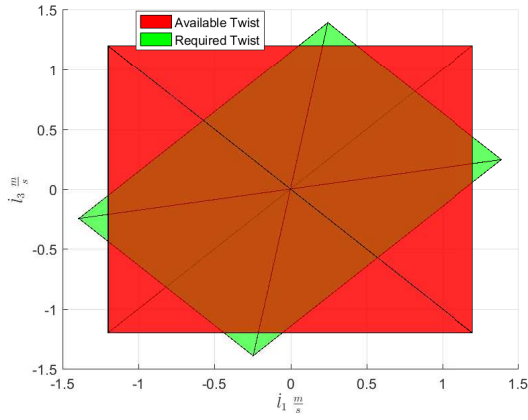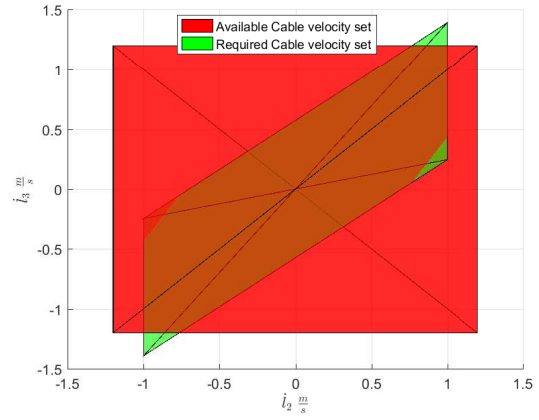
(a) $\mathscr{L}$ and $\mathscr{V}$

(b) Image of $\mathscr{L}$ and $\mathscr{V}$ into $(\dot{l}_1, \dot{l}_2)$-space

(c) Image of $\mathscr{L}$ and $\mathscr{V}$ into $(\dot{l}_1, \dot{l}_3)$-space

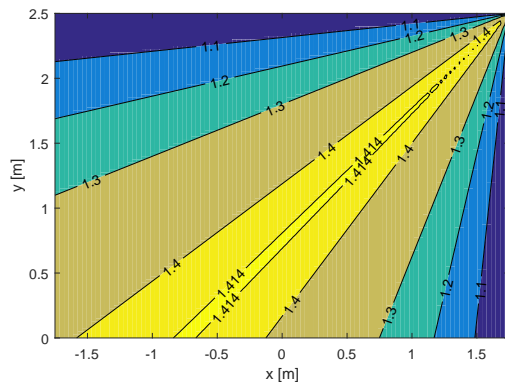**(d)** Image of $\mathscr{L}$ and $\mathscr{V}$ into $(\dot{l}_2, \dot{l}_3)$-space

Figure B.8: Required cable velocity polytope, $\mathscr{L}$ and available cable velocity polytope, $\mathscr{V}$ for the given pose of the case study, shown in Fig. B.6
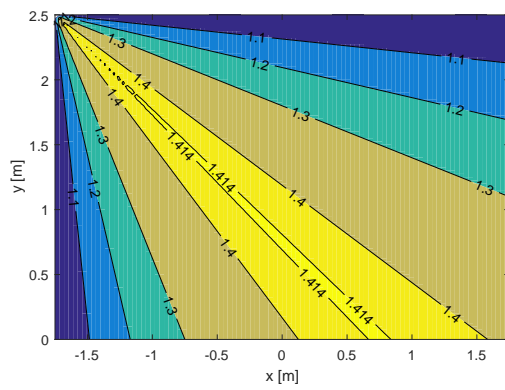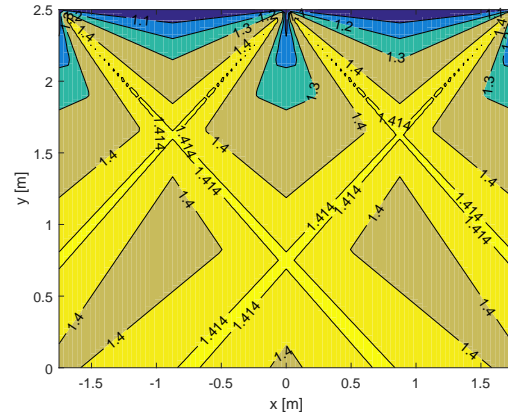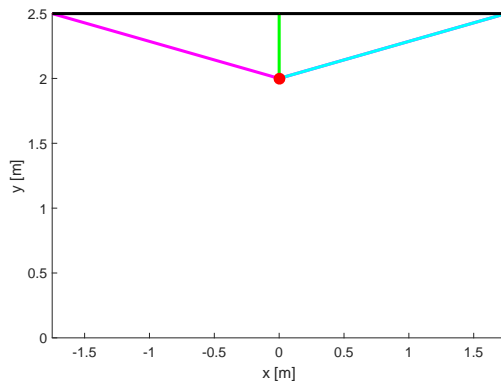
(a) Cable 1 MRCV
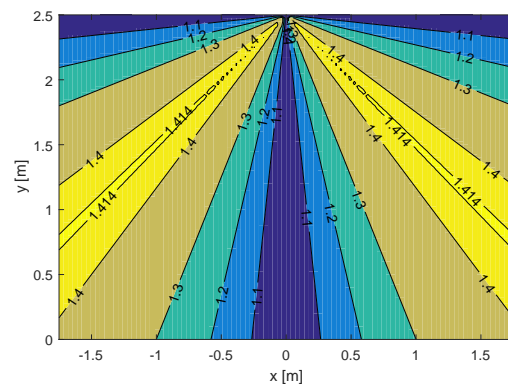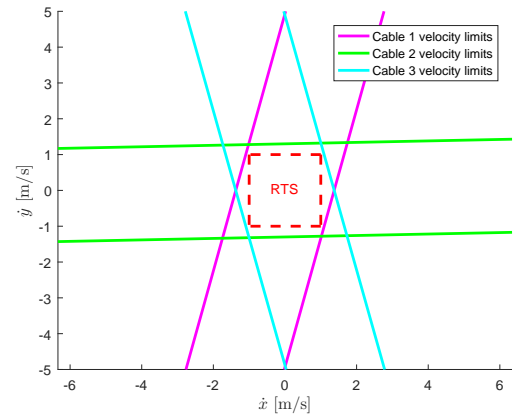
(b) Cable 2 MRCV

(c) Cable 3 MRCV

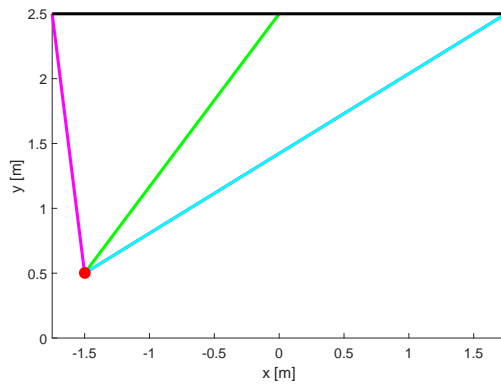**(d)** Cables 1, 2 and 3 MRCV

Figure B.9: Maximum Required Cable Velocity (MRCV) of each cable through the Cartesian space for the RTS shown in Fig. B.7b
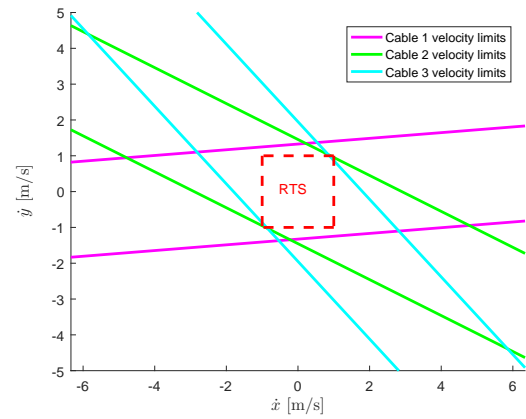
(a) A feasible twist pose

(b) The RTS is included into the ATS

(c) An infeasible twist pose

(d) The RTS is partially outside the ATS

Figure B.10: A feasible twist pose and an infeasible twist pose of the CDPR

(a) $\dot{l}_{i,max} = 1.12 \text{ m.s}^{-1}$

(b) $\dot{l}_{i,max} = 1.32 \text{ m.s}^{-1}$

(c) $\dot{l}_{i,max} = 1.4 \text{ m.s}^{-1}$

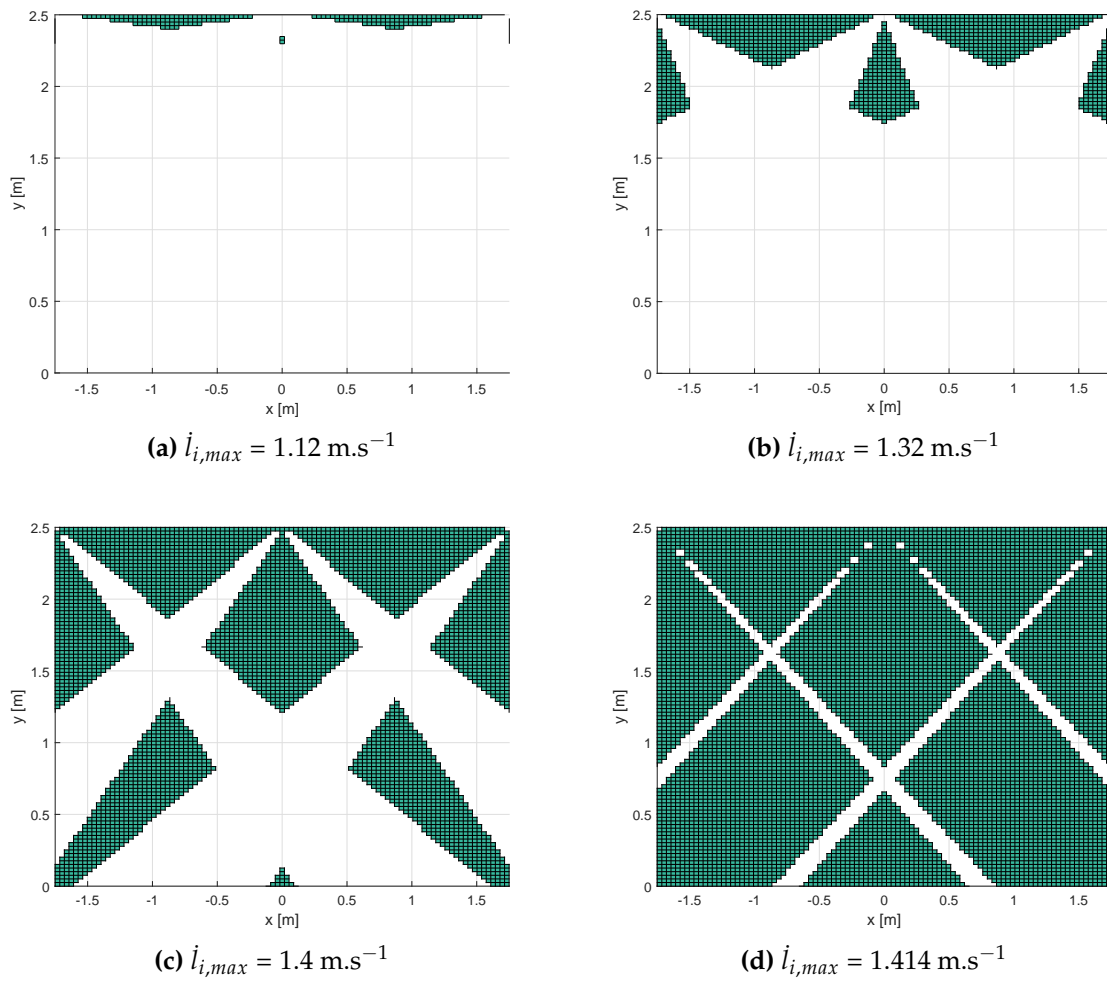**(d)** $\dot{l}_{i,max} = 1.414 \text{ m.s}^{-1}$

Figure B.11: TFW of the planar CDPR for four maximum cable velocity limits and for the RTS shown in Fig. B.7b

of CDPRs by formulating the boundaries of the cable velocities. This analytical approach is a fast solution to find constant-orientation TFW without discretization of the task space.

We start with rewriting Eq. (B.5) for a CDPR with m cables and only linear velocities of the moving-platform as follows:

$$
\begin{bmatrix} \dot{\mathbf{u}}_1 \\ \vdots \\ \dot{\mathbf{u}}_m \end{bmatrix} \begin{bmatrix} \dot{x} \\ \dot{y} \\ \dot{z} \end{bmatrix} = \begin{bmatrix} \dot{l}_1 \\ \vdots \\ \dot{l}_m \end{bmatrix}
\tag{B.19}
$$

The following equation associates the moving-platform twist and cable velocities and holds for twist feasible workspace. From Eqs. (B.11) and (B.19) we can write the following equation:

$$
\begin{cases}
\dot{l}_{1,min} \leq \dfrac{(x_{A1} - x_{B1})\dot{x} + (y_{A1} - y_{B1})\dot{y} + (z_{A1} - z_{B1})\dot{z}}{\sqrt{(x_{A1} - x_{B1})^2 + (y_{A1} - y_{B1})^2 + (z_{A1} - z_{B1})^2}} \leq \dot{l}_{1,max} \\
\qquad\qquad\qquad\qquad \vdots \\
\dot{l}_{m,min} \leq \dfrac{(x_{Am} - x_{Bm})\dot{x} + (y_{Am} - y_{Bm})\dot{y} + (z_{Am} - z_{Bm})\dot{z}}{\sqrt{(x_{Am} - x_{Bm})^2 + (y_{Am} - y_{Bm})^2 + (z_{Am} - z_{Bm})^2}} \leq \dot{l}_{m,max}
\end{cases}
\tag{B.20}
$$

By replacing $[x_i,\ y_i,\ z_i]^T$ with $[x_{B,i},\ y_{B,i},\ z_{B,i}]^T$ in Eq. (B.20), we can trace the position of the moving-platform which satisfies the twist feasibility for the ith cable. We can assume that, $\dot{l}_{i,min} = -\dot{l}_{i,max}$ for $i = 1, ..., m$, and rewrite Eq. (B.20) for the maximum admissible cable velocity as follows.

$$
\begin{cases}
[(x_{A1} - x_1)\dot{x} + (y_{A1} - y_1)\dot{y} + (z_{A1} - z_1)\dot{z}]^2 - \dot{l}_{1,max}^2 \left[(x_{A1} - x_1)^2 + (y_{A1} - y_1)^2 + (z_{A1} - z_1)^2\right] \leq 0 \\
\qquad\qquad\qquad\qquad\qquad\qquad \vdots \\
[(x_{Am} - x_m)\dot{x} + (y_{Am} - y_m)\dot{y} + (z_{Am} - z_m)\dot{z}] - \dot{l}_{m,max}^2 \left[(x_{Am} - x_m)^2 + (y_{Am} - y_m)^2 + (z_{Am} - z_m)^2\right] \leq 0
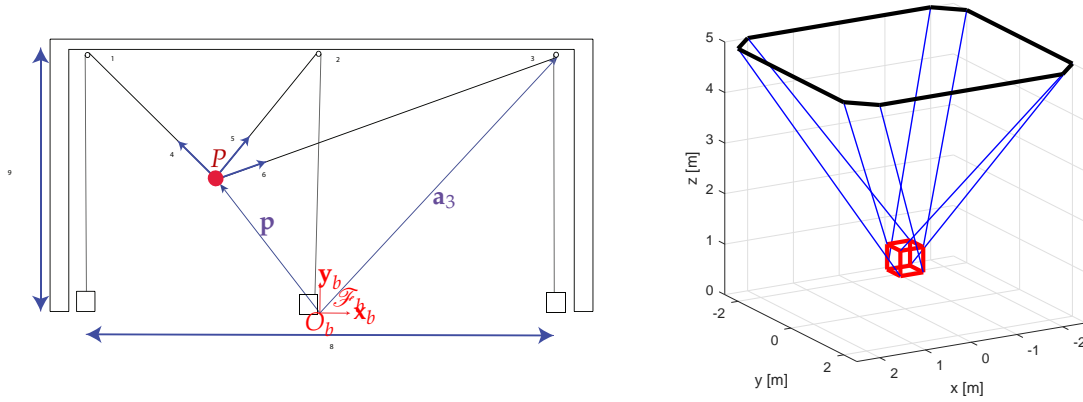\end{cases}
\tag{B.21}
$$

For a given required twist, $\mathbf{t}_w$ and the maximum admissible cable velocity, $\dot{l}_i$, $i = 1, ..., m$, Eq. (B.21) yields the quadratic surface areas which forms TFW area in Cartesian space.

Comparison Between Two Approaches

In order to prove the outcomes of this implementation are reliable, we compare the TFW obtained by two approaches. The comparison is done for planar and spacial CDPRs shown in Fig. B.12.

Case Study 1

Figure B.12a illustrates the architecture and configuration of a CDPR. The comparison between TFWs obtained by two approaches detailed in previous section. In this

(a) Case Study 1- A planar CDPR with a point-mass suspended by three cables

(b) Case Study 2- A spatial CDPR with a suspended MP suspended by eight cables

Figure B.12: Planar and spacial CDPRs for analysis of TFW

case study, TFW is computed for the following required twist, namely, $[\mathbf{t}_w]_r$.

$$
\begin{aligned}
-1 \; m.s^{-1} &\le \dot{x} \le 1 \; m.s^{-1} \\
-1 \; m.s^{-1} &\le \dot{y} \le 1 \; m.s^{-1}
\end{aligned}
\tag{B.22}
$$

Case Study 2

A spacial CDPR is studied as the second case study. The architecture and configuration of the robot is detailed in Fig. B.12b. In the second case study, TFW is computed for the following required twist, namely, $[\mathbf{t}_w]_r$.

$$
\begin{aligned}
-1 \; m.s^{-1} &\le \dot{x} \le 1 \; m.s^{-1} \\
-1 \; m.s^{-1} &\le \dot{y} \le 1 \; m.s^{-1} \\
-1 \; m.s^{-1} &\le \dot{z} \le 1 \; m.s^{-1}
\end{aligned}
\tag{B.23}
$$

The TFWs plotted by two approaches in Figs. B.13-B.14 are identical for the case study 1 presented in Fig. B.12a. Similarly, identical TFWs are obtained by two approaches as presented in Fig. B.15 for the second case study shown in Fig. B.12b.

B.2.4   Conclusion

In summary, this chapter presents two methods for determining the twist-feasibility of a CDPR. The first method uses a set of required mobile platform twists to compute the corresponding required cable velocities, the latter corresponds to cable winding speeds at the winches. The second method takes the opposite route, i.e., it uses the available cable velocities to compute the corresponding set of available
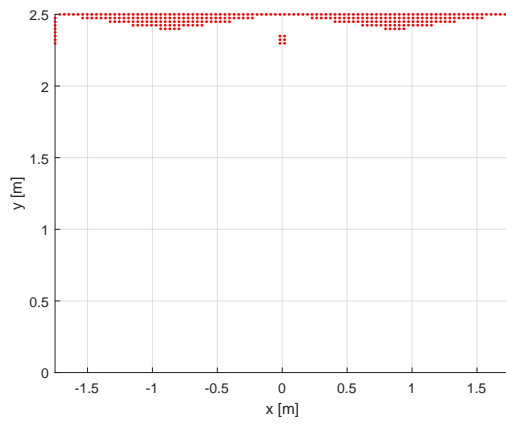
(a) $\dot{l}_{i,max} = 1.12 \ m.s^{-1}$
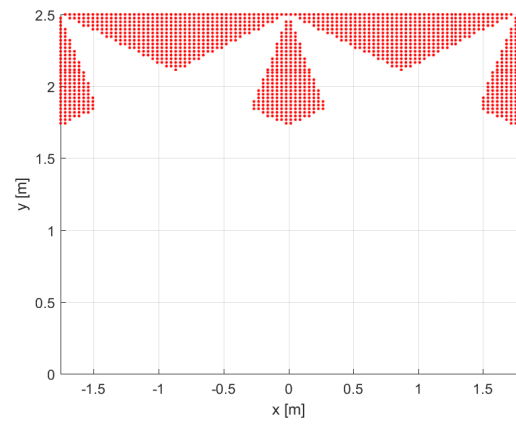
(b) $\dot{l}_{i,max} = 1.32 \ m.s^{-1}$
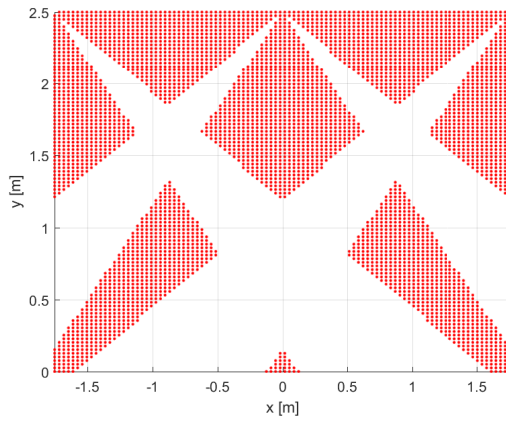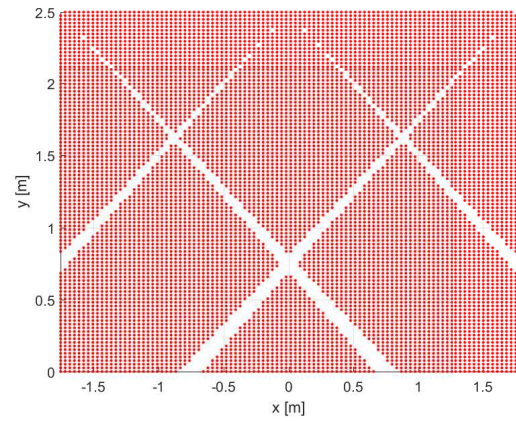
(c) $\dot{l}_{i,max} = 1.4 \ m.s^{-1}$

(d) $\dot{l}_{i,max} = 1.414 \ m.s^{-1}$

Figure B.13: TFW of case study 1 calculated by CMI approach for different $\dot{l}_{i,max}$
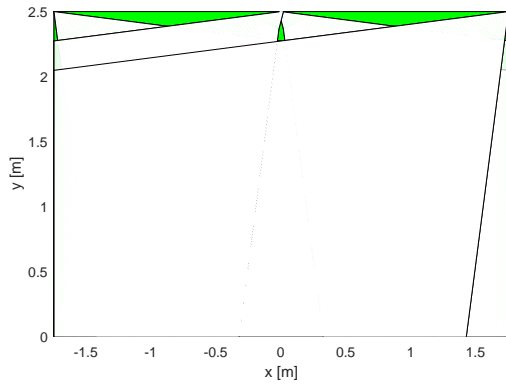
(a) TFW for $\dot{l}_{i,max} = 1.12 \; m.s^{-1}$
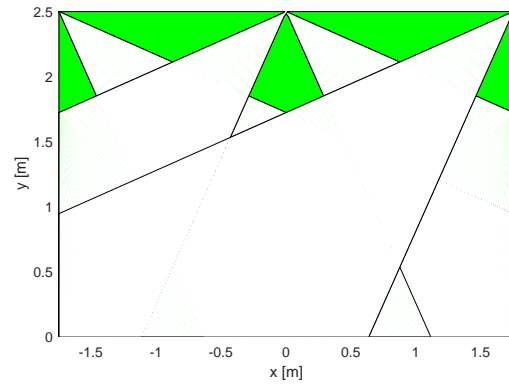
(b) TFW for $\dot{l}_{i,max} = 1.32 \; m.s^{-1}$
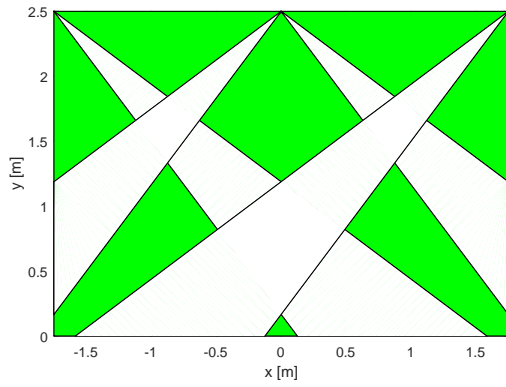
(c) TFW for $\dot{l}_{i,max} = 1.4 \; m.s^{-1}$
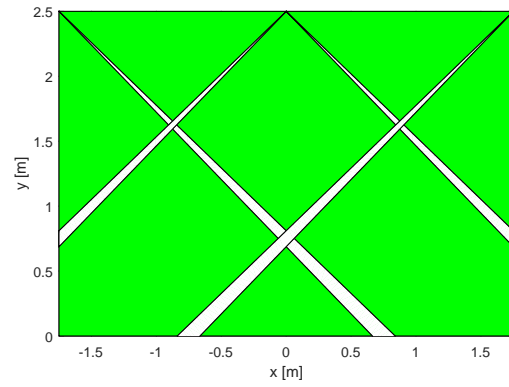
(d) TFW for $\dot{l}_{i,max} = 1.414 \; m.s^{-1}$

Figure B.14: TFW of case study 1 calculated by cable velocity boundary approach for different $\dot{l}_{i,max}$
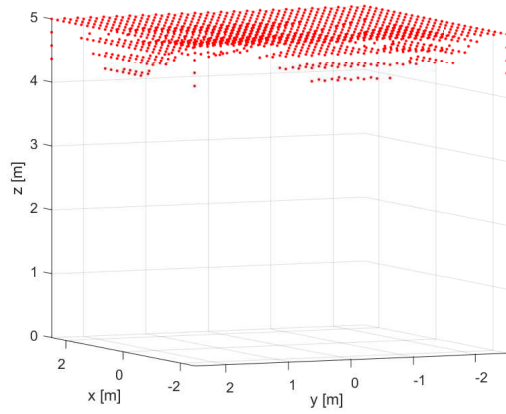
(a) TFW calculated by MDCS approach for $\dot{l}_{i,max} = 1.5 \ m.s^{-1}$
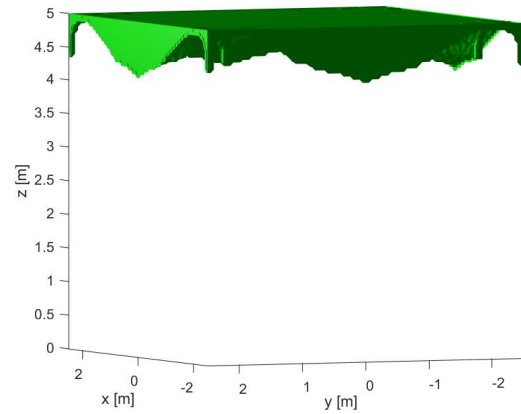
(b) TFW calculated by cable velocety boundary approach for $\dot{l}_{i,max} = 1.5 \ m.s^{-1}$
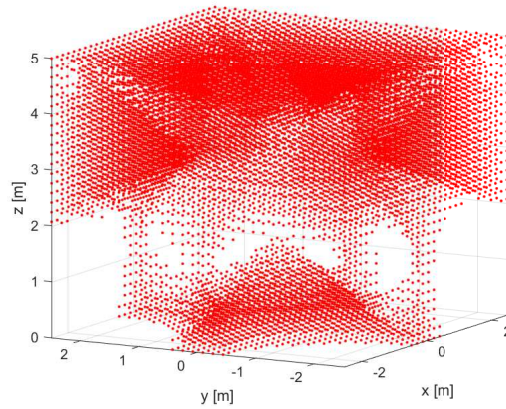
(c) TFW calculated by MDCS approach for $\dot{l}_{i,max} = 1.7 \ m.s^{-1}$
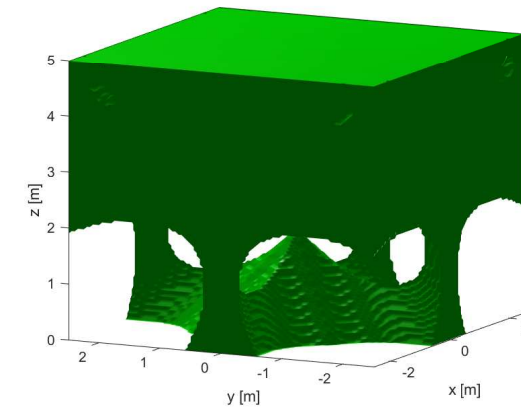
(d) TFW calculated by cable velocety boundary approach for $\dot{l}_{i,max} = 1.7 \ m.s^{-1}$

Figure B.15: TFW of case study 2 calculated by different approaches for different $\dot{l}_{i,max}$

mobile platform twists. The second method can be applied to compute the twist-feasible workspace, i.e., to determine the set of mobile platform poses where a prescribed polyhedral required twist set is contained within the available twist set. This method can thus be used to analyze the CDPR speed capabilities over its workspace, which should prove useful in high-speed CDPR applications.

The proposed method can be seen as a dual to the one used to compute the wrench-feasible workspace of a CDPR, just as the velocity equations may be seen as dual to static equations. From a mathematical standpoint, however, the problem is much simpler in the case of the twist-feasible workspace, as the feasibility conditions can be obtained explicitly. Nevertheless, the authors believe that the present chapter complements nicely the previous works on wrench feasibility.

Finally, we should point out that the proposed method does not deal with the issue of guaranteeing the magnitudes of the mobile platform point-velocity or angular velocity. In such a case, the required twist set becomes a ball or an ellipsoid, and thus is no longer polyhedral. This ellipsoid could be approximated by a polytope in order to apply the method proposed in this chapter. However, since the accuracy of the approximation would come at the expense of the number of conditions to be numerically verified, part of our future work will be dedicated to the problem of determining the twist-feasibility of CDPRs for ellipsoidal required twist sets.

Appendix C

Publications

Journals

[1] Saman Lessanibahri, Philippe Cardou, and Stéphane Caro. *A Cable-Driven Parallel Robot with an Embedded Tilt-Roll Wrist*, ASME Journal of Mechanisms and Robotics, 2020.

[2] Saman Lessanibahri, Philippe Cardou, and Stéphane Caro. Parasitic inclinations in cable-driven parallel robots using cable loops. *Procedia CIRP*, 70:296–301, 2018.

International Conferences

[1] Saman Lessanibahri, Marc Gouttefarde, Stéphane Caro, and Philippe Cardou. Twist feasibility analysis of cable-driven parallel robots. In *Cable-Driven Parallel Robots*, pages 128–139. Springer, 2018.

[2] Saman Lessanibahri, Philippe Cardou, and Stéphane Caro. Kinetostatic analysis of a simple cable-driven parallel crane. In *ASME 2018 International Design Engineering Technical Conferences and Computers and Information in Engineering Conference*. American Society of Mechanical Engineers Digital Collection, 2018.

[3] Saman Lessanibahri, Philippe Cardou, and Stéphane Caro. Kinetostatic modeling of a cable-driven parallel robot using a tilt-roll wrist. In *International Conference on Cable-Driven Parallel Robots*, pages 109–120. Springer, 2019.

[4] Saman Lessanibahri, Philippe Cardou, and Stéphane Caro. A cable-driven parallel robot with an embedded tilt-roll wrist. In *ASME 2019 International Design Engineering Technical Conferences and Computers and Information in Engineering Conference*. American Society of Mechanical Engineers Digital Collection, 2019.

[5] Marceau Métillon, Saman Lessanibahri, Philippe Cardou, Kévin Subrin and Stéphane Caro. A cable-driven parallel robot with a full-circle end-effector. In *ASME 2020 International Design Engineering Technical Conferences and Computers*

and Information in Engineering Conference. American Society of Mechanical Engineers Digital Collection, 2020. (Accepted)

Bibliography

[ABD93]   J. Albus, R. Bostelman, and N. Dagalakis. "The NIST Robocrane". In: *Journal of Robotic Systems* 10.2 (1993), pp. 709–724.

[Ang15]   PLATIS Angelos. *Master Thesis: A 6-dof Cable-Driven Parallel Robot with a large orientation workspace*. 2015.

[BA05]   SP Bai and Jorge Angeles. "The design of a gearless pitch-roll wrist". In: *Robotics and Automation, 2005. ICRA 2005. Proceedings of the 2005 IEEE International Conference on*. IEEE. 2005, pp. 3213–3218.

[Bak+17]   Sana Baklouti, Eric Courteille, Stéphane Caro, and Mohamed Dkhil. "Dynamic and Oscillatory Motions of Cable-Driven Parallel Robots Based on a Nonlinear Cable Tension Model". In: *Journal of Mechanisms and Robotics* 9.6 (Oct. 2017). 061014. ISSN: 1942-4302. DOI: 10.1115/1.4038068. URL: https://doi.org/10.1115/1.4038068.

[Bak+19]   Sana Baklouti, Eric Courteille, Philippe Lemoine, and Stéphane Caro. "Vibration reduction of Cable-Driven Parallel Robots through elasto-dynamic model-based control". In: *Mechanism and Machine Theory* 139 (2019), pp. 329–345.

[Bal00]   Robert S. Ball. *A treatise on the theory of screws, by Sir Robert Stawell Ball*. Cambridge: University Press, 1900. DOI: 10.5962/bhl.title.18548.

[Beh+03]   Saeed Behzadipour, Robert Dekker, Amir Khajepour, and Edmon Chan. "DeltaBot: A new cable-based ultra high speed robot". In: *ASME 2003 international mechanical engineering congress and exposition*. American Society of Mechanical Engineers Digital Collection. 2003, pp. 533–537.

[BG04]   Lionel Birglen and Clément M Gosselin. "Kinetostatic analysis of underactuated fingers". In: *IEEE Transactions on Robotics and Automation* 20.2 (2004), pp. 211–221.

[BG06]   Lionel Birglen and Clément M Gosselin. "Force analysis of connected differential mechanisms: Application to grasping". In: *The International Journal of Robotics Research* 25.10 (2006), pp. 1033–1046.

[BG15]   Eric Barnett and Clément Gosselin. "Large-scale 3D printing with a cable-suspended robot". In: *Additive Manufacturing* 7 (2015), pp. 27–44.

[BGM10a]   S. Bouchard, C. M. Gosselin, and B. Moore. "On the Ability of a Cable-Driven Robot to Generate a Prescribed Set of Wrenches". In: *ASME Journal of Mechanisms and Robotics* 2.1 (2010), pp. 1–10.

[BGM10b]   Samuel Bouchard, Clément Gosselin, and Brian Moore. "On the ability of a cable-driven robot to generate a prescribed set of wrenches". In: *Journal of Mechanisms and Robotics* 2.1 (2010), p. 011010.

[BJB99]   Roger Bostelman, Adam Jacoff, and Robert Bunch. "Delivery of an Advanced Double-Hull Ship Welding System using RoboCrane." In: *IIA/SOCO*. 1999.

[BK06]   Saeed Behzadipour and Amir Khajepour. "Stiffness of cable-based parallel manipulators with application to stability analysis". In: *Journal of mechanical design* 128.1 (2006), pp. 303–310.

[Bos+94]   Roger Bostelman, James Albus, Nicholas Dagalakis, Adam Jacoff, and John Gross. "Applications of the NIST RoboCrane". In: *Proceedings of the 5th International Symposium on Robotics and Manufacturing*. 1994, pp. 14–18.

[BREU06]   P. Bosscher, A. T. Riechel, and I. Ebert-Uphoff. "Wrench-Feasible Workspace Generation for Cable-Driven Robots". In: *IEEE Trans. on Robotics* 22.5 (Oct. 2006), pp. 890–902.

[Bru+09]   Tobias Bruckmann, Lars Mikelsons, Thorsten Brandt, Manfred Hiller, and Dieter Schramm. "Design approaches for wire robots". In: *ASME 2009 International Design Engineering Technical Conferences and Computers and Information in Engineering Conference*. American Society of Mechanical Engineers. 2009, pp. 25–34.

[Bru+13a]   Tobias Bruckmann, Wildan Lalo, Christian Sturm, Dieter Schramm, and Manfred Hiller. "Design and realization of a high rack storage and retrieval machine based on wire robot technology". In: *DINAME* (2013).

[Bru+13b]   Tobias Bruckmann, Wildan Lalo, Khoa Nguyen, and Bashir Salah. "Development of a storage retrieval machine for high racks using a wire robot". In: *ASME 2012 International Design Engineering Technical Conferences and Computers and Information in Engineering Conference*. American Society of Mechanical Engineers Digital Collection. 2013, pp. 771–780.

[Car13]   Marco Carricato. "Inverse geometrico-static problem of underconstrained cable-driven parallel robots with three cables". In: *Journal of Mechanisms and Robotics* 5.3 (2013), p. 031002.

[Che+13]   Quanzhu Chen, Weihai Chen, Guilin Yang, and Rong Liu. "An integrated two-level self-calibration method for a cable-driven humanoid arm". In: *IEEE Transactions on Automation Science and Engineering* 10.2 (2013), pp. 380–391.

[CN12]   David W Crawford and Edward A Nemeth. *Amusement park ride with cable-suspended vehicles*. US Patent 8,147,344. 2012.

[Con85]   Lawrence L Cone. "Skycam-an aerial robotic camera system". In: *Byte* 10.10 (1985), p. 122.

[CR+15]   A. Cruz Ruiz, S. Caro, P. Cardou, and F. Guay. "ARACHNIS : Analysis of Robots Actuated by Cables with Handy and Neat Interface Software". In: *Mechanisms and Machine Science Volume*. Vol. 32. 2015, pp. 293–305.

[CSS11]   Alon Capua, Amir Shapiro, and Shraga Shoval. "Spiderbot: a cable suspended mobile robot". In: *2011 IEEE International Conference on Robotics and Automation*. IEEE. 2011, pp. 3437–3438.

[Dua+09]   BY Duan, YY Qiu, FS Zhang, and B Zi. "On design and experiment of the feed cable-suspended structure for super antenna". In: *Mechatronics* 19.4 (2009), pp. 503–509.

[Dua99]   BY Duan. "A new design project of the line feed structure for large spherical radio telescope and its nonlinear dynamic analysis". In: *Mechatronics* 9.1 (1999), pp. 53–64.

[Ede+16]   J. Eden, D. Lau, Y. Tan, and D. Oetomo. "Available acceleration set for the study of motion capabilities for cable-driven robots". In: *Mechanism and Machine Theory* 105 (2016), pp. 320–336.

[EUV04]   Imme Ebert-Uphoff and Philip A Voglewede. "On the connections between cable-driven robots, parallel manipulators and grasping". In: *IEEE International Conference on Robotics and Automation, 2004. Proceedings. ICRA'04. 2004*. Vol. 5. IEEE. 2004, pp. 4521–4526.

[Fuk]   K. Fukuda. *Frequently Asked Questions in Polyhedral Computation*. Tech. rep. http://www.ifor.math.ethz.ch/~fukuda/polyfaq/polyfaq.html.

[Gag+15]   L. Gagliardini, S. Caro, M. Gouttefarde, and A. Girin. "Dimensioning of Cable-Driven Parallel Robot Actuators, Gearboxes And Winches According To The Twist Feasible Work-space". In: *Proc. IEEE Int. Conf. on Automation Science and Engineering*. Gothenburg, Sweden, 2015.

[Gag+16a]   L. Gagliardini, S. Caro, M. Gouttefarde, and A. Girin. "Discrete reconfiguration planning for cable-driven parallel robots". In: *Mechanism and Machine Theory* 100 (2016), pp. 313–337.

[Gag+16b]   Lorenzo Gagliardini, Stéphane Caro, Marc Gouttefarde, and Alexis Girin. "Discrete reconfiguration planning for cable-driven parallel robots". In: *Mechanism and Machine Theory* 100 (2016), pp. 313–337.

[Gag+16c]   Lorenzo Gagliardini, Stéphane Caro, Marc Gouttefarde, and Alexis Girin. "Discrete reconfiguration planning for cable-driven parallel robots". In: *Mechanism and Machine Theory* 100 (2016), pp. 313–337.

[GCG15]   Lorenzo Gagliardini, Stéphane Caro, and Marc Gouttefarde. "Dimensioning of cable-driven parallel robot actuators, gearboxes and winches according to the twist feasible workspace". In: *2015 IEEE International Conference on Automation Science and Engineering (CASE)*. IEEE. 2015, pp. 99–105.

[GG06]   M. Gouttefarde and C. M. Gosselin. "Analysis of the Wrench-Closure Workspace of Planar Parallel Cable-Driven Mechanisms". In: *IEEE Trans. on Robotics* 22.3 (June 2006), pp. 434–445.

[GGC16]   L. Gagliardini, M. Gouttefarde, and S. Caro. "Determination of a Dynamic Feasible Workspace for Cable-Driven Parallel Robots". In: *The 15th International Symposium on Advances in Robot Kinematics*. Grasse, France, 2016.

[GK10]   M. Gouttefarde and S. Krut. "Characterization of Parallel Manipulator Available Wrench Set Facets". In: *Advanced in Robot Kinematics*. Portoroz, Slovenia, 2010.

[GMD07]   Marc Gouttefarde, Jean-Pierre Merlet, and David Daney. "Wrench-feasible workspace of parallel cable-driven mechanisms". In: *Proceedings 2007 IEEE International Conference on Robotics and Automation*. IEEE. 2007, pp. 1492–1497.

[Gos07]   F. Gosselin. *Haptic interface provided with a tight cable structure, with a large maneuver angle*. PCT patent: PCT/EP2007/064537. 2007.

[Gou+08] Marc Gouttefarde, Sébastien Krut, François Pierrot, Nacim Ramdani, et al. "On the design of fully constrained parallel cable-driven robots". In: *Advances in Robot Kinematics: Analysis and Design*. Springer, 2008, pp. 71–78.

[Gou+15a] M. Gouttefarde, J. Lamaury, C. Reichert, and T. Bruckmann. "A versatile tension distribution algorithm for n-DOF parallel robots driven by n+2 cables". In: *IEEE Trans. on Robotics* 31.6 (2015), pp. 1444–1457.

[Gou+15b] Marc Gouttefarde, Jean-François Collard, Nicolas Riehl, and Cédric Baradat. "Geometry selection of a redundantly actuated cable-suspended parallel robot". In: *IEEE Transactions on Robotics* 31.2 (2015), pp. 501–510.

[Gou57]   VE Gough. "Contribution to discussion of papers on research in automobile stability, control and tyre performance". In: *Proc. of Auto Div. Inst. Mech. Eng.* 171 (1957), pp. 392–395.

[GRR01]   P. Gallina, G. Rosati, and A. Rossi. "3-DOF wire driven planar haptic interface". In: *Journal of Intelligent and Robotic Systems* 32.1 (2001), pp. 23–36.

[Gua+14] François Guay, Philippe Cardou, Ana Lucia Cruz-Ruiz, and Stéphane Caro. "Measuring how well a structure supports varying external wrenches". In: *New Advances in Mechanisms, Transmissions and Applications*. Springer, 2014, pp. 385–392.

[Han+12] Blake Hannaford, Jacob Rosen, Diana W Friedman, Hawkeye King, Phillip Roan, Lei Cheng, Daniel Glozman, Ji Ma, Sina Nia Kosari, and Lee White. "Raven-II: an open platform for surgical robotics research". In: *IEEE Transactions on Biomedical Engineering* 60.4 (2012), pp. 954–959.

[HBA06]   S Hernandez, Shaoping Bai, and J Angeles. "The design of a chain of spherical Stephenson mechanisms for a gearless robotic pitch-roll wrist". In: *Journal of Mechanical Design* 128.2 (2006), pp. 422–429.

[Hil+05] M. Hiller, S. Fang, S. Mielczarek, R. Verhoeven, and D. Franitza. "Design, analysis and realization of tendon-based parallel manipulators". In: *Mech. and Mach. Theory* 40.4 (Apr. 2005), pp. 429–445.

[HK11]   M. Hassan and A. Khajepour. "Analysis of Bounded Cable Tensions in Cable-Actuated Parallel Manipulators". In: *IEEE Trans. on Robotics* 27.5 (2011), pp. 891–900.

[HK92]   Kazuhito Hyodo and Hiroaki Kobayashi. "Kinematic and Control Issues on Tendon Controlled Wrist Mechanism". In: *Robotics, Mechatronics and Manufacturing Systems edited by T. Takamori, K. Tsuchiya*. Elsevier, 1992, pp. 89–94.

[Jeo+98]   Jae Won Jeong, Soo Hyun Kim, Yoon Keun Kwak, and Craig C Smith. "Development of a parallel wire mechanism for measuring position and orientation of a robot end-effector". In: *Mechatronics* 8.8 (1998), pp. 845–861.

[JKK99]   Jae Won Jeong, Soo Hyun Kim, and Yoon Keun Kwak. "Kinematics and workspace analysis of a parallel wire mechanism for measuring a robot pose". In: *Mechanism and Machine Theory* 34.6 (1999), pp. 825–841.

[KB14]   Hamed Khakpour and Lionel Birglen. "Workspace augmentation of spatial 3-DOF cable parallel robots using differential actuation". In: *Intelligent Robots and Systems (IROS 2014), 2014 IEEE/RSJ International Conference on*. IEEE. 2014, pp. 3880–3885.

[KBR16]   Daniel Krebs, Gunnar Borchert, and Annika Raatz. "Simulation and design of an orientation mechanism for assembly systems". In: *Procedia CIRP* 44 (2016), pp. 245–250.

[KBT14]   Hamed Khakpour, Lionel Birglen, and Souheil-Antoine Tahan. "Synthesis of differentially driven planar cable parallel manipulators". In: *IEEE Transactions on Robotics* 30.3 (2014), pp. 619–630.

[KBT15]   Hamed Khakpour, Lionel Birglen, and Souheil-Antoine Tahan. "Analysis and optimization of a new differentially driven cable parallel robot". In: *Journal of Mechanisms and Robotics* 7.3 (2015), p. 034503.

[KCP04]   S. Krut, O. Company, and F. Pierrot. "Velocity performance indices for parallel mechanisms with actuation redundancy". In: *Robotica* 22 (2004), pp. 129–139.

[KD04]   Wisama Khalil and Etienne Dombre. *Modeling, identification and control of robots*. Butterworth-Heinemann, 2004.

[KK15]   Hitoshi Kino and Sadao Kawamura. "Mechanism and control of parallel-wire driven system". In: *Journal of Robotics and Mechatronics* 27.6 (2015), pp. 599–607.

[KKW00a]   S. Kawamura, H. Kino, and C. Won. "High-speed manipulation by using parallel wire-driven robots". In: *Robotica* 18 (2000), pp. 13–21.

[KKW00b]   Sadao Kawamura, Hitoshi Kino, and Choe Won. "High-speed manipulation by using parallel wire-driven robots". In: *Robotica* 18.1 (2000), pp. 13–21.

[KN02]   Craig Kossowski and Leila Notash. "CAT4 (Cable actuated truss—4 Degrees of Freedom): a novel 4 DOF cable actuated parallel manipulator". In: *Journal of Robotic Systems* 19.12 (2002), pp. 605–615.

[KS13]   Alexander Konyukhov and Karl Schweizerhof. *Computational Contact Mechanics*. Vol. 67. Berlin, Heidelberg: Springer Berlin Heidelberg, 2013. ISBN: 978-3-642-31530-5. DOI: 10.1007/978-3-642-31531-2.

[KZW06]   Kris Kozak, Qian Zhou, and Jinsong Wang. "Static analysis of cable-driven manipulators with non-negligible cable mass". In: *IEEE Transactions on Robotics* 22.3 (2006), pp. 425–433.

[Lab]   UW BioRobotics Lab. URL: http://brl.ee.washington.edu/category/surgical-robotics/raven/.

[Lam13]   Johann Lamaury. "Contribution a la commande des robots parallèles a câbles à redondance d'actionnement". PhD thesis. 2013.

[LBS13]   W Lalo, T Bruckmann, and D Schramm. "Optimal control for a wire-based storage retrieval machine". In: *New Trends in Mechanism and Machine Science*. Springer, 2013, pp. 631–639.

[LDN16]   Tam Nhat Le, Hiroki Dobashi, and Kiyoshi Nagai. "Configuration of redundant drive wire mechanism using double actuator modules". In: *ROBOMECH Journal* 3.1 (2016), p. 25.

[LG13]   Johann Lamaury and Marc Gouttefarde. "Control of a large redundantly actuated cable-suspended parallel robot". In: *2013 IEEE International Conference on Robotics and Automation*. IEEE. 2013, pp. 4659–4664.

[LGG16]   Rongfu Lin, Weizhong Guo, and Feng Gao. "On Parasitic Motion of Parallel Mechanisms". In: *ASME 2016 International Design Engineering Technical Conferences and Computers and Information in Engineering Conference*. American Society of Mechanical Engineers. 2016, V05BT07A077–V05BT07A077.

[Li94]   S-H Li. "An Ultrahigh Speed Assembly Robot System: Part II Design". In: *Proc. 1994 Japan-USA Symposium on Flexible Automation*. 1994.

[LNC07]   C. Lambert, M. Nahon, and D. Chalmers. "Implementation of an Aerostat Positioning System With Cable Control". In: *IEEE/ASME Transactions on Mechatronics* 12(1) (2007), pp. 32–40.

[Mao+14]   Ying Mao, Xin Jin, Geetanjali Gera Dutta, John P Scholz, and Sunil K Agrawal. "Human movement training with a cable driven arm exoskeleton (CAREX)". In: *IEEE Transactions on Neural Systems and Rehabilitation Engineering* 23.1 (2014), pp. 84–92.

[Mer06]   Jean-Pierre Merlet. *Parallel robots*. Vol. 128. Springer Science & Business Media, 2006.

[Mét+ l]   Marceau Métillon, Saman Lessanibahri, Philippe Cardou, Kévin Subrin, and Stéphane Caro. "A cable-driven parallel robot with a full-circle end-effector". In: *Proceedings of the ASME 2020 International Design Engineering Technical Conferences & Computers and Information in Engineering Conference IDETC/CIE 2020*. St. Louis, Missouri, USA, August 16–19, 2020.

[Mét19]   Marceau Métillon. *Cable-Driven Parallel Robot with a Large Orientation Workspace, Master Thesis, CNRS, Laboratoire des Sciences du Numérique de Nantes*. 2019.

[Mie+16]   Philipp Miermeister, Maria Lächele, Rainer Boss, Carlo Masone, Christian Schenk, Joachim Tesch, Michael Kerger, Harald Teufel, Andreas Pott, and Heinrich H Bülthoff. "The cablerobot simulator large scale motion platform based on cable robot technology". In: *2016 IEEE/RSJ International Conference on Intelligent Robots and Systems (IROS)*. IEEE. 2016, pp. 3024–3029.

[Min94]   Aiguo Ming. "Study on Multiple Degree-of-Freedom Positioning Mechanism Using Wires (Part I)-Concept, Design and Control". In: *International Journal of the Japan Society for Precision Engineering* 28.2 (1994), pp. 131–138.

[MP15]   Philipp Miermeister and Andreas Pott. "Design of cable-driven parallel robots with multiple platforms and endless rotating axes". In: *Interdisciplinary Applications of Kinematics*. Springer, 2015, pp. 21–29.

[Nag+11]   Kiyoshi Nagai, Tam Nhat Le, Yoshikatsu Hayashi, and Koji Ito. "Proposal of a Redundant Drive Wire Mechanism for producing motions with high acceleration and high precision". In: *2011 IEEE/SICE International Symposium on System Integration (SII)*. IEEE. 2011, pp. 1049–1054.

[Nag+12]   Kiyoshi Nagai, Tam Nhat Le, Yoshikatsu Hayashi, and Koji Ito. "Kinematical analysis of redundant drive wire mechanisms with velocity constraint". In: *Mechatronics and Automation (ICMA), 2012 International Conference on*. IEEE. 2012, pp. 1496–1501.

[OCP10]   Erika Ottaviano, Marco Ceccarelli, and Francesco Palmucci. "An application of CaTraSys, a cable-based parallel measuring system for an experimental characterization of human walking". In: *Robotica* 28.1 (2010), pp. 119–133.

[OHK09]   Ryuta Ozawa, Kazunori Hashirii, and Hiroaki Kobayashi. "Design and control of underactuated tendon-driven mechanisms". In: *2009 IEEE International Conference on Robotics and Automation*. IEEE. 2009, pp. 1522–1527.

[PD14]   Zoran Pandilov and Vladimir Dukovski. "Comparison of the characteristics between serial and parallel robots". In: *Acta Technica Corvininesis-Bulletin of Engineering* 7.1 (2014).

[Ped+19]   Nicolò Pedemonte, Tahir Rasheed, David Marquez-Gamez, Philip Long, Étienne Hocquard, Francois Babin, Charlotte Fouché, Guy Caverot, Alexis Girin, and Stéphane Caro. "FASTKIT: A Mobile Cable-Driven Parallel Robot for Logistics". In: *Advances in Robotics Research: From Lab to Market: ECHORD++: Robotic Science Supporting Innovation* 132 (2019), p. 141.

[Per+10]   S. Perreault, P. Cardou, C. Gosselin, and M. Otis. "Geometric Determination of the Interference-Free Constant-Orientation Workspace of Parallel Cable-Driven Mechanisms". In: *ASME Journal of Mechanisms and Robotics* 2.3 (2010).

[Pla+18]   Angelos Platis, Tahir Rasheed, Philippe Cardou, and Stéphane Caro. "Isotropic Design of the Spherical Wrist of a Cable-Driven Parallel Robot". In: *Advances in Robot Kinematics 2016*. Springer, 2018, pp. 321–330.

[Pot10]   Andreas Pott. "An algorithm for real-time forward kinematics of cable-driven parallel robots". In: *Advances in Robot Kinematics: Motion in man and machine*. Springer, 2010, pp. 529–538.

[Pot+13]   Andreas Pott, Hendrick Mütherich, Werner Kraus, Valentine Schmidt, Philipp Miermeister, and Alexander Verl. "IPAnema: a family of cable-driven parallel robots for industrial applications". In: *Cable-Driven Parallel Robots*. Springer, 2013, pp. 119–134.

[Pot18]   Andreas Pott. *Cable-driven parallel robots: theory and application*. Vol. 120. Springer, 2018.

[Qia+18]   Sen Qian, Bin Zi, Wei-Wei Shang, and Qing-Song Xu. "A review on cable-driven parallel robots". In: *Chinese Journal of Mechanical Engineering* 31.1 (2018), p. 66.

[Ras+18]   Tahir Rasheed, Philip Long, David Marquez-Gamez, and Stéphane Caro. "Tension distribution algorithm for planar mobile cable-driven parallel robots". In: *Cable-Driven Parallel Robots*. Springer, 2018, pp. 268–279.

[Rei+19]   Thomas Reichenbach, Philipp Tempel, Alexander Verl, and Andreas Pott. "Static Analysis of a Two-Platform Planar Cable-Driven Parallel Robot with Unlimited Rotation". In: *International Conference on Cable-Driven Parallel Robots*. Springer. 2019, pp. 121–133.

[REU04]   A. T. Riechel and I. Ebert-Uphoff. "Force-Feasible Workspace Analysis for Underconstrained Point-Mass Cable Robots". In: *Proc. IEEE Int. Conf. Robotics and Automation (ICRA)*. New Orleans, LA, 2004, pp. 4956–4962.

[RG98]   R. G. Roberts and T. Graham T.and Lippitt. "On the Inverse Kinematics, Statics, and Fault Tolerance of Cable-Suspended Robots". In: *Journal of Robotic Systems* 15.10 (Oct. 1998), pp. 581–597.

[Ros+05]   Giulio Rosati, Paolo Gallina, Stefano Masiero, and Aldo Rossi. "Design of a new 5 dof wire-based robot for rehabilitation". In: *9th International Conference on Rehabilitation Robotics, 2005. ICORR 2005*. IEEE. 2005, pp. 430–433.

[RSBT17]   Peter Racioppo, Wael Saab, and Pinhas Ben-Tzvi. "Design and Analysis of Reduced Degree of Freedom Modular Snake Robot". In: *ASME 2017 International Design Engineering Technical Conferences and Computers and Information in Engineering Conference*. American Society of Mechanical Engineers. 2017, V05BT08A009–V05BT08A009.

[Rui13]   Ana Lucia Cruz Ruiz. "A graphical user interface for the design of cable-driven parallel robots". PhD thesis. Master's thesis, Ecole Centrale de Nantes, 2013.

[Rui+15]   Ana Lucia Cruz Ruiz, Stéphane Caro, Philippe Cardou, and François Guay. "Arachnis: Analysis of robots actuated by cables with handy and neat interface software". In: *Cable-Driven Parallel Robots*. Springer, 2015, pp. 293–305.

[RZA11]   G. Rosati, D. Zanotto, and S. K. Agrawal. "On the Design of Adaptive Cable-Driven Systems". In: *Journal of Mechanisms and Robotics* 3 (2011).

[SB04]   Dragoljub Surdilovic and Rolf Bernhardt. "STRING-MAN: a new wire robot for gait rehabilitation". In: *IEEE International Conference on Robotics and Automation, 2004. Proceedings. ICRA'04. 2004*. Vol. 2. IEEE. 2004, pp. 2031–2036.

[SGW16]   Stefano Seriani, Paolo Gallina, and A Wedler. "A modular cable robot for inspection and light manipulation on celestial bodies". In: *Acta Astronautica* 123 (2016), pp. 145–153.

[SHH93]   Andre Sharon, Neville Hogan, and David E Hardt. "The macro/micro manipulator: An improved architecture for robot control". In: *Robotics and computer-integrated manufacturing* 10.3 (1993), pp. 209–222.

[Shi11]   Joseph Edward Shigley. *Shigley's mechanical engineering design*. Tata McGraw-Hill Education, 2011.

[Skya]   URL: http://skycam.tv/.

[Skyb]   URL: https://www.wired.com/2016/01/the-cameras-thatll-make-the-super-bowl-way-more-interesting-this-year.

[Ste65]   Doug Stewart. "A platform with six degrees of freedom". In: *Proceedings of the institution of mechanical engineers* 180.1 (1965), pp. 371–386.

[Tah16]   Rasheed Tahir. *Optimum Design, Prototyping and Control of a 6-dof Cable Driven Parallel Robot with a large orientational workspace, Master Thesis, CNRS, Laboratoire des Sciences du Numérique de Nantes*. 2016.

[Tem+15] Philipp Tempel, Fabian Schnelle, Andreas Pott, and Peter Eberhard. "Design and programming for cable-driven parallel robots in the German pavilion at the expo 2015". In: *Machines* 3.3 (2015), pp. 223–241.

[TOC06]   Cristina Tavolieri, Erika Ottaviano, and Marco Ceccarelli. "Pose determination for a rigid body by means of CaTraSys II (Cassino Tracking System)". In: *Proceedings of EuCoMeS, the first European Conference on Mechanism Science*. 2006, pp. 21–26.

[Ver04]   R. Verhoeven. "Analysis of the Workspace of Tendon-Based Stewart-Platforms". PhD thesis. Germany: Univ. Duisburg-Essen, 2004.

[VH00]   Richard Verhoeven and Manfred Hiller. "Estimating the controllable workspace of tendon-based Stewart platforms". In: *Advances in Robot Kinematics*. Springer, 2000, pp. 277–284.

[WR15]   R Williams and L Robert. "Five-hundred meter aperture spherical radio telescope (FAST) cable-Suspended robot model and comparison with the Arecibo observatory". In: *Internet Publication, www.ohio.edu/people/williar4/html/pdf/FAST.pdf* (2015).

[Yos90]   T. Yoshikawa. *Foundations of Robotics*. 2nd ed. Boston, MA: MIT Press, 1990.

[Zak+19] Z. Zake, F. Chaumette, N. Pedemonte, and S. Caro. "Vision-Based Control and Stability Analysis of a Cable-Driven Parallel Robot". In: *IEEE Robotics and Automation Letters* 4.2 (2019), pp. 1029–1036. DOI: 10.1109/LRA.2019.2893611.

[Zie94]   G. M. Ziegler. *Lectures on Polytopes*. Springer-Verlag, Graduate Texts in Mathematics 152, 1994.

Résumé : Les Robots Parallèles à Câbles (RPC) sont considérés comme des manipulateurs parallèles avec des câbles flexibles au lieu de liens rigides. Un RPC se compose d'un bâti, d'une plate-forme mobile et de câbles les reliant l'un à l'autre. Les RPC sont réputés pour leurs performances avantageuses par rapport aux robots parallèles classiques en termes d'espace de travail en translation, de reconfigurabilité, de capacité de charge utile importante et de performances dynamiques élevées.

Cependant, l'amplitude de rotation de la plateforme mobile des RPC est généralement limitée en raison des collisions de types câble/câble et câble/plateforme mobile.

L'objectif de cette thèse est ainsi de concevoir, d'analyser et de prototyper des RPC hybrides ayant à la fois un grand espace de travail en translation et un grand espace de travail en orientation en utilisant des boucles de câbles.

Ce travail de recherche présente le développement de trois RPC hybrides adaptés aux tâches nécessitant de grands espaces de travail en orientation et en translation comme le balayage tomographique, les dispositifs d'orientation de caméras et l'inspection.

Abstract : Cable-Driven Parallel Robots (CDPRs) also noted as wire-driven robots are parallel manipulators with flexible cables instead of rigid links. A CDPR consists of a base frame, a moving-platform and a set of cables connecting the moving-platform to the base frame. CDPRs are well-known for their advantageous performance over classical parallel robots in terms of translation workspace, reconfigurability, payload capacity and high dynamic performance.

However, most of the CDPRs provide limited amplitudes of rotation of the moving-platform due to cable/cable and cable/moving-platform collisions.

The objective of this thesis is to design, analyze and build hybrid CDPRs to enlarge the orientation workspace in addition to their large translation workspace by exploiting cable-loops.

This research work presents development of three hybrid CDPRs with drastically augmented orientation workspace suitable for tasks requiring large orientation and translational workspaces like tomography scanning, camera-orienting devices, visual surveillance and inspection.